VIRGINIA TECH

CPES

Modeling and Control of Three-Phase High-Power High-Frequency Converters

Presented by:

Dushan Boroyevich, Rolando Burgos,

Igor Cvetkovic, and Bo Wen

IEEE COMPEL 2018
Padova, Italy, June 25-28, 2018

pels IEEE POWER ELECTRONICS SOCIETY Powering a Sustainable Future

IEEE

UNIVERSITÀ DEGLI STUDI DI PADOVA

Outline

1. Introduction
2. Mathematical Framework
3. Switching Modeling and PWM
4. Average Modeling
5. Small-Signal Modeling
6. Closed-Loop Control
7. 3-Level Converters
8. Control System Synchronization
9. AC System Interactions
10. Electronic Synchronous Machine (Voltage Controlling Converter)

Three-Phase Applications

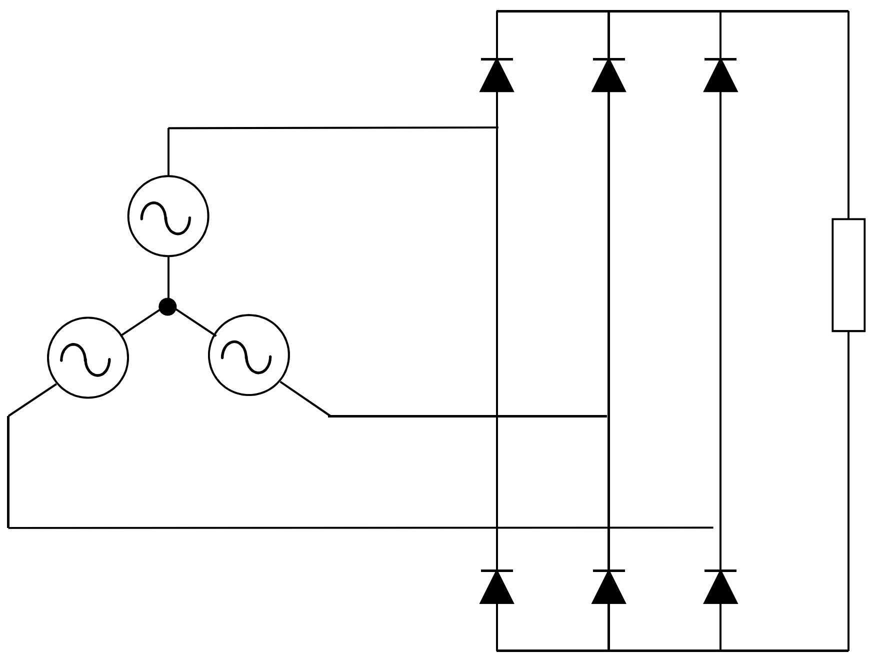

Diode Rectifier

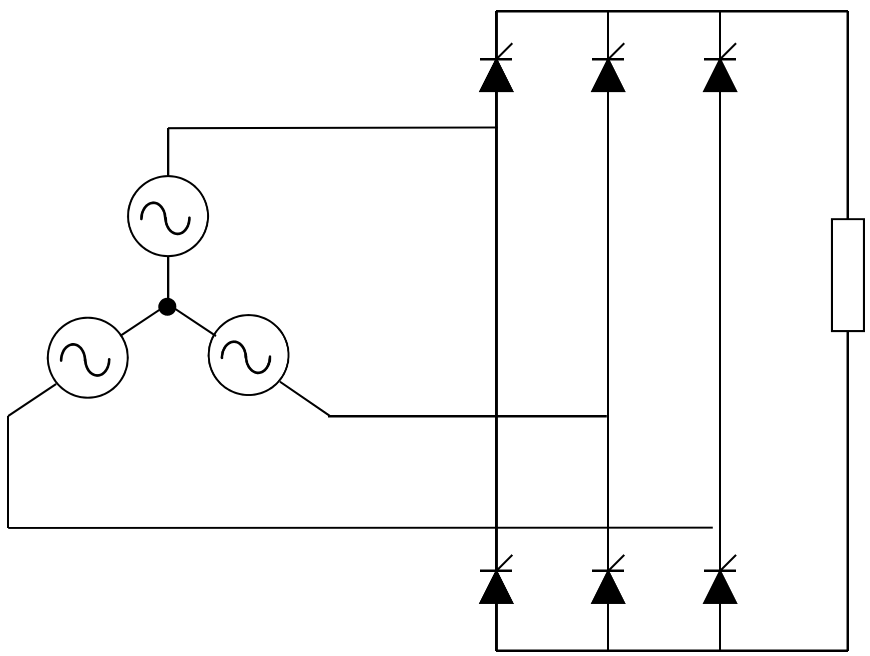

SCR Rectifier

Diode Rectifiers

THD ≅ 90%

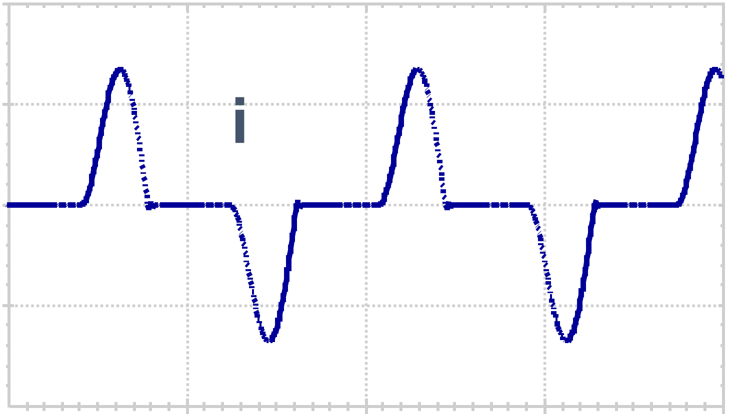

THD ≅ 80%

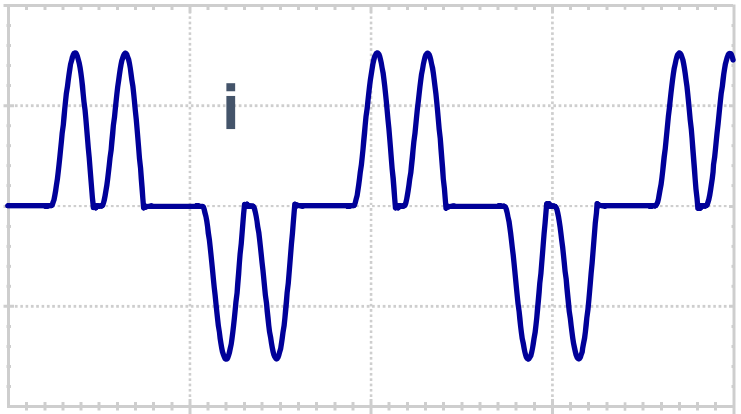

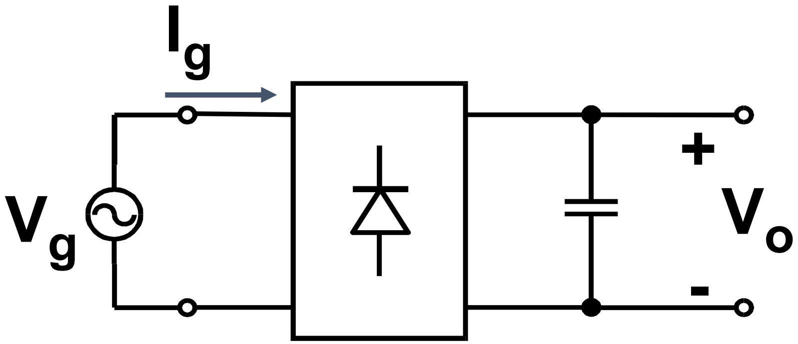

Single-phase rectifier

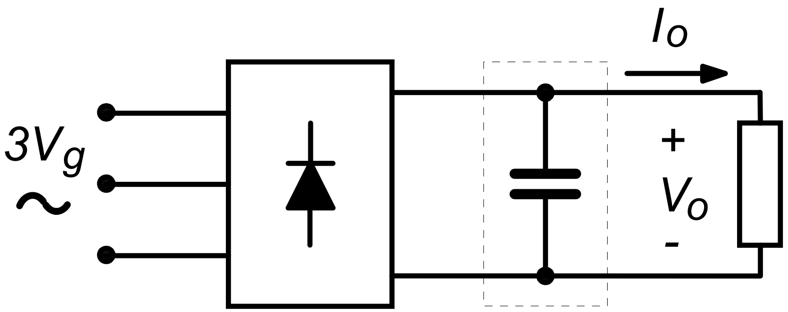

Three-phase rectifier

Diode Rectifiers

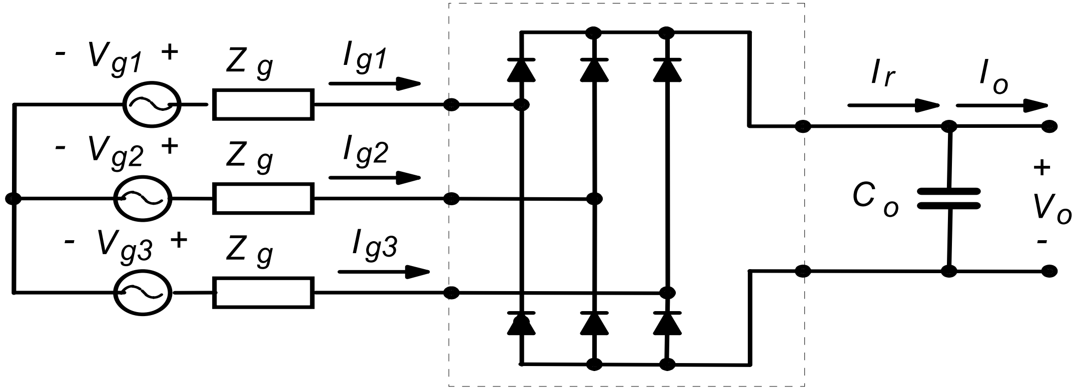

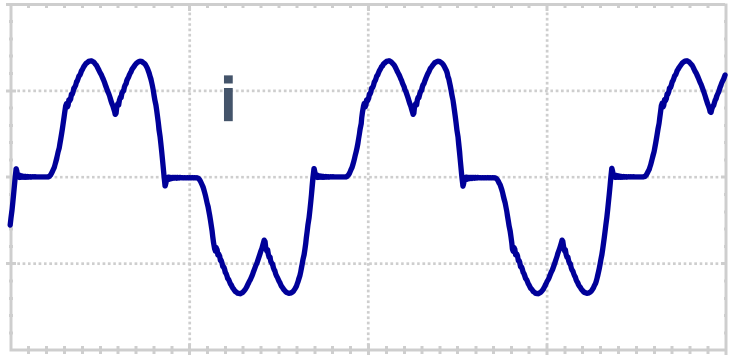

Three-phase rectifier with inductive filter

THD ≅ 40%

Three-Phase Applications

- Power Factor Correction

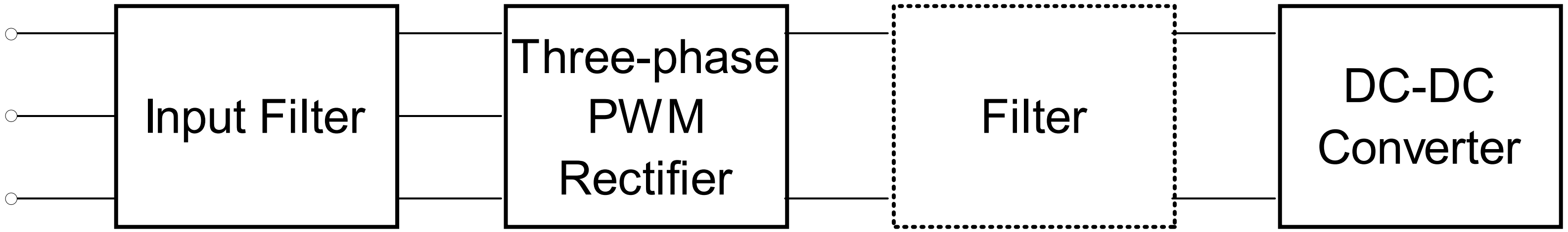

  - Sinusoidal input current and unity power factor
  - Bidirectional power flow capabilities

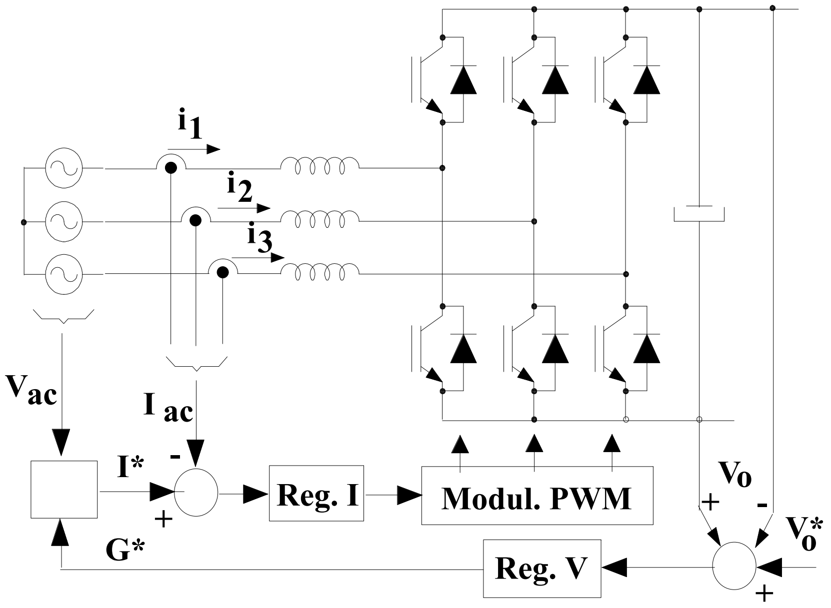

Circuit and control diagram

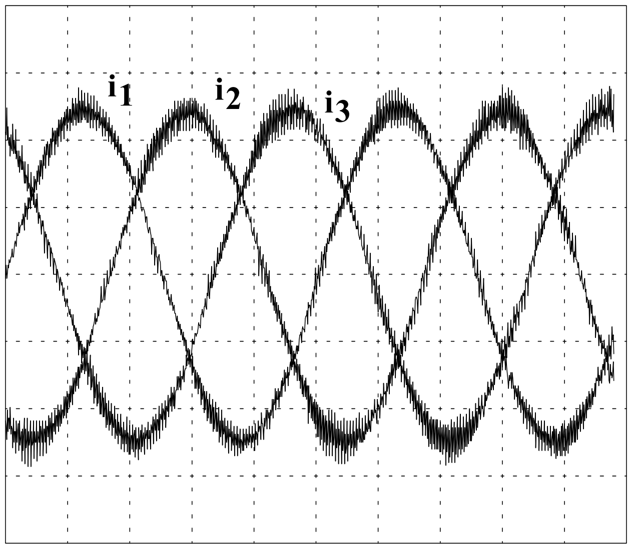

Input current waveform

Other Three-Phase Converters

- AC-DC rectifier
- DC-fed inverter
- AC-DC-AC power converter
- AC-AC power converter
- Uninterruptible power system
- Active filters
- STATCOM
- HVDC transmission station
- DC-AC grid-interface

Three-Phase Applications: Grid-Interface Converters

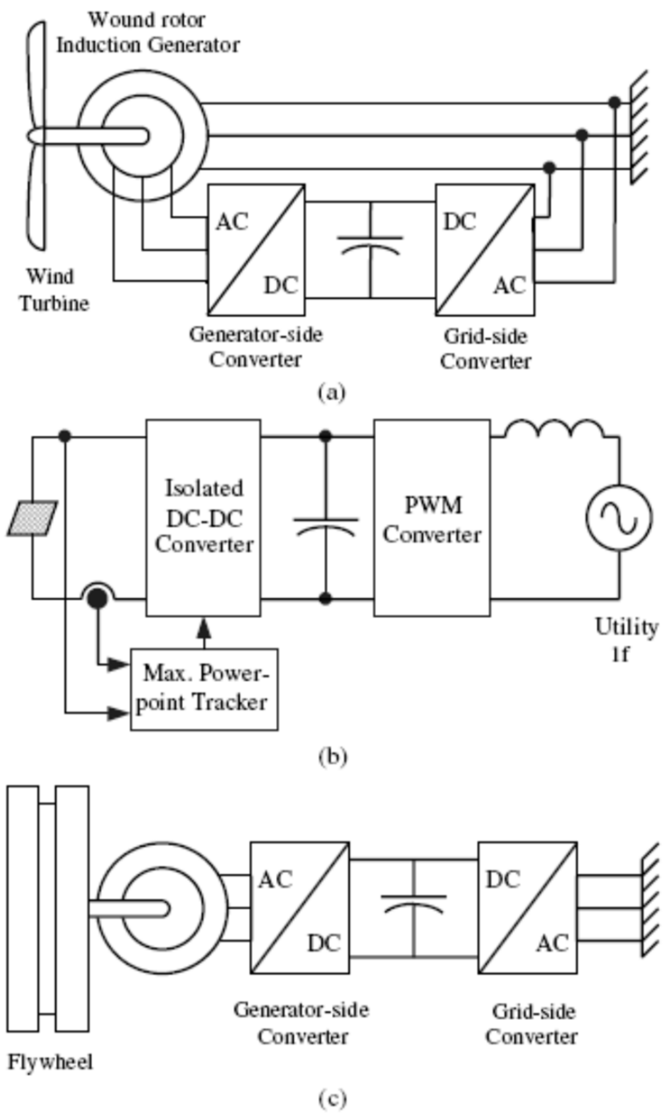

- Wind power applications
- Photovoltaic applications
- Energy Storage

Three-Phase Applications
Two-Level Power Converters

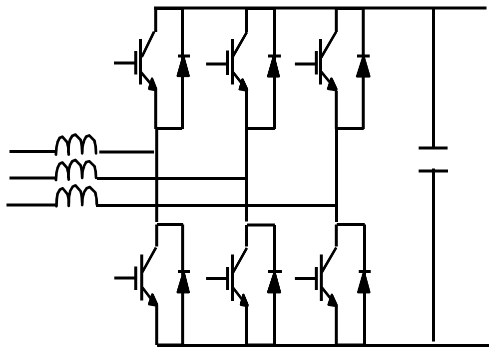

Boost Rectifier

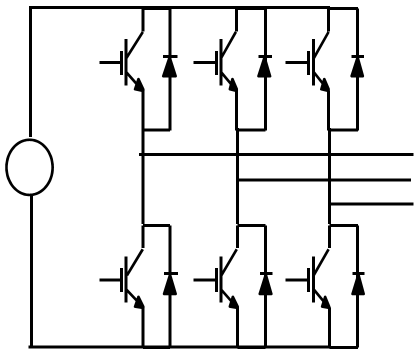

Buck Inverter (VSI)

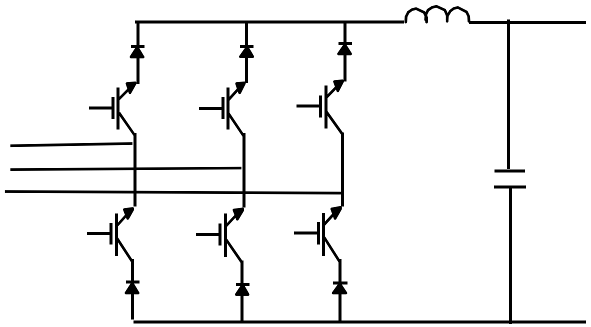

Buck Rectifier

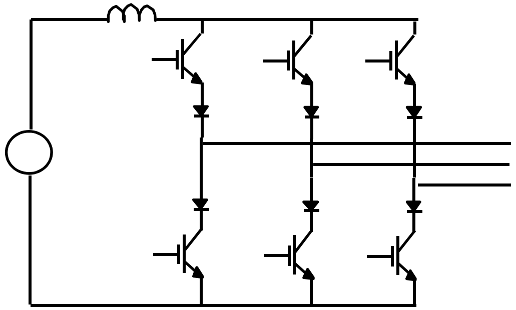

Boost Inverter (CSI)

Generalized Structure of a Power Converter

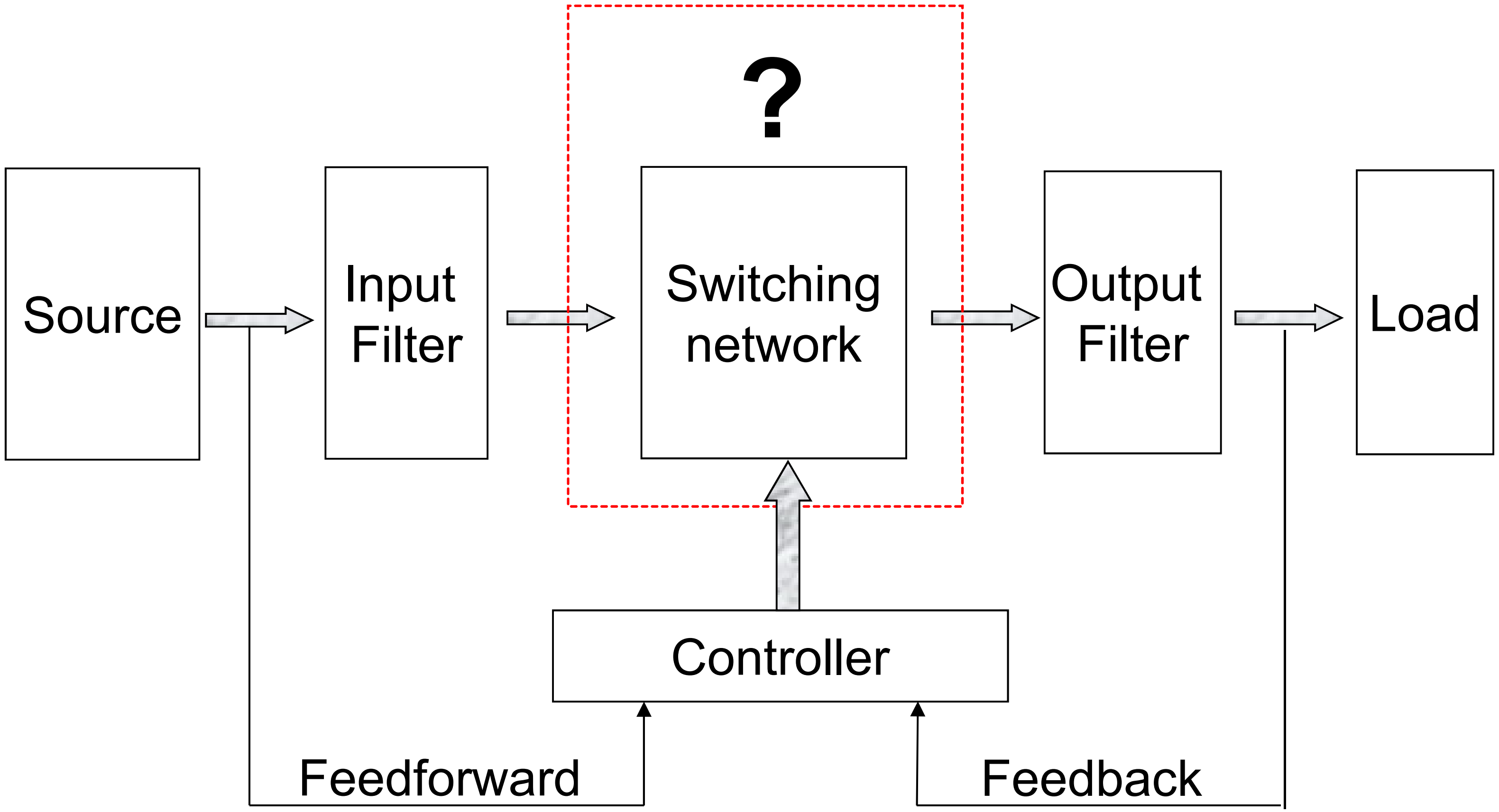

- Switching network is discontinuous and nonlinear

Steps in Modeling Three-Phase PWM Converters

1. Switching model
   - ▪ Time-discontinuous
   - ▪ Time-varying
   - ▪ Nonlinear

2. Average model in stationary frame
   - ✓ Time-continuous
   - ▪ Time-varying
   - ▪ Nonlinear

3. Average model in rotating d-q frame
   - ✓ Time-continuous
   - ✓ Time-invariant
   - ▪ Nonlinear

4. Small-signal model in rotating d-q frame
   - ✓ Time-continuous
   - ✓ Time-invariant
   - ✓ Linear

Outline

Three-Phase Variables

Y-connection

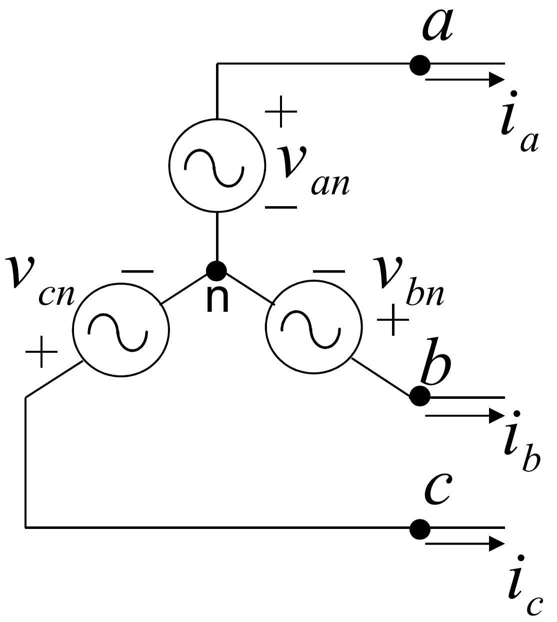

$$v_{ab} = v_a - v_b$$
$$v_{bc} = v_b - v_c$$
$$v_{ca} = v_c - v_a$$

$$i_a = i_{ca} - i_{ab}$$
$$i_b = i_{ab} - i_{bc}$$
$$i_c = i_{bc} - i_{ca}$$

$$i_a + i_b + i_c \equiv 0$$
$$v_{ab} + v_{bc} + v_{ca} \equiv 0$$
$$v_{an} + v_{bn} + v_{cn} \neq 0$$

Δ-connection

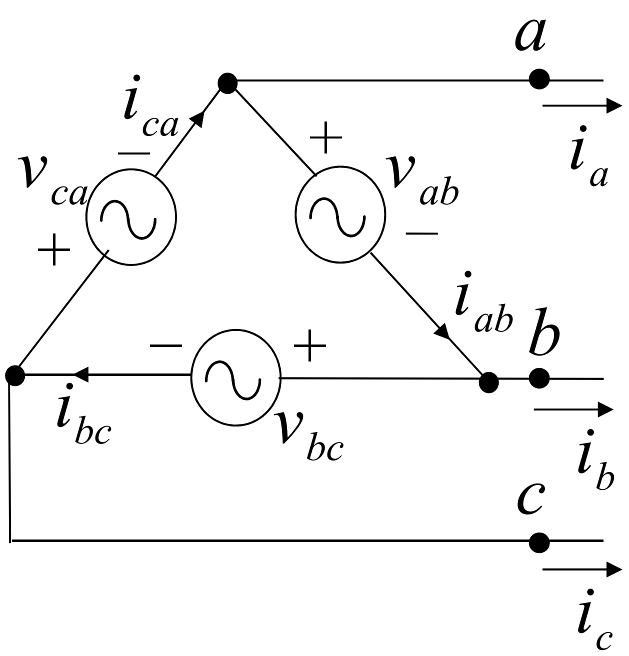

$$i_a + i_b + i_c \equiv 0$$
$$v_{ab} + v_{bc} + v_{ca} \equiv 0$$
$$i_{ab} + i_{bc} + i_{ca} \neq 0$$

Vector Representations of the Three-Phase Variables

Euclid vector representations

$$\vec{v} = \begin{bmatrix} v_a(t) \\ v_b(t) \\ v_c(t) \end{bmatrix} \qquad \vec{i} = \begin{bmatrix} i_a(t) \\ i_b(t) \\ i_c(t) \end{bmatrix}$$

Euclid Space:

$$\vec{u}_a = \begin{bmatrix} 1 \\ 0 \\ 0 \end{bmatrix} \quad \vec{u}_b = \begin{bmatrix} 0 \\ 1 \\ 0 \end{bmatrix} \quad \vec{u}_c = \begin{bmatrix} 0 \\ 0 \\ 1 \end{bmatrix}$$

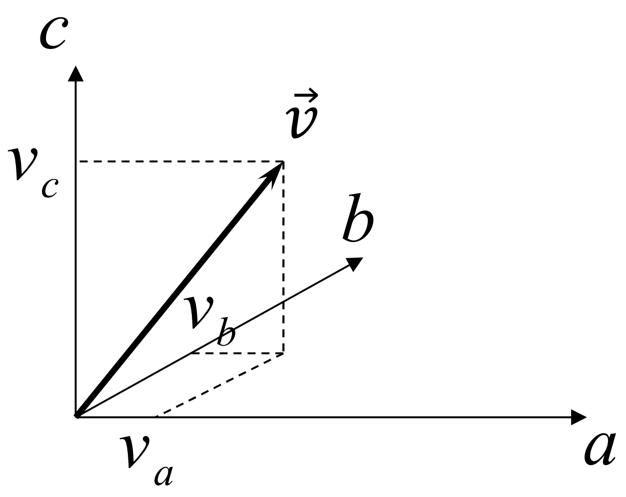

Change of Coordinates (*abc* to $\alpha\beta\gamma$)

$$i_a + i_b + i_c \equiv 0 \qquad\qquad v_{ab} + v_{bc} + v_{ca} \equiv 0$$

This defines a 2-dimensional subspace χ , perpendicular to the vector $\begin{bmatrix}1 & 1 & 1\end{bmatrix}^T$ in abc-space.

$\alpha\beta\gamma$ -space is traditionally defined by:

- α -axis is chosen as projection of the a-axis onto χ ,
- γ -axis is co-linear with vector $\begin{bmatrix}1 & 1 & 1\end{bmatrix}^T$
- β - axis is defined by right-hand rule.

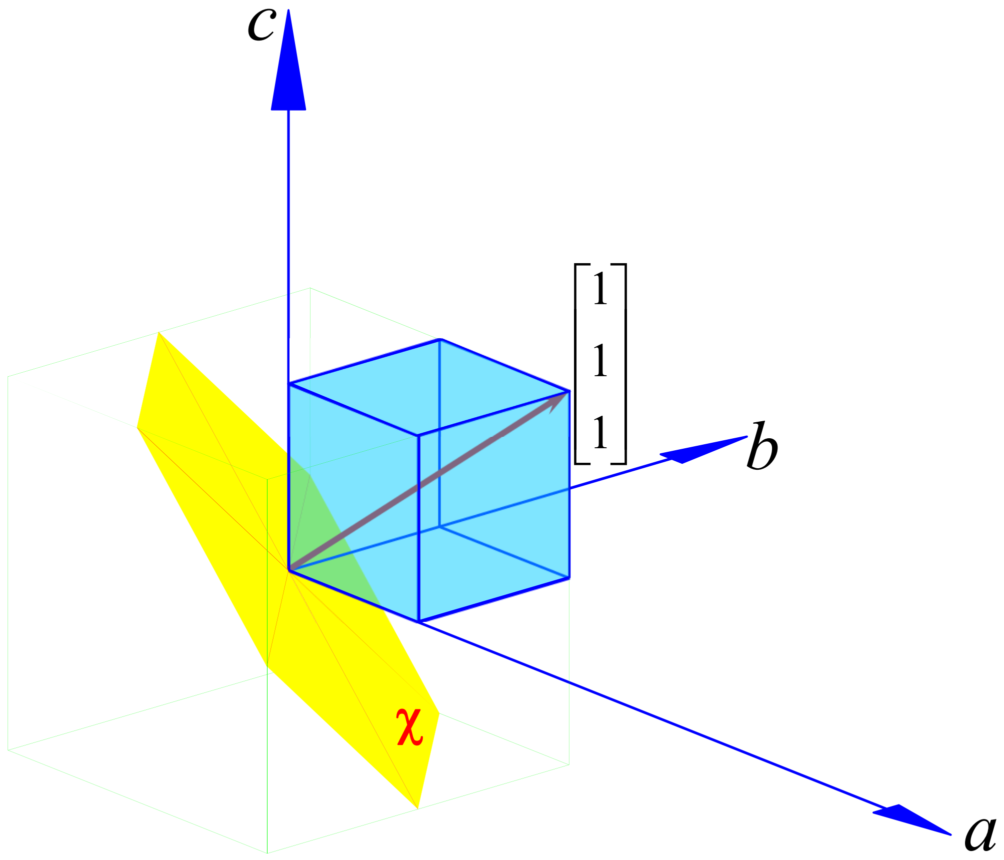

Transformation Matrix $T_{\alpha\beta\gamma/abc}$

The transformation matrix

$$\| T_{\alpha\beta\gamma\,/\,abc} \| = 1$$

$$T_{\alpha\beta\gamma/abc} = \sqrt{\frac{2}{3}} \begin{bmatrix} 1 & -\frac{1}{2} & -\frac{1}{2} \\ 0 & \frac{\sqrt{3}}{2} & -\frac{\sqrt{3}}{2} \\ \frac{1}{\sqrt{2}} & \frac{1}{\sqrt{2}} & \frac{1}{\sqrt{2}} \end{bmatrix}$$

$$\vec{v}_{\alpha\beta\gamma} = T_{\alpha\beta\gamma/abc} \cdot \vec{v}_{abc}$$
$$\vec{\imath}_{\alpha\beta\gamma} = T_{\alpha\beta\gamma/abc} \cdot \vec{\imath}_{abc}$$

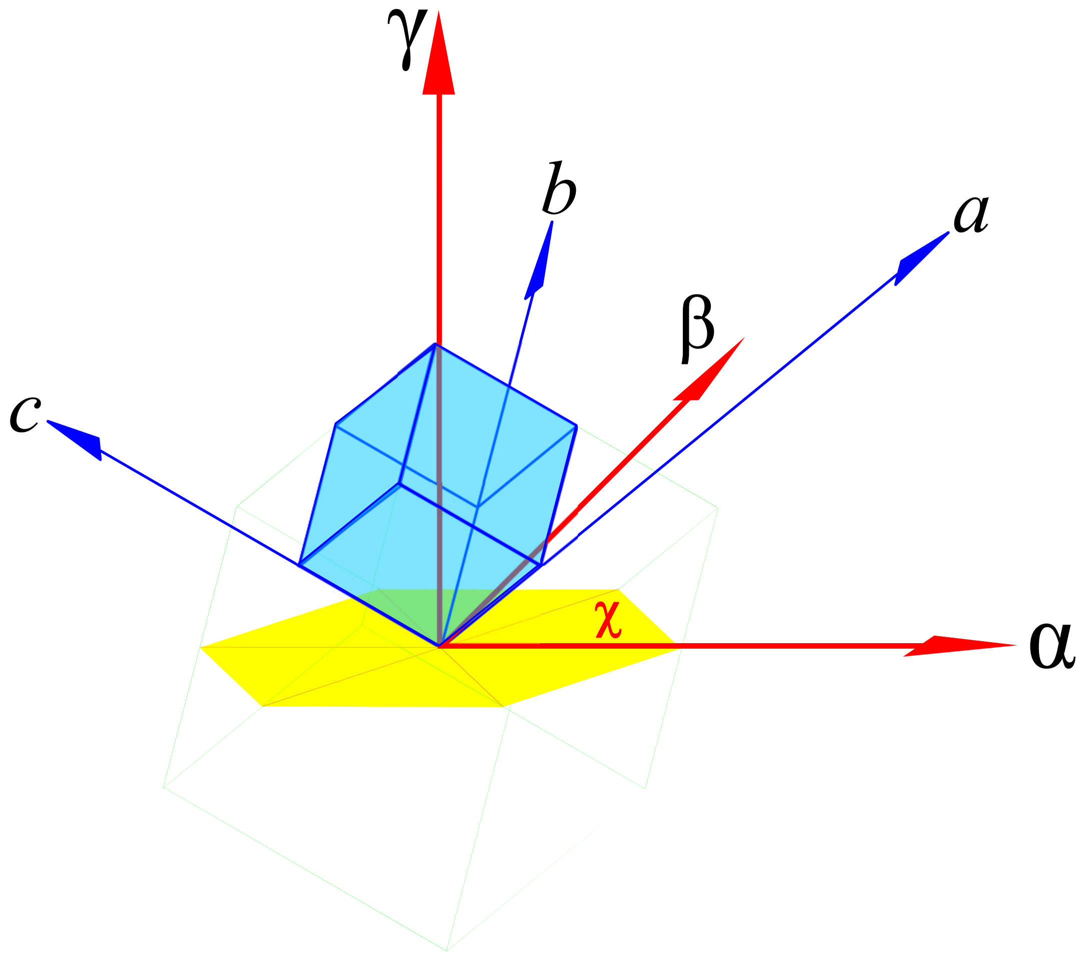

Example: State-Space Equations

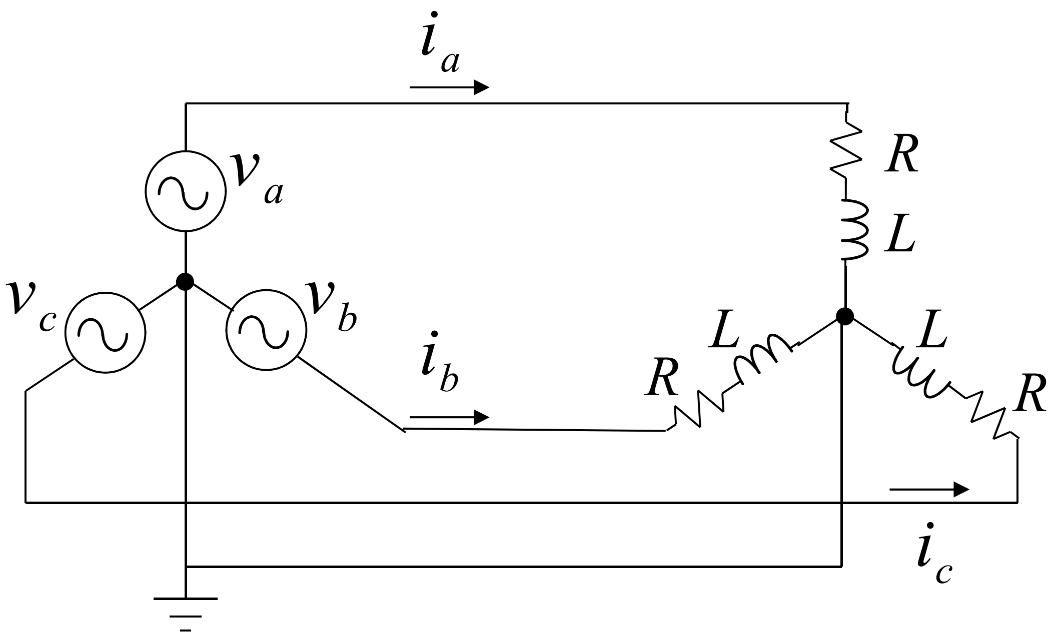

$$\vec{v} = \begin{bmatrix} v_a \\ v_b \\ v_c \end{bmatrix} \begin{bmatrix} V_m \cos(\omega t) \\ V_m \cos(\omega t - 2\pi/3) \\ V_m \cos(\omega t + 2\pi/3) \end{bmatrix}$$

$$\mathbf{R} = \begin{bmatrix} R & 0 & 0 \\ 0 & R & 0 \\ 0 & 0 & R \end{bmatrix}$$

$$\vec{v} = \mathbf{R}\vec{i} + \mathbf{L}\frac{d\vec{i}}{dt}$$

$$\vec{i} = \begin{bmatrix} i_a \\ i_b \\ i_c \end{bmatrix}$$

$$\mathbf{L} = \begin{bmatrix} L & 0 & 0 \\ 0 & L & 0 \\ 0 & 0 & L \end{bmatrix}$$

$$\frac{d\vec{i}}{dt} = -\mathbf{L}^{-1}\mathbf{R}\vec{i} + \mathbf{L}^{-1}\vec{v}$$

Example: State-Space Equations

$$\begin{bmatrix} i_a \\ i_b \\ i_c \end{bmatrix} = I_m \cdot \begin{bmatrix} \cos(\omega t - \phi) \\ \cos(\omega t - 120^\circ - \phi) \\ \cos(\omega t + 120^\circ - \phi) \end{bmatrix}$$

$$I_m = \frac{V_m}{\sqrt{R^2 + \omega^2 L^2}}$$

$$\phi = \arctan \frac{\omega L}{R}$$

$$\begin{bmatrix} i_\alpha \\ i_\beta \end{bmatrix} = \sqrt{\frac{3}{2}} \cdot I_m \cdot \begin{bmatrix} \cos(\omega t - \phi) \\ \sin(\omega t - \phi) \end{bmatrix}$$

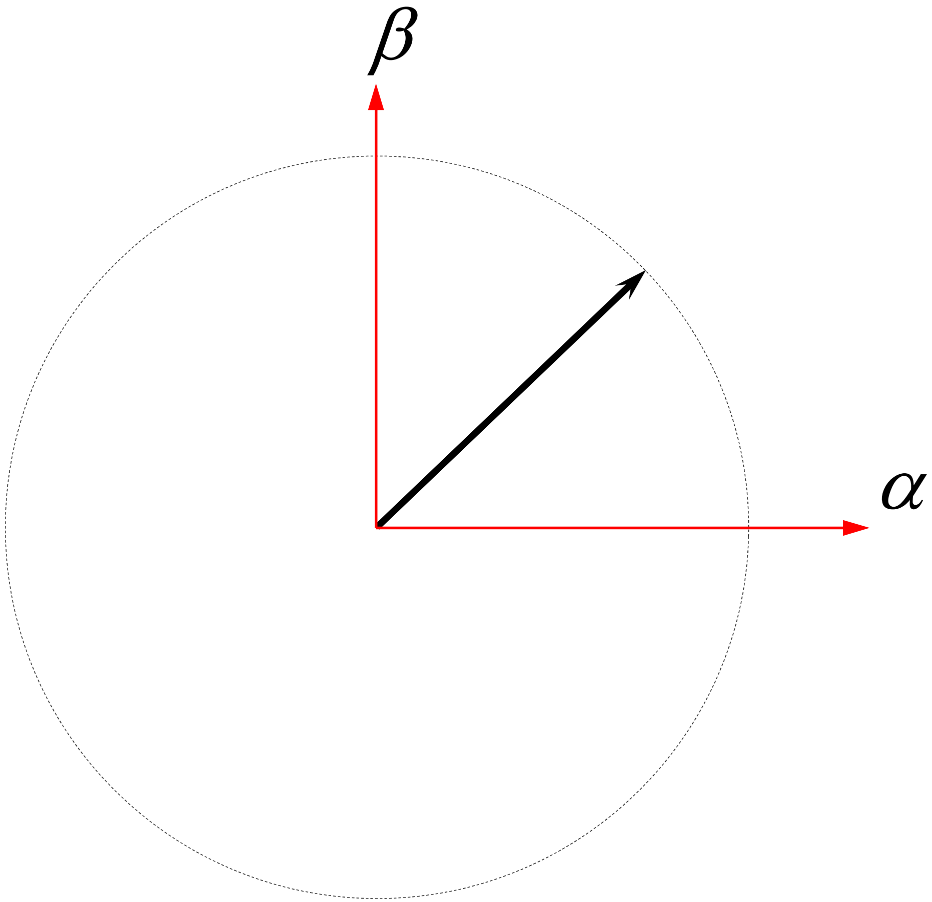

$$\begin{bmatrix} i_d \\ i_q \end{bmatrix} = \sqrt{\frac{3}{2}} \cdot I_m \cdot \begin{bmatrix} \cos\phi \\ -\sin\phi \end{bmatrix}$$

Transformation Matrix $T_{dq/\alpha\beta}$

A rotating vector in $\alpha\beta\gamma$ space can be a constant vector in a rotating space

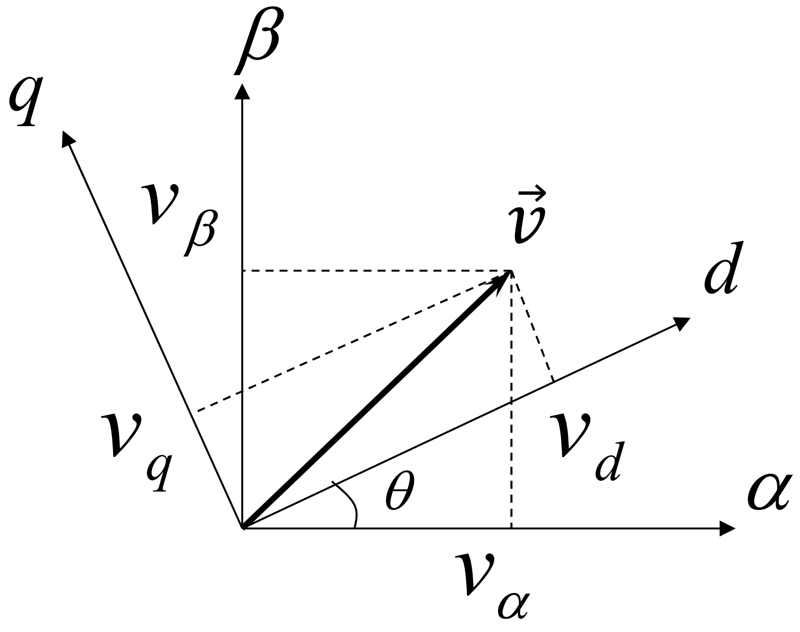

$$\begin{bmatrix} v_d \\ v_q \end{bmatrix} = \begin{bmatrix} \cos\theta & \sin\theta \\ -\sin\theta & \cos\theta \end{bmatrix} \begin{bmatrix} v_\alpha \\ v_\beta \end{bmatrix}$$

$$\theta = \int_0^t \omega(\tau)d\tau + \theta(0)$$

Where ω is the rotating speed

Transformation Matrix $T_{dq0/\alpha\beta\gamma}$

Preserve the same third axis, that is 0-axis is the same as γ-axis

$$\begin{bmatrix} v_d \\ v_q \\ v_0 \end{bmatrix} = \begin{bmatrix} \cos\theta & \sin\theta & 0 \\ -\sin\theta & \cos\theta & 0 \\ 0 & 0 & 1 \end{bmatrix} \begin{bmatrix} v_\alpha \\ v_\beta \\ v_\gamma \end{bmatrix}$$

Therefore

$$\mathrm{T}_{dq0/\alpha\beta\gamma} = \begin{bmatrix} \cos\theta & \sin\theta & 0 \\ -\sin\theta & \cos\theta & 0 \\ 0 & 0 & 1 \end{bmatrix}$$

$$\| T_{dq0/\alpha\beta\gamma} \| = 1$$

$$\boxed{T_{\alpha\beta\gamma/dq0} = T_{dq0/\alpha\beta\gamma}^{-1} = T_{dq0/\alpha\beta\gamma}^{T}}$$

Example: Stationary and Rotating Reference Frame

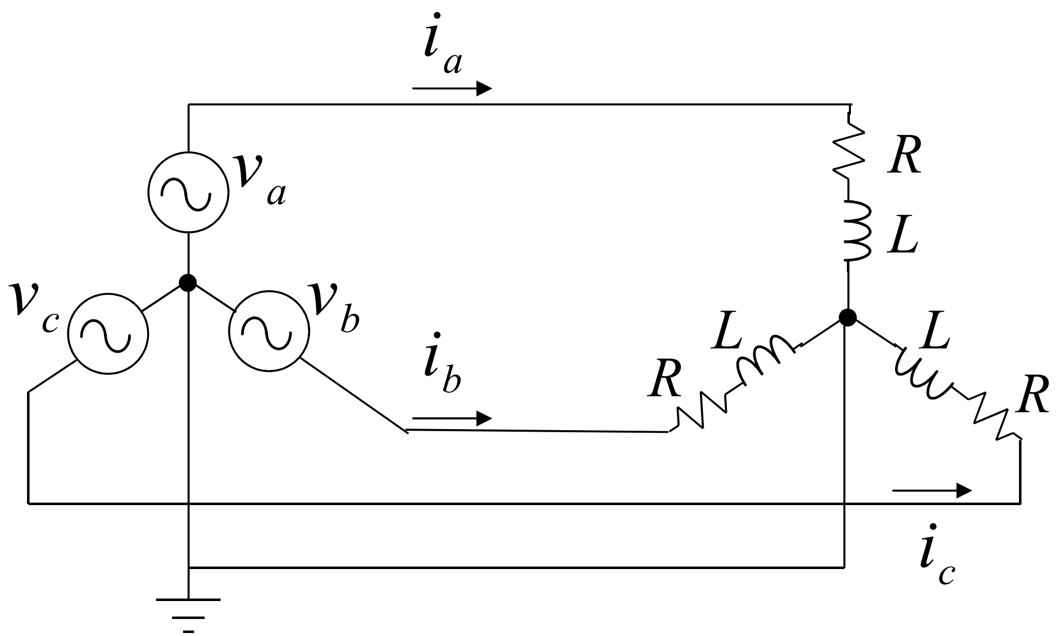

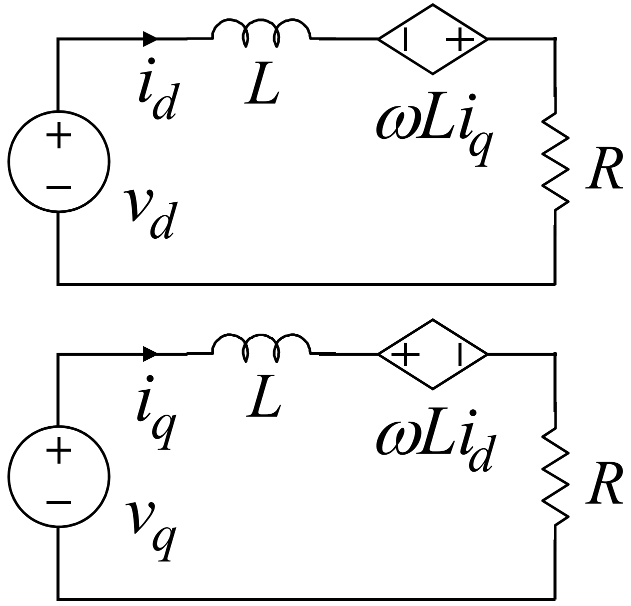

$$\vec{v} = \mathbf{R}\vec{i} + \mathbf{L}\frac{d\vec{i}}{dt}$$

$$\lim_{t\to\infty}\left(\frac{d\vec{i}}{dt}\right) \neq 0$$

$$\vec{v} = \mathbf{R}\vec{i} + \begin{bmatrix} 0 & -\omega L \\ \omega L & 0 \end{bmatrix}\begin{bmatrix} i_d \\ i_q \end{bmatrix} + \frac{d\vec{i}}{dt}$$

$$\lim_{t\to\infty}\left(\frac{d\vec{i}}{dt}\right) = 0$$

Outline

Basic Topologies

Boost Rectifier

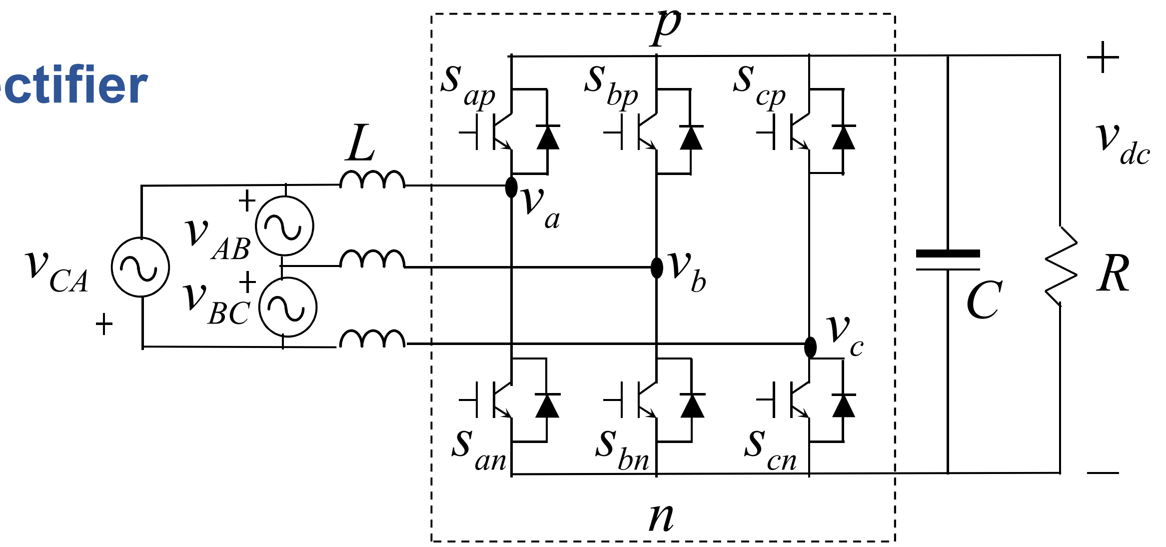

$$V_{dc} > V_m$$

where V_m is the peak value of the line-to-line input voltage

Voltage Source Inverter (VSI)

$$V_{dc} > V_m$$

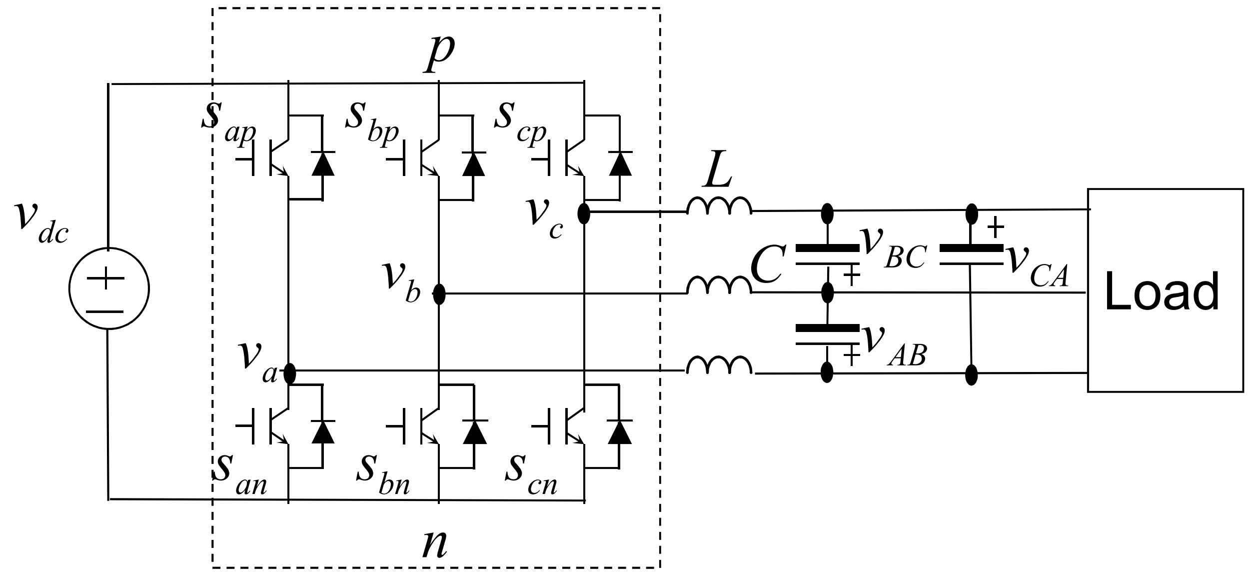

Basic Topologies

Buck Rectifier

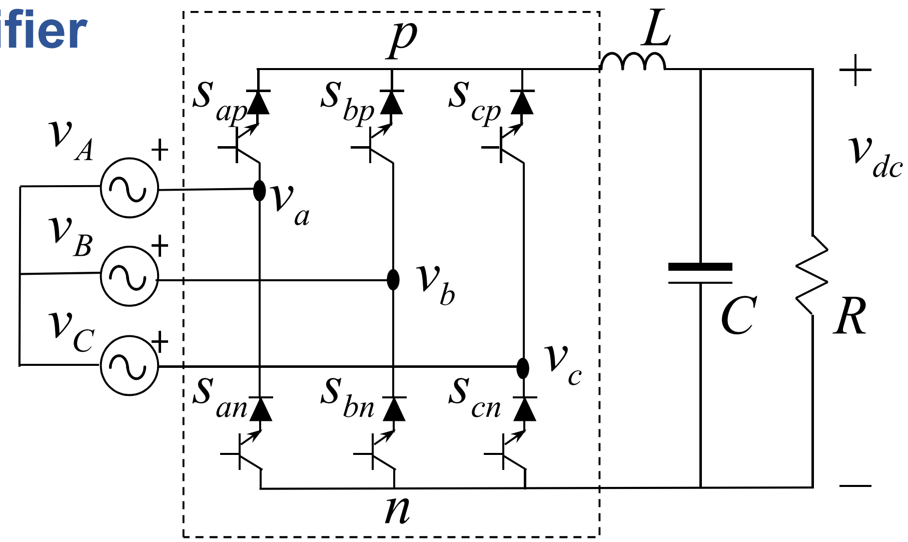

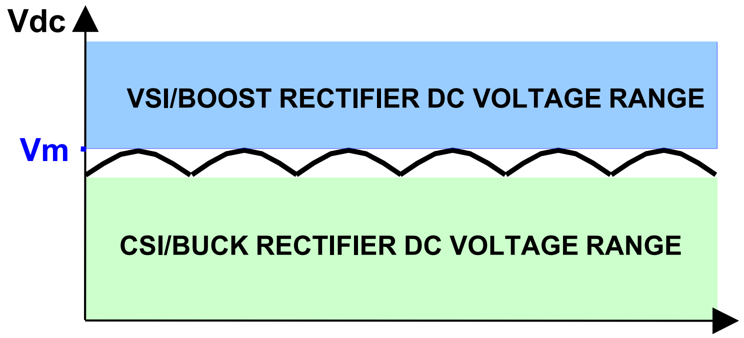

$$V_{dc} < \frac{\sqrt{3}}{2} V_m$$

Current Source Inverter (CSI)

$$V_{dc} < \frac{\sqrt{3}}{2} V_m$$

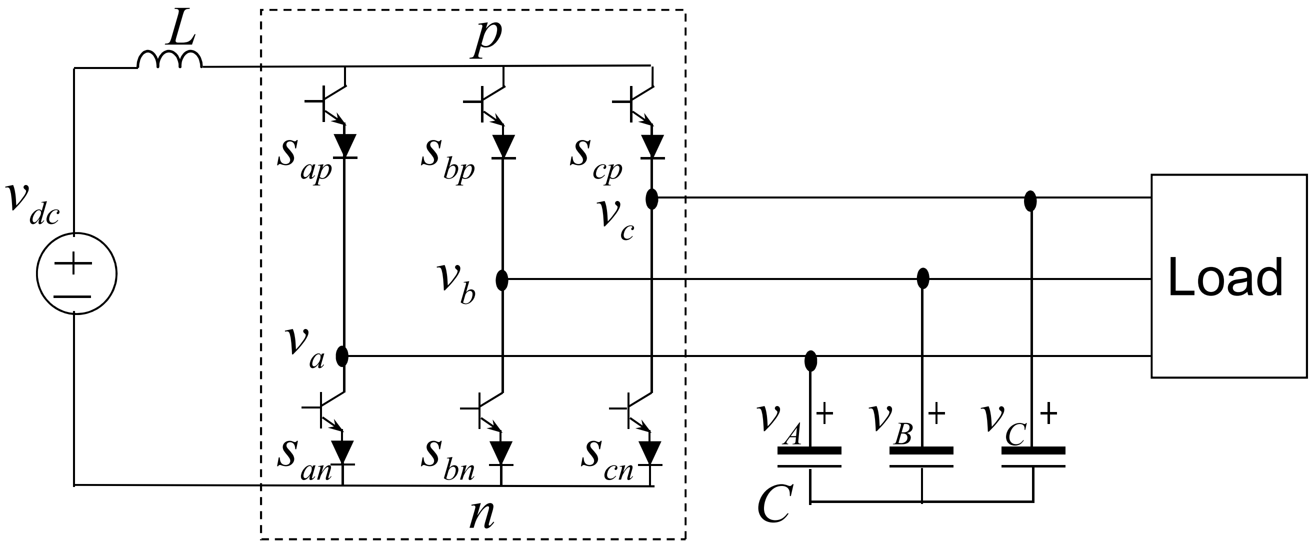

Method of Modeling Switching Networks

Current bi-directional two-quadrant switch

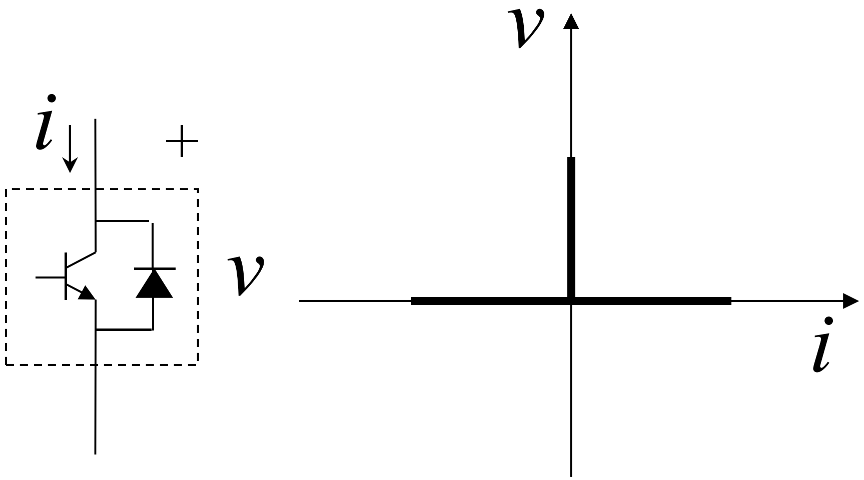

Switching Function

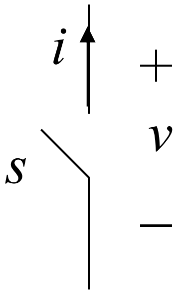

$$s = \begin{cases} 1, \; v = 0, \text{ if switch } s \text{ is closed} \\ 0, \; i = 0, \text{ if switch } s \text{ is open} \end{cases}$$

Switching Constraints

- Voltage source or capacitor cannot be shorted
- Current source or inductor cannot be open

Voltage-Unidirectional Three-Phase Switching Network

Three-Switch (Single-Pole-Double-Throw)

- Boost Rectifier
- Voltage Source Inverter

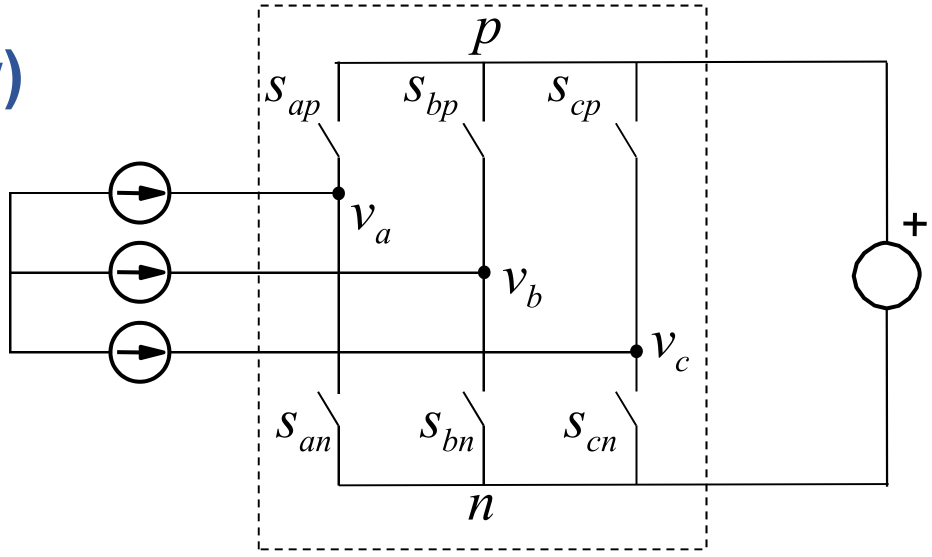

Allowed switching combinations:

$$s_{ip} + s_{in} = 1; \quad i \in \{a, b, c\}$$

Defining:

- Voltage-unidirectional single-pole-double-throw switch
- Switching functions

$$s_i = s_{ip} = 1 - s_{in}; \quad i \in \{a, b, c\}$$

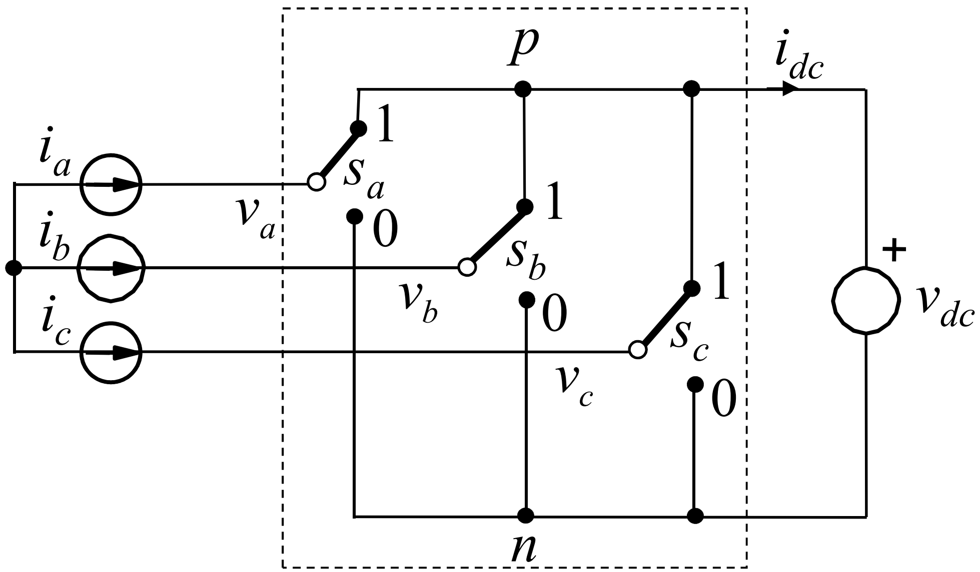

Current-Unidirectional Three-Phase Switching Network

Topology

- Three-phase terminals are voltage controlled
- DC port is current controlled
- Six current-unidirectional, voltage-bi-directional, switches

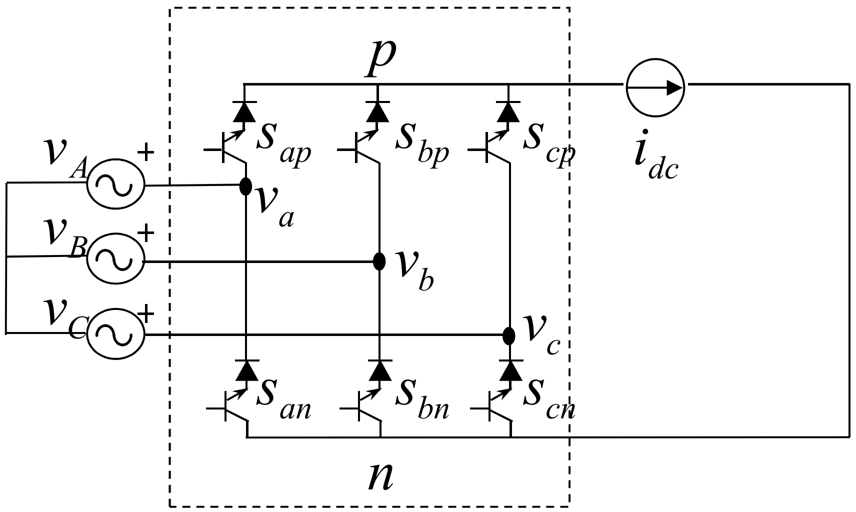

Allowed switching combinations:

$$s_{ak} + s_{bk} + s_{ck} = 1; \qquad k \in \{p, n\}$$

- Two single-pole-triple-throw (SPTT) current-unidirectional switches

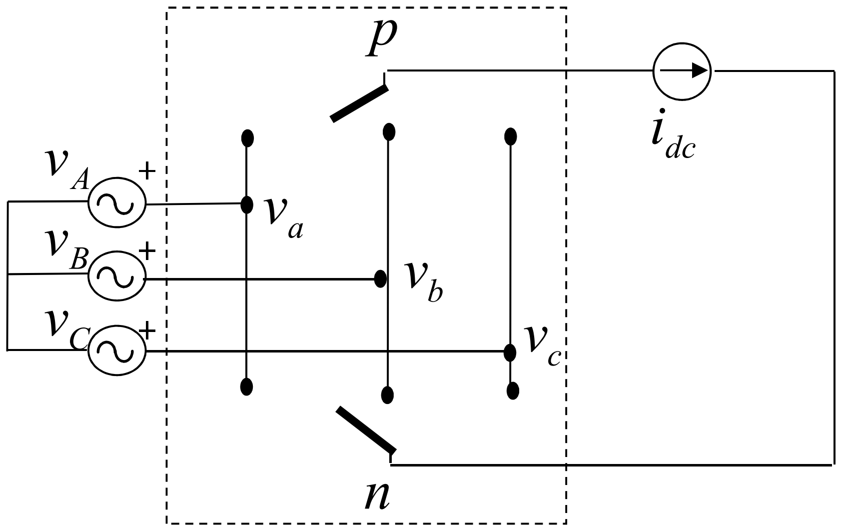

Switching Model—Line Variables
Boost Rectifier/Voltage Source Inverter

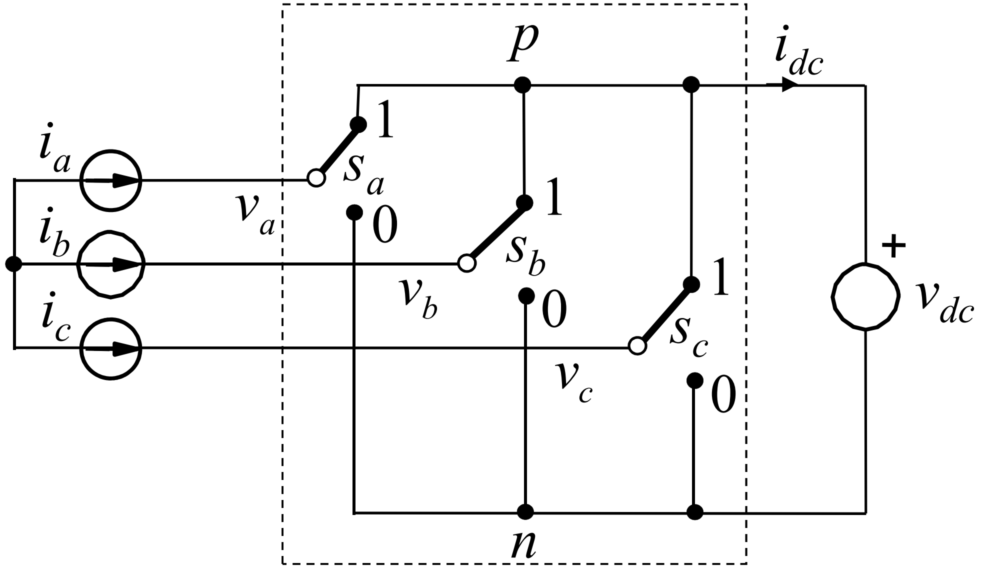

Instantaneous voltage equation

$$\begin{bmatrix} v_{ab} \\ v_{bc} \\ v_{ca} \end{bmatrix} = \begin{bmatrix} S_a - S_b \\ S_b - S_c \\ S_c - S_a \end{bmatrix} v_{dc} = \begin{bmatrix} S_{ab} \\ S_{bc} \\ S_{ca} \end{bmatrix} v_{dc}$$

Instantaneous current equation

$$i_{dc} = [S_a \quad S_b \quad S_c] \cdot \begin{bmatrix} i_a \\ i_b \\ i_c \end{bmatrix}$$

Note that: $S_{ab} = S_a - S_b;\ \ldots \qquad v_{ab} = v_a - v_b;\ \ldots$

Relationship between Line-to-Line Current and Phase Current

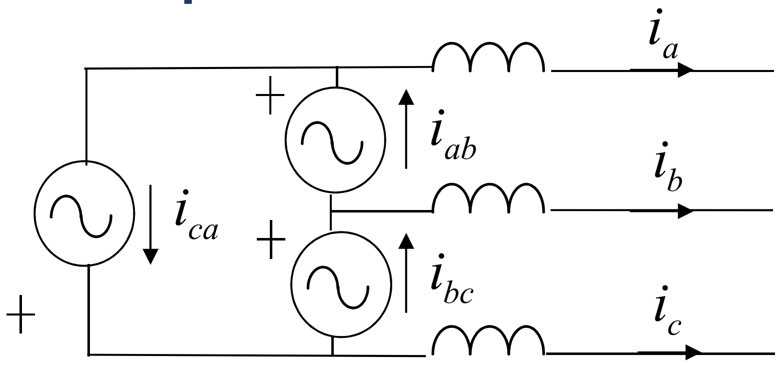

$$i_a = i_{ab} - i_{ca}$$
$$i_b = i_{bc} - i_{ab}$$
$$i_c = i_{ca} - i_{bc}$$

$$i_a - i_b = i_{ab} - i_{ca} - (i_{bc} - i_{ab}) = 2i_{ab} - (i_{ca} + i_{bc}) = 3i_{ab}$$

Assuming that $i_{ab} + i_{bc} + i_{ca} = 0$

$$i_{ab} = \frac{1}{3}(i_a - i_b)$$ Similarly $$i_{bc} = \frac{1}{3}(i_b - i_c) \qquad i_{ca} = \frac{1}{3}(i_c - i_a)$$

$$i_{dc} = S_a i_a + S_b i_b + S_c i_c = S_a(i_{ab} - i_{ca}) + S_b(i_{bc} - i_{ab}) + S_c(i_{ca} - i_{bc})$$

$$i_{dc} = i_{ab}(S_a - S_b) + i_{bc}(S_b - S_c) + i_{ca}(S_c - S_a) = [S_{ab} \quad S_{bc} \quad S_{ca}]\begin{bmatrix} i_{ab} \\ i_{bc} \\ i_{ca} \end{bmatrix}$$

Switching Model – Line Variables
Boost Rectifier / Voltage Source Inverter

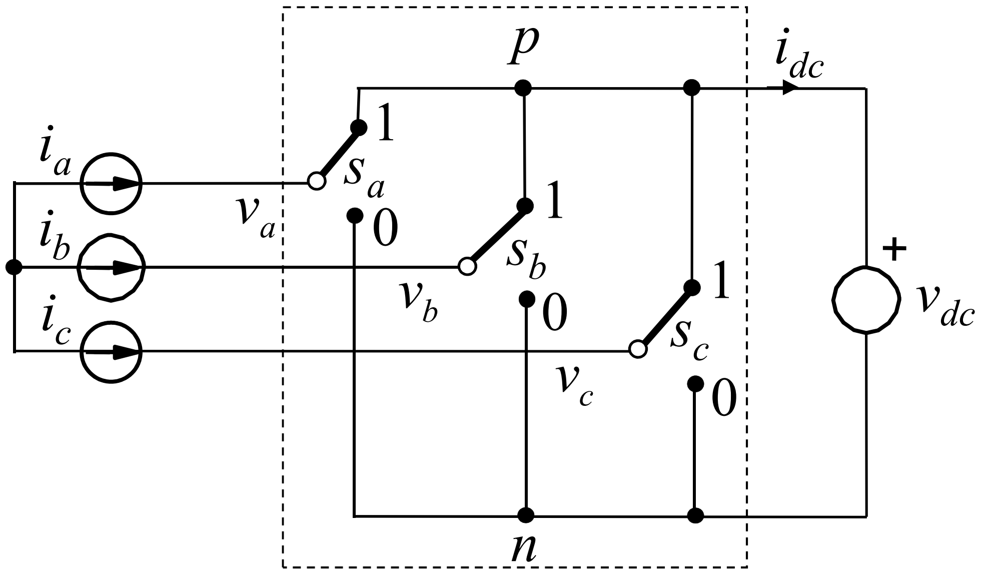

$$v_{l-l} = S_{l-l} \cdot v_{dc}$$

$$i_{dc} = S_{l-l}^{T} \cdot i_{l-l}$$

Where:

$$v_{l-l} = \begin{bmatrix} v_{ab} \\ v_{bc} \\ v_{ca} \end{bmatrix} = \begin{bmatrix} v_{an} - v_{bn} \\ v_{bn} - v_{cn} \\ v_{cn} - v_{an} \end{bmatrix} \qquad S_{l-l} = \begin{bmatrix} S_{ab} \\ S_{bc} \\ S_{ca} \end{bmatrix} = \begin{bmatrix} S_a - S_b \\ S_b - S_c \\ S_c - S_a \end{bmatrix} \qquad i_{l-l} = \begin{bmatrix} i_{ab} \\ i_{bc} \\ i_{ca} \end{bmatrix}$$

Switching Model—Phase Variables

Boost Rectifier/Voltage Source Inverter

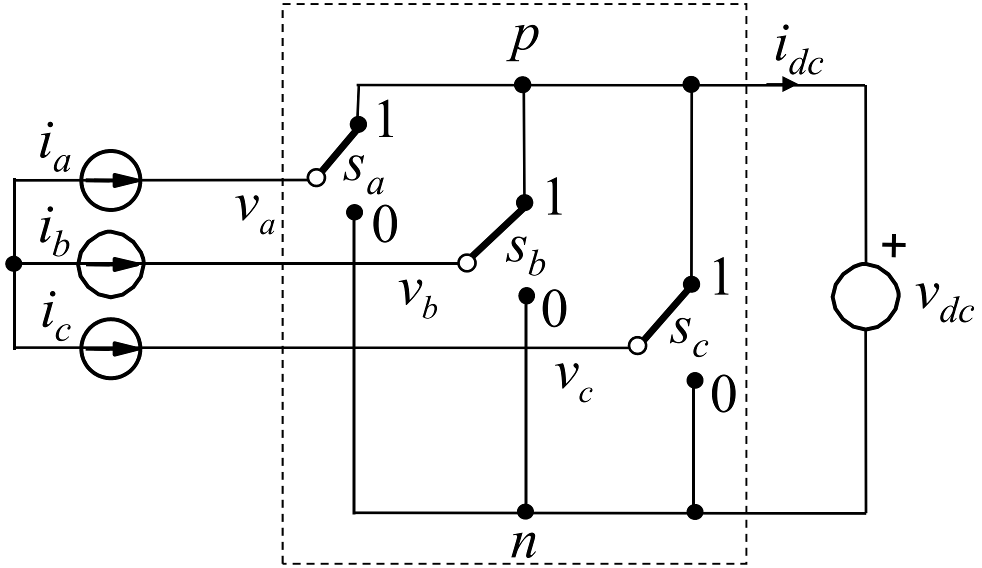

$$v_{abc} = S_{abc} \cdot v_{dc}$$

$$i_{dc} = S_{abc}^T \cdot i_{abc}$$

Where:

$$v_{abc} = \begin{bmatrix} v_a \\ v_b \\ v_c \end{bmatrix} = \begin{bmatrix} v_{an} \\ v_{bn} \\ v_{cn} \end{bmatrix} \qquad S_{abc} = \begin{bmatrix} S_a \\ S_b \\ S_c \end{bmatrix} \qquad i_{abc} = \begin{bmatrix} i_a \\ i_b \\ i_c \end{bmatrix}$$

Outline

Average Circuit Modeling

- Applying an average operator to the switching model:

$$\boxed{\bar{x}(t) = \frac{1}{T}\int_{t-T}^{t} x(\tau)d\tau}$$

- Switch duty cycle $$d_{ap} = \bar{s}_{ap}(t) = \frac{1}{T}\int_{t-T}^{t} s_{ap}(\tau)d\tau$$
- Phase-leg duty cycle $$d_a = d_{ap} = 1 - d_{an}$$
- Line-to-line duty cycle $$d_{ab} = \bar{s}_{ab}(t) = \frac{1}{T}\int_{t-T}^{t} s_{ab}(\tau)d\tau = d_a - d_b$$
- KVL and KCL $$\Sigma\bar{v} = 0 \qquad \Sigma\bar{i} = 0$$
- Linear components $$\bar{v}_R = R\bar{i}_R \qquad \bar{v}_L = L\frac{d\bar{i}_L}{dt} \qquad \bar{i}_C = C\frac{d\bar{v}_C}{dt}$$

Averaging of Quadratic Terms

$$v_{ab} = s_{ab} \cdot v_{dc}$$

$$\overline{v}_{ab} = \frac{1}{T} \int_{t-T}^{t} s_{ab}(\tau) \cdot v_{dc}(\tau) d\tau \approx \overline{s}_{ab} \cdot \overline{v}_{dc} = d_{ab} \cdot \overline{v}_{dc}$$

If maximum-frequency components of $v_{dc}(t)$ are $\ll \frac{1}{2T}$

$$\overline{\vec{S}_{l-l} \cdot v_{dc}} \approx \overline{\vec{S}_{l-l}} \cdot \overline{v_{dc}} = \vec{d}_{l-l} \cdot \overline{v_{dc}}$$

$$\overline{\vec{S}_{l-l}^{T} \cdot \vec{i}_{l-l}} \approx \overline{\vec{S}_{l-l}^{T}} \cdot \overline{\vec{i}_{l-l}} = \vec{d}_{l-l}^{T} \cdot \overline{\vec{i}_{l-l}}$$

Average Model of Three-Phase Boost Rectifier

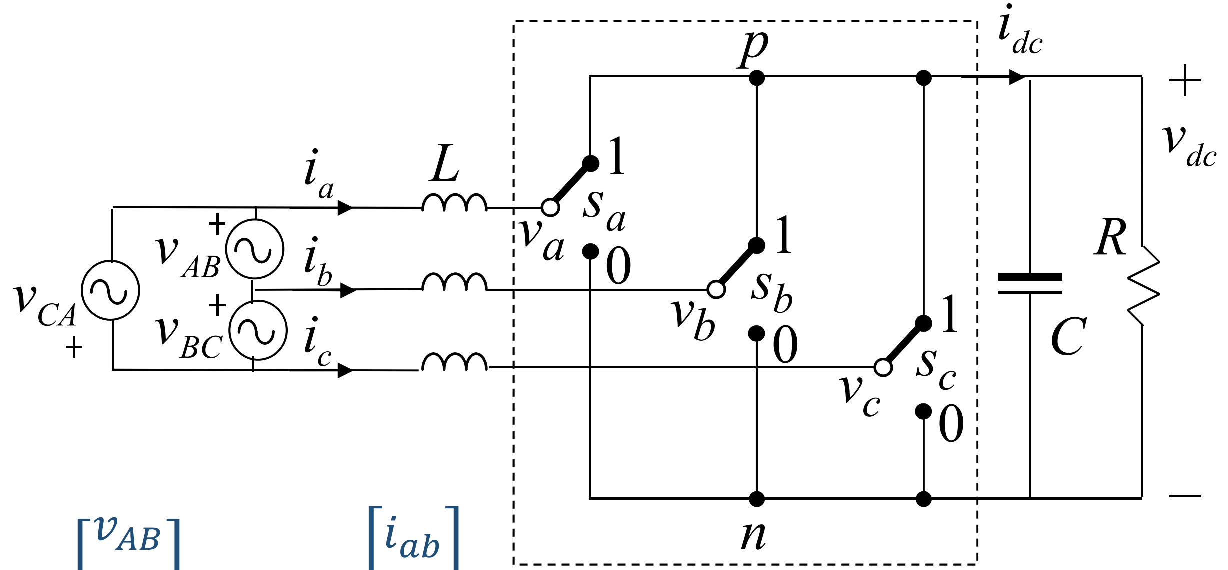

$$v_{l-l} = \begin{bmatrix} v_{AB} \\ v_{BC} \\ v_{CA} \end{bmatrix} \qquad i_{l-l} = \begin{bmatrix} i_{ab} \\ i_{bc} \\ i_{ca} \end{bmatrix}$$

Averaging

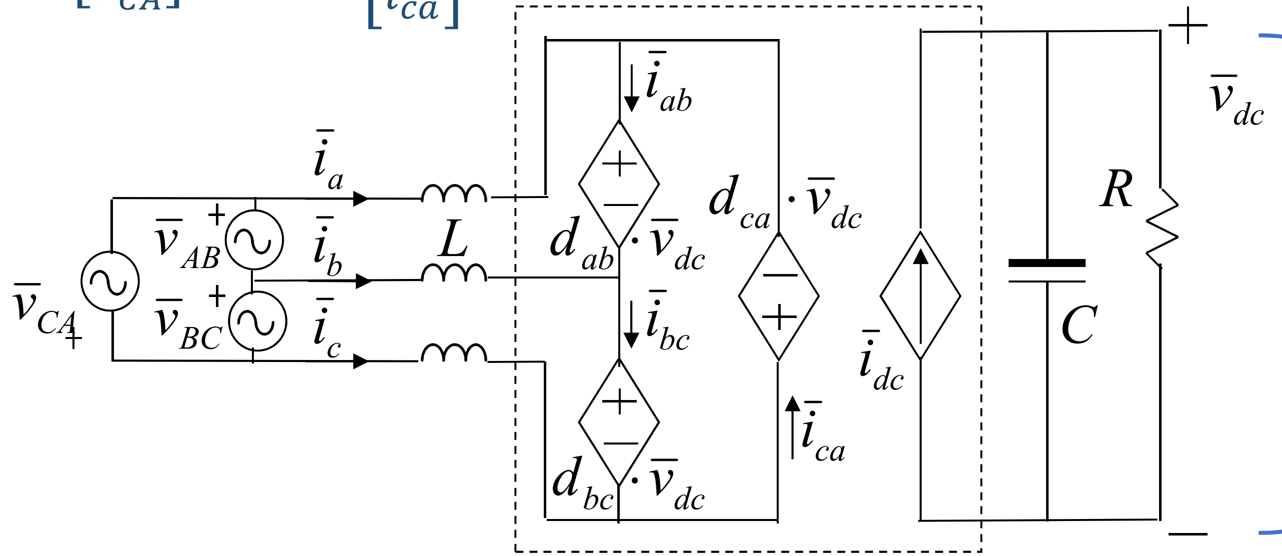

Switching Model

$$\frac{d\vec{i}_{l-l}}{dt} = \frac{1}{3L}\vec{v}_{l-l} - \frac{1}{3L}\vec{S}_{l-l} \cdot v_{dc}$$

$$\frac{dv_{dc}}{dt} = \frac{1}{C}\vec{S}^{T}_{l-l} \cdot \vec{i}_{l-l} - \frac{v_{dc}}{RC}$$

$$S_{l-l} = \begin{bmatrix} S_{ab} \\ S_{bc} \\ S_{ca} \end{bmatrix} = \begin{bmatrix} S_a - S_b \\ S_b - S_c \\ S_c - S_a \end{bmatrix} \qquad \bar{d}_{l-l} = \begin{bmatrix} d_{ab} \\ d_{bc} \\ d_{ca} \end{bmatrix}$$

Average Model

$$\frac{d\bar{i}_{l-l}}{dt} = \frac{1}{3L}\bar{v}_{l-l} - \frac{1}{3L}\bar{d}_{l-l} \cdot \bar{v}_{dc}$$

$$\frac{dv_{dc}}{dt} = \frac{1}{C}\bar{d}^{T}_{l-l} \cdot \bar{i}_{l-l} - \frac{\bar{v}_{dc}}{RC}$$

Another Equivalent Circuit of the Boost Rectifier

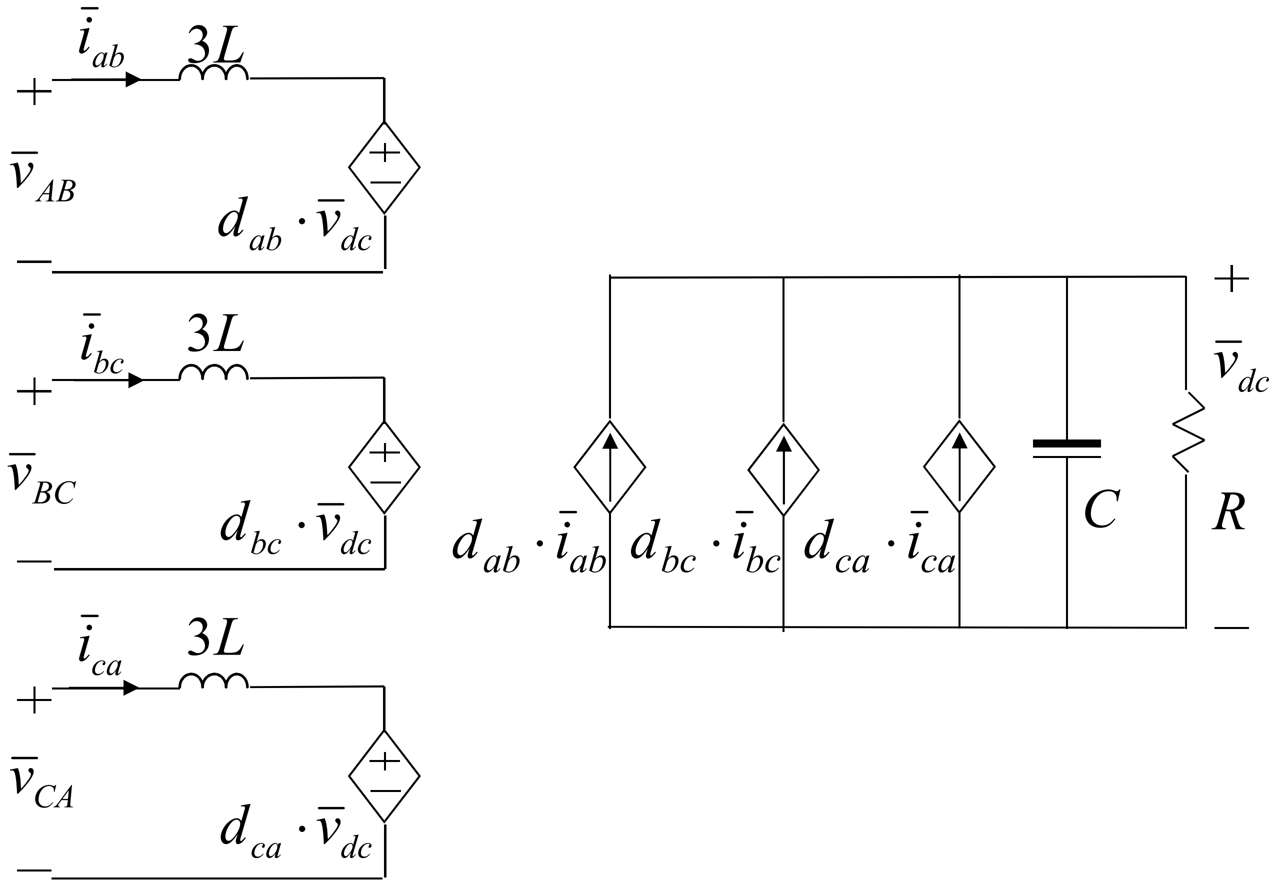

- Third order system due to degeneration

State-Space Equations in abc and dq0 Frames—Boost Rectifier

$$\frac{d}{dt}\begin{bmatrix}\bar{i}_{ab}\\ \bar{i}_{bc}\\ \bar{i}_{ca}\end{bmatrix} = \frac{1}{3L}\begin{bmatrix}\bar{v}_{AB}\\ \bar{v}_{BC}\\ \bar{v}_{CA}\end{bmatrix} - \frac{1}{3L}\begin{bmatrix}d_{ab}\\ d_{bc}\\ d_{ca}\end{bmatrix}\cdot \bar{v}_{dc}$$

$$\frac{d\bar{v}_{dc}}{dt} = \frac{1}{C}\begin{bmatrix}d_{ab} & d_{bc} & d_{ca}\end{bmatrix}\cdot\begin{bmatrix}\bar{i}_{ab}\\ \bar{i}_{bc}\\ \bar{i}_{ca}\end{bmatrix} - \frac{\bar{v}_{dc}}{RC}$$

abc coordinates

$$\frac{d}{dt}\begin{bmatrix}\bar{i}_{d}\\ \bar{i}_{q}\\ \bar{i}_{0}\end{bmatrix} = \frac{1}{3L}\begin{bmatrix}\bar{v}_{d}\\ \bar{v}_{q}\\ \bar{v}_{0}\end{bmatrix} - \begin{bmatrix}0 & -\omega & 0\\ \omega & 0 & 0\\ 0 & 0 & 0\end{bmatrix}\begin{bmatrix}\bar{i}_{d}\\ \bar{i}_{q}\\ \bar{i}_{0}\end{bmatrix} - \frac{1}{3L}\begin{bmatrix}d_{d}\\ d_{q}\\ d_{0}\end{bmatrix}\cdot \bar{v}_{dc}$$

$$\frac{d\bar{v}_{dc}}{dt} = \frac{1}{C}\begin{bmatrix}d_{d} & d_{q} & d_{0}\end{bmatrix}\cdot\begin{bmatrix}\bar{i}_{d}\\ \bar{i}_{q}\\ \bar{i}_{0}\end{bmatrix} - \frac{\bar{v}_{dc}}{RC}$$

dq0 coordinates

Equivalent Circuit in dq0 Frame—Boost Rectifier

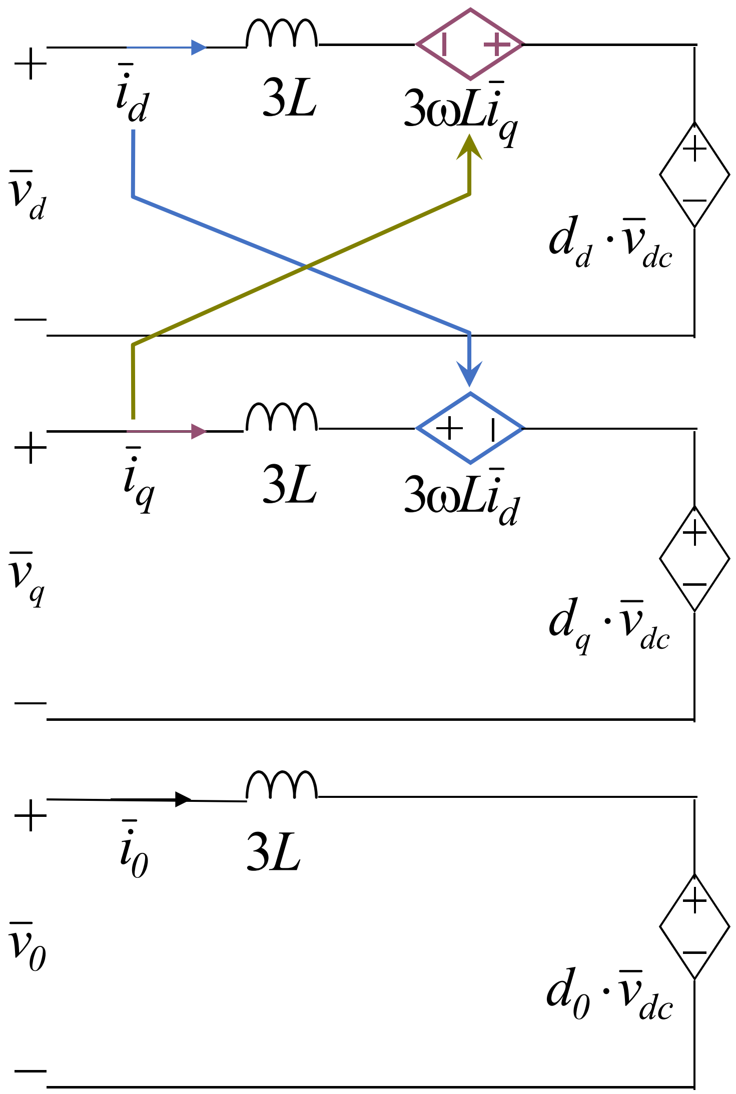

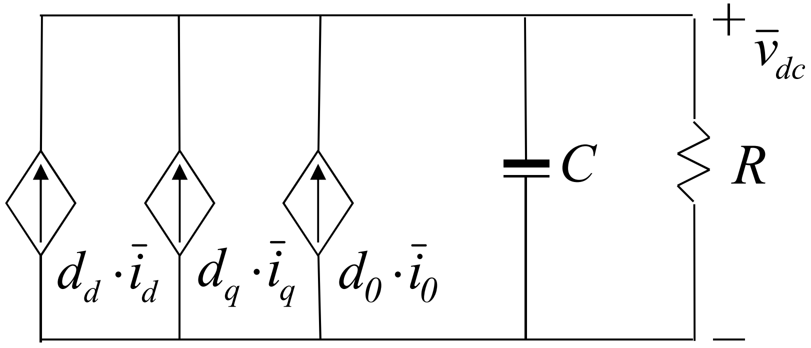

- The cross-coupling terms $3\omega L\bar{\imath}_q$ and $3\omega L\bar{\imath}_d$ in dq0 coordinates account for the voltage drops across the inductances, at line frequency, in abc coordinates ($j3\omega L\bar{\imath}_{ab}$, $j3\omega L\bar{\imath}_{bc}$, and $j3\omega L\bar{\imath}_{ca}$)

0-Channel

Since

$$\begin{cases} \bar{v}_{AB} + \bar{v}_{BC} + \bar{v}_{CA} \equiv 0 \\ \bar{\imath}_{ab} + \bar{\imath}_{bc} + \bar{\imath}_{ca} \equiv 0 \\ d_{ab} + d_{bc} + d_{ca} \equiv 0 \end{cases} \Rightarrow \begin{matrix} \bar{v}_0 \equiv 0 \\ \bar{\imath}_0 \equiv 0 \\ d_0 \equiv 0 \end{matrix}$$

- 0-channel can be omitted

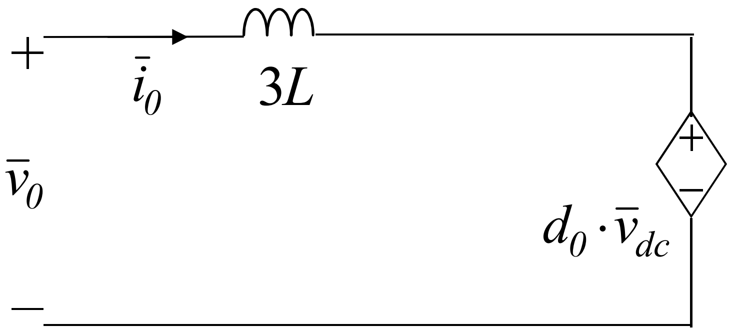

Equivalent Circuit in dq0 Frame—Boost Rectifier

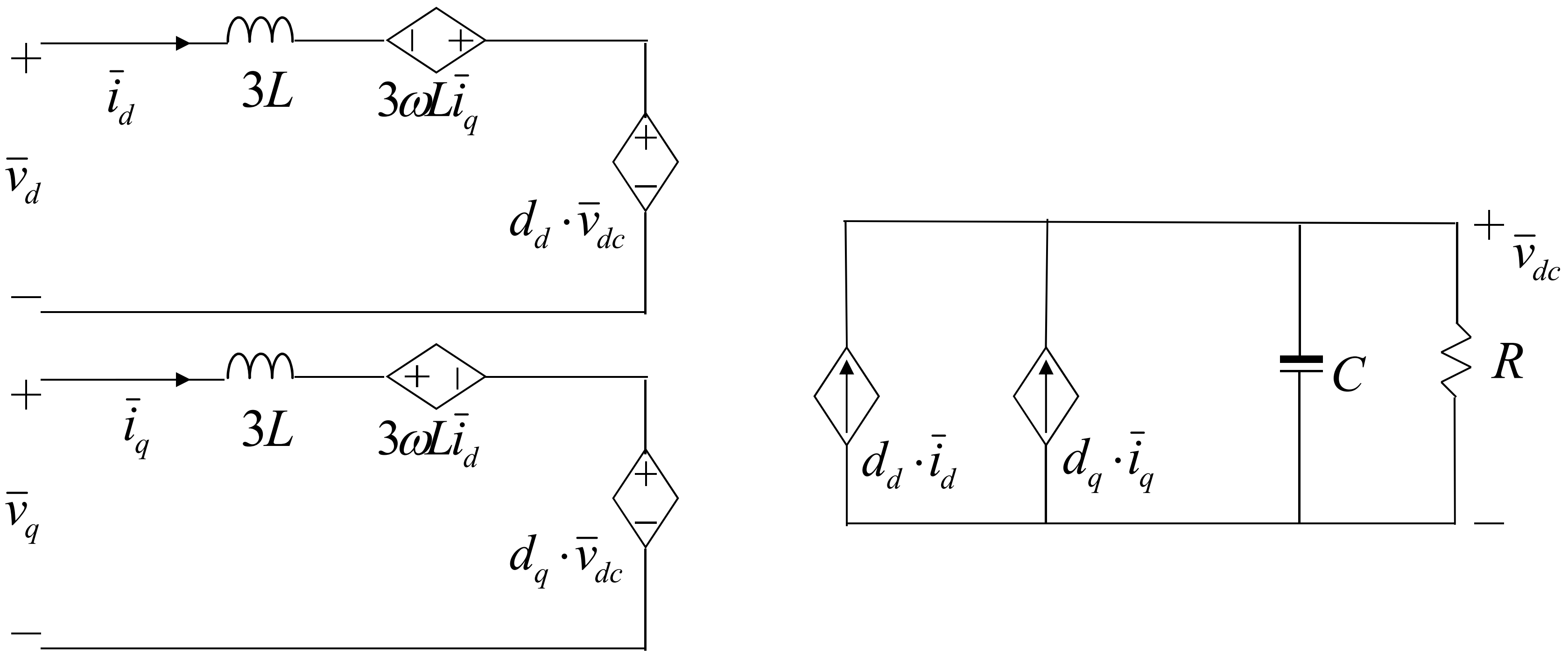

$$\left.\begin{aligned}
\frac{d}{dt}\begin{bmatrix}\bar{\imath}_d\\ \bar{\imath}_q\end{bmatrix} &= \frac{1}{3L}\begin{bmatrix}\bar{v}_d\\ \bar{v}_q\end{bmatrix} - \begin{bmatrix}0 & -\omega\\ \omega & 0\end{bmatrix}\begin{bmatrix}\bar{\imath}_d\\ \bar{\imath}_q\end{bmatrix} - \frac{1}{3L}\begin{bmatrix}d_d\\ d_q\end{bmatrix}\cdot \bar{v}_{dc}\\
\frac{d\bar{v}_{dc}}{dt} &= \frac{1}{C}\begin{bmatrix}d_d & d_q\end{bmatrix}\cdot\begin{bmatrix}\bar{\imath}_d\\ \bar{\imath}_q\end{bmatrix} - \frac{\bar{v}_{dc}}{RC}
\end{aligned}\right\}\ \text{dq coordinates}$$

Equivalent Circuits in dq0 Frame

Boost Rectifier

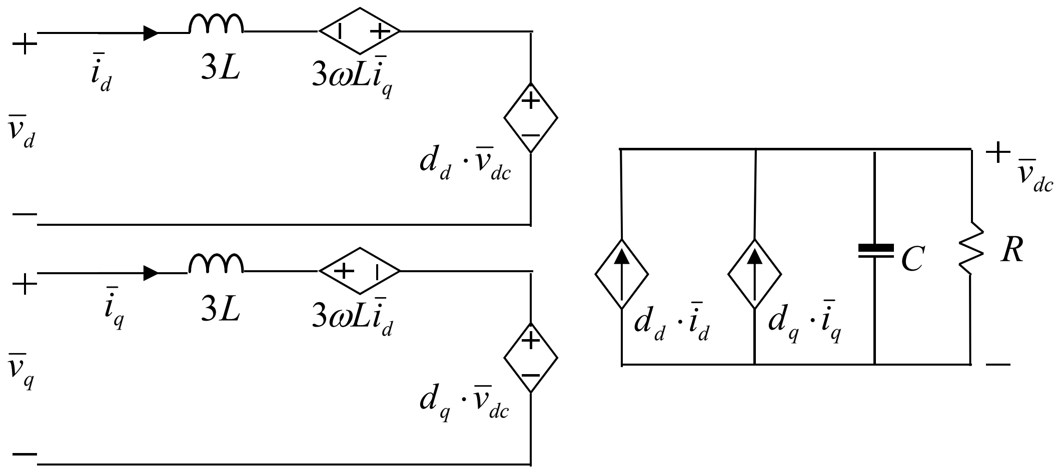

Buck Rectifier

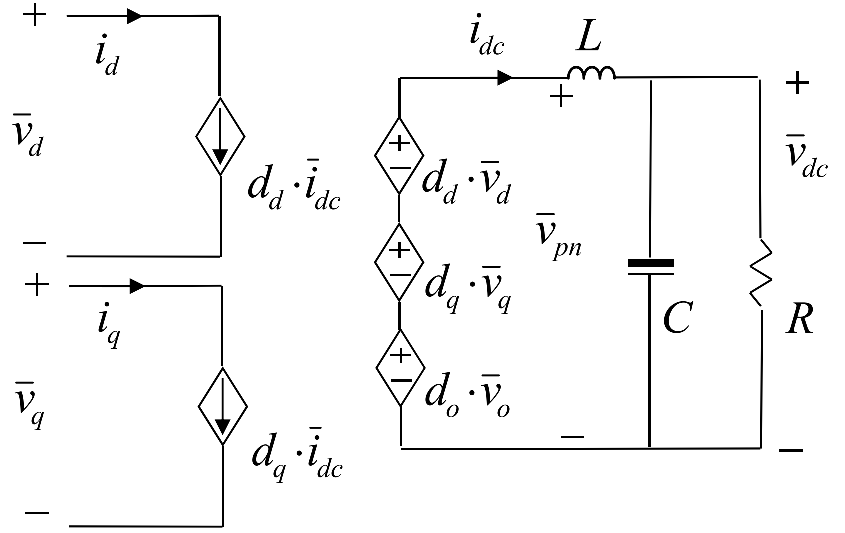

VSI

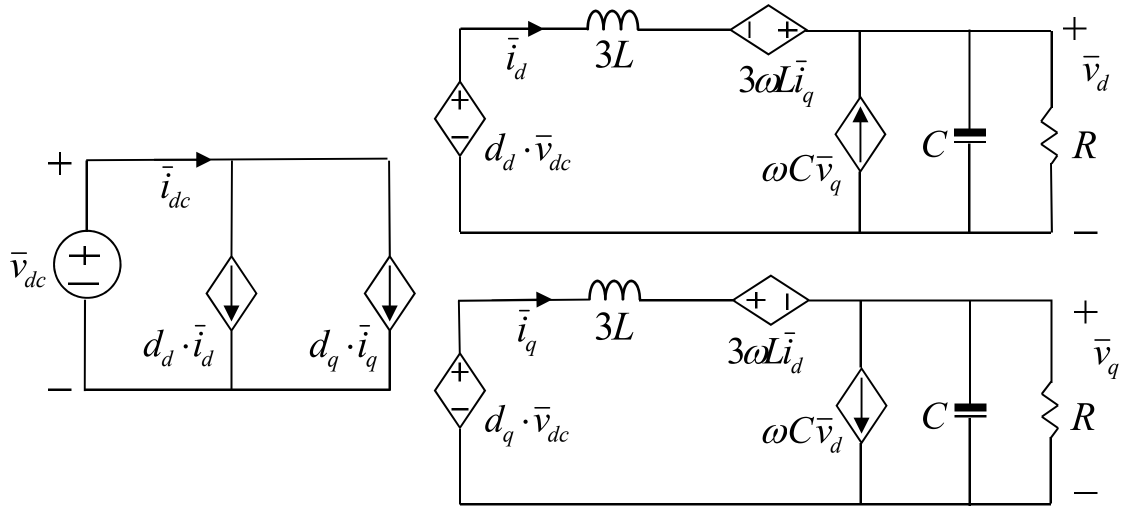

CSI

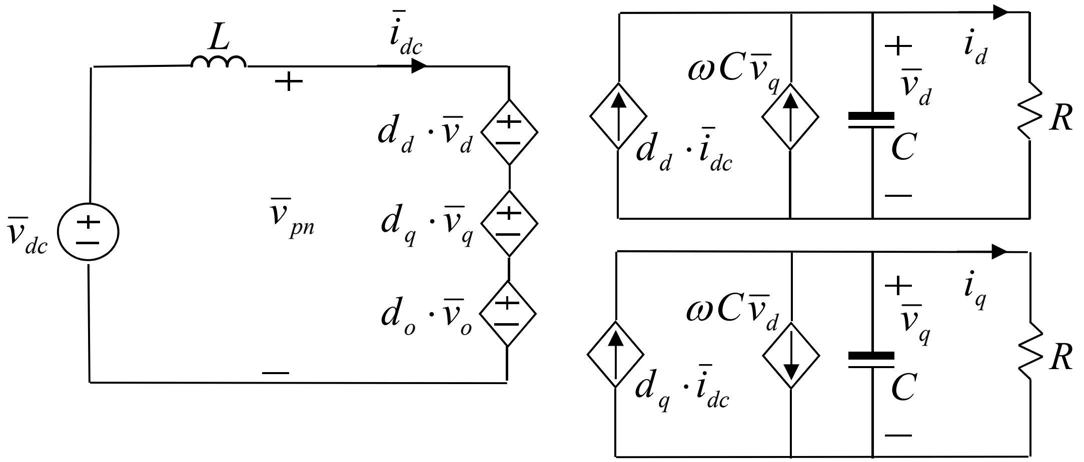

Outline

Linearization

Autonomous dynamic system: $\dfrac{d\vec{x}}{dt} = \vec{f}(\vec{x}, \vec{u})$

If $\vec{f}$ is analytic it can be expressed as Taylor series:

$$\vec{f}(\vec{x}, \vec{u}) = \vec{f}(\vec{x}_0, \vec{u}_0) + \frac{\partial \vec{f}(\vec{x}_0, \vec{u}_0)}{\partial \vec{x}} \cdot (\vec{x} - \vec{x}_0) + \frac{\partial \vec{f}(\vec{x}_0, \vec{u}_0)}{\partial \vec{u}} \cdot (\vec{u} - \vec{u}_0) + \frac{1}{2!} \cdot$$
$$\left[\frac{\partial^2 \vec{f}(\vec{x}_0, \vec{u}_0)}{\partial \vec{x}^2} \cdot (\vec{x} - \vec{x}_0)^2 + 2\frac{\partial^2 \vec{f}(\vec{x}_0, \vec{u}_0)}{\partial \vec{x} \partial \vec{u}} \cdot (\vec{x} - \vec{x}_0)(\vec{u} - \vec{u}_0) + \frac{\partial^2 \vec{f}(\vec{x}_0, \vec{u}_0)}{\partial \vec{u}^2} \cdot (\vec{u} - \vec{u}_0)^2\right] + K$$

Retaining the first 3 terms results in linear approximation of $\vec{f}$:

$$\vec{f}(\vec{x}, \vec{u}) = \vec{f}(\vec{x}_0, \vec{u}_0) + \frac{\partial \vec{f}(\vec{x}_0, \vec{u}_0)}{\partial \vec{x}} \cdot (\vec{x} - \vec{x}_0) + \frac{\partial \vec{f}(\vec{x}_0, \vec{u}_0)}{\partial \vec{u}} \cdot (\vec{u} - \vec{u}_0)$$

But the dynamic system is **NOT** in canonical form:

$$\underbrace{\frac{d\vec{x}}{dt}}_{\dot{\vec{x}} =} \cong \underbrace{\frac{\partial \vec{f}(\vec{x}_0, \vec{u}_0)}{\partial \vec{x}}}_{\mathbf{A}} \cdot \underbrace{\vec{x}}_{\vec{x}} + \underbrace{\frac{\partial \vec{f}(\vec{x}_0, \vec{u}_0)}{\partial \vec{u}}}_{\mathbf{B}} \cdot \underbrace{\vec{u}}_{\vec{u}} + \underbrace{\vec{f}(\vec{x}_0, \vec{u}_0) - \frac{\partial \vec{f}(\vec{x}_0, \vec{u}_0)}{\partial \vec{x}} \cdot \vec{x}_0 - \frac{\partial \vec{f}(\vec{x}_0, \vec{u}_0)}{\partial \vec{u}} \cdot \vec{u}_0}_{+\vec{g} \neq 0}$$

Linearization

$$\frac{d\vec{x}}{dt} = \vec{f}(\vec{x},\vec{u}) \cong \vec{f}(\vec{x}_0,\vec{u}_0) + \frac{\partial \vec{f}(\vec{x}_0,\vec{u}_0)}{\partial \vec{x}} \cdot (\vec{x} - \vec{x}_0) + \frac{\partial \vec{f}(\vec{x}_0,\vec{u}_0)}{\partial \vec{u}} \cdot (\vec{u} - \vec{u}_0)$$

If $(\vec{x}_0,\vec{u}_0)$ is an equilibrium point $\left(\vec{X},\vec{U}\right)$, and $(\tilde{x},\tilde{u})$ is perturbation around it:

$$\vec{f}\left(\vec{X},\vec{U}\right) \equiv 0 \qquad \vec{x} = \vec{X} + \tilde{\vec{x}} \qquad \vec{u} = \vec{U} + \tilde{\vec{u}} \qquad \vec{x} - \vec{X} = \tilde{\vec{x}} \qquad \vec{u} - \vec{U} = \tilde{\vec{u}}$$

$$\frac{d\vec{X}}{dt} = 0 \qquad \Rightarrow \qquad \frac{d\vec{x}}{dt} = \frac{d\vec{X}}{dt} + \frac{d\tilde{\vec{x}}}{dt} = \frac{d\tilde{\vec{x}}}{dt}$$

$$\frac{d\tilde{\vec{x}}}{dt} \cong \left.\frac{\partial \vec{f}(\vec{x},\vec{u})}{\partial \vec{x}}\right|_{(\vec{X},\vec{U})} \cdot \tilde{\vec{x}} + \left.\frac{\partial \vec{f}(\vec{x},\vec{u})}{\partial \vec{u}}\right|_{(\vec{X},\vec{U})} \cdot \tilde{\vec{u}}$$

$$\begin{cases} \dot{\tilde{\vec{x}}} = \mathbf{A} \cdot \tilde{\vec{x}} + \mathbf{B} \cdot \tilde{\vec{u}} \\ \mathbf{A} = \left.\frac{\partial \vec{f}(\vec{x},\vec{u})}{\partial \vec{x}}\right|_{(\vec{X},\vec{U})} \qquad \mathbf{B} = \left.\frac{\partial \vec{f}(\vec{x},\vec{u})}{\partial \vec{u}}\right|_{(\vec{X},\vec{U})} \end{cases}$$

Average Large-Signal Model—Boost Rectifier

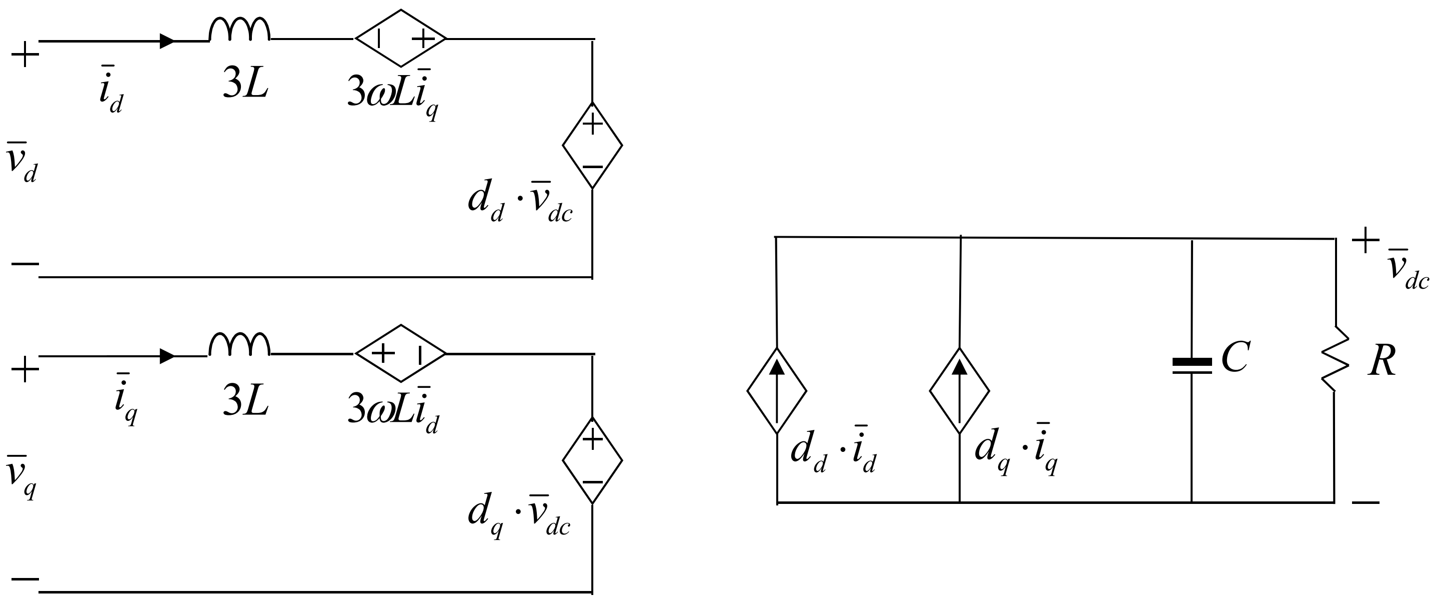

A steady-state operating point:

$$V_d = \sqrt{\frac{3}{2}} \cdot V_m$$ (V_m: Max line-to-line voltage)

$$V_q = 0$$

$$D_d = \frac{V_d}{V_{dc}} \qquad I_d = \frac{V_{dc}}{R \cdot D_d}$$

$$D_q = -\frac{3\omega L I_d}{V_{dc}} \qquad I_q = 0$$

Small-Signal State-Space Model – Boost Rectifier

$$\underbrace{\frac{d}{dt}\begin{bmatrix}\tilde{i}_d\\ \tilde{i}_q\\ \tilde{v}_{dc}\end{bmatrix}}_{\dot{\vec{x}}} = \underbrace{\begin{bmatrix}0 & \omega & -\frac{D_d}{3L}\\ -\omega & 0 & -\frac{D_q}{3L}\\ \frac{D_d}{C} & \frac{D_q}{C} & -\frac{1}{RC}\end{bmatrix}}_{\mathbf{A}}\underbrace{\begin{bmatrix}\tilde{i}_d\\ \tilde{i}_q\\ \tilde{v}_{dc}\end{bmatrix}}_{\vec{x}} + \underbrace{\begin{bmatrix}-\frac{V_{dc}}{3L} & 0\\ 0 & -\frac{V_{dc}}{3L}\\ \frac{I_d}{C} & \frac{I_q}{C}\end{bmatrix}}_{\mathbf{B}}\underbrace{\begin{bmatrix}\tilde{d}_d\\ \tilde{d}_q\end{bmatrix}}_{\vec{u}} + \underbrace{\begin{bmatrix}\frac{1}{3L} & 0\\ 0 & \frac{1}{3L}\\ 0 & 0\end{bmatrix}}_{\mathbf{D}}\underbrace{\begin{bmatrix}\tilde{v}_d\\ \tilde{v}_q\end{bmatrix}}_{\vec{v}}$$

$$\underbrace{\dot{\vec{x}} = \mathbf{A}\vec{x}}_{\text{Intrinsic System Dynamics}} + \underbrace{\mathbf{B}\vec{u}}_{\text{Control Input}} + \underbrace{\mathbf{D}\vec{v}}_{\text{Disturbance Input}}$$

Intrinsic
System Dynamics

Control
Input

Disturbance
Input

Small-Signal Circuit Model – Boost Rectifier

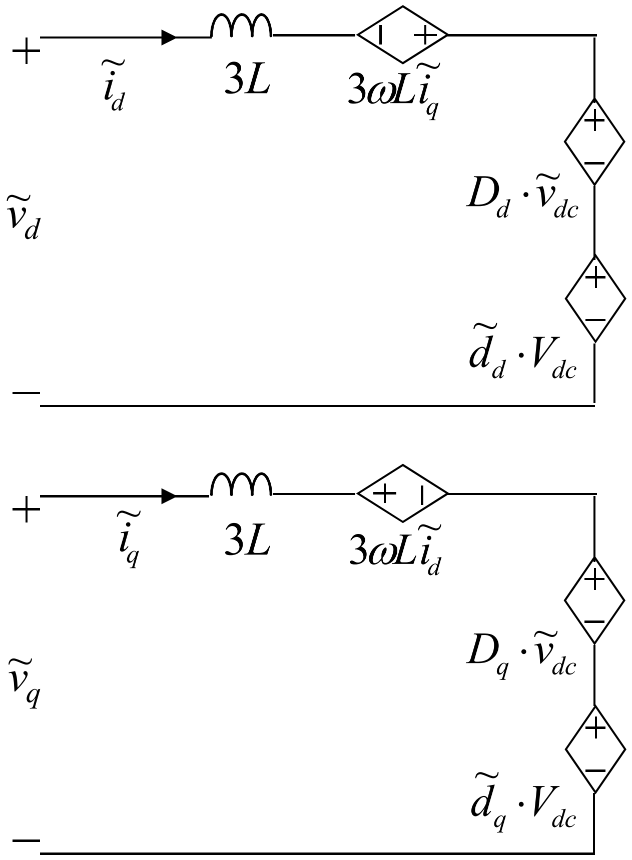

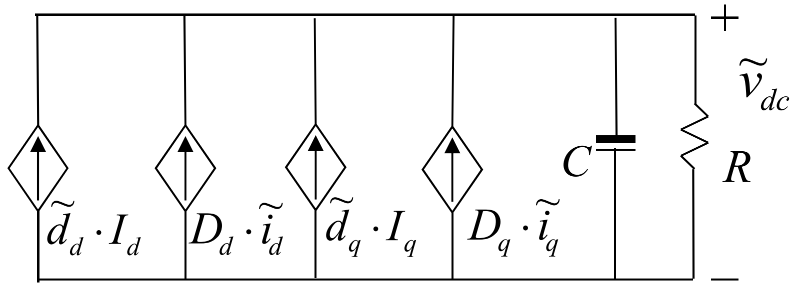

Boost Rectifier Open-Loop Transfer Functions

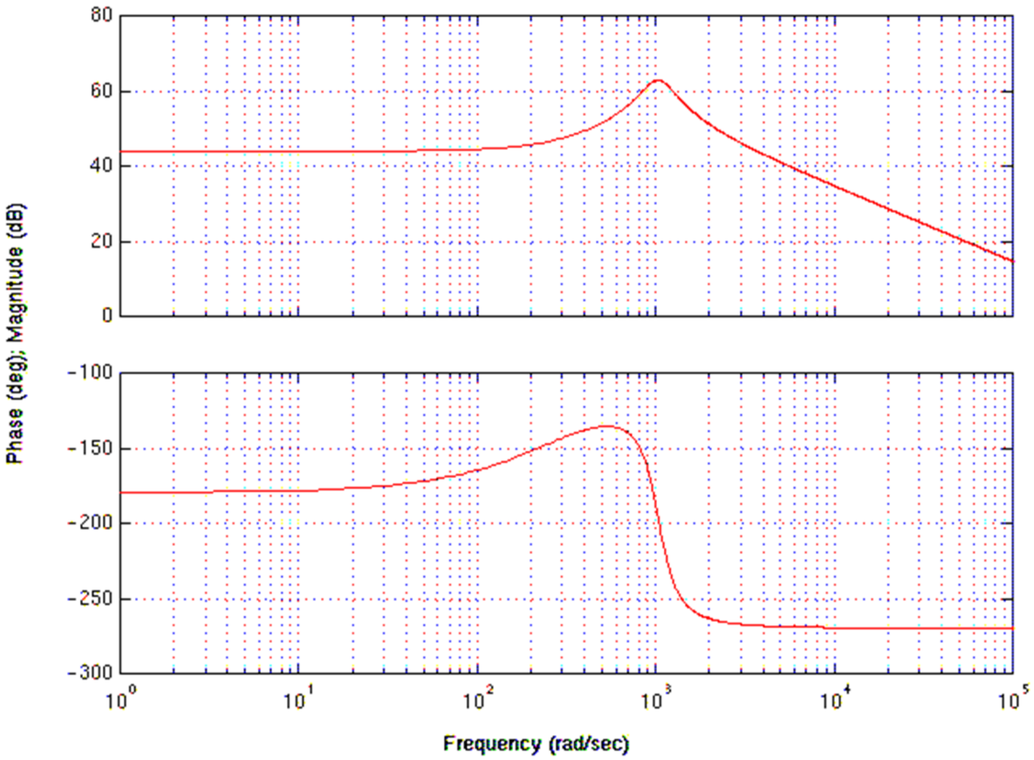

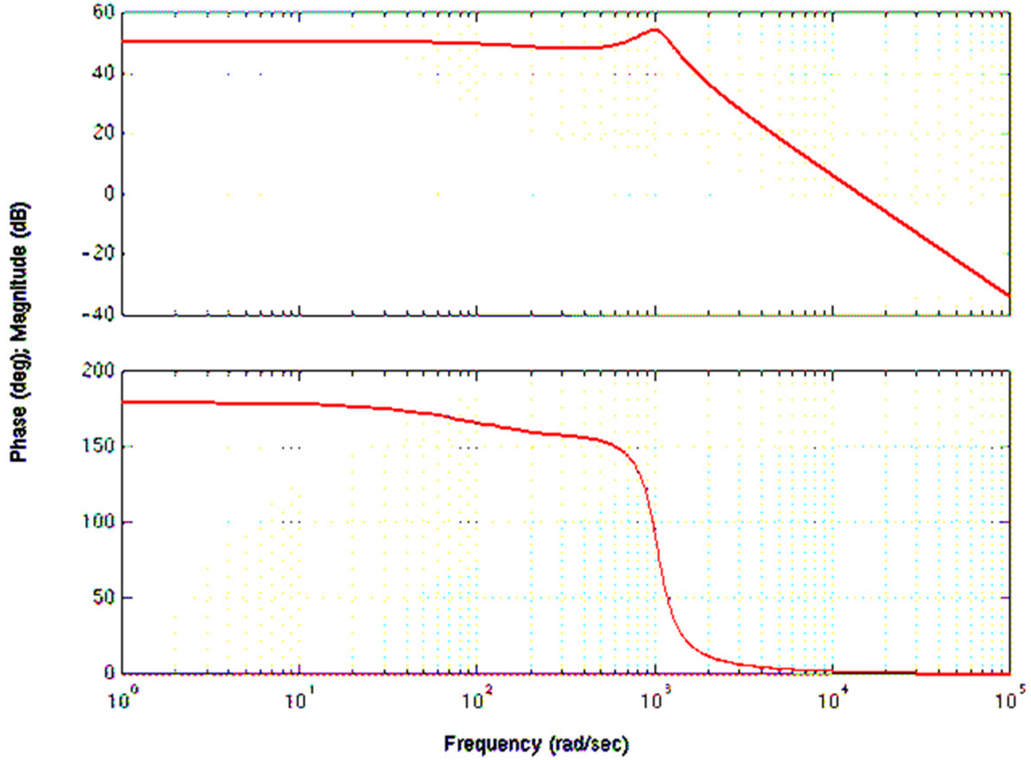

$$\frac{\tilde{i}_d}{\tilde{d}_d} = \frac{K_{iddd} \cdot (s + z_{iddd\,1}) \cdot (s + z_{iddd\,2})}{(s + p_1) \cdot (s + p_2) \cdot (s + p_2^*)}$$

$$\frac{\tilde{i}_d}{\tilde{d}_q} = \frac{K_{iddq} \cdot (s + z_{iddq})}{(s + p_1) \cdot (s + p_2) \cdot (s + p_2^*)}$$

Boost Rectifier Open-Loop Transfer Functions

$$\frac{\tilde{v}_{dc}}{\tilde{d}_d} = \frac{K_{vdcdd} \cdot (s + z_{vdcdd\,1}) \cdot (s + z_{vdcdd\,2}) \cdot (s - z_{RHP})}{(s + p_1) \cdot (s + p_2) \cdot (s + p_2^*)}$$

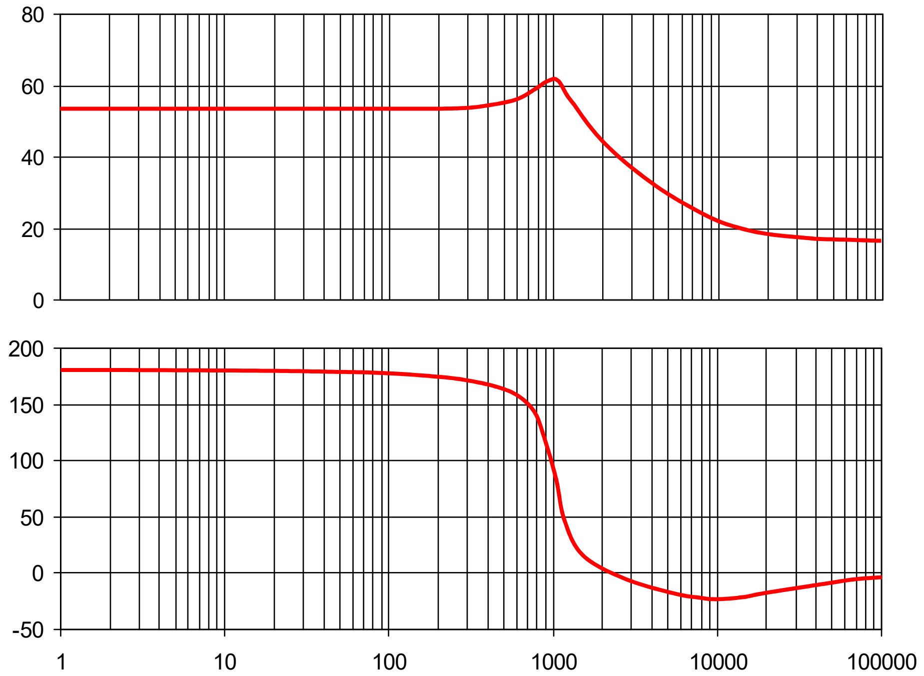

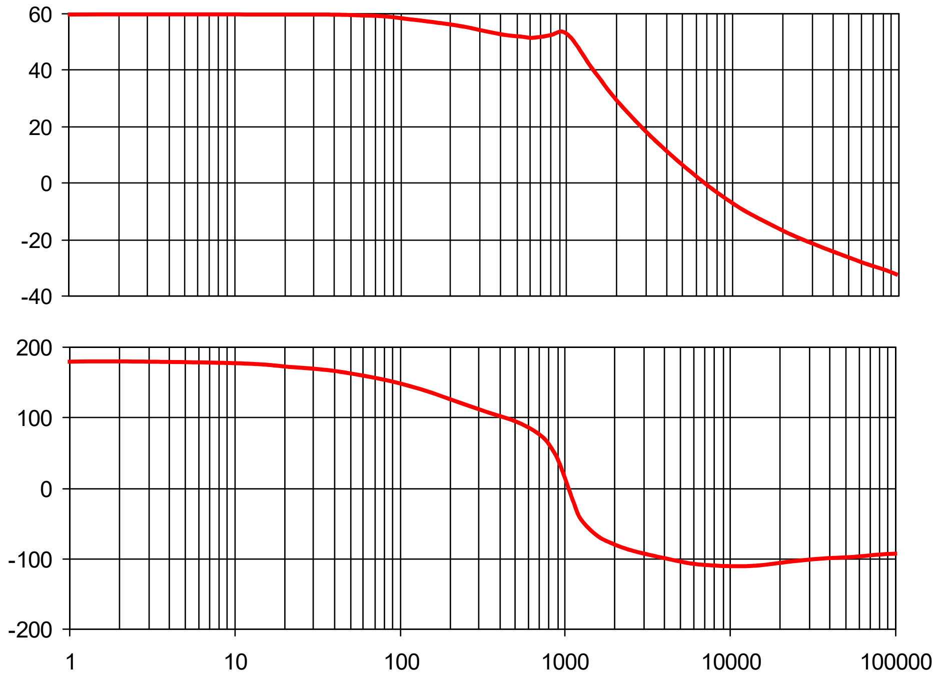

$$\frac{\tilde{v}_{dc}}{\tilde{d}_q} = \frac{K_{vdcdq} \cdot (s + z_{vdcdq\,1}) \cdot (s - z_{RHP})}{(s + p_1) \cdot (s + p_2) \cdot (s + p_2^*)}$$

Poles of Boost Rectifier

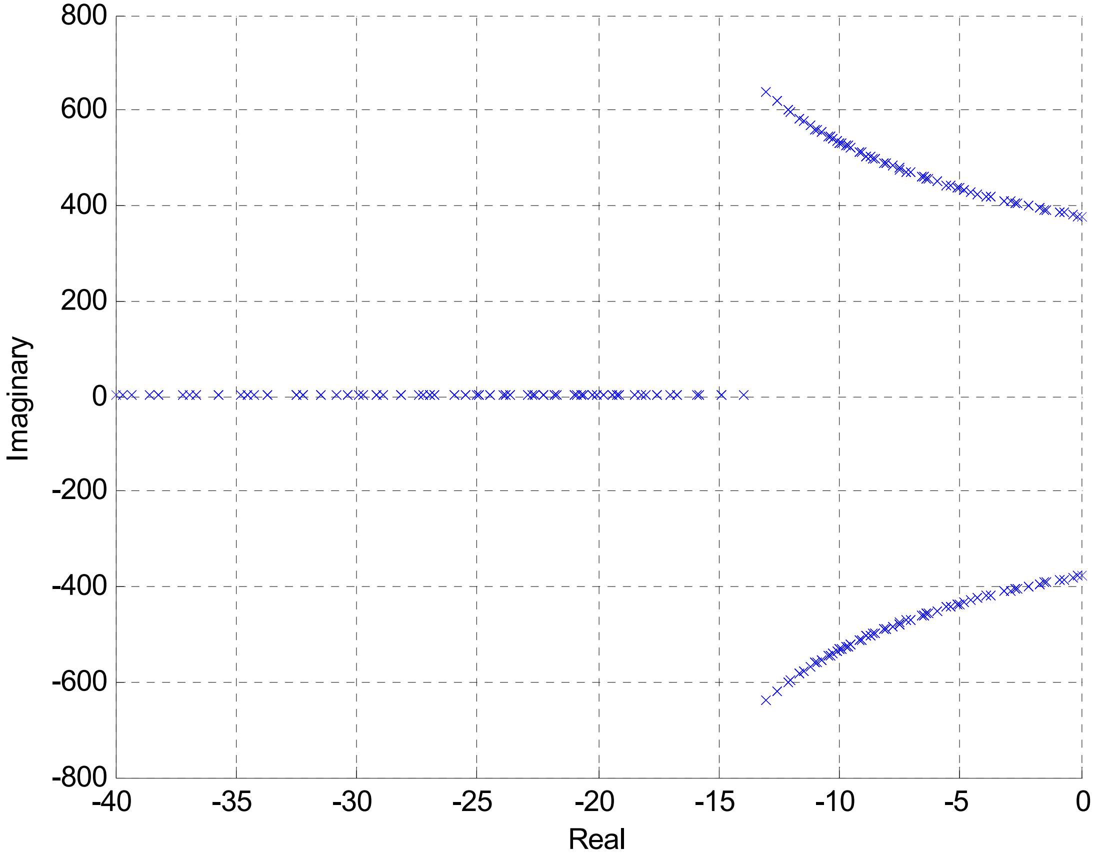

Pole map for –1 < Dd < 1 and –1 < Dq < 1 and:

$$V_d = \sqrt{\frac{3}{2}} \cdot \sqrt{6} \cdot 230 \qquad \omega = 60 \cdot 2\pi \qquad L = 1\,\mathrm{mH}$$

$$V_q = 0 \qquad R = 10\,\Omega \qquad C = 2.5\,\mathrm{mF}$$

Digital Delay

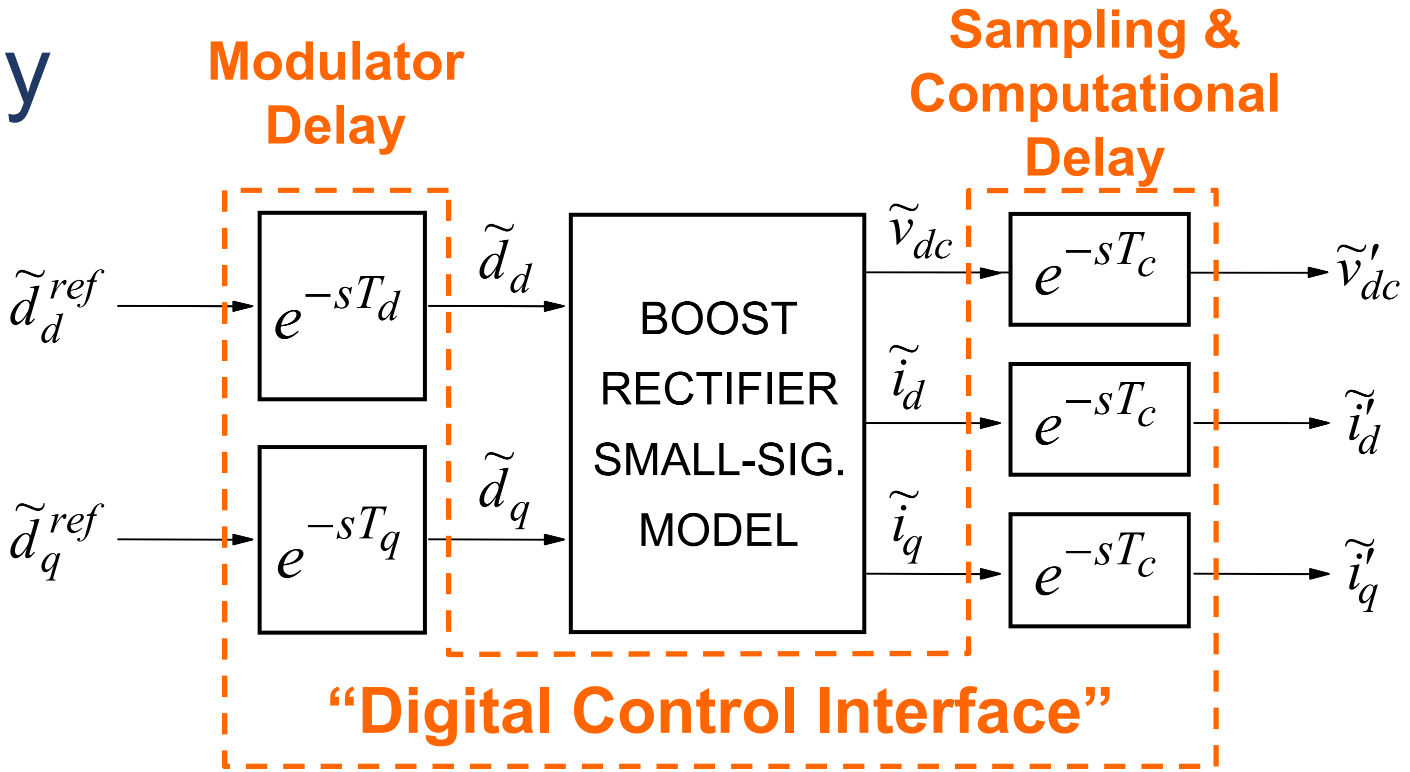

Simplified approximations in continuous time domain:

$$e^{-sT_{del}} \approx \frac{1 - \frac{sT_{del}}{2} + \frac{(sT_{del})^2}{12}}{1 + \frac{sT_{del}}{2} + \frac{(sT_{del})^2}{12}}$$

Often choose: $T_{del} \approx T_c \approx T_d \approx T_q \approx T_{sampling} = T_{switching}$ Total digital delay $\approx 2 \cdot T_{switching}$

Outline

AC Sweep in Switching Model Simulation (PLECS)

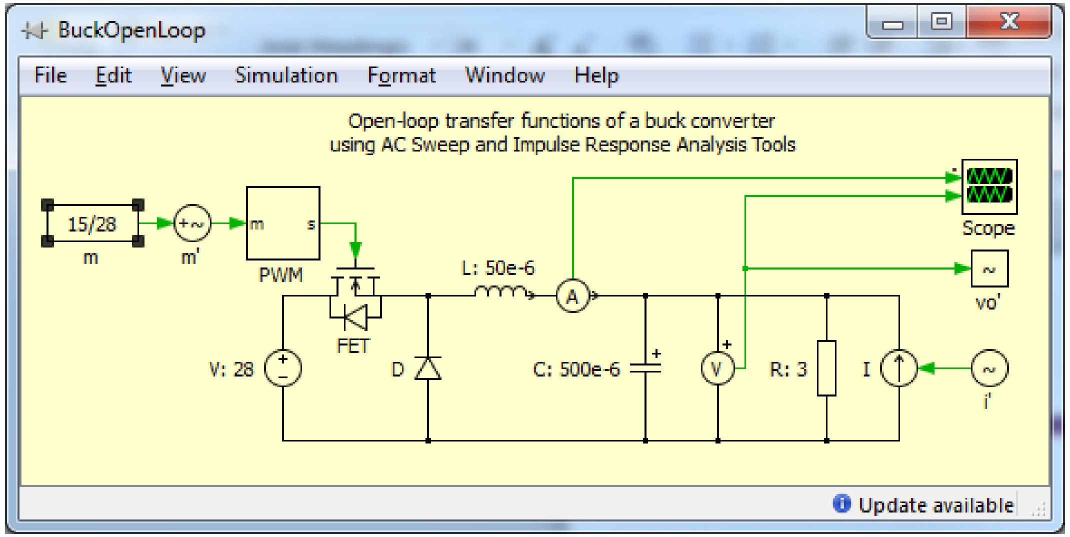

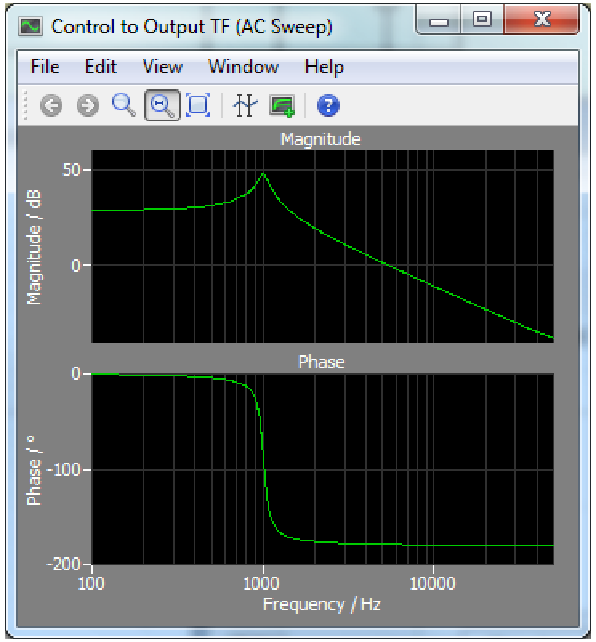

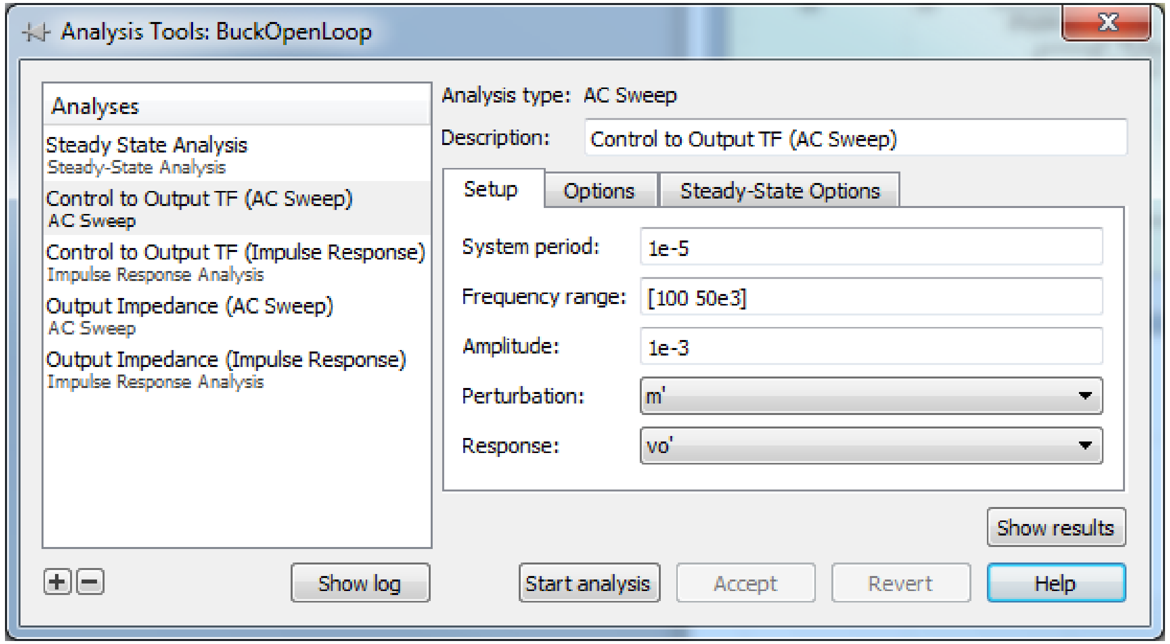

Measurement Set-up

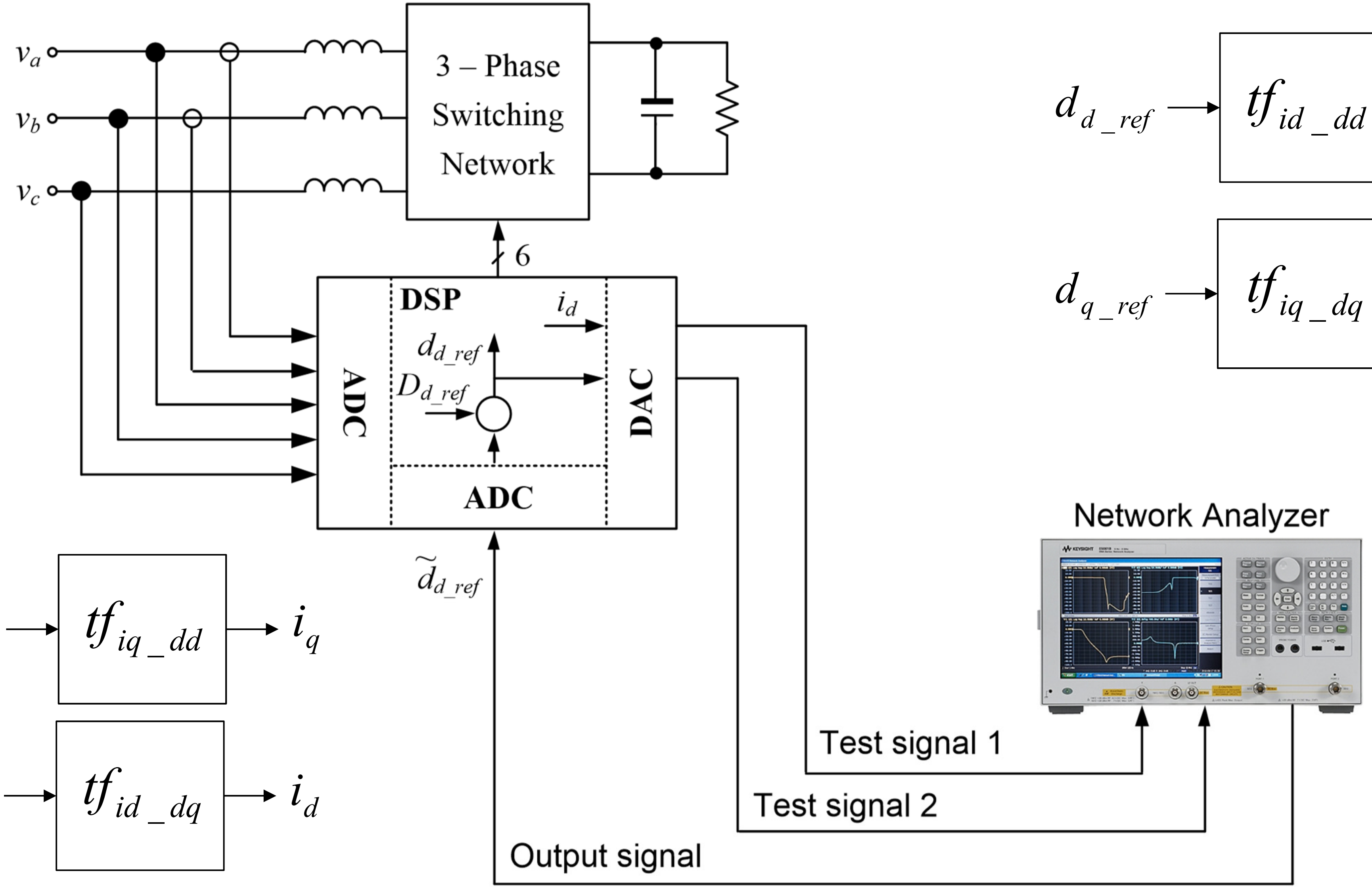

$$d_{d\_ref} \rightarrow \boxed{tf_{id\_dd}} \rightarrow i_d$$

$$d_{q\_ref} \rightarrow \boxed{tf_{iq\_dq}} \rightarrow i_q$$

$$d_{d\_ref} \rightarrow \boxed{tf_{iq\_dd}} \rightarrow i_q$$

$$d_{q\_ref} \rightarrow \boxed{tf_{id\_dq}} \rightarrow i_d$$

http://www.keysight.com/en/pdx-x201771-pn-E5061B/ena-series-network-analyzer?cc=GB&lc=eng

Software Frequency Response Analyser Tool

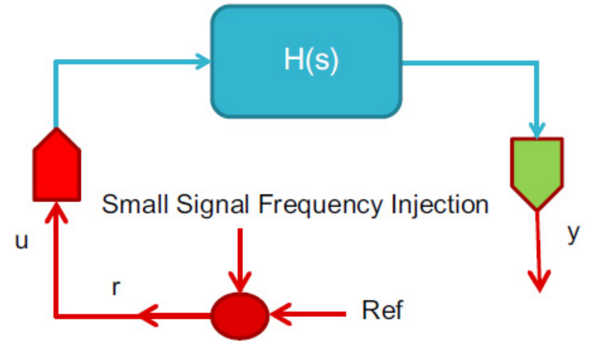

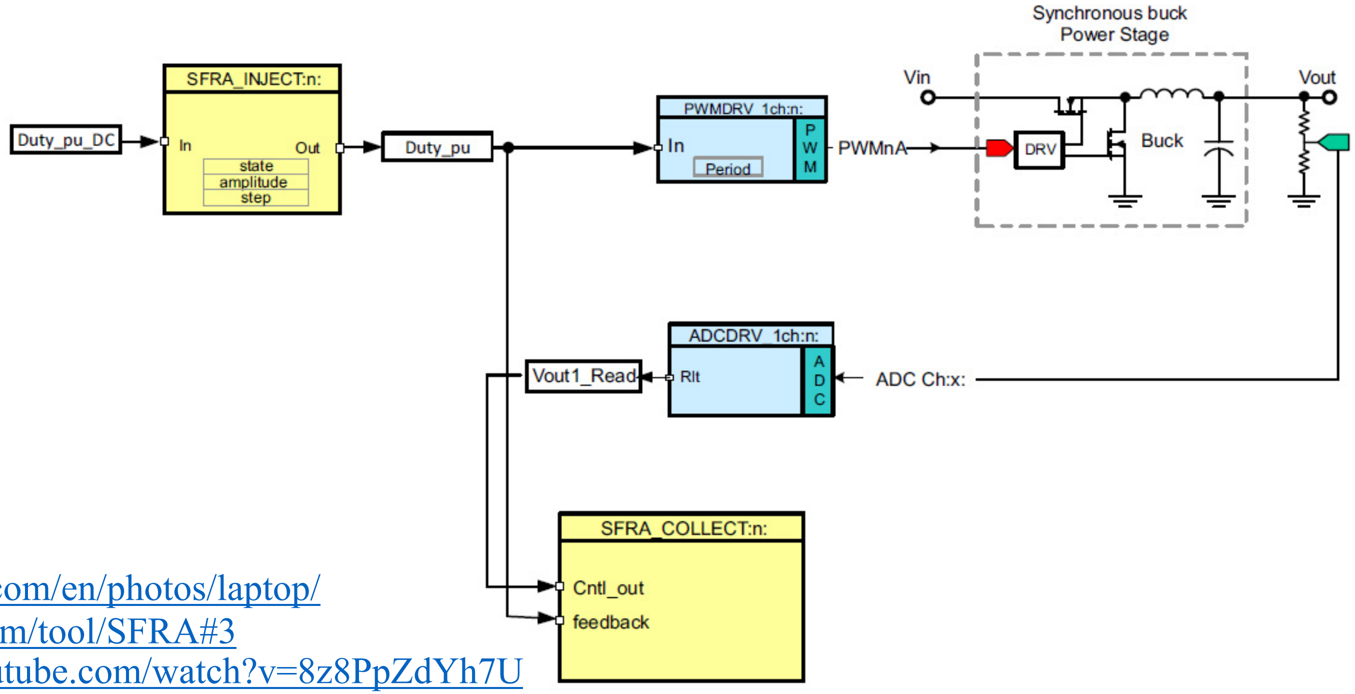

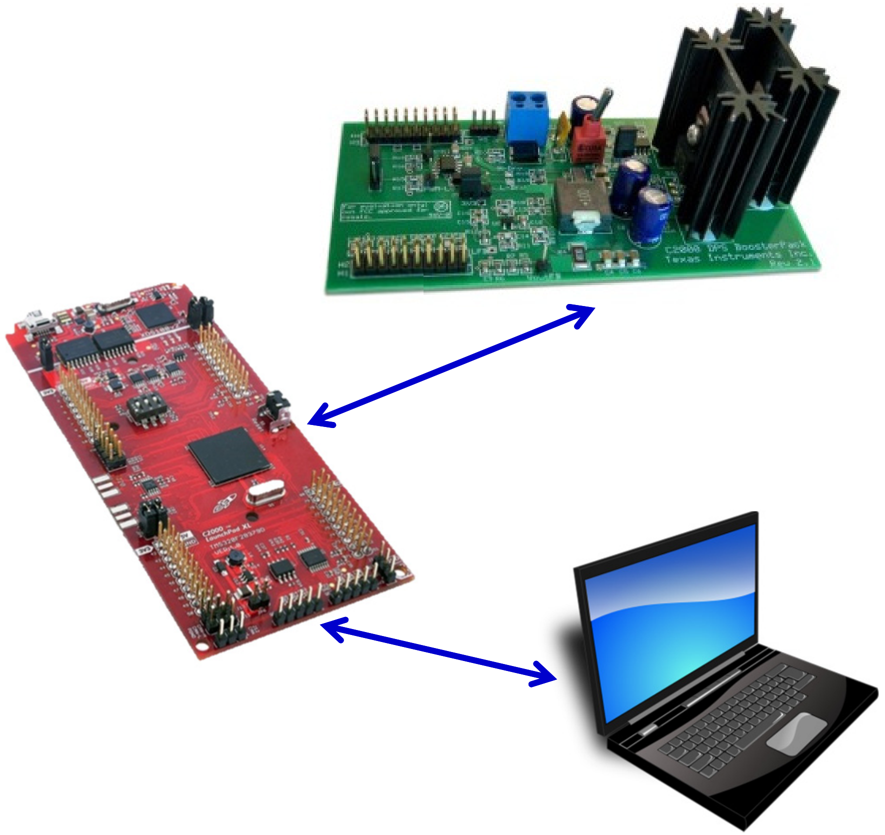

https://pixabay.com/en/photos/laptop/
http://www.ti.com/tool/SFRA#3
https://www.youtube.com/watch?v=8z8PpZdYh7U
https://store.ti.com/LAUNCHXL-F28379D-C2000-Delfino-MCUs-F28379D-LaunchPad-Development-Kit-P50584.aspx?HQS=ecm-tistore-promo-janlaunchpad-null-store-LAUNCHXL-F28379D-wwe

Current Loop Design—Boost Rectifier

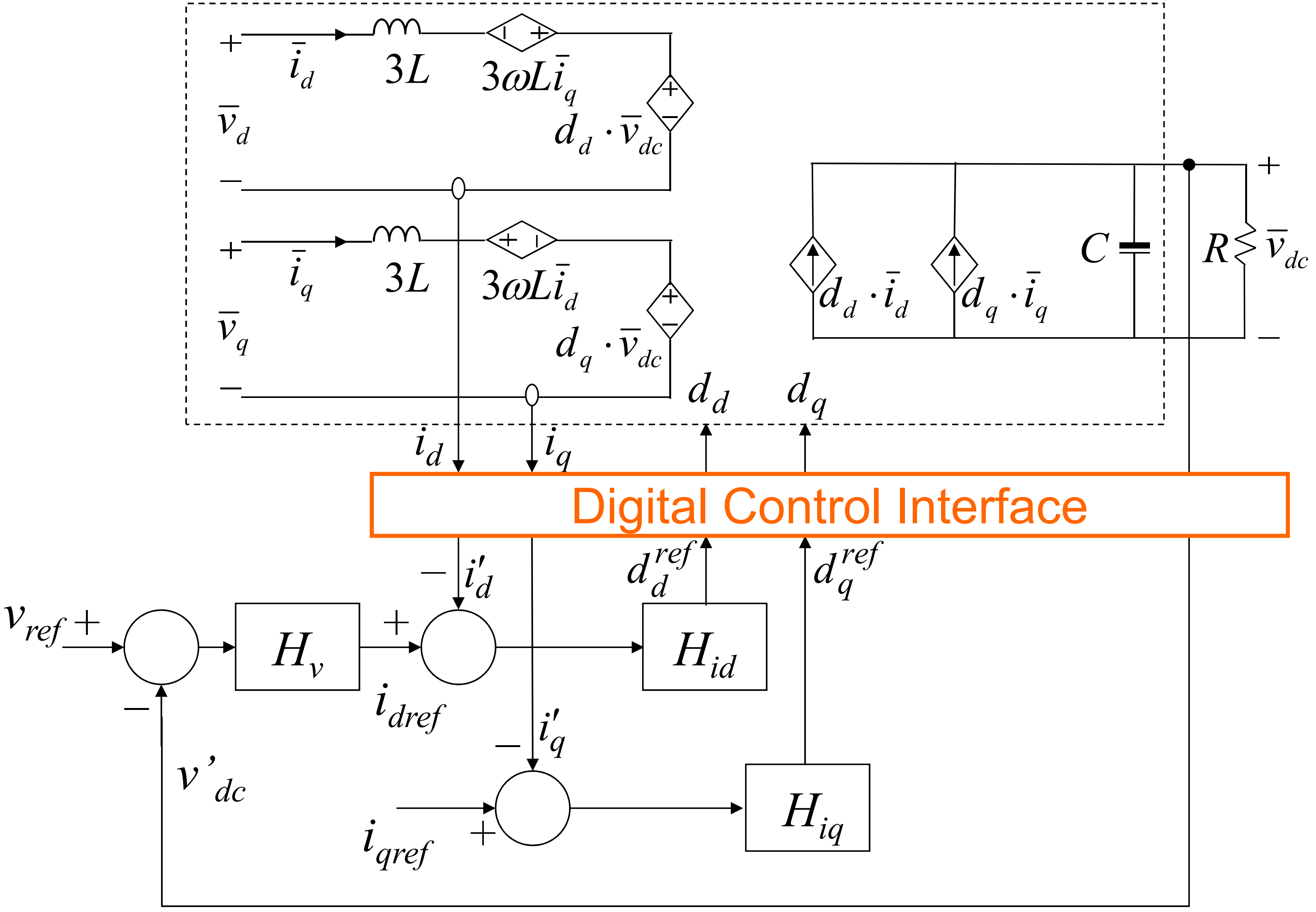

Control-to-Current Transfer Function

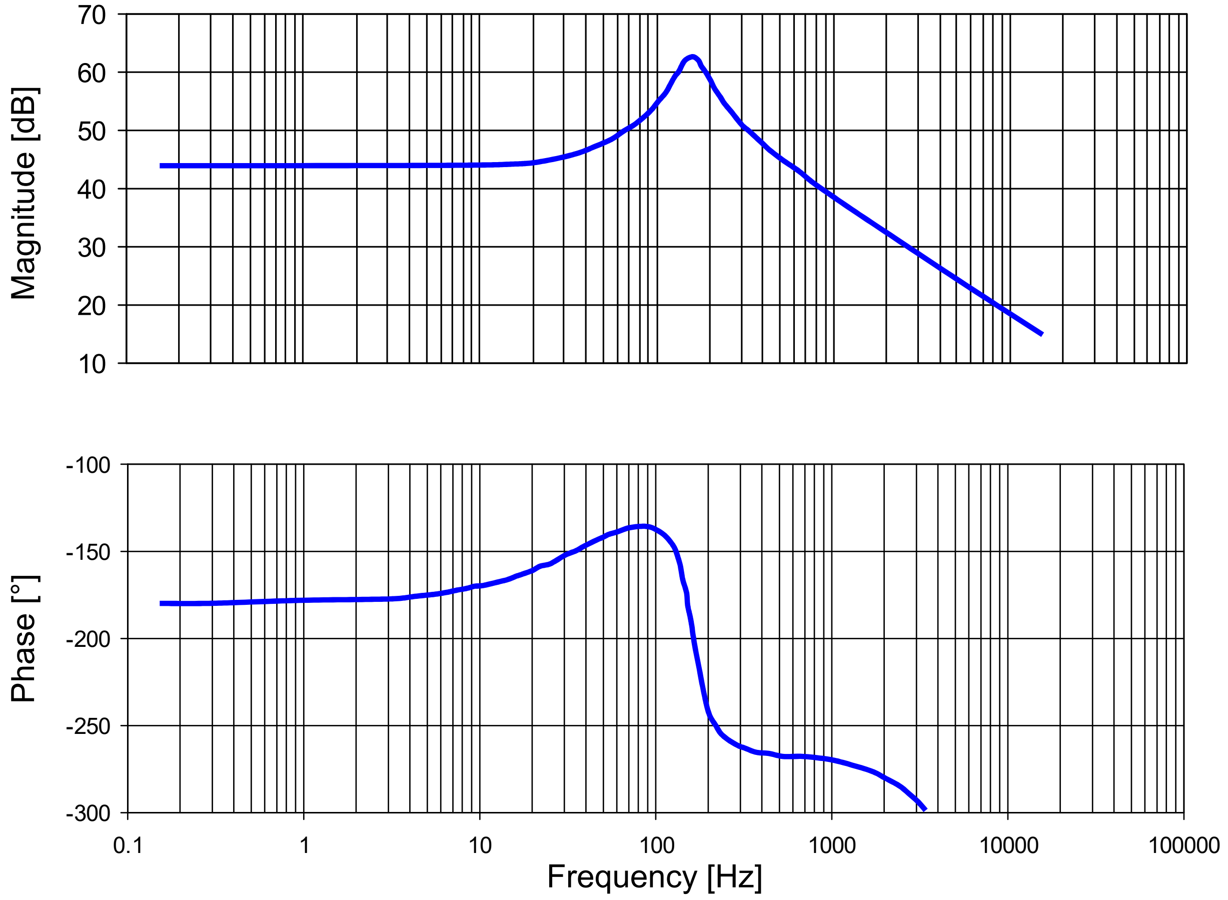

$$\frac{\tilde{i}_d}{\tilde{d}_d} = \frac{K_{iddd} \cdot (s + z_{iddd\,1}) \cdot (s + z_{iddd\,2})}{(s + p_1) \cdot (s + p_2) \cdot (s + p_2^*)}$$

Control-to-Current Transfer Function

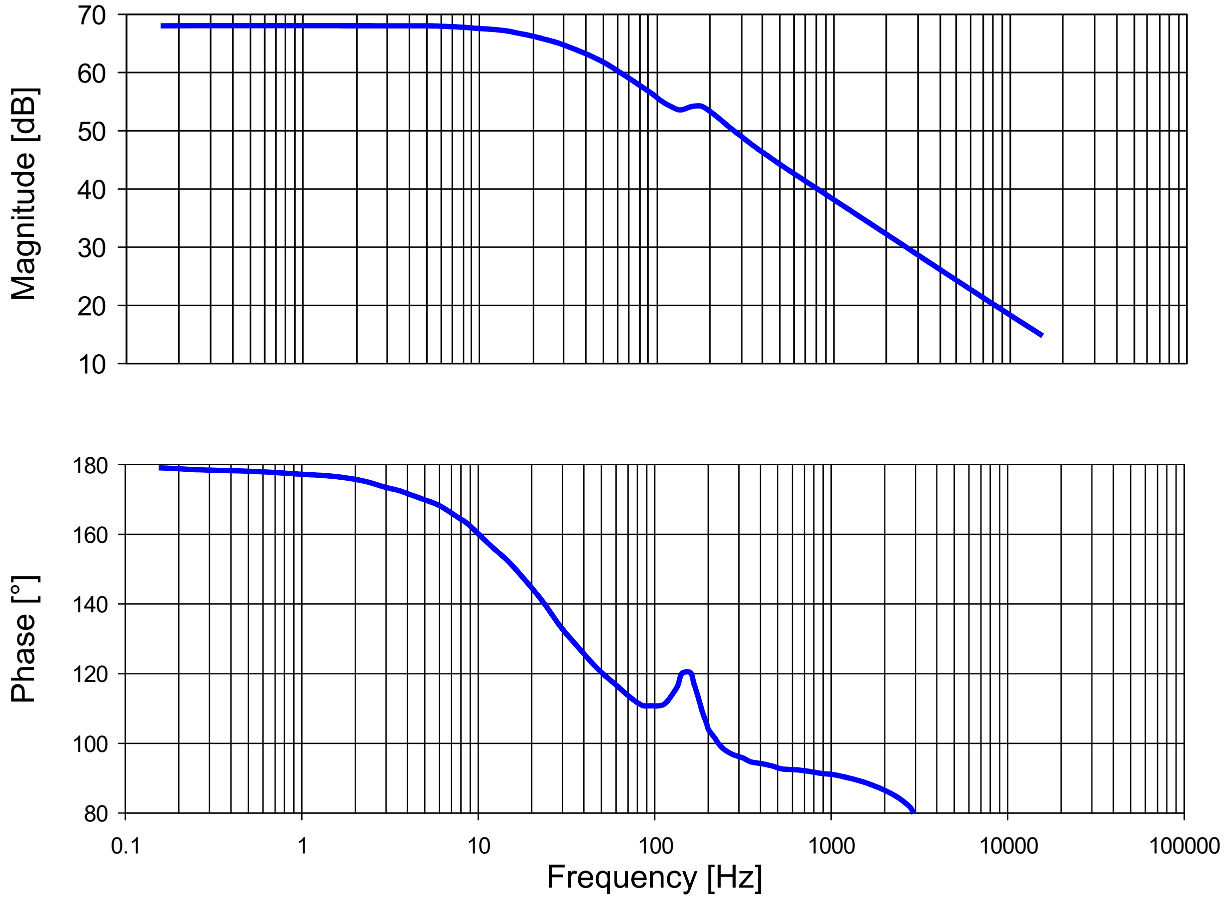

$$\frac{\tilde{i}_q}{\tilde{d}_q} = \frac{K_{iqdq} \cdot (s + z_{iqdq}) \cdot (s + z^*_{iqdq})}{(s + p_1) \cdot (s + p_2) \cdot (s + p^*_2)}$$

Current Loop Gain

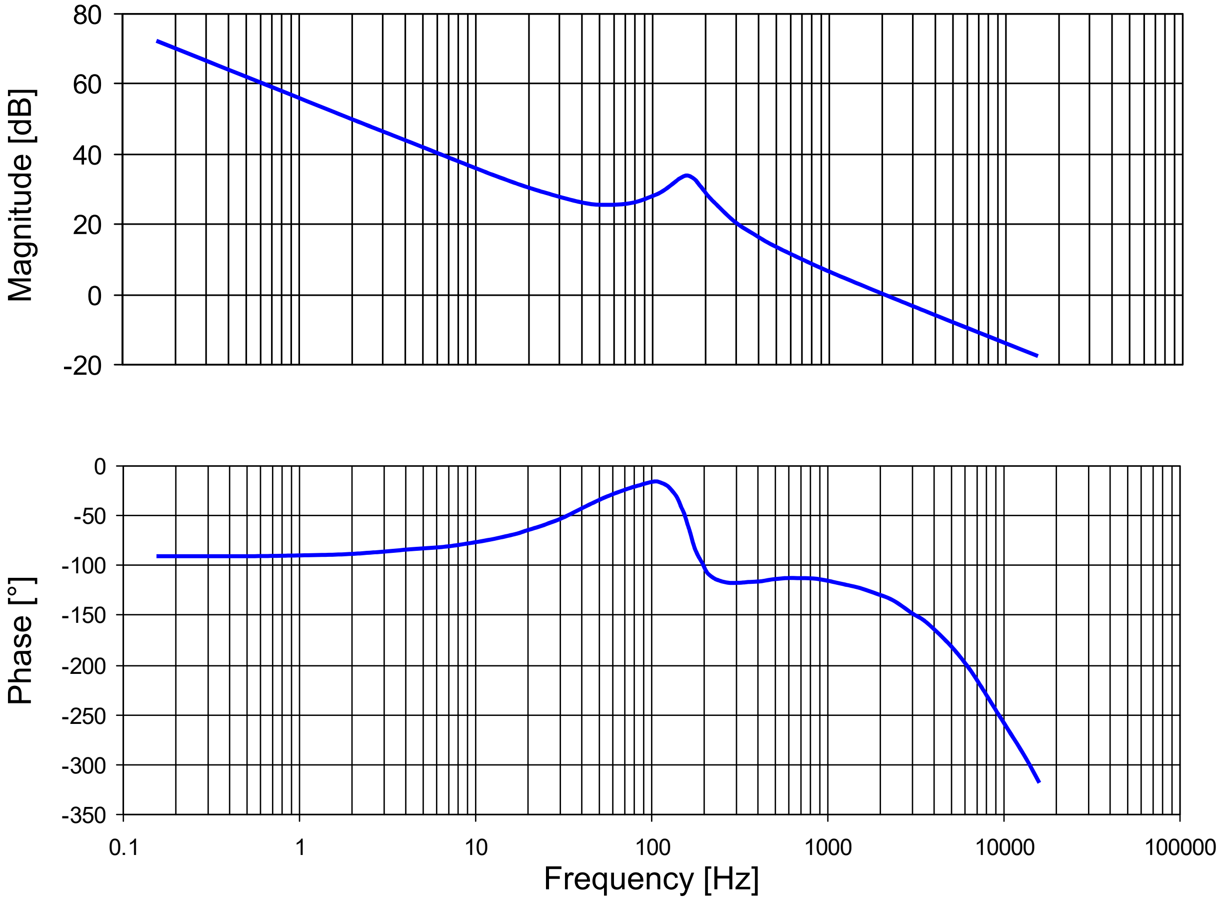

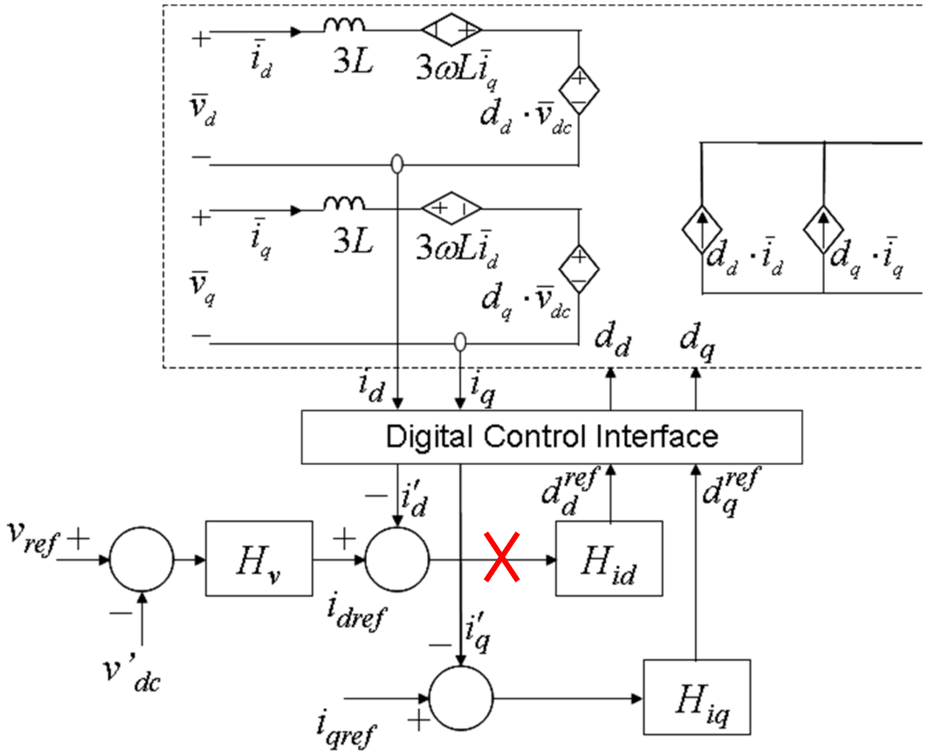

- D channel loop-gain
- Bandwidth is limited by delay (f_{sw}=20kHz)

Current Loop Gain

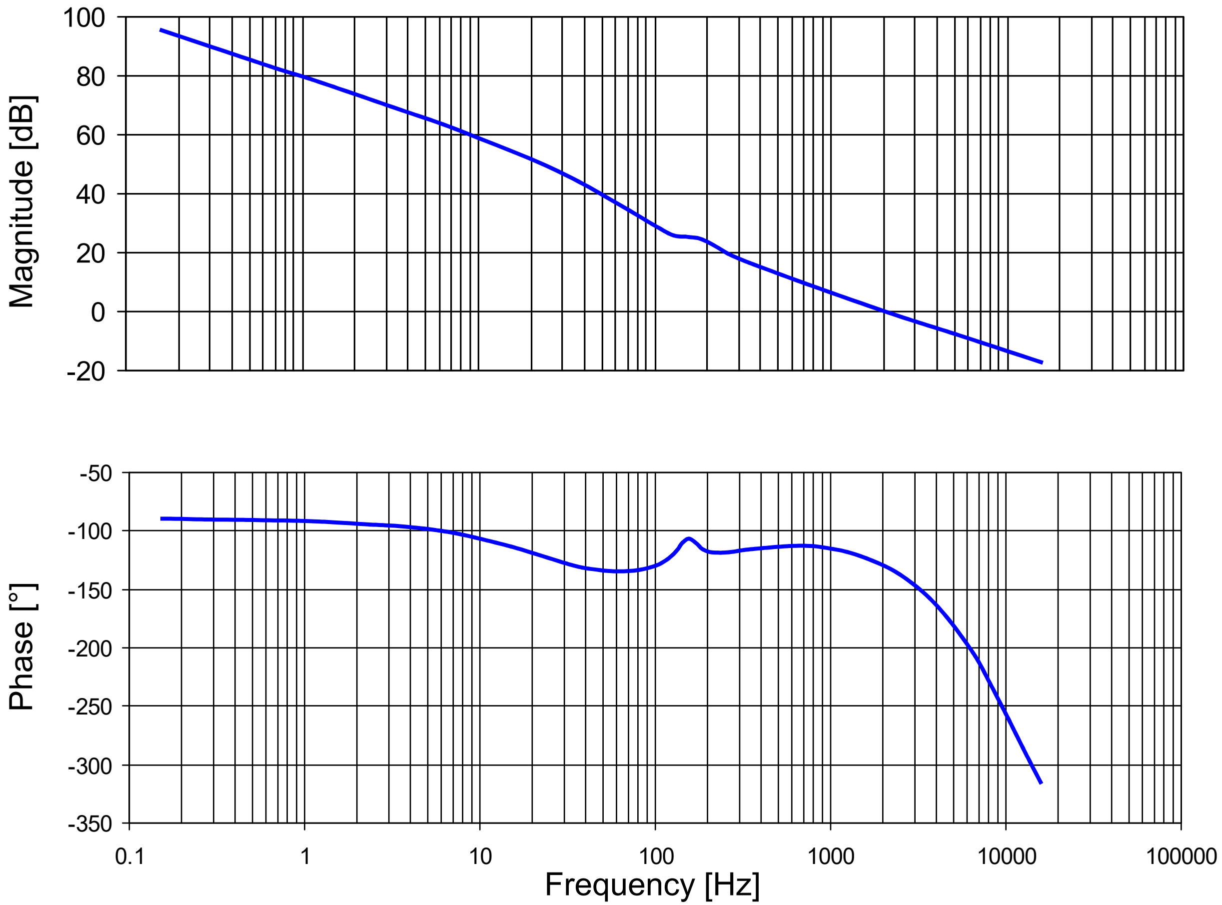

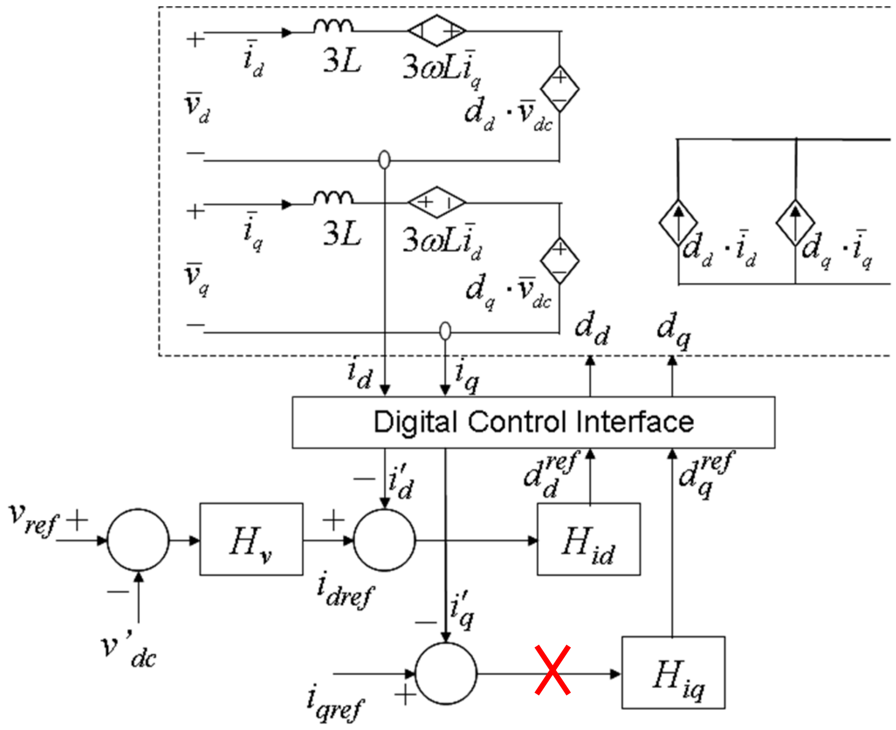

- Q channel loop-gain
- Bandwidth is limited by delay (f_{sw}=20kHz)

Current Regulation

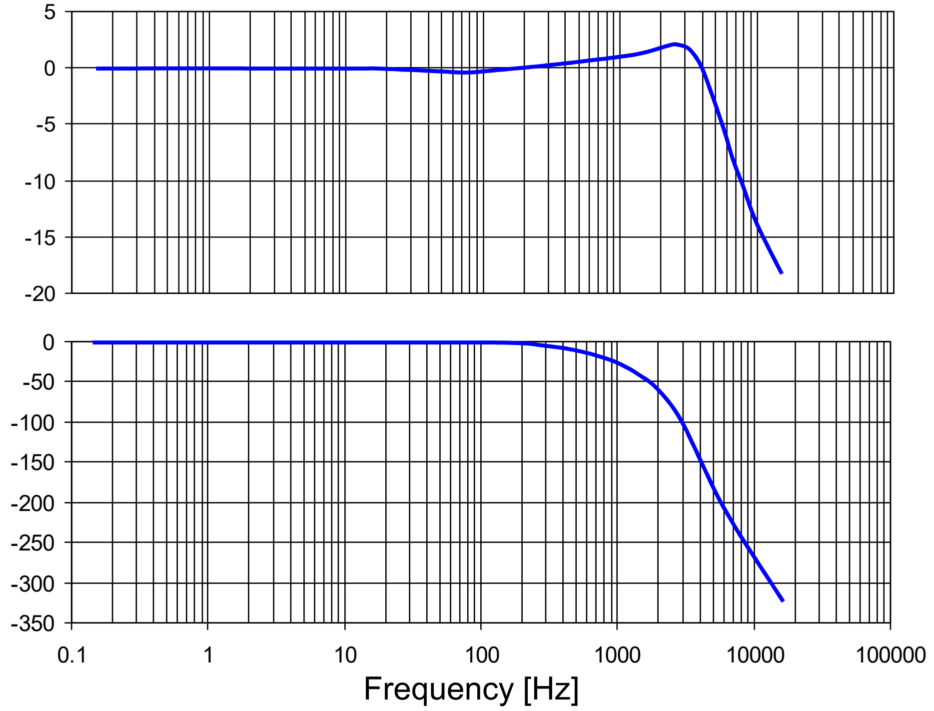

$$\frac{\tilde{i}'_d}{\tilde{i}_{dref}}$$

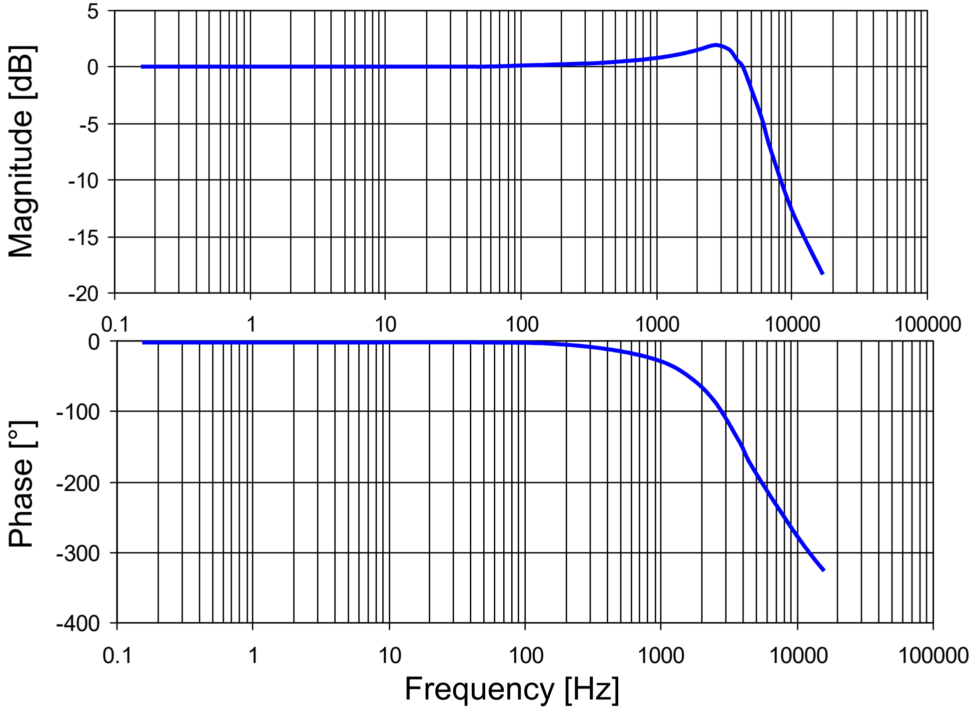

$$\frac{\tilde{i}'_q}{\tilde{i}_{qref}}$$

- Peak is more pronounced when gain increases

Current Loop with D and Q Decoupling

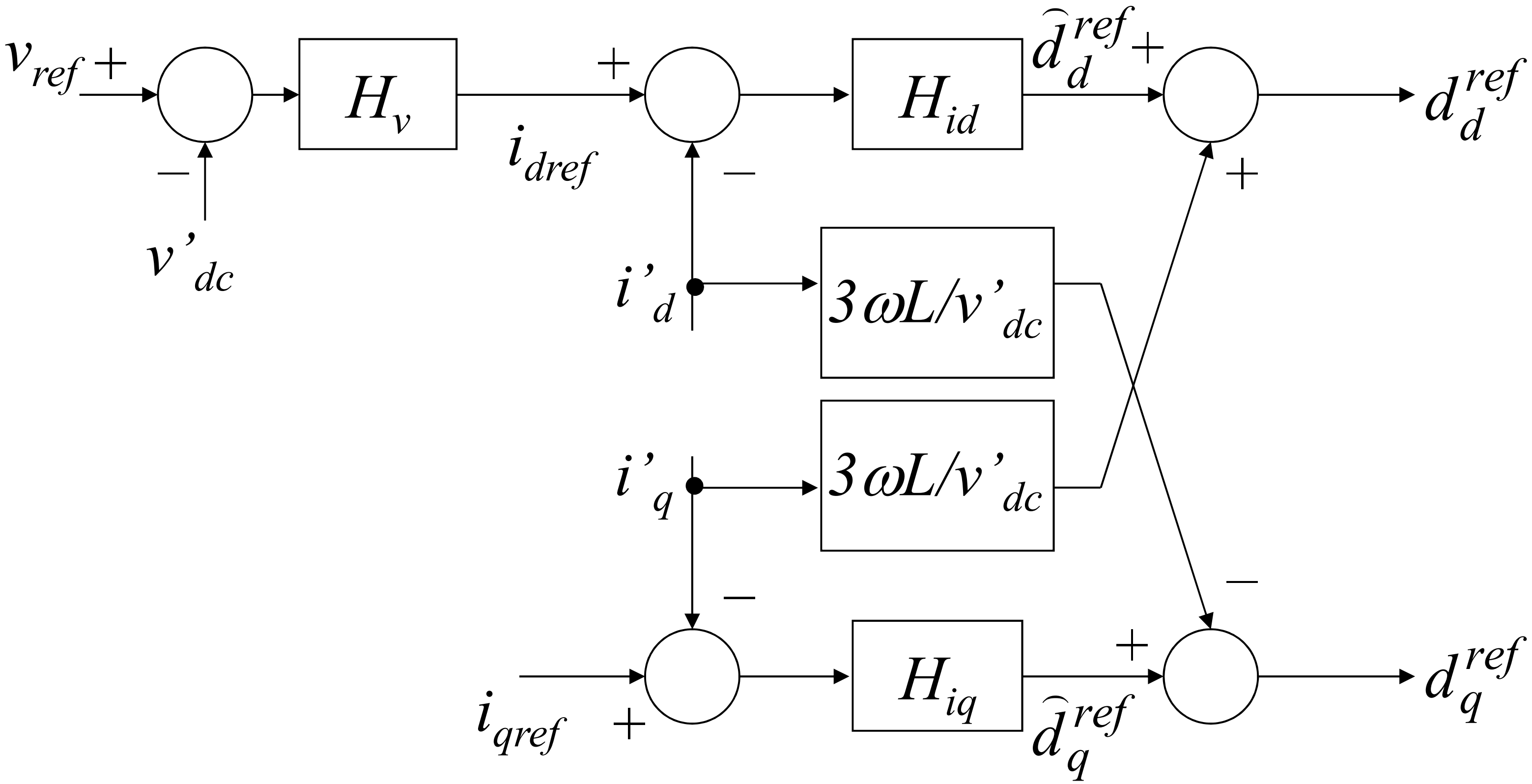

$$d_d = d_d^{ref} e^{-sT_d} = \left(\hat{d}_d^{ref} + 3\omega L i'_q / v'_{dc}\right) e^{-sT_d} = \hat{d}_d + 3\omega L \frac{1}{v'_{dc}} e^{-sT_d} i'_q$$

$$d_q = d_q^{ref} e^{-sT_q} = \left(\hat{d}_q^{ref} + 3\omega L i'_d / v'_{dc}\right) e^{-sT_q} = \hat{d}_q - 3\omega L \frac{1}{v'_{dc}} e^{-sT_q} i'_d$$

Decoupled D and Q Channels

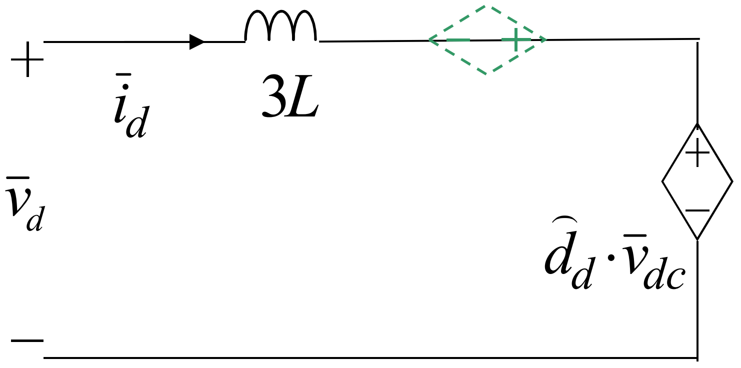

$$d_d\bar{v}_{dc} - 3\omega L\bar{i}_q = \hat{d}_d\bar{v}_{dc} + \overbrace{3\hat{\omega}\hat{L}\frac{\bar{v}_{dc}}{v'_{dc}}e^{-sT_d}i'_q - 3\omega L\bar{i}_q}^{\approx 0}$$

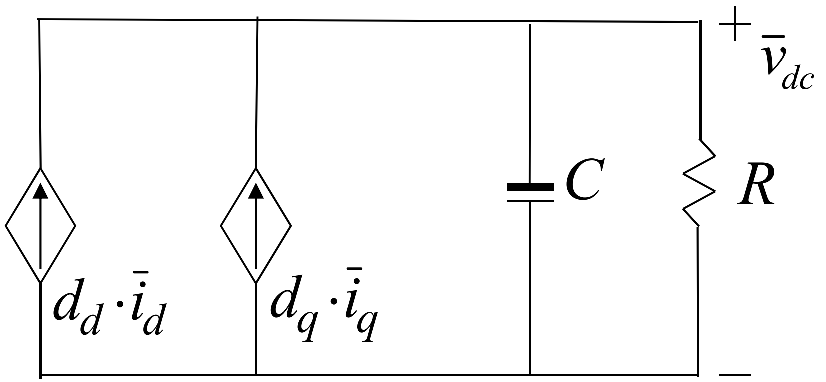

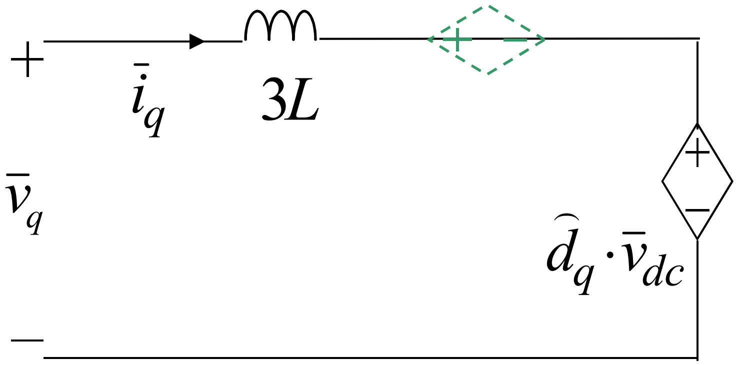

$$d_q\bar{v}_{dc} + 3\omega L\bar{i}_d = \hat{d}_q\bar{v}_{dc} \underbrace{- 3\hat{\omega}\hat{L}\frac{\bar{v}_{dc}}{v'_{dc}}e^{-sT_q}i'_d + 3\omega L\bar{i}_d}_{\approx 0}$$

- Similar to two parallel dc-dc boost converters after d and q decoupled

Output Voltage Loop Design

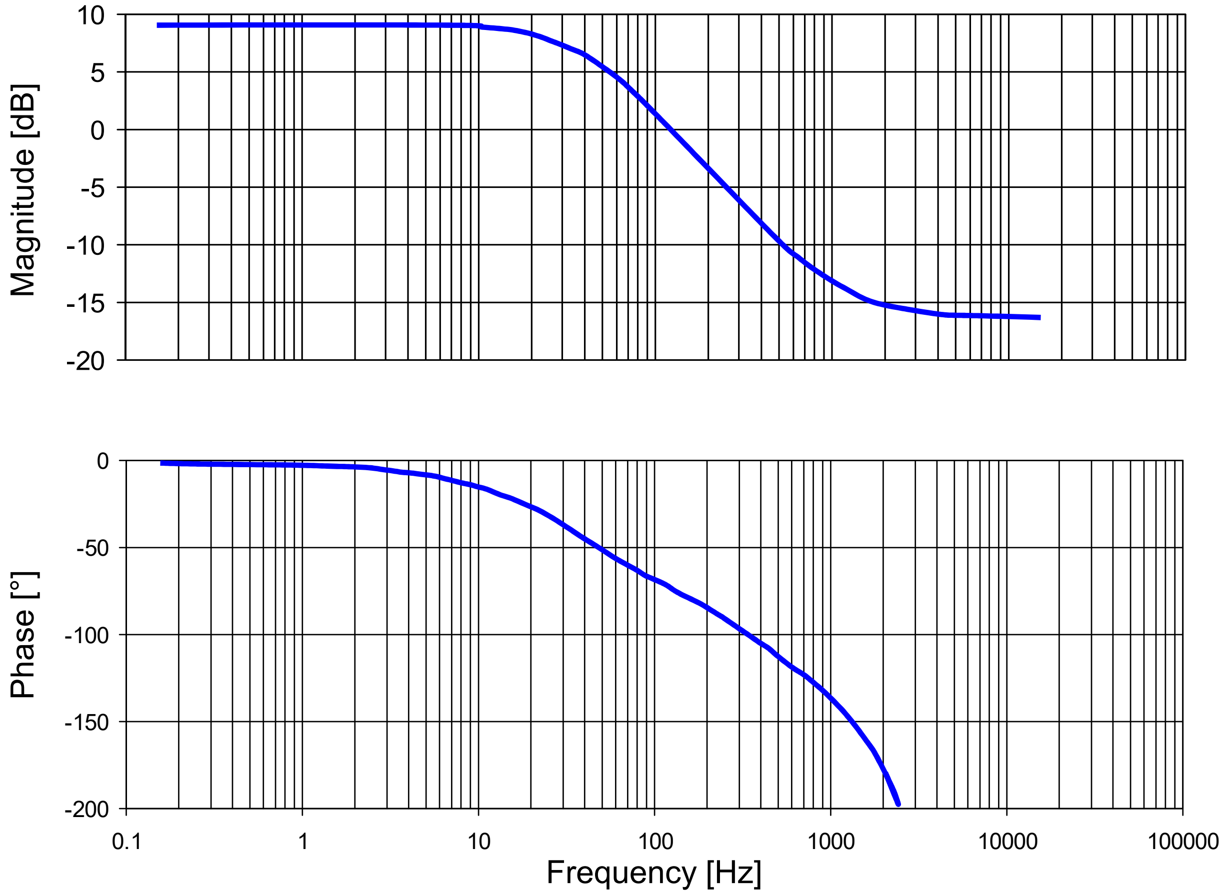

$$G_c = \frac{\tilde{v}_{dc}}{\tilde{i}_{dref}} = \frac{K \cdot (s - z_{RHP})}{(s + p_L) \cdot (s + p_H)}$$

Compensator Design

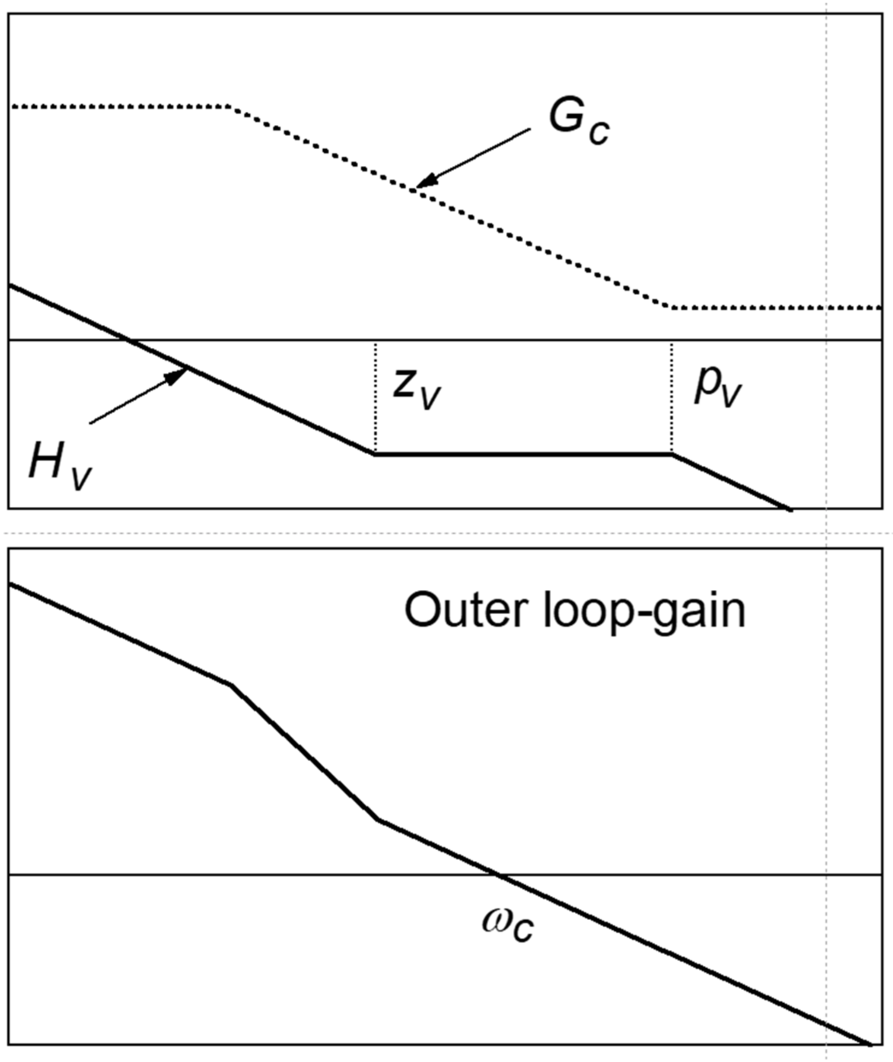

- Voltage compensator: $H_v = \dfrac{K_v\left(1+\dfrac{s}{z_v}\right)}{s(1+s/p_v)}$
  - Place z_v as high as possible for required phase margin
  - Place p_v for loop-gain attenuation
  - Attainable voltage-loop bandwidth: $\omega_c < \frac{1}{4} Z_{RHP}$

➢ p_v should be close to RHP zero to provide sufficient gain margin and loop gain attenuation beyond crossover frequency

➢ With high enough K_v the dominant pole of closed-loop system will be close to z_v

Time-Domain Simulation Results

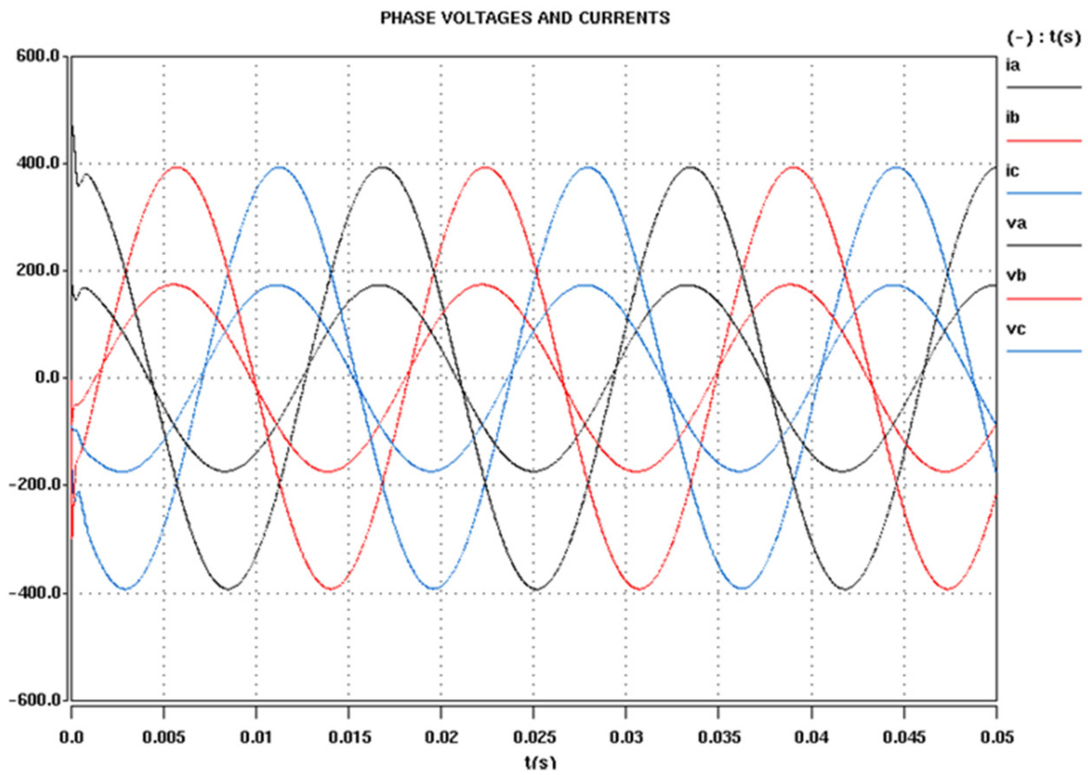

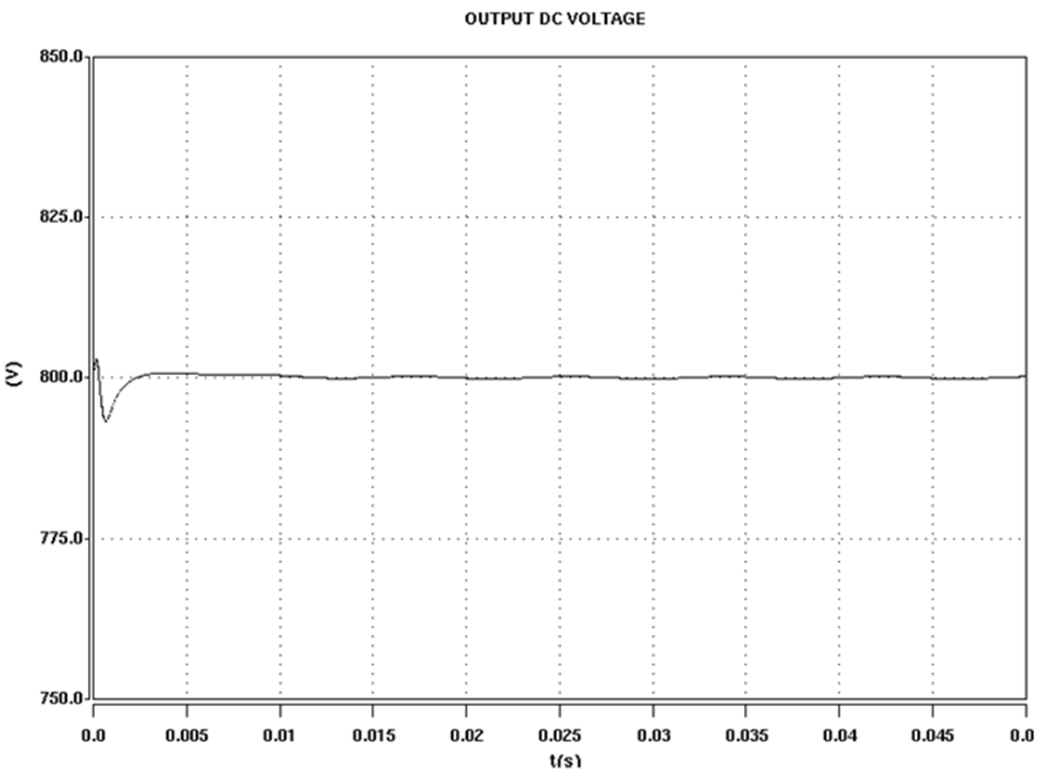

Phase voltage and current in PFC operation

Dc bus output voltage

Control Design of Voltage Source Inverter

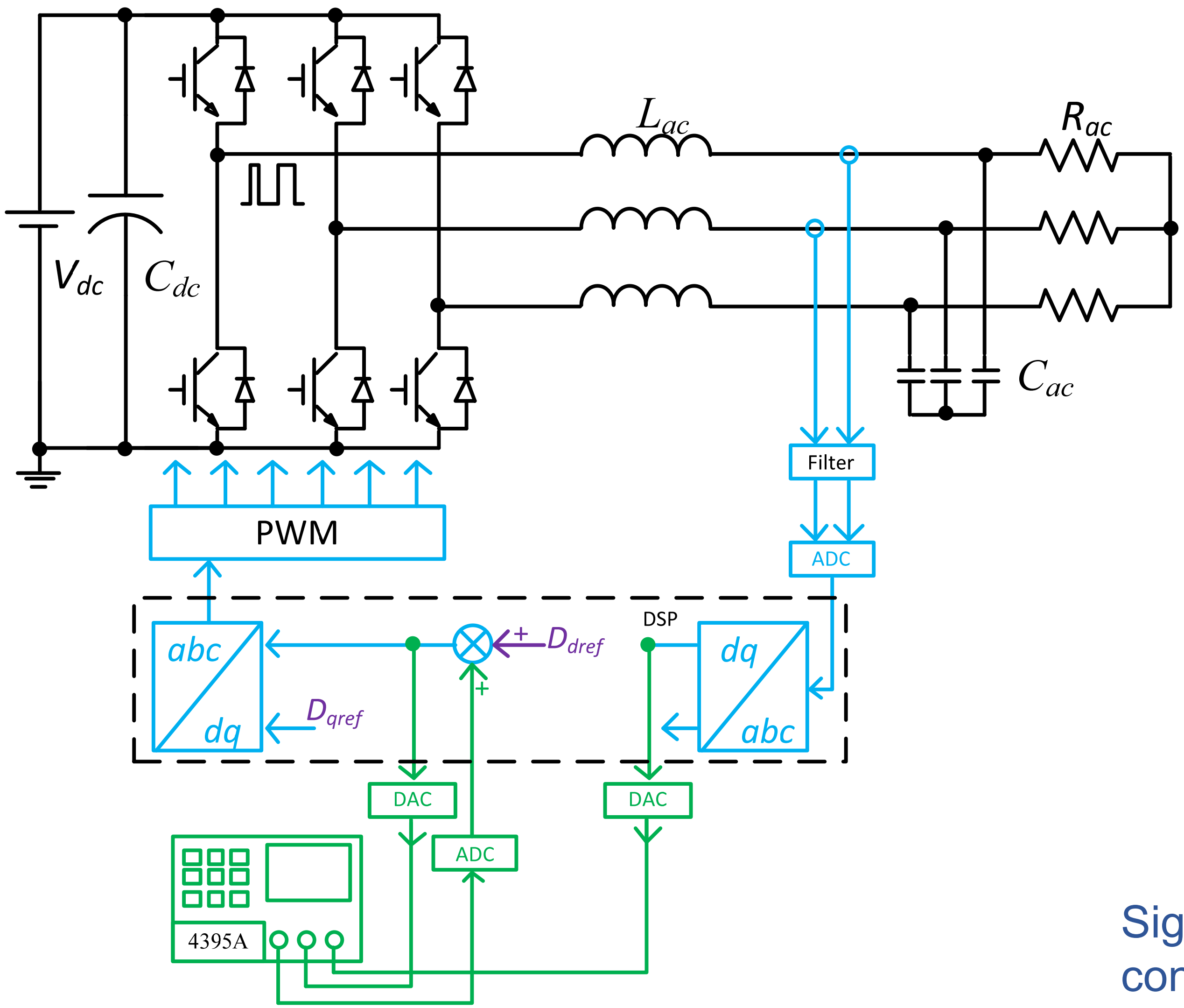

Signal sensing and digital control delays are included

Control-to-Current Transfer Function

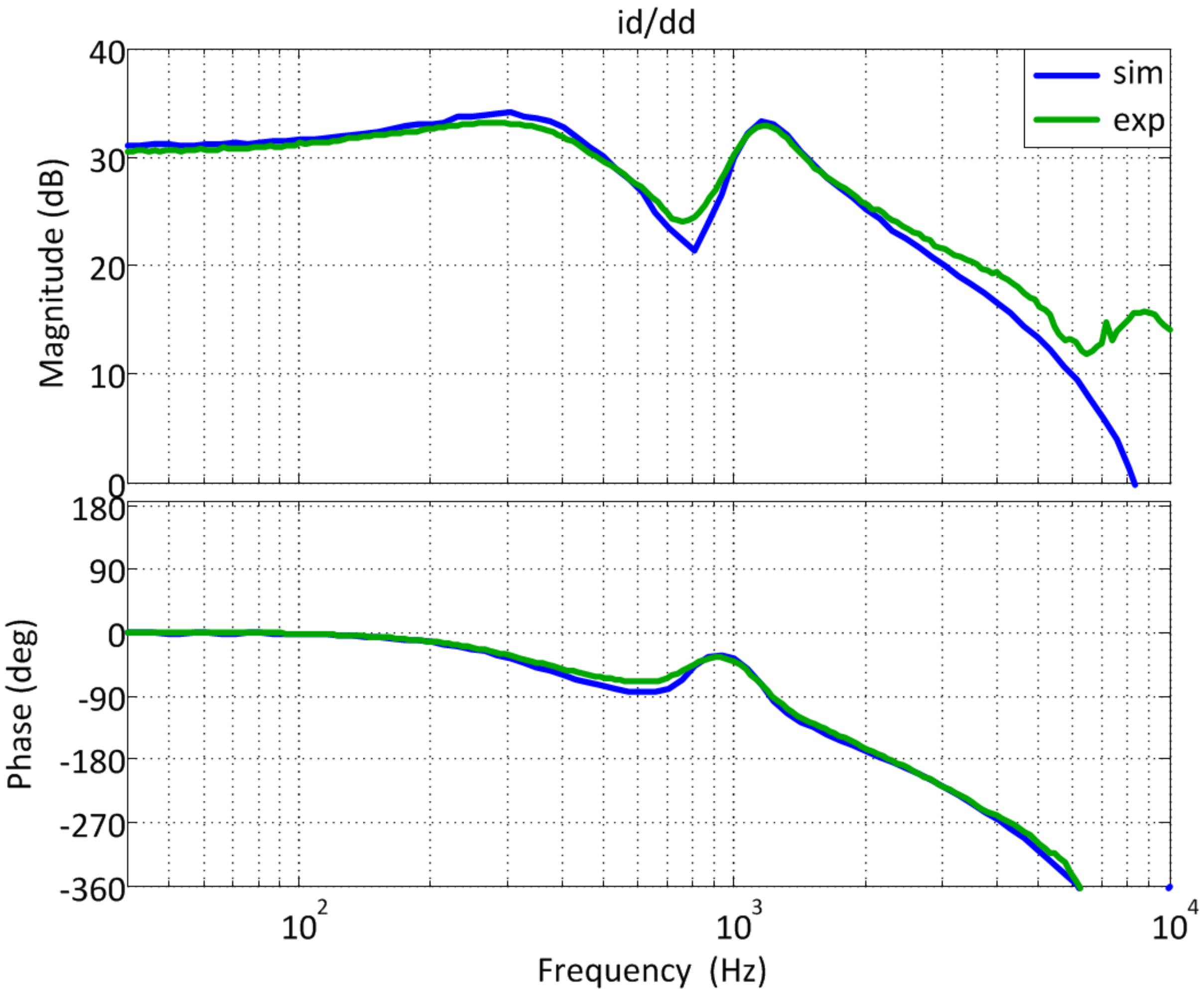

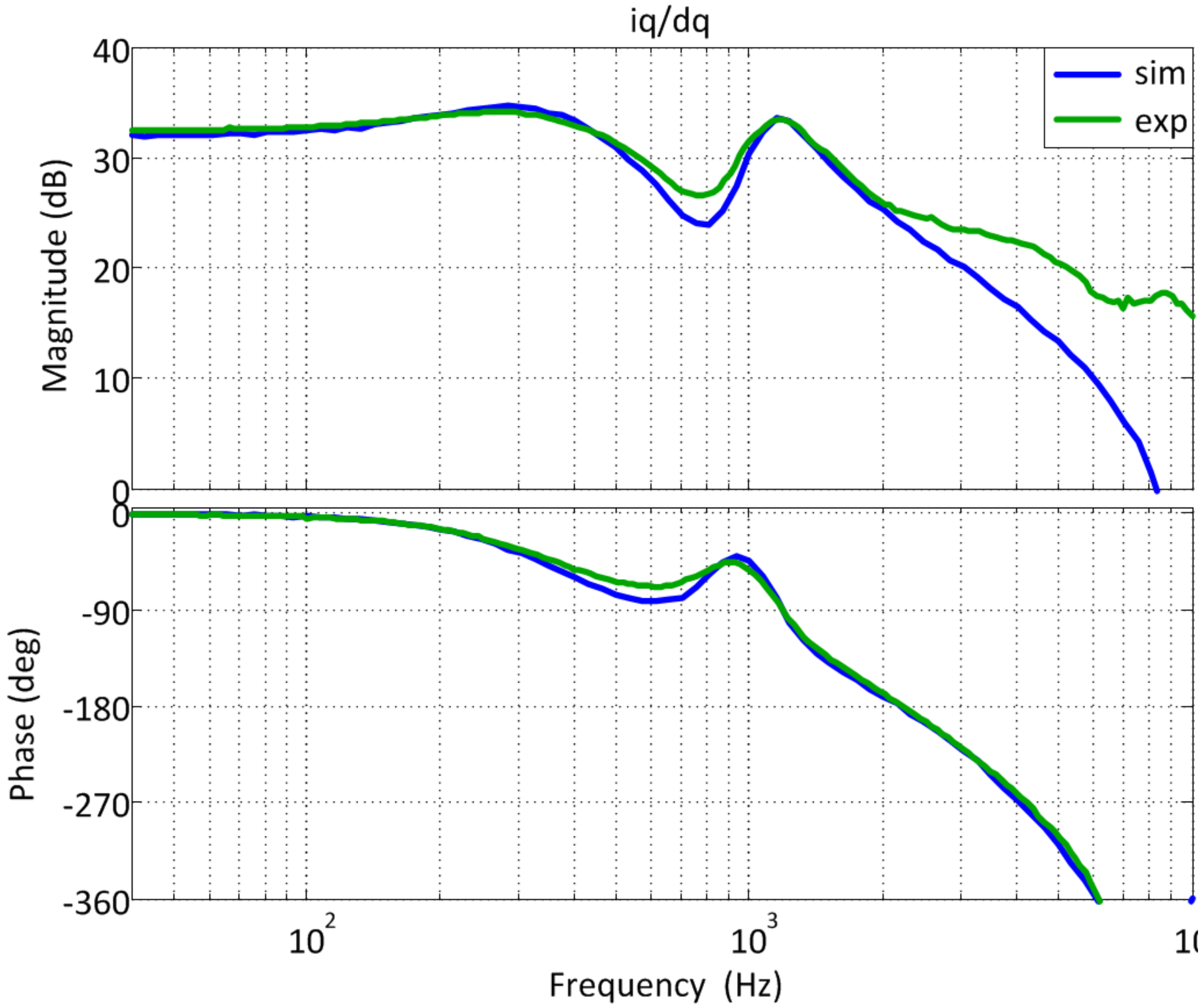

Control-to-Current Cross Transfer Functions

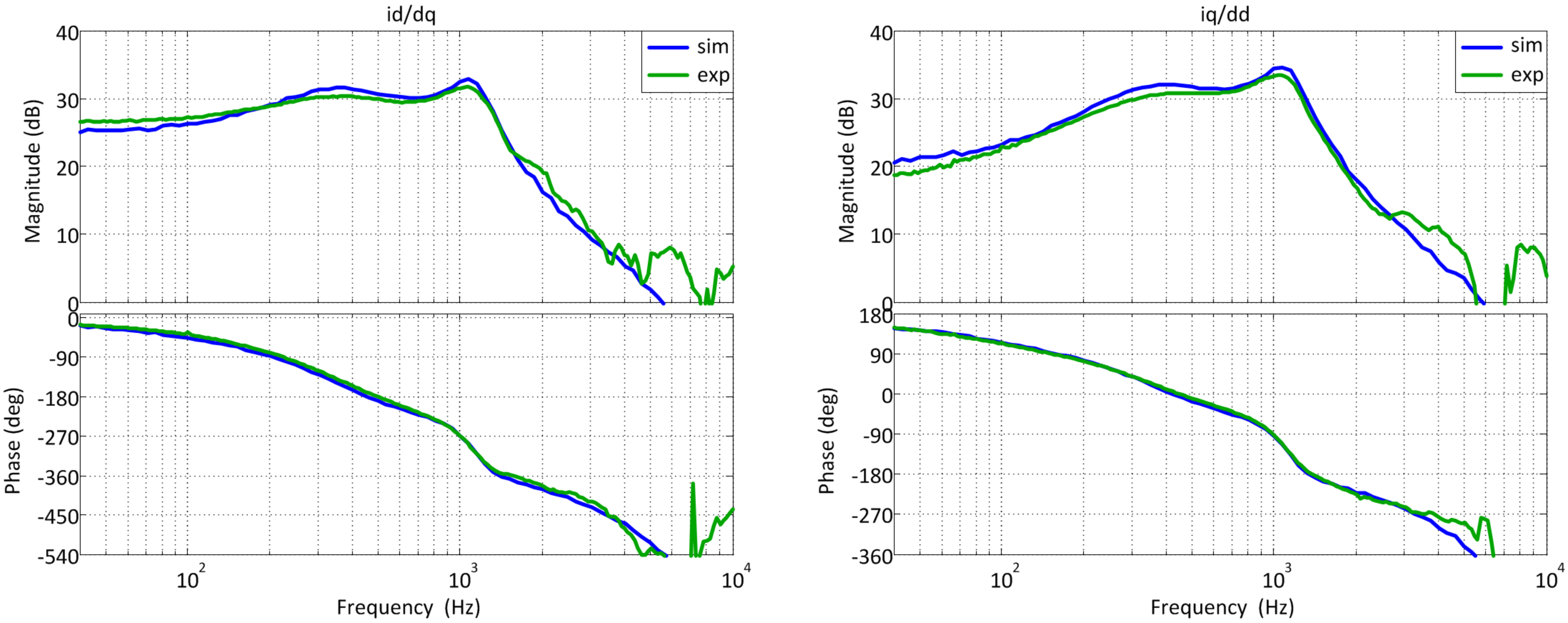

Current Loop Gain

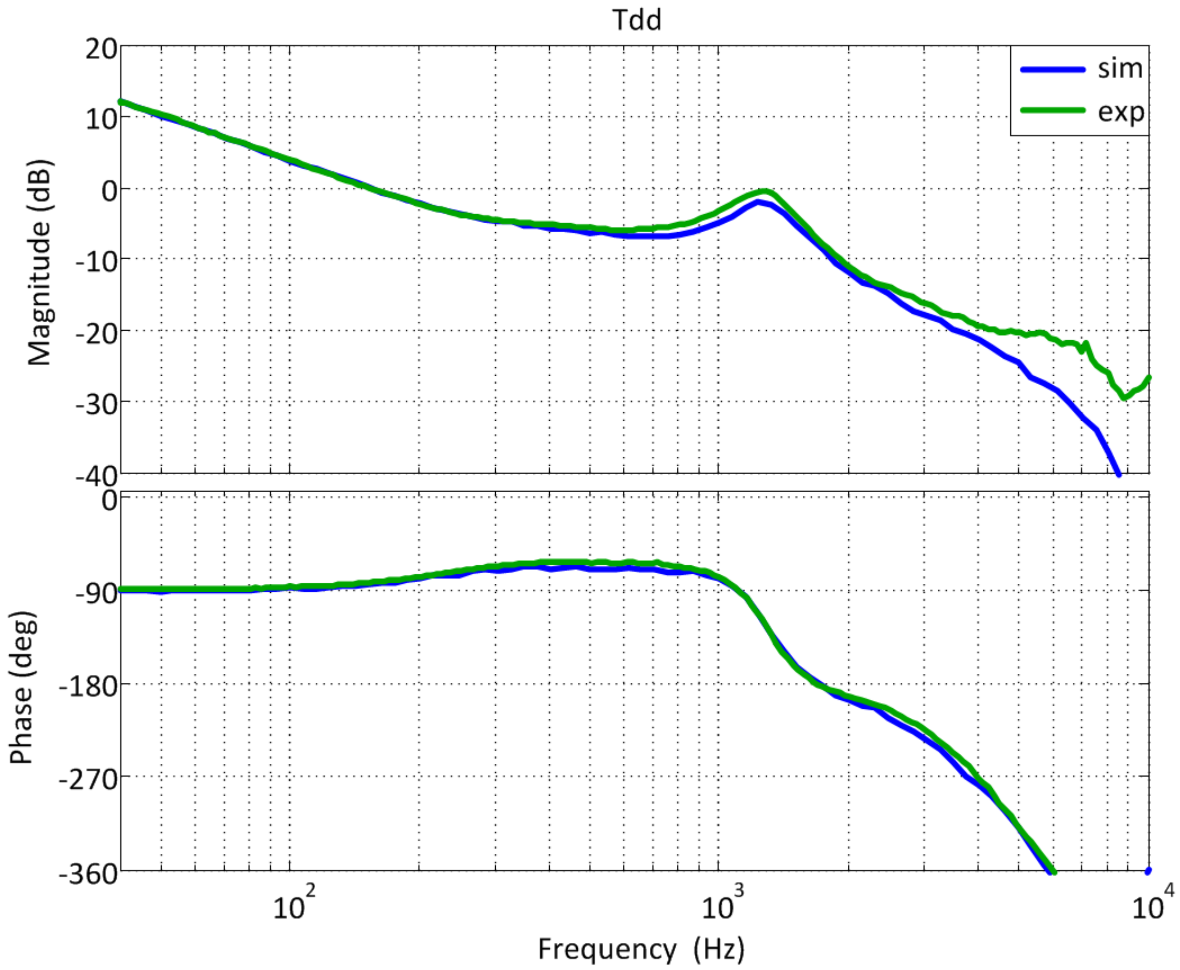

D-Channel Loop-Gain

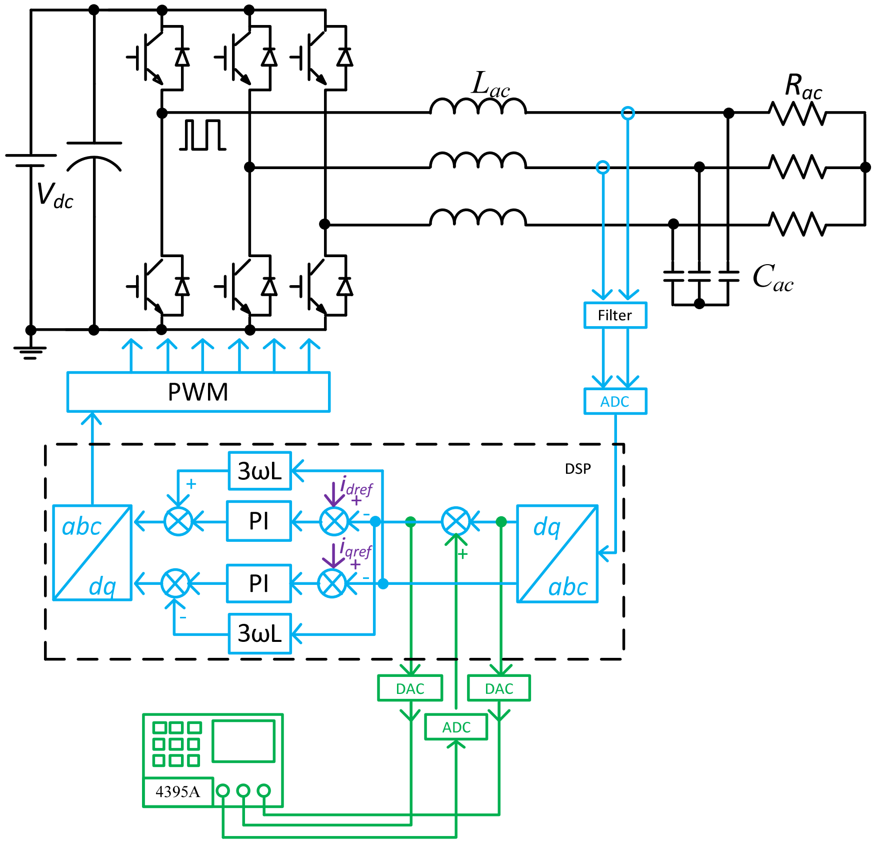

$$H_{id} = K_p + \frac{K_i}{s} \qquad H_{iq} = K_p + \frac{K_i}{s}$$

Current Regulation

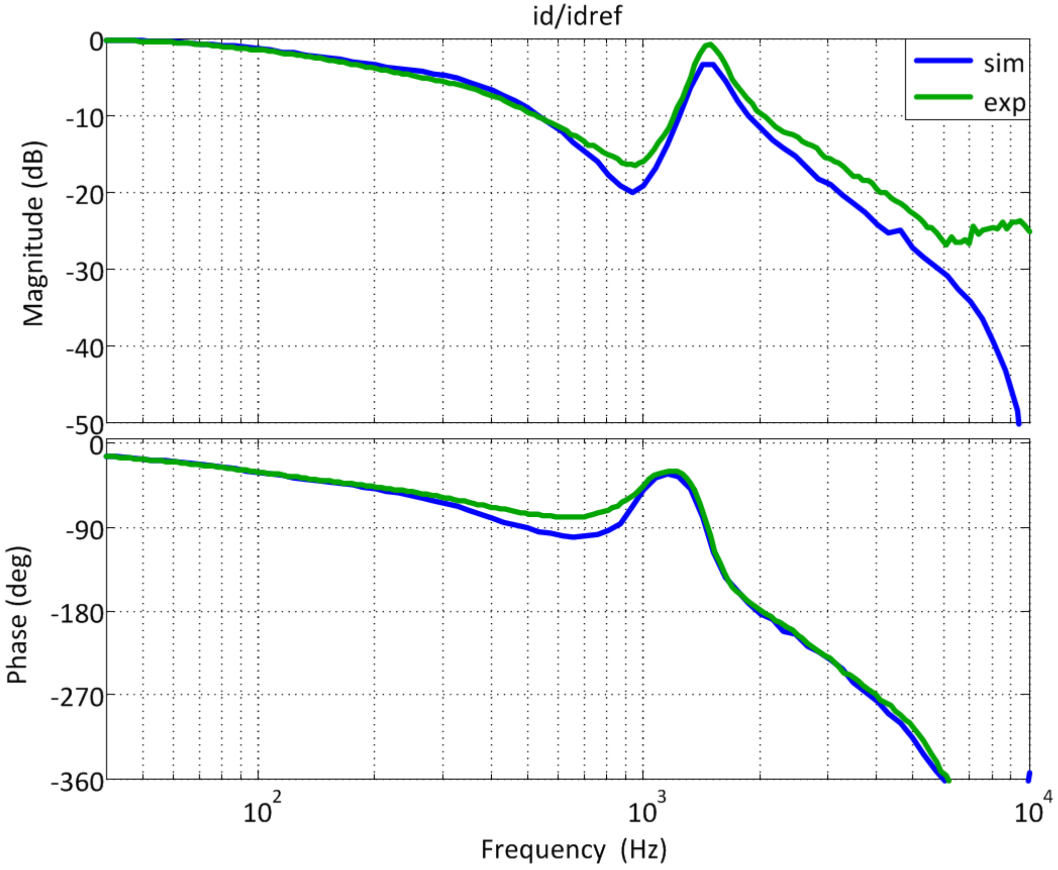

$$\frac{\tilde{i}_d}{\tilde{i}_{dref}}$$

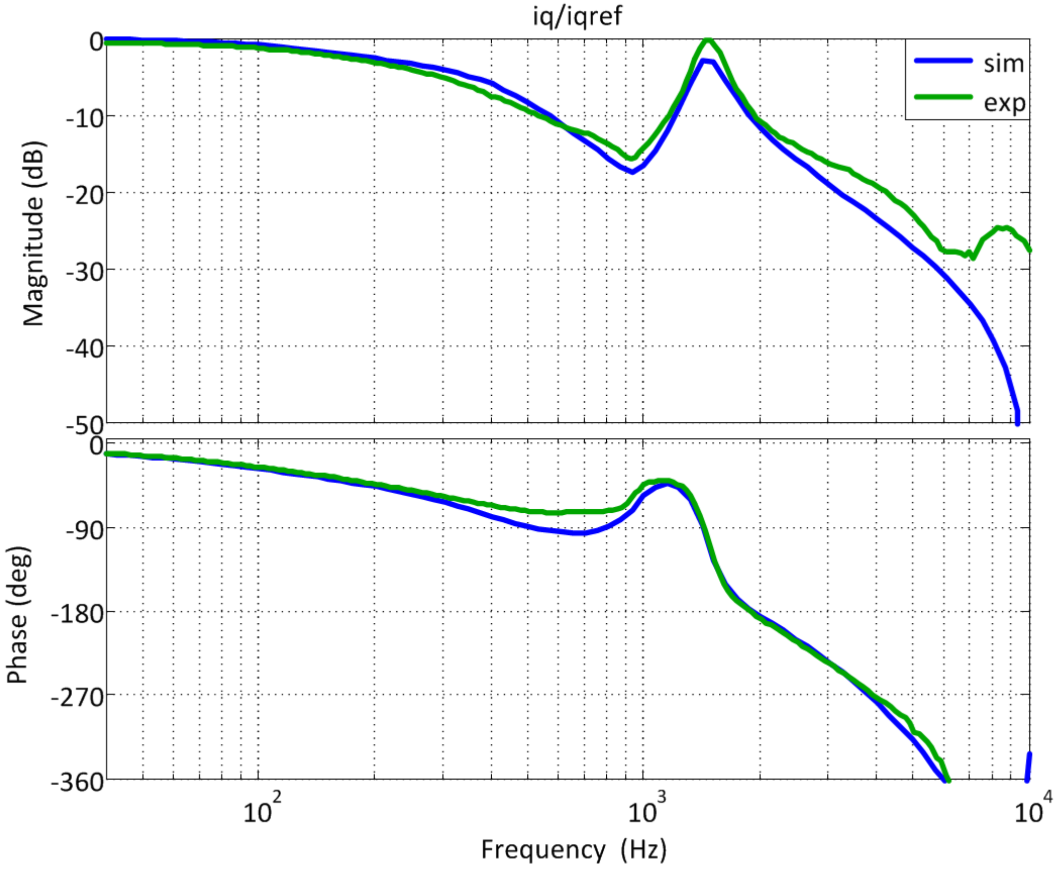

$$\frac{\tilde{i}_q}{\tilde{i}_{qref}}$$

AC Voltage Loop

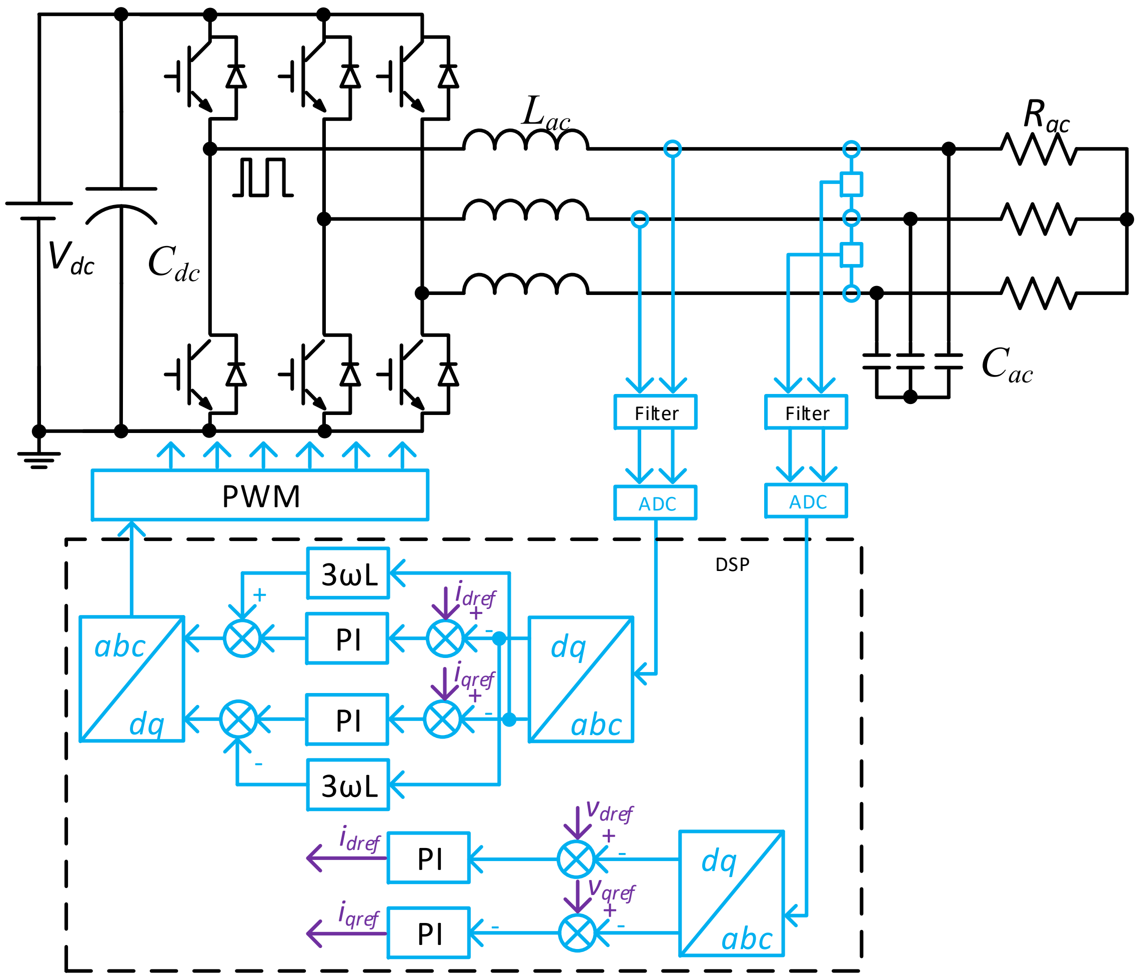

$$H_{vd} = K_p + \frac{K_i}{s}$$

$$H_{vq} = K_p + \frac{K_i}{s}$$

Current Reference-to-Voltage Transfer Function

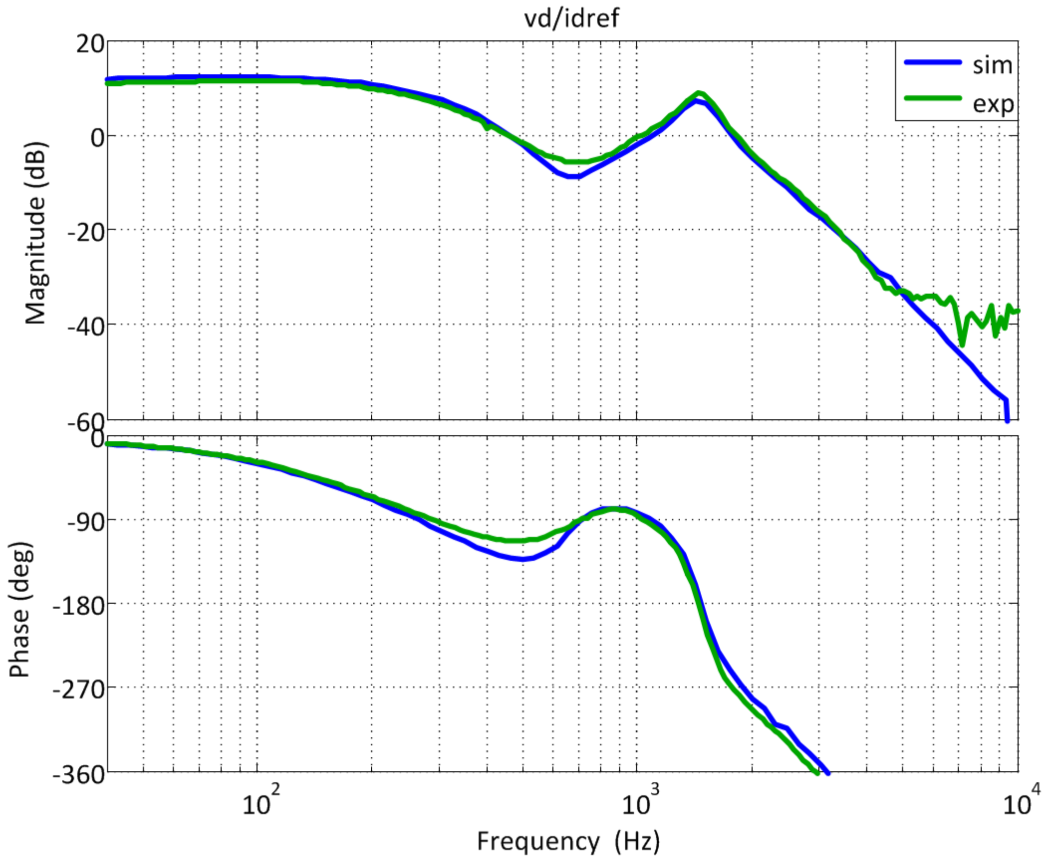

$$\frac{\tilde{v}_d}{\tilde{i}_{dref}}$$

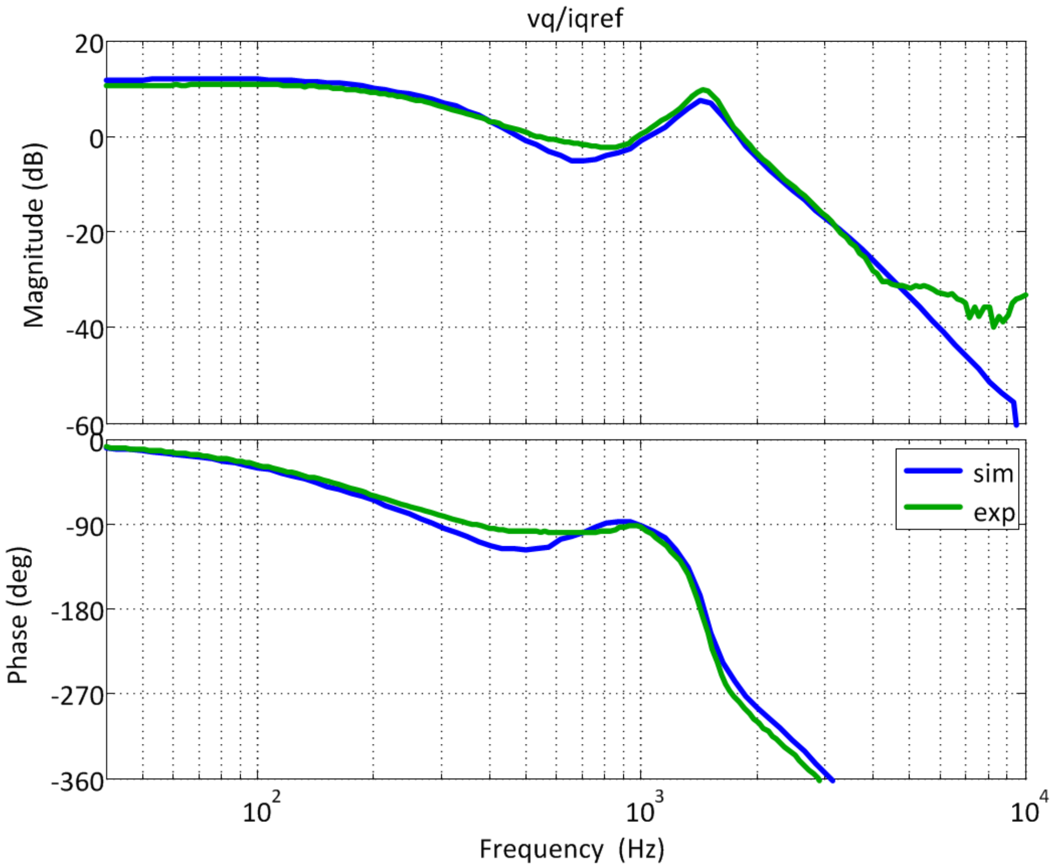

$$\frac{\tilde{v}_q}{\tilde{i}_{qref}}$$

Improving Voltage Source

DQ-Frame Decoupled Controller for VSI

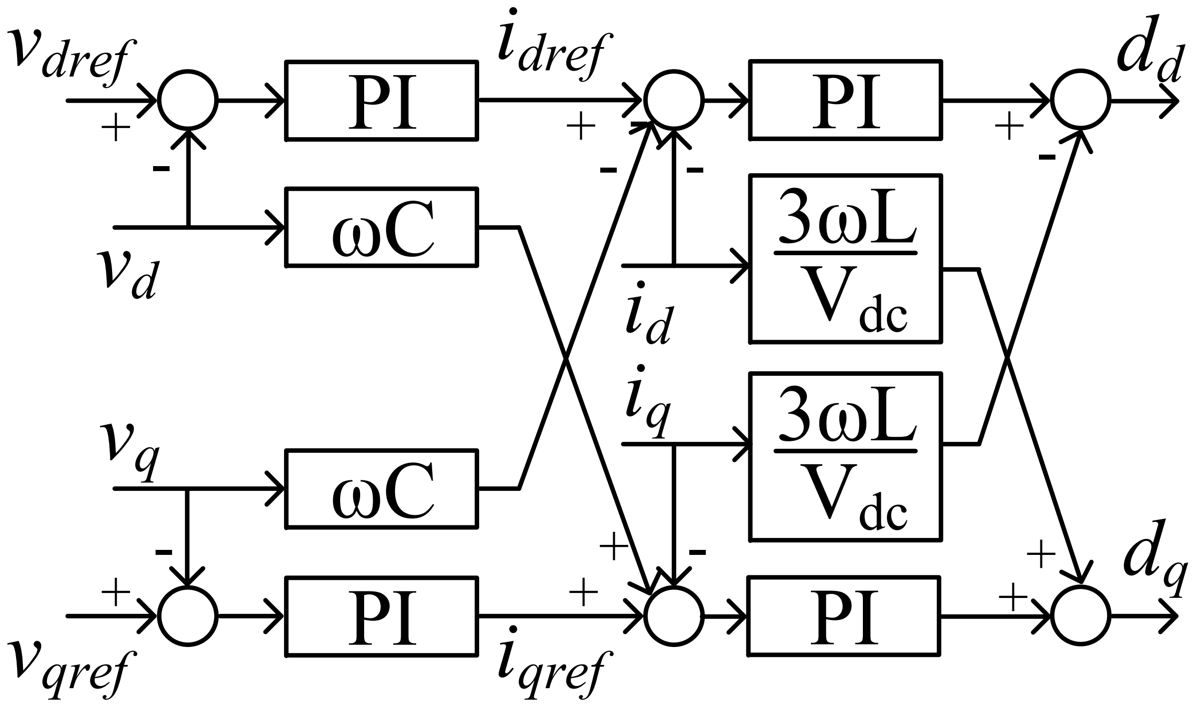

Experimental D-Q Frame Impedance

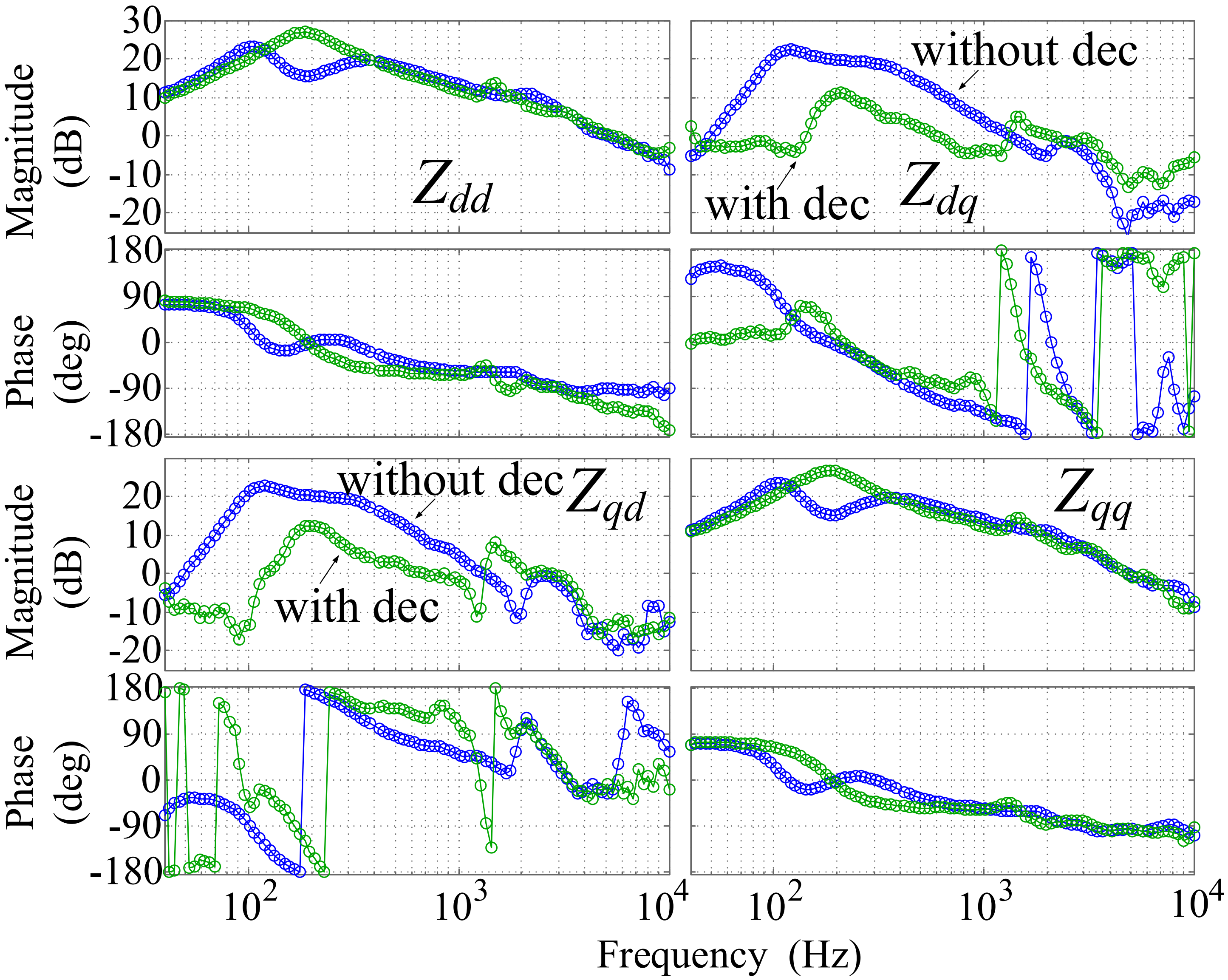

Software Frequency Response Analyzer—STATCOM

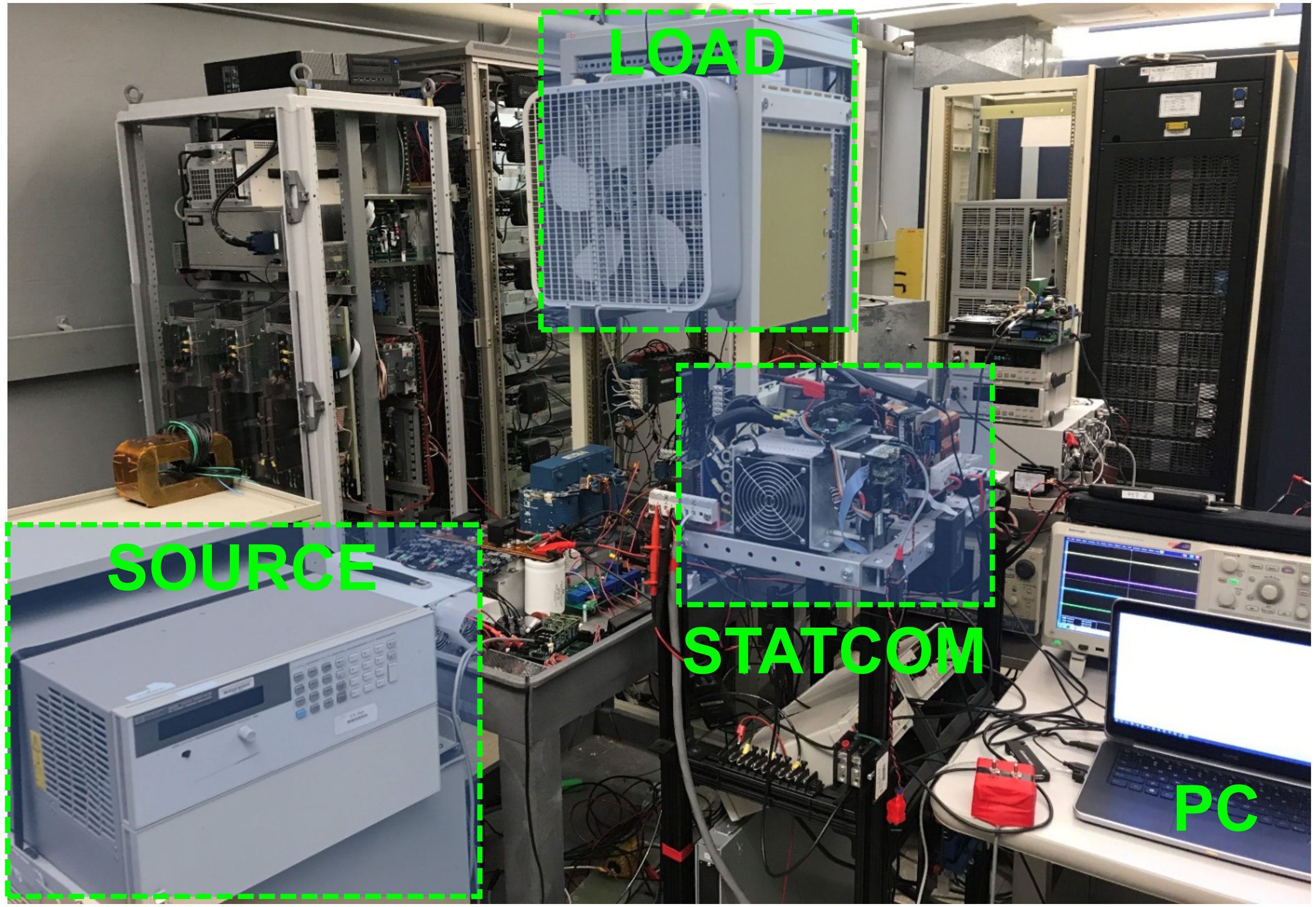

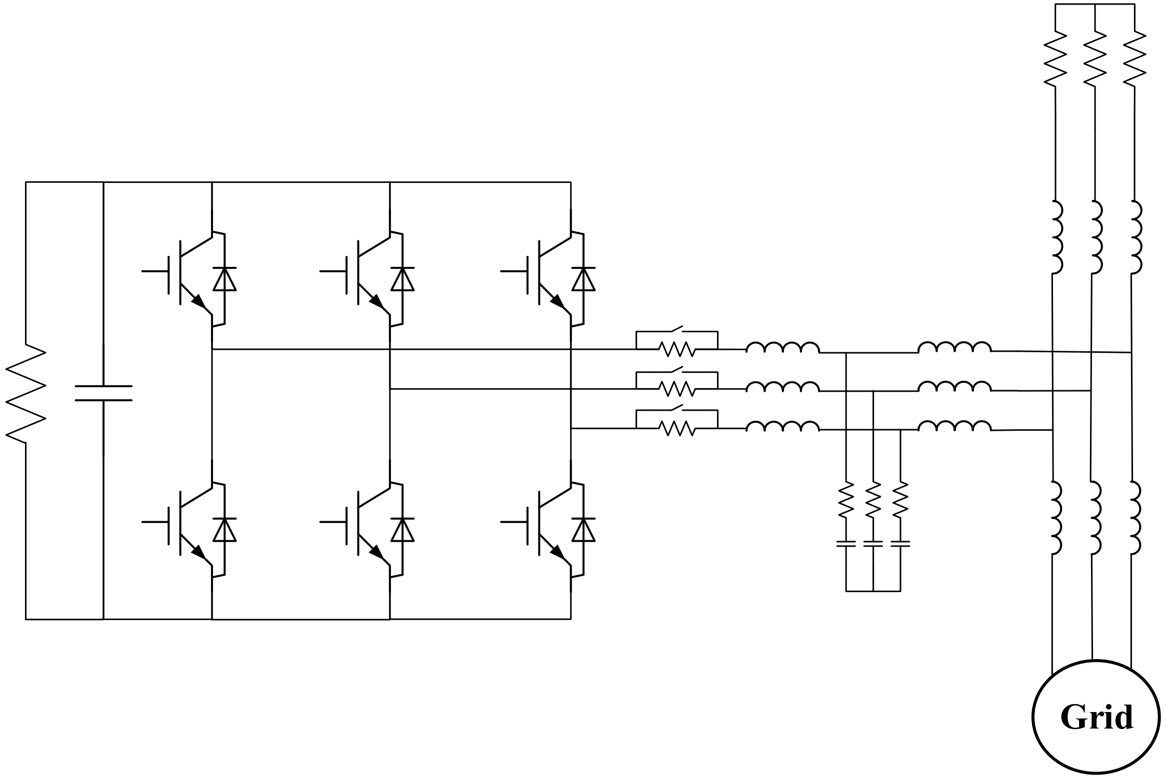

STATCOM Controller

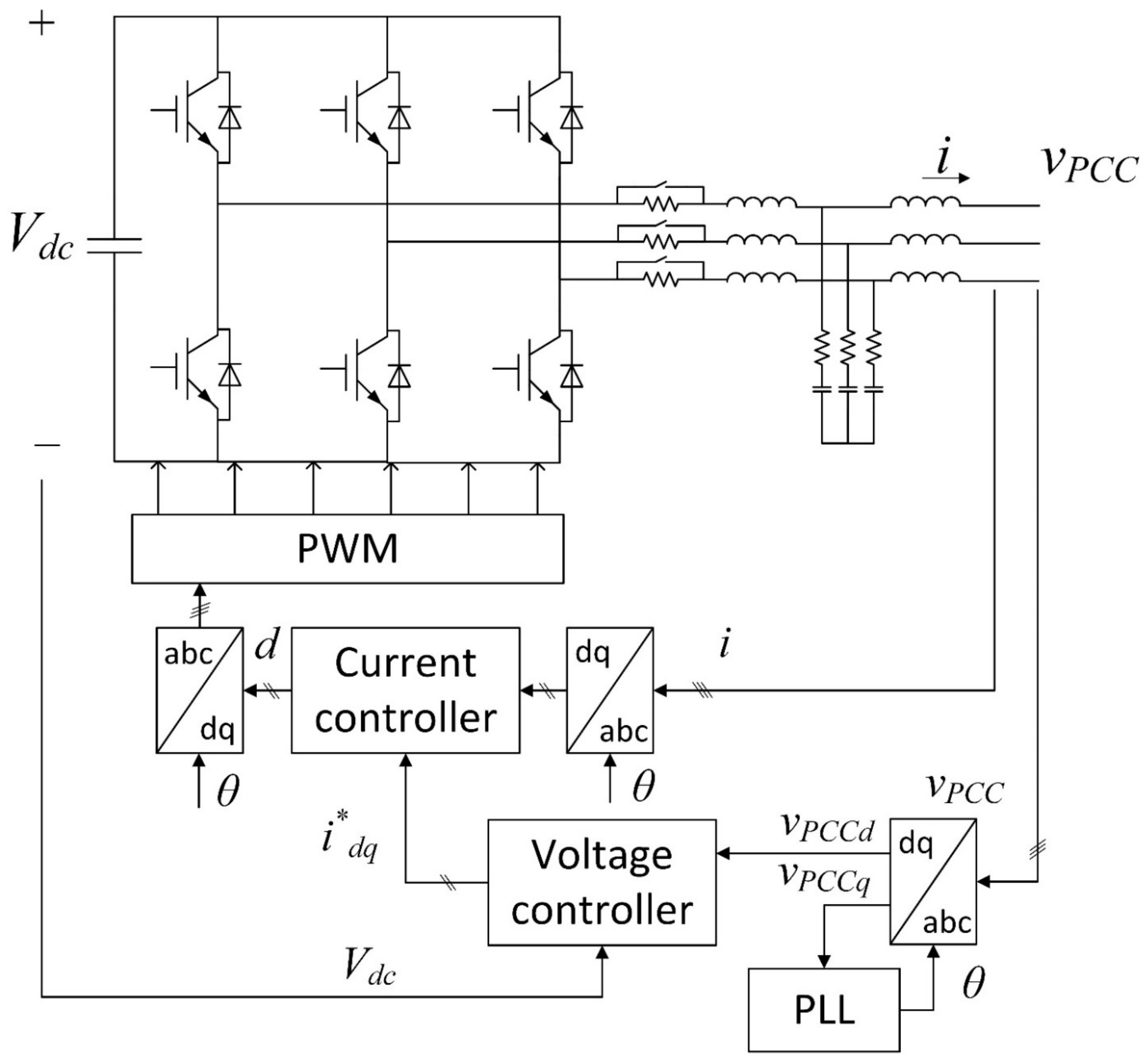

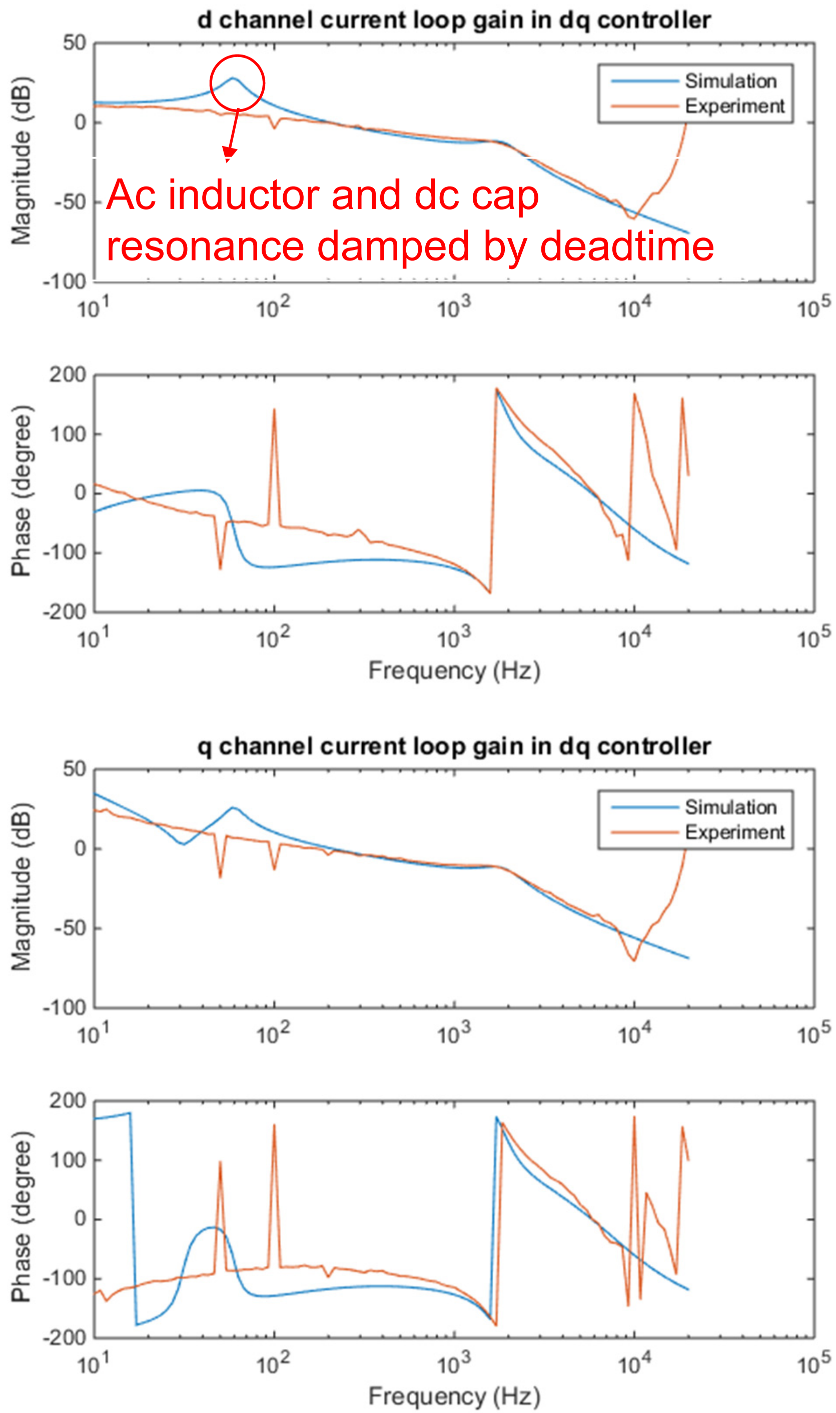

STATCOM Outer Loop-Gains

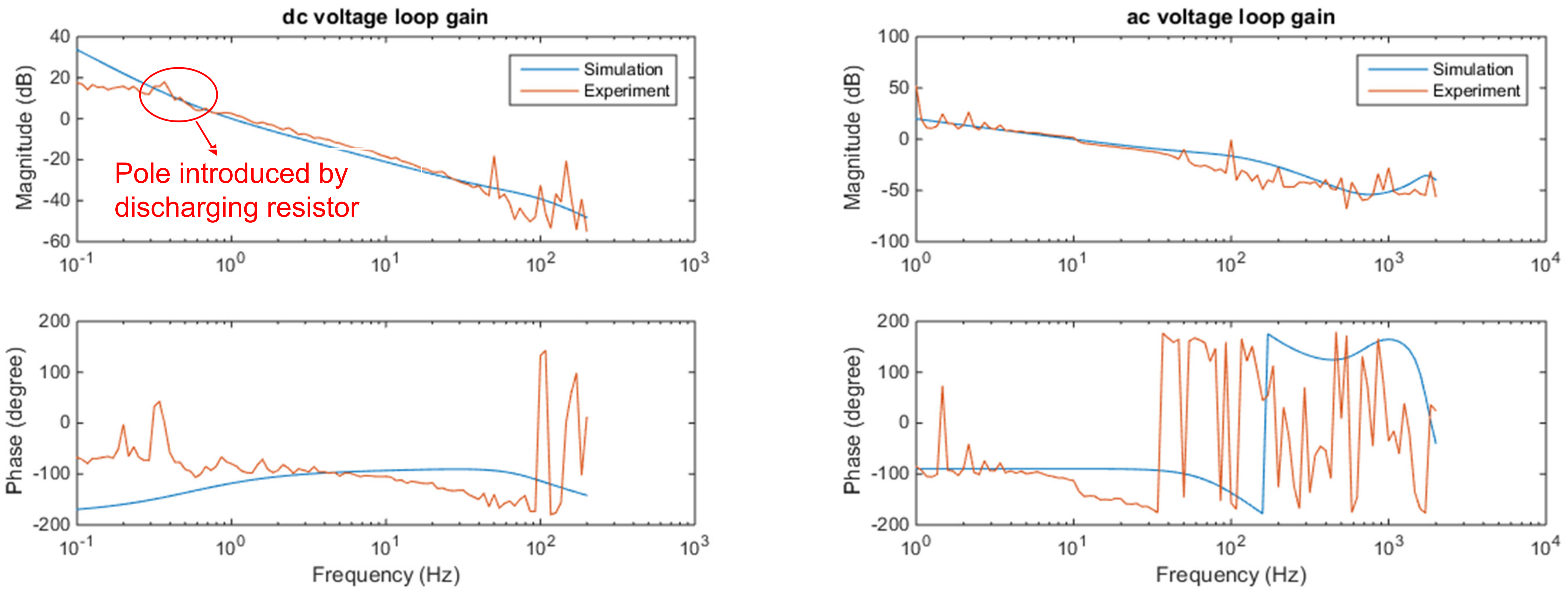

Software Frequency Response Analyzer—Boost Rectifier

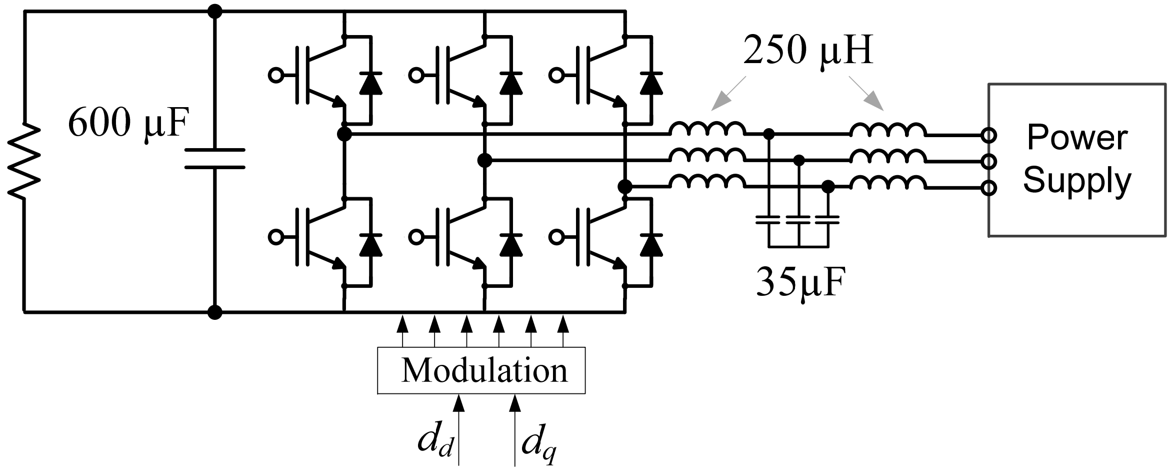

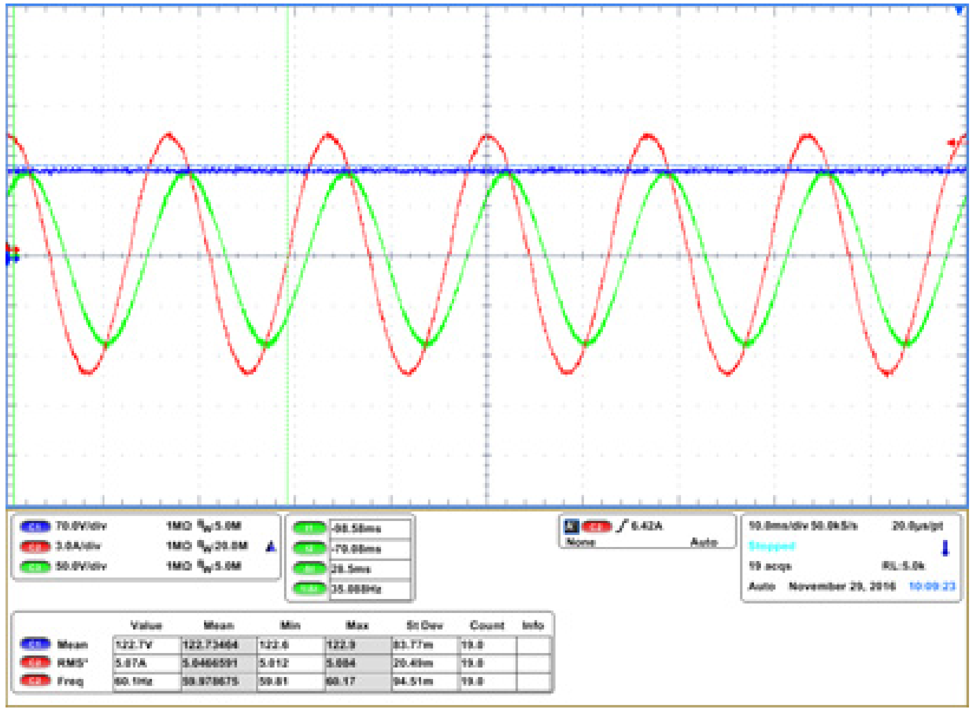

D-Axis Control-to-Current Loop-Gain

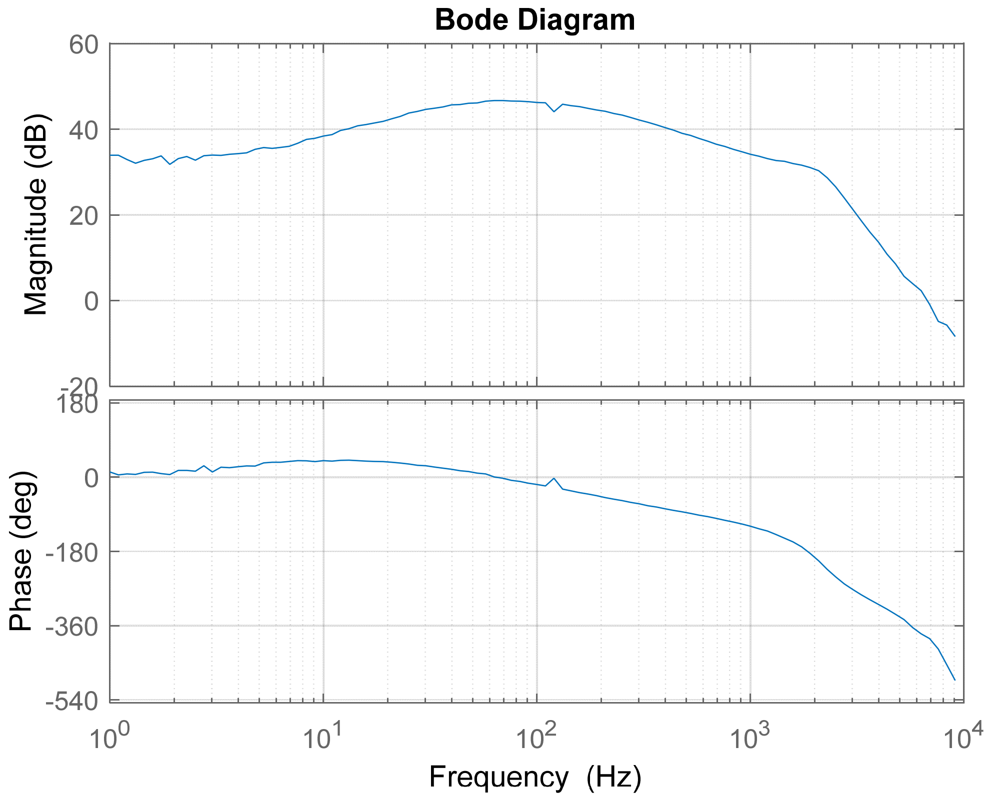

$$\frac{\tilde{i}_d}{\tilde{d}_d}$$

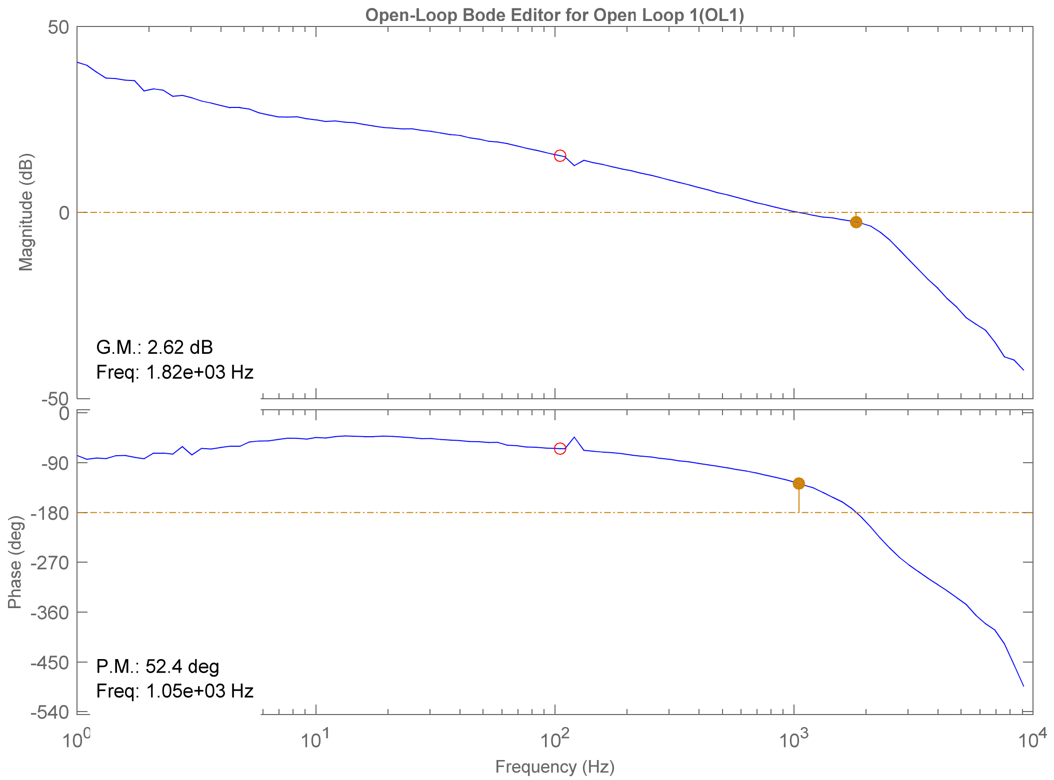

$$\frac{\tilde{i}_d}{\tilde{i}_{dref}}$$

Q-Axis Control-to-Current Loop-Gain

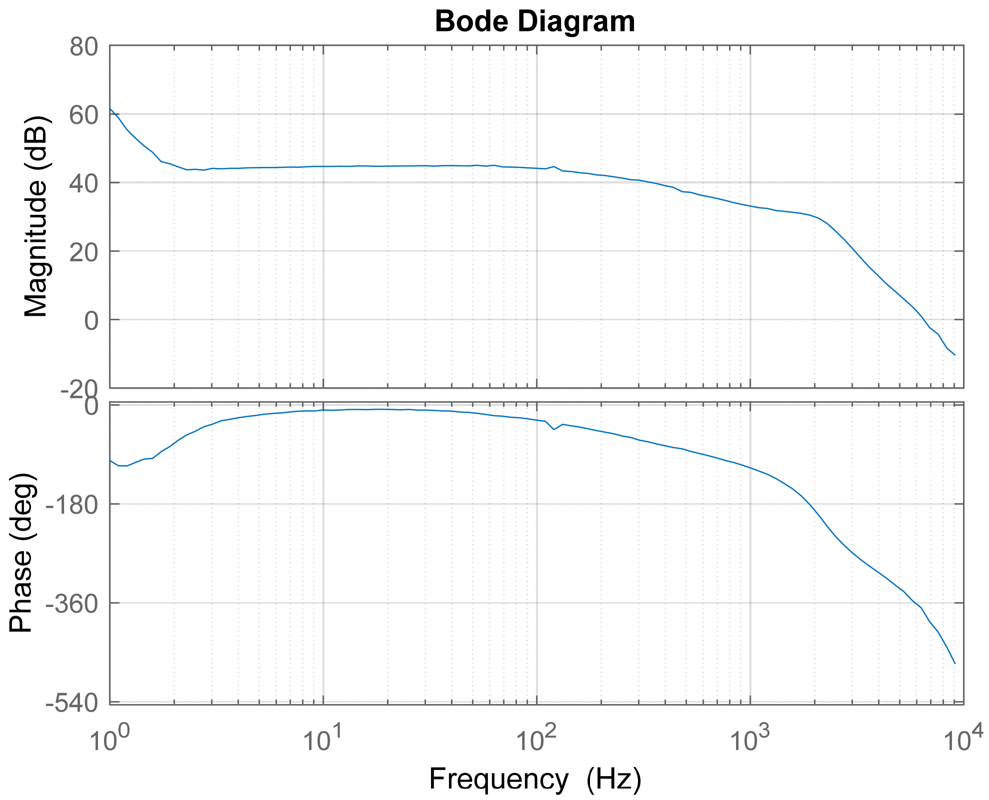

$$\frac{\tilde{i}_q}{\tilde{d}_q}$$

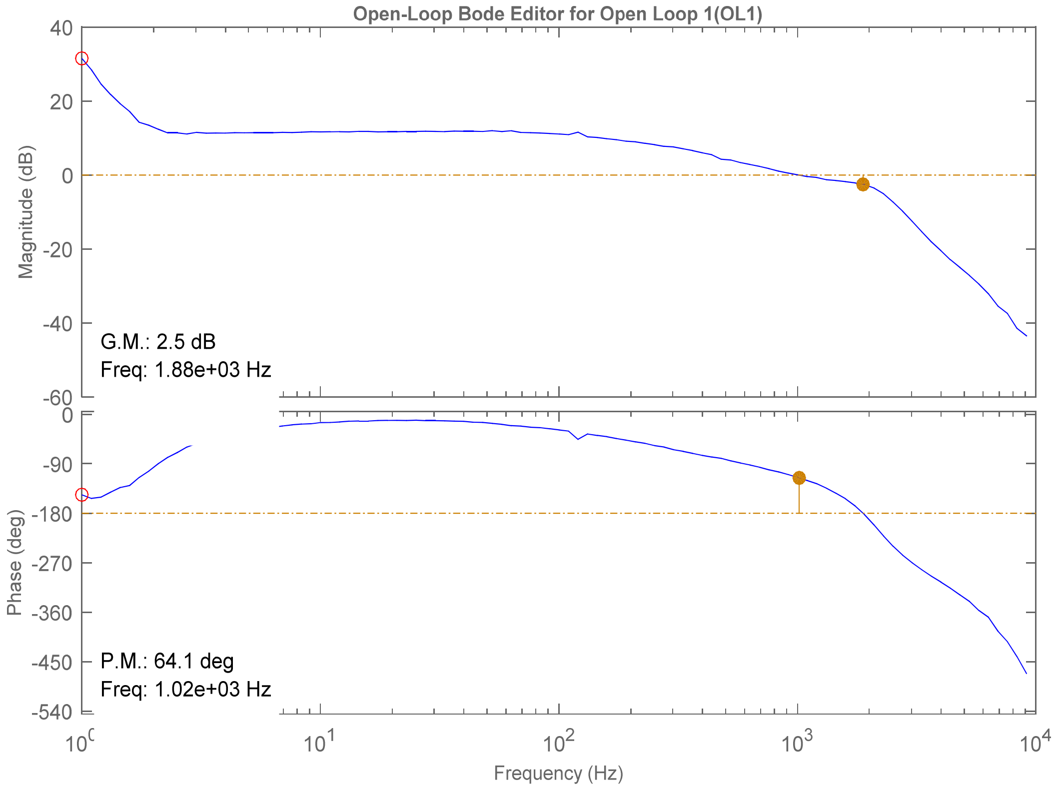

$$\frac{\tilde{i}_q}{\tilde{i}_{qref}}$$

Outline

1. Introduction
2. Mathematical Framework
3. Switching Modeling and PWM
4. Average Modeling
5. Small-Signal Modeling
6. Closed-Loop Control
7. 3-Level Converters
8. Control System Synchronization
9. AC System Interactions
10. Electronic Synchronous Machine (Voltage Controlling Converter)

Vienna (Type) Rectifier Topology Used

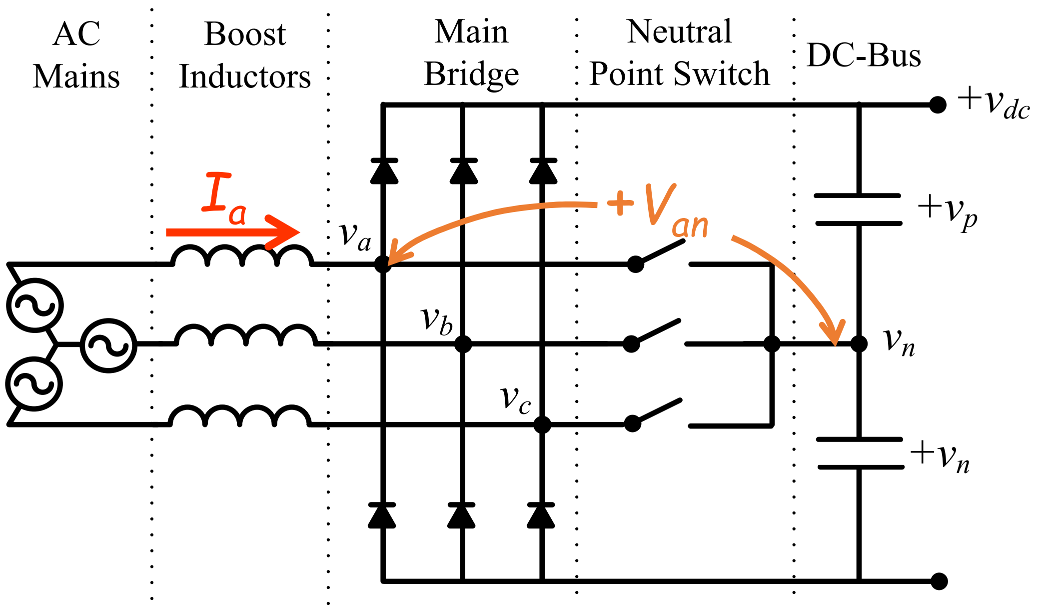

Three-level non-regenerative rectifier

Developed originally as front-end for power supplies

Has good *power density* characteristics

Space Vectors and Duty Cycles

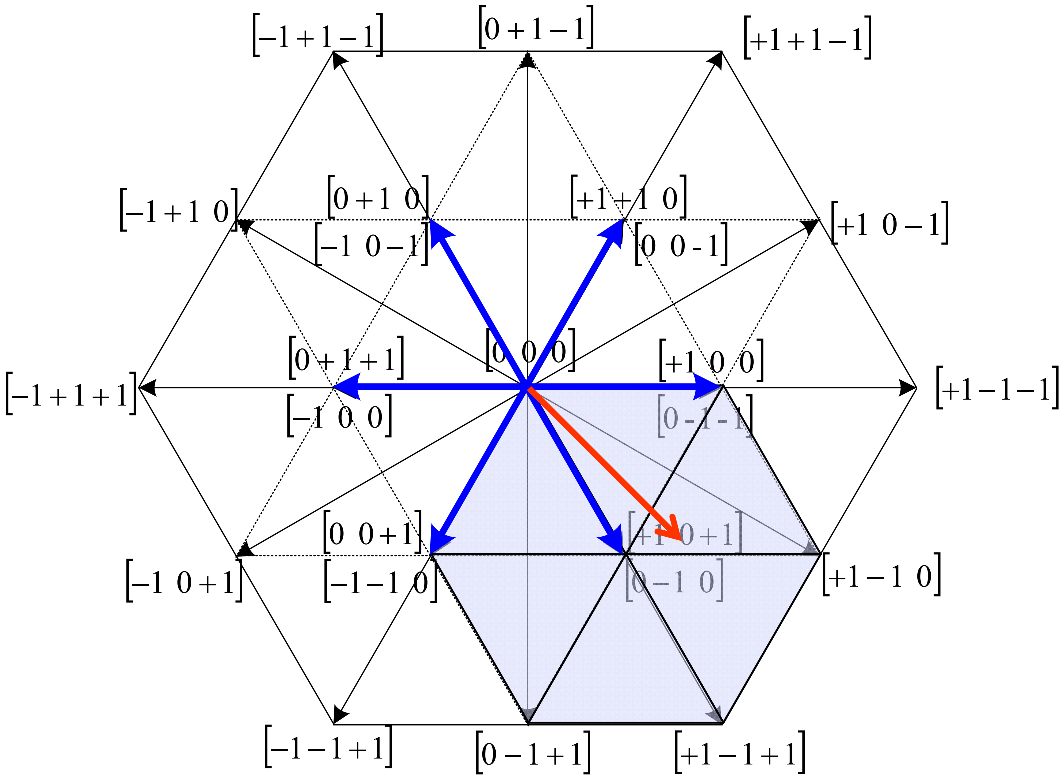

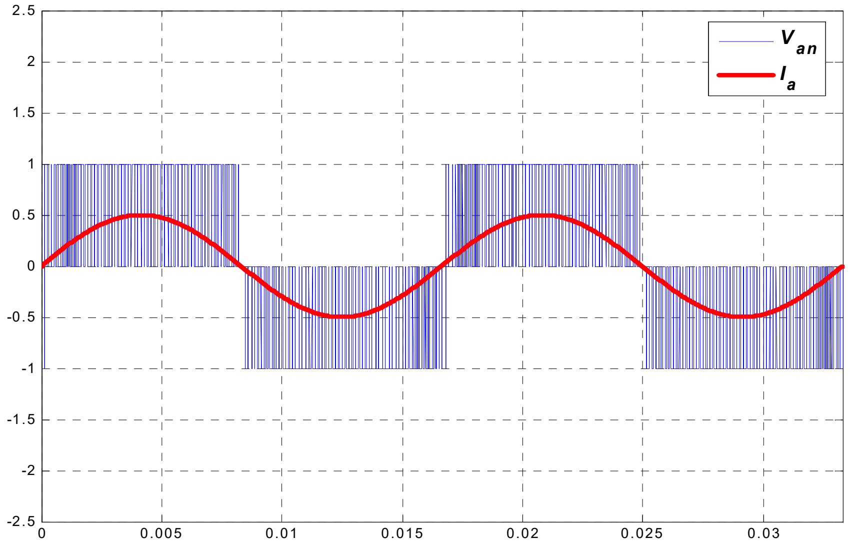

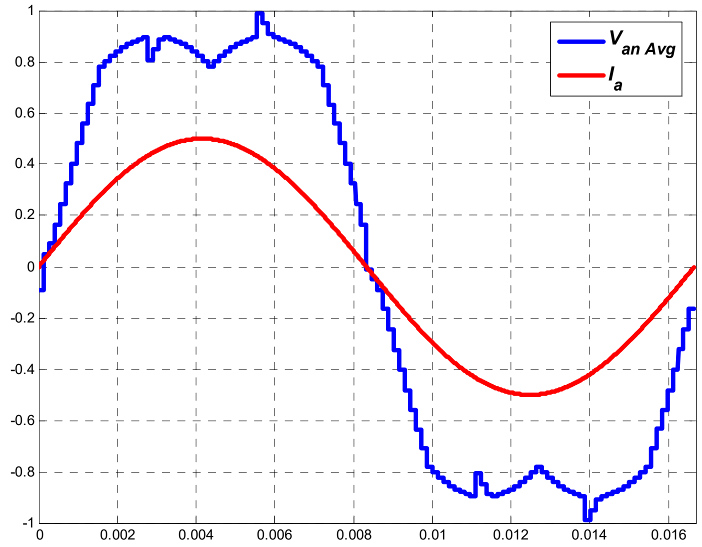

Twenty five total space vectors

Space Vectors and Duty Cycles

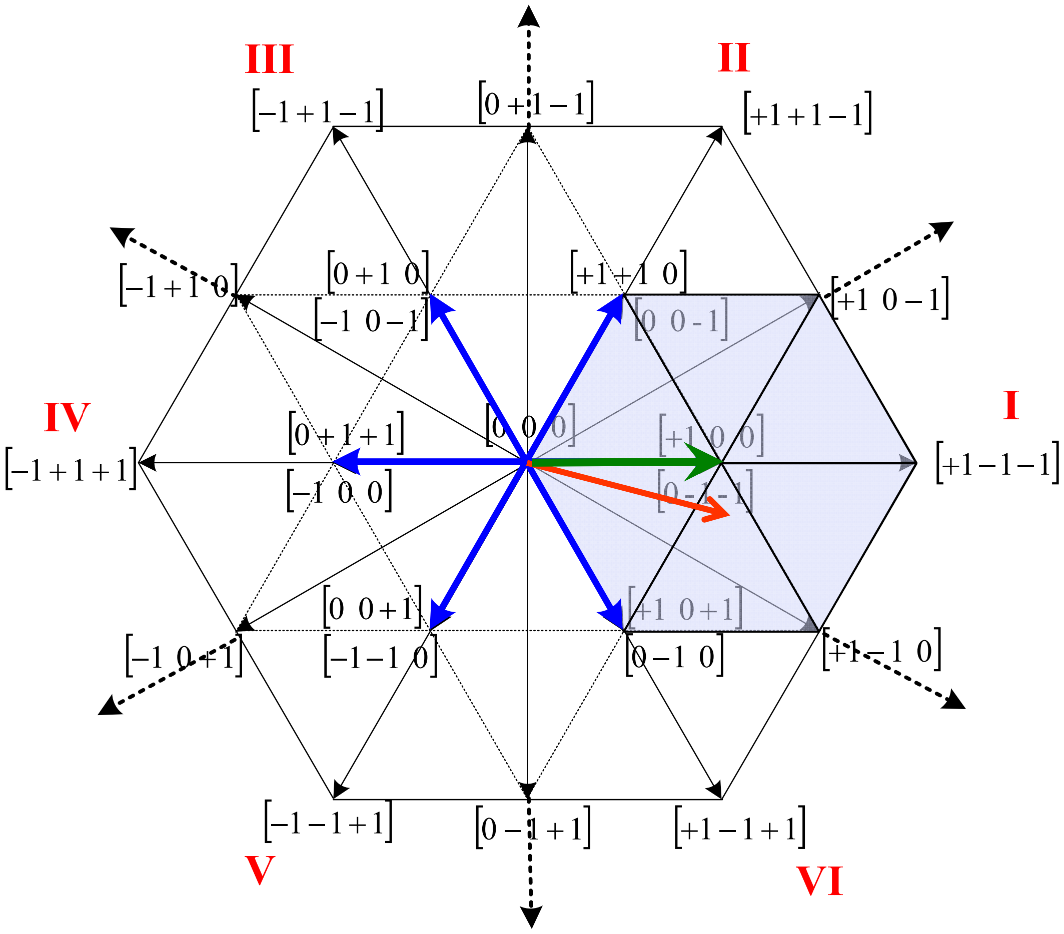

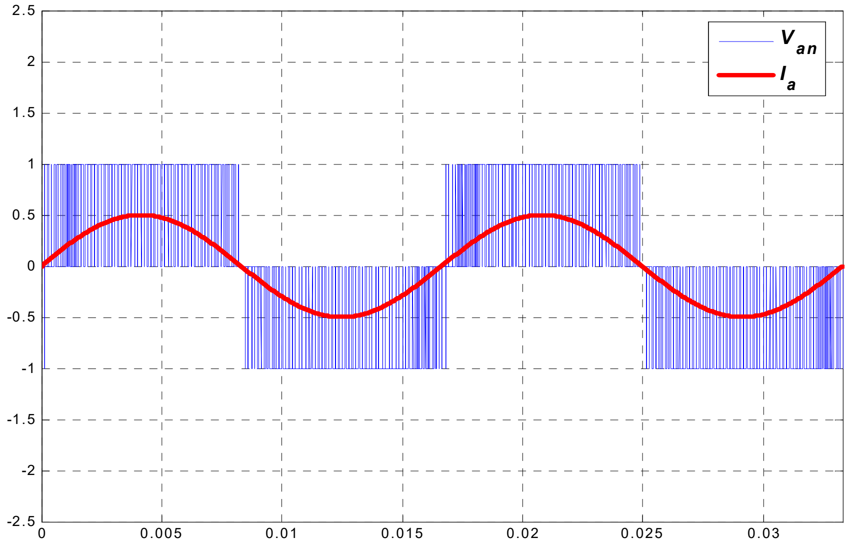

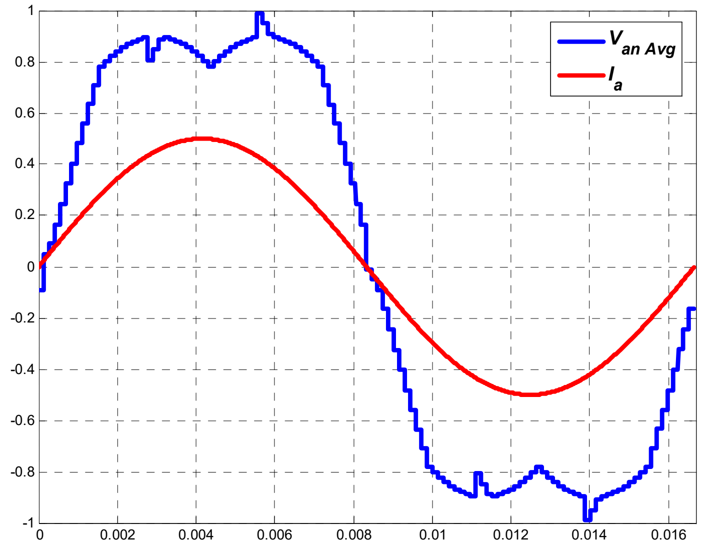

Twenty five total space vectors

Eight vectors active at a time, one double vector

Circuit-Oriented Modeling Approach

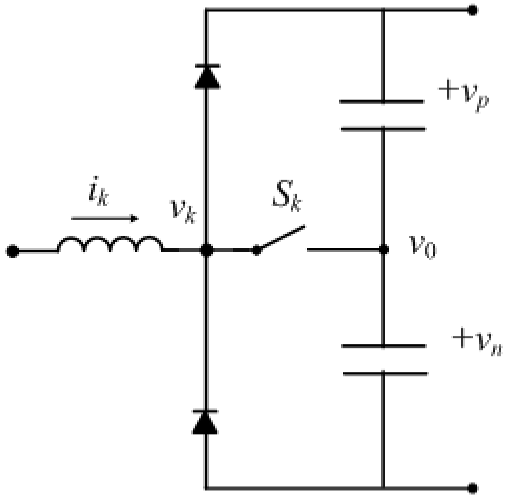

$$v_{k0} = \left(\frac{v_p + v_n}{2} sign(i_k) + \frac{v_p - v_n}{2} \right) \cdot (1 - S_k)$$

$$\frac{d}{dt} i_k = -\frac{R}{L} i_k + \frac{1}{L} v_{sk} - \frac{1}{L} \underbrace{\boxed{\left(\frac{v_p + v_n}{2} sign(i_k) + \frac{v_p - v_n}{2} \right)(1 - S_k)}}_{v_{k0}} - \frac{1}{L} v_{0n}$$

$$\frac{d}{dt} v_{p/n} = \pm \frac{1}{2C} \sum_{k=a,b,c} (1 - S_k) \cdot i_k \cdot [(1 \pm sign(i_k))] - \frac{1}{C} i_{dc}$$

Switching-Transfer-Function Based Modeling

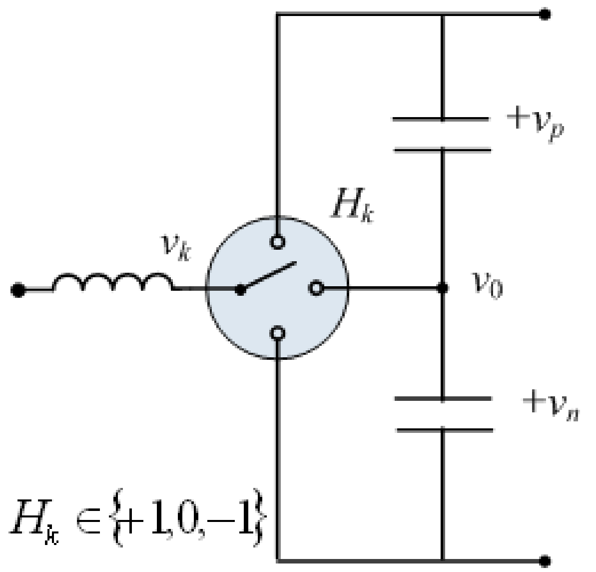

$$v_{k0} = H_k \frac{v_p + v_n}{2} + |H_k| \frac{v_p - v_n}{2}$$

$$v_{k0} = H_k \frac{H_k + 1}{2} v_p - H_k \frac{H_k - 1}{2} v_n$$

$$v_{k0} = S_{kp} v_p - S_{kn} v_n$$

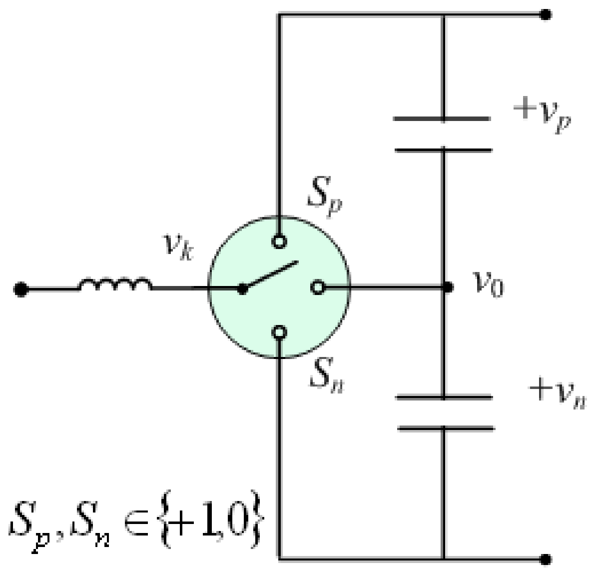

Phase-leg model is equivalent to three-level NPC converter

Assumption:
Switching functions S_{kp} comply with topological restrictions of Vienna-type rectifiers

Switching and Average Models in abc-Coordinates

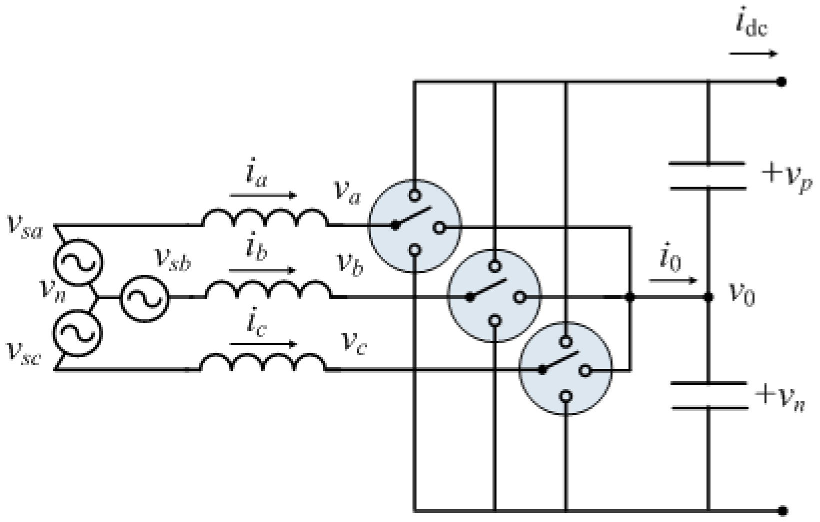

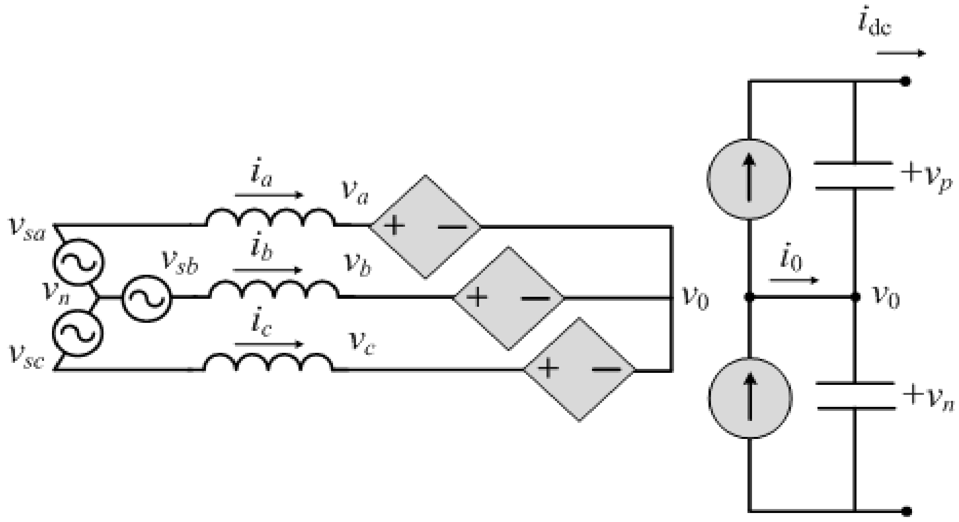

$$\frac{d}{dt}i_k = -\frac{R}{L}i_k + \frac{1}{L}v_{sk} - \frac{1}{L}\left(S_{kp}v_p - S_{kn}v_n\right) - \frac{1}{L}v_{0n}$$

$$\frac{d}{dt}v_p = \frac{1}{C}\sum_{k=a,b,c} S_{kp} \cdot i_k - \frac{1}{C}i_{dc}$$

$$\frac{d}{dt}v_n = -\frac{1}{C}\sum_{k=a,b,c} S_{kn} \cdot i_k - \frac{1}{C}i_{dc}$$

$$\frac{d}{dt}i_k = -\frac{R}{L}i_k + \frac{1}{L}v_{sk} - \frac{1}{L}\left(d_{kp}v_p - d_{kn}v_n\right) - \frac{1}{L}v_{0n}$$

$$\frac{d}{dt}v_p = \frac{1}{C}\sum_{k=a,b,c} d_{kp} \cdot i_k - \frac{1}{C}i_{dc}$$

$$\frac{d}{dt}v_n = -\frac{1}{C}\sum_{k=a,b,c} d_{kn} \cdot i_k - \frac{1}{C}i_{dc}$$

Average Model in D-Q Frame

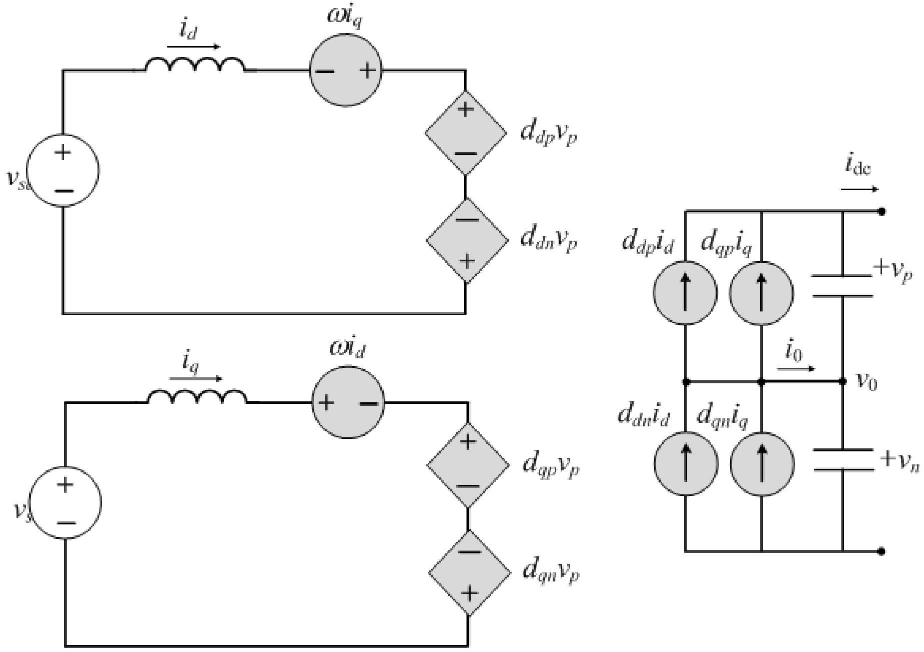

$$\frac{d}{dt}\begin{bmatrix} i_d \\ i_q \end{bmatrix} = -\frac{R}{L}\begin{bmatrix} i_d \\ i_q \end{bmatrix} + \frac{1}{L}\begin{bmatrix} v_{sd} \\ v_{sq} \end{bmatrix} - \frac{1}{L}\begin{bmatrix} d_{dp} & -d_{dn} \\ d_{qp} & -d_{qn} \end{bmatrix}\begin{bmatrix} v_p \\ v_n \end{bmatrix} - \frac{1}{L}\begin{bmatrix} v_{0n} \\ v_{0n} \end{bmatrix}$$

$$\frac{d}{dt}\begin{bmatrix} v_p \\ v_n \end{bmatrix} = \frac{1}{C}\begin{bmatrix} d_{dp} & -d_{dn} \\ d_{qp} & -d_{qn} \end{bmatrix}^T \begin{bmatrix} i_d \\ i_q \end{bmatrix} - \frac{1}{C}\begin{bmatrix} i_{dc} \\ i_{dc} \end{bmatrix}$$

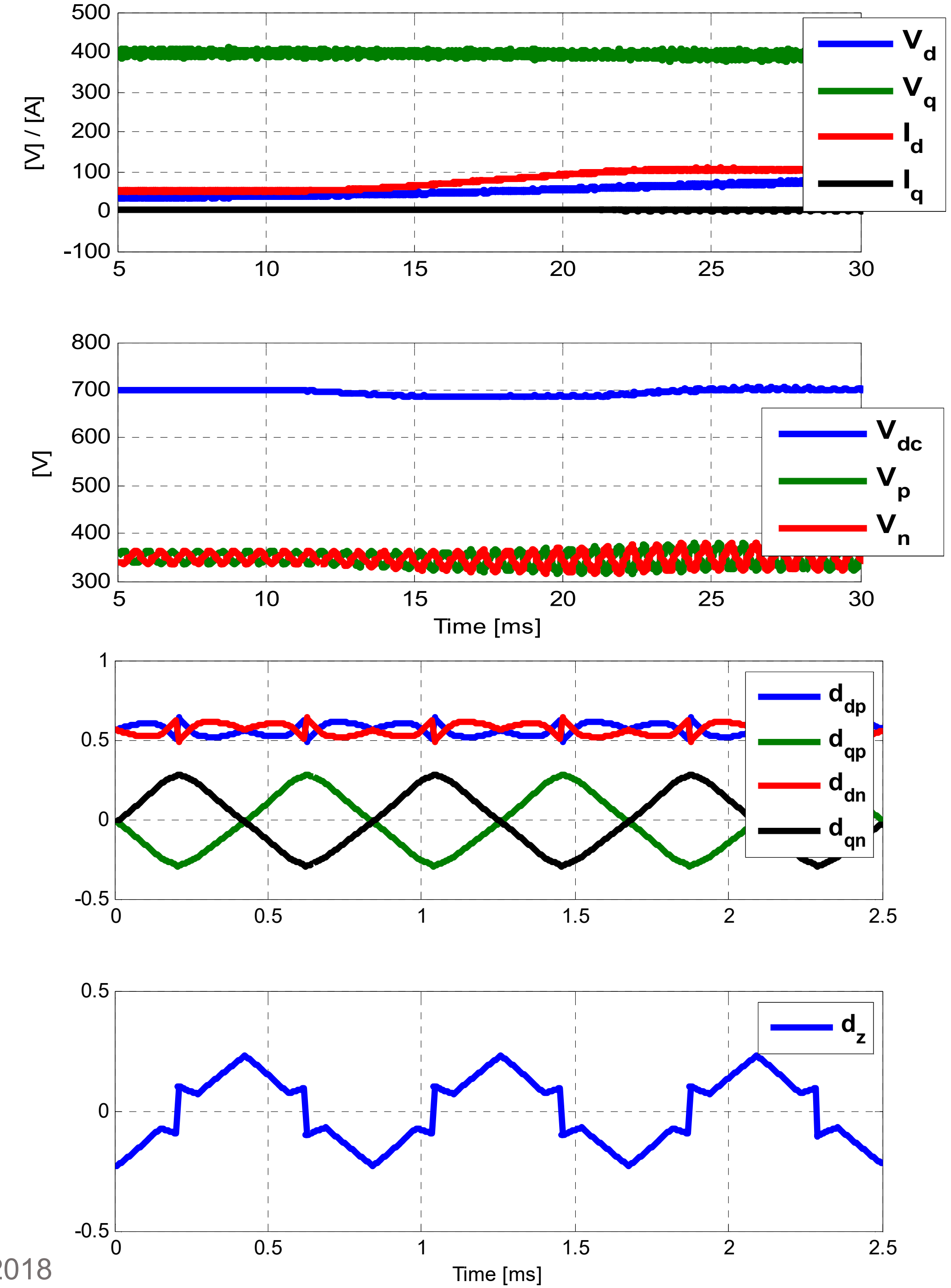

D & Q Axes Current-Control Loop-Gains

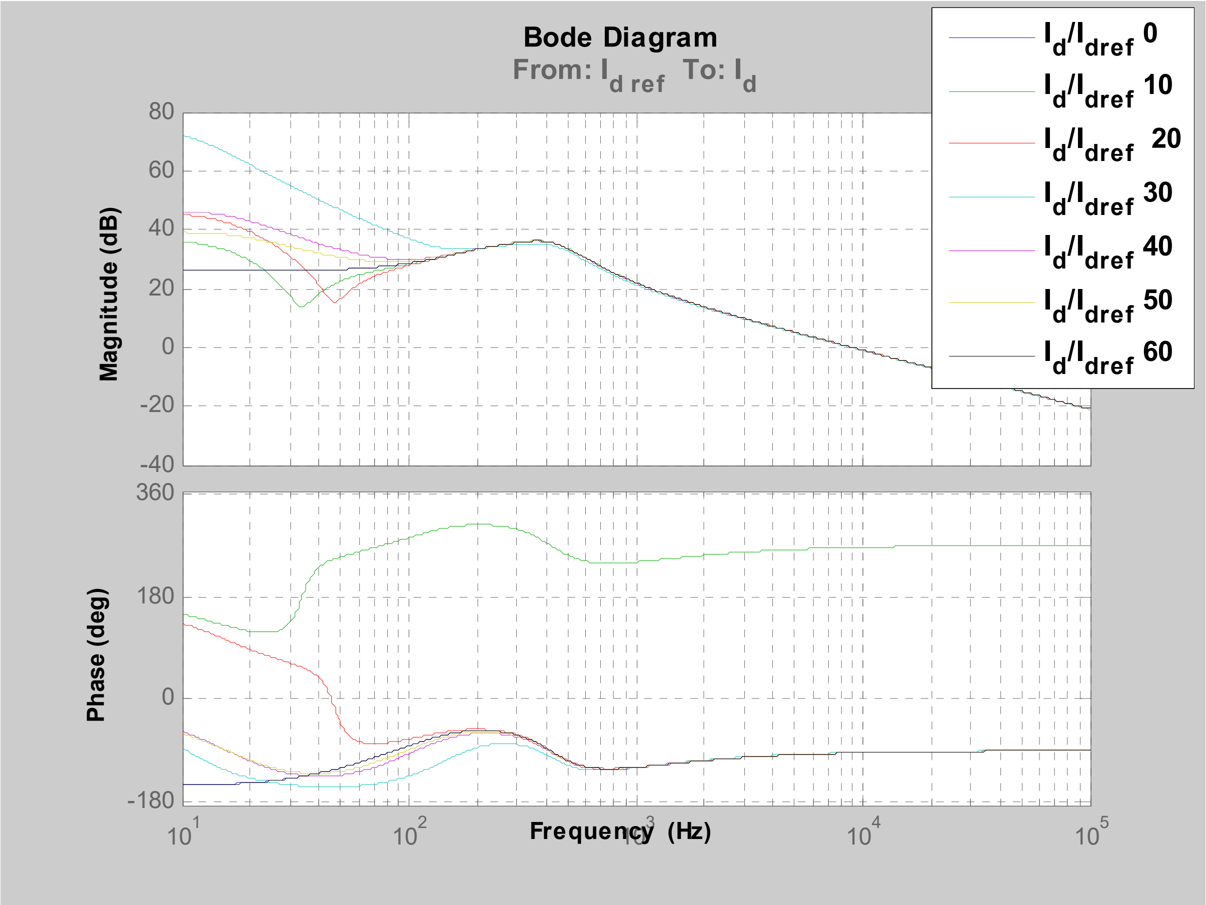

$$\frac{\tilde{i}_d}{\tilde{i}_{dref}}$$

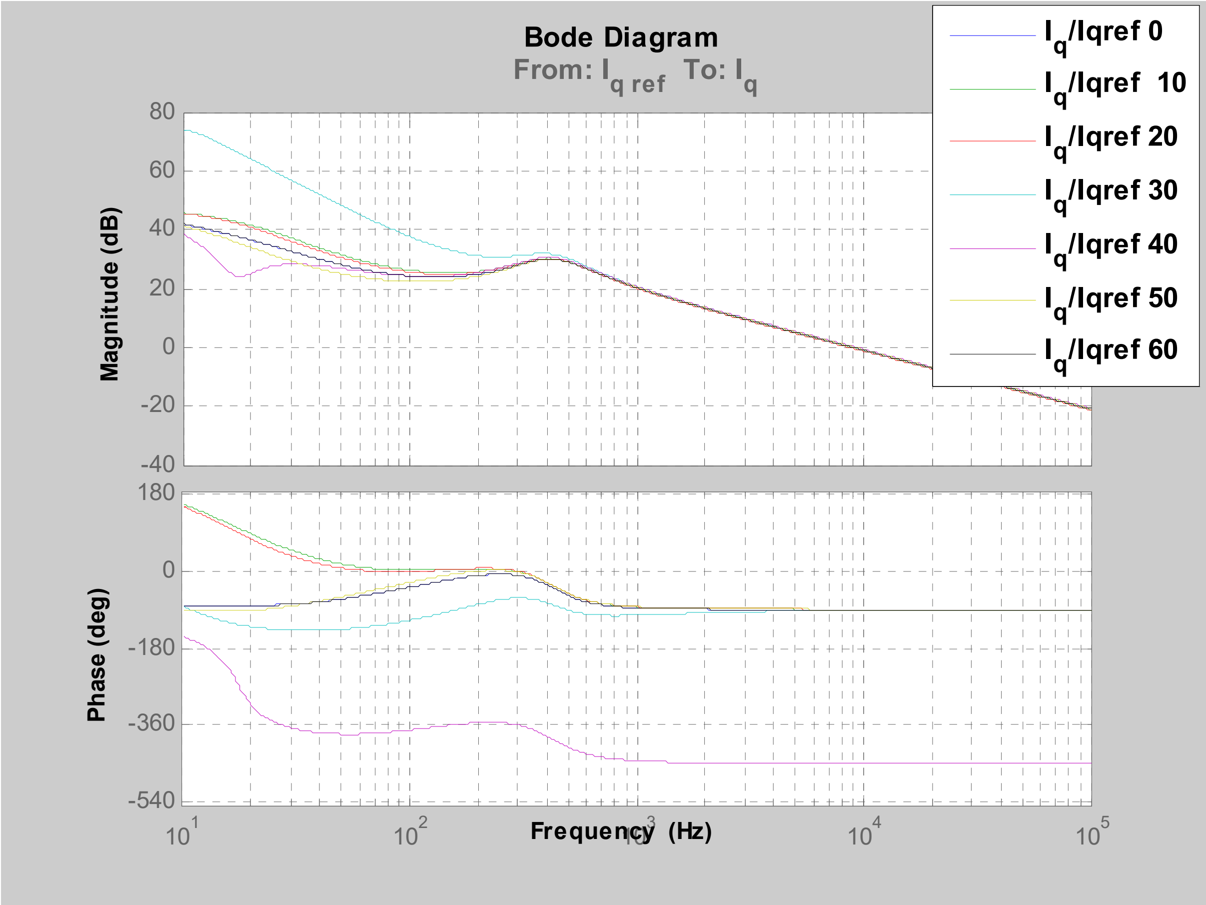

$$\frac{\tilde{i}_q}{\tilde{i}_{qref}}$$

Neutral-Point Loop-Gain and Output Impedance

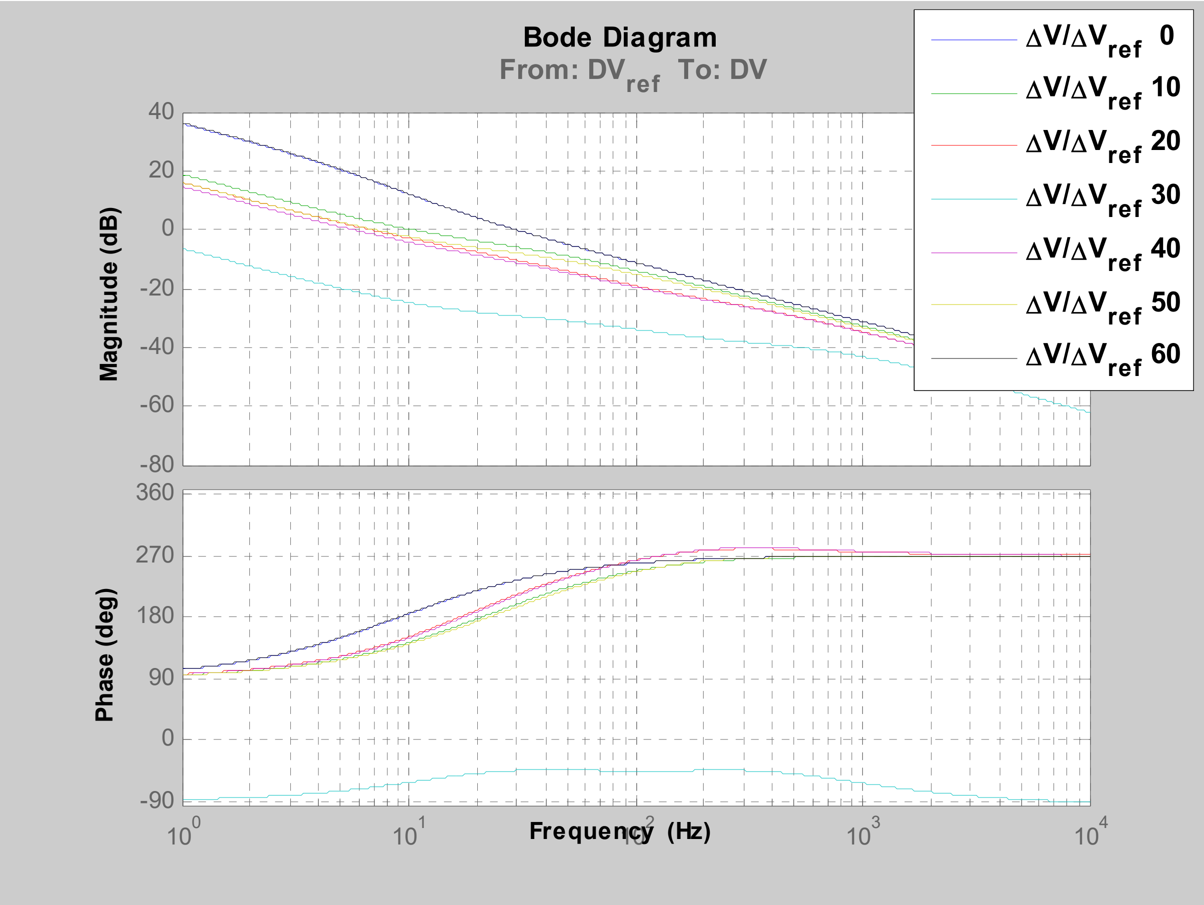

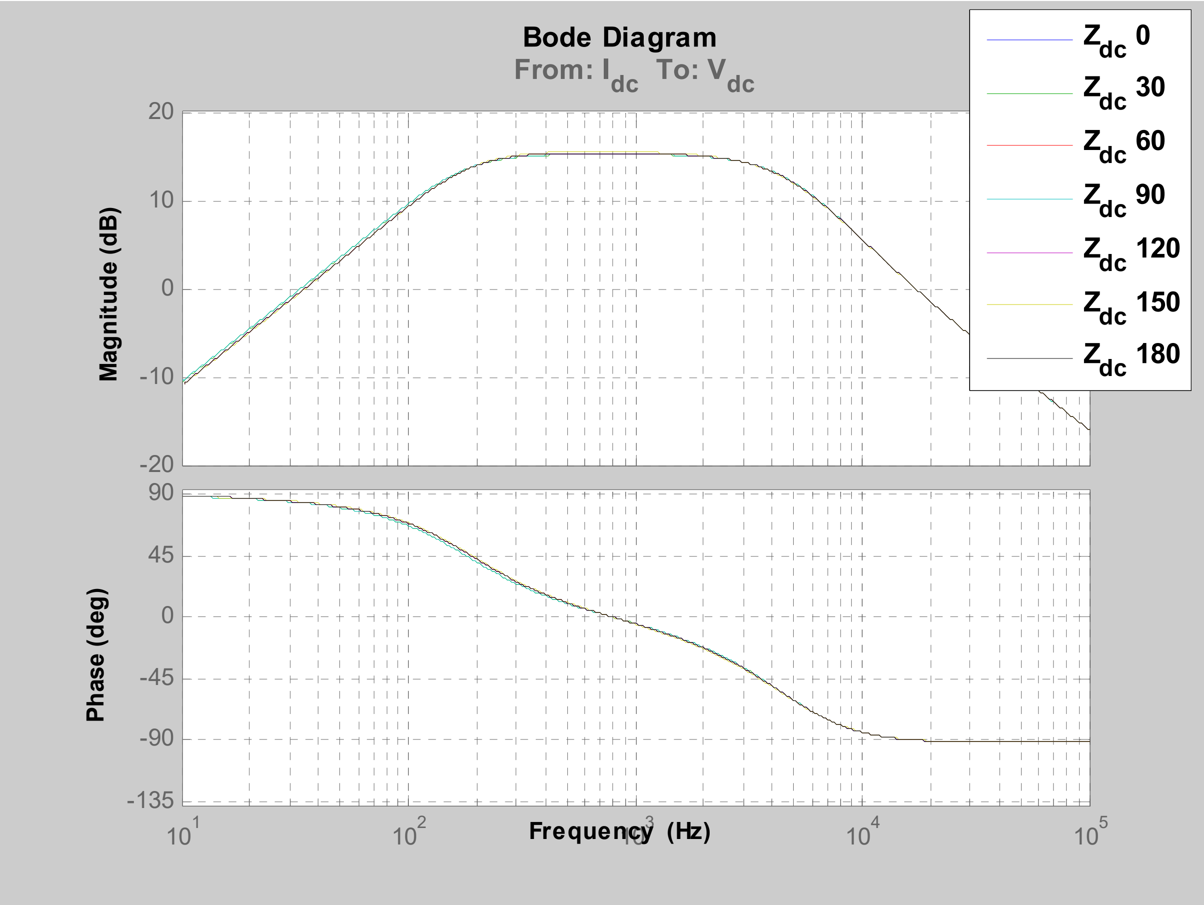

$$\frac{\widetilde{\Delta v}_{dc}}{\widetilde{\Delta v}_{dcref}}$$

$$Z_{out} = \frac{\tilde{v}_{dc}}{\tilde{\imath}_{dc}}$$

AC Terminal Input Admittance

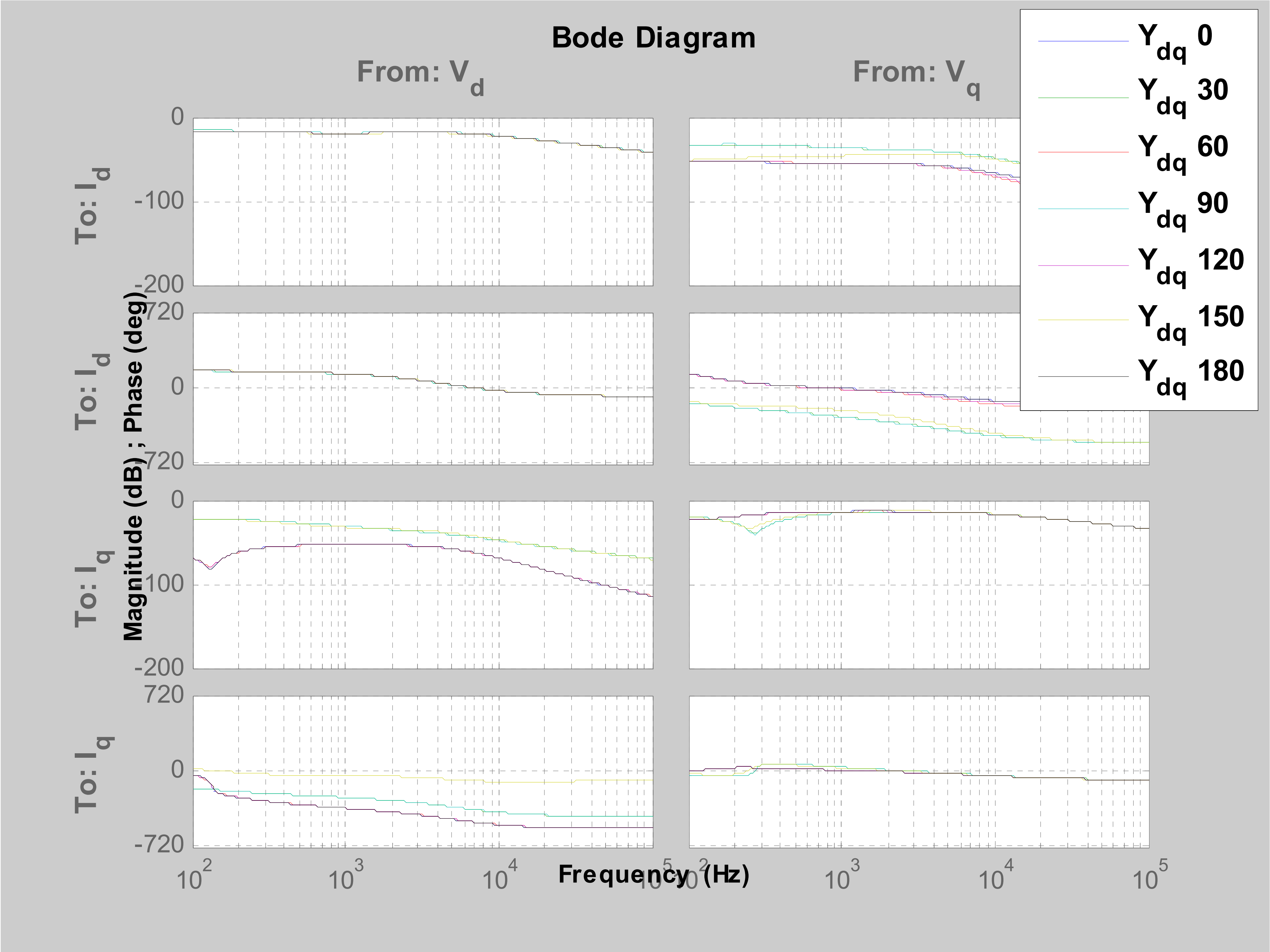

$$Y_{in} = \frac{\tilde{i}_{dq}}{\tilde{v}_{dq}}$$

Outline

1. Introduction
2. Mathematical Framework
3. Switching Modeling and PWM
4. Average Modeling
5. Small-Signal Modeling
6. Closed-Loop Control
7. 3-Level Converters
8. Control System Synchronization
9. AC System Interactions
10. Electronic Synchronous Machine (Voltage Controlling Converter)

Phase-Locked Loop (PLL) Controller Synchronization

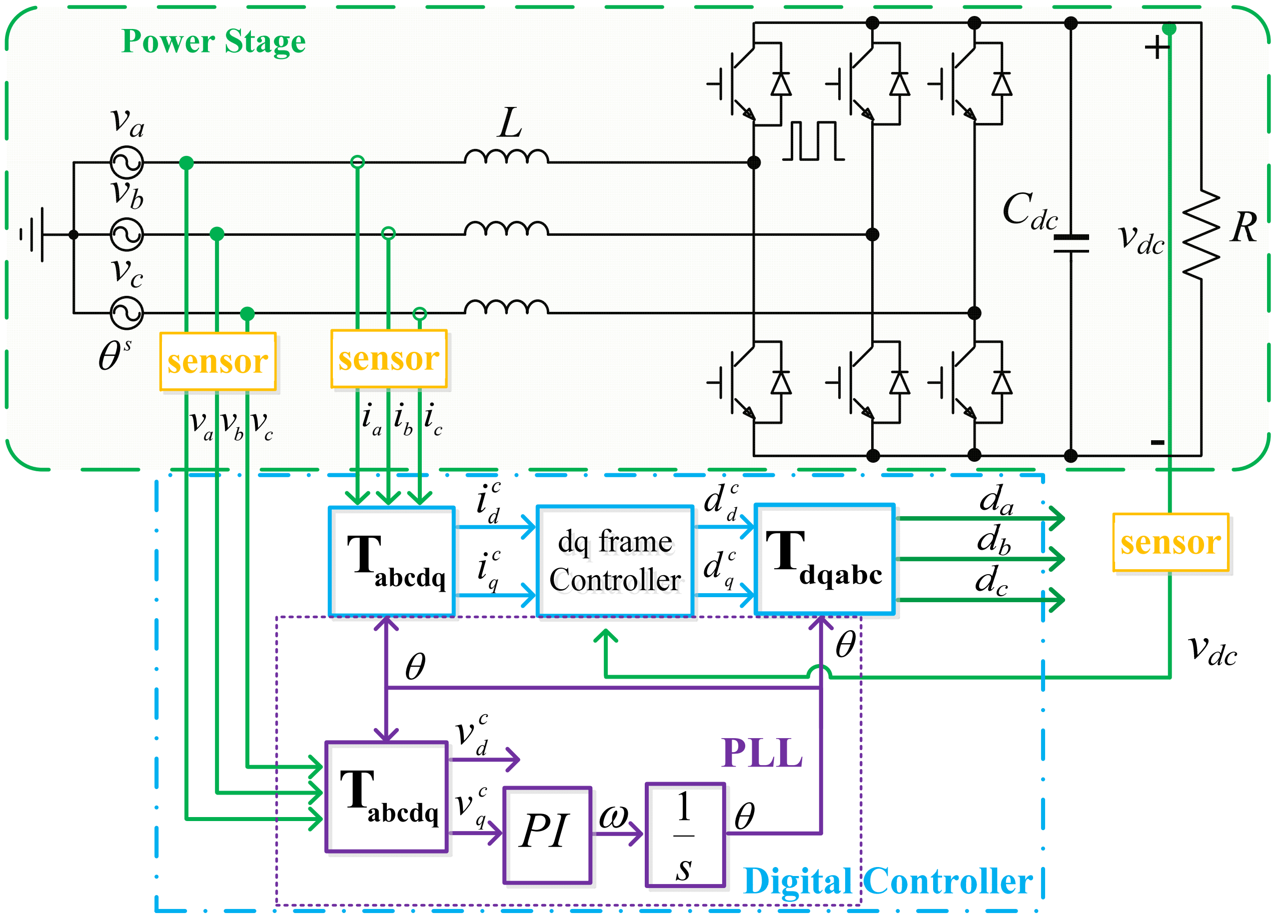

- PLL finds the angle of the voltage source, so that controller can control the variables in correct dq frame
- Controller commands need to be transferred back to abc frame with correct angle

Synchronous D-Q Frame PLL

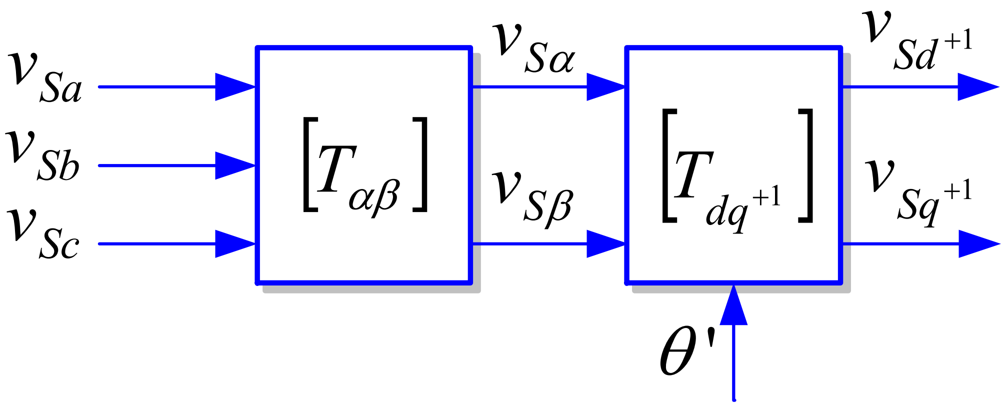

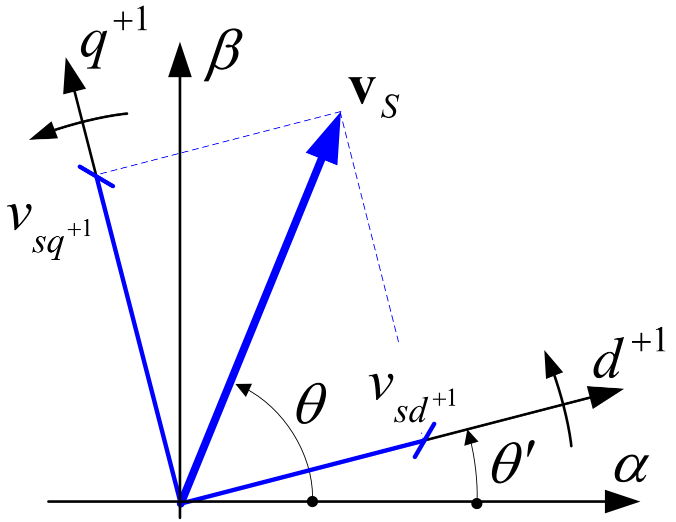

Phase-lock Loop (PLL)

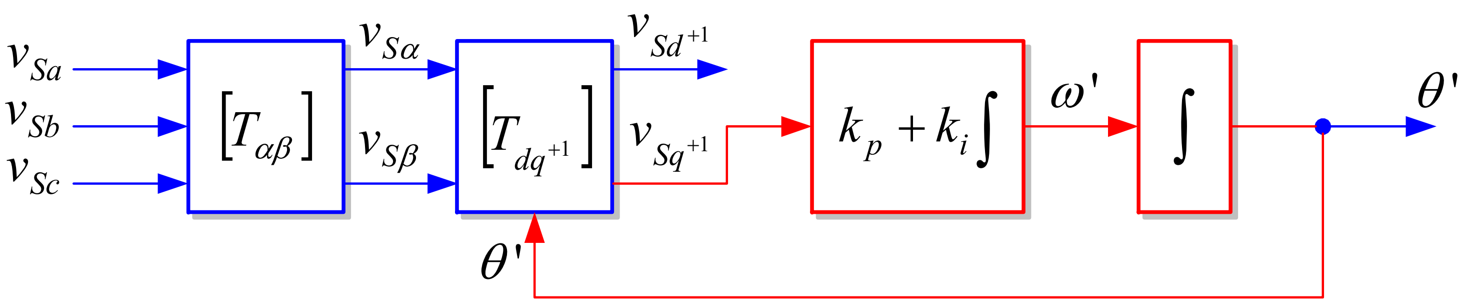

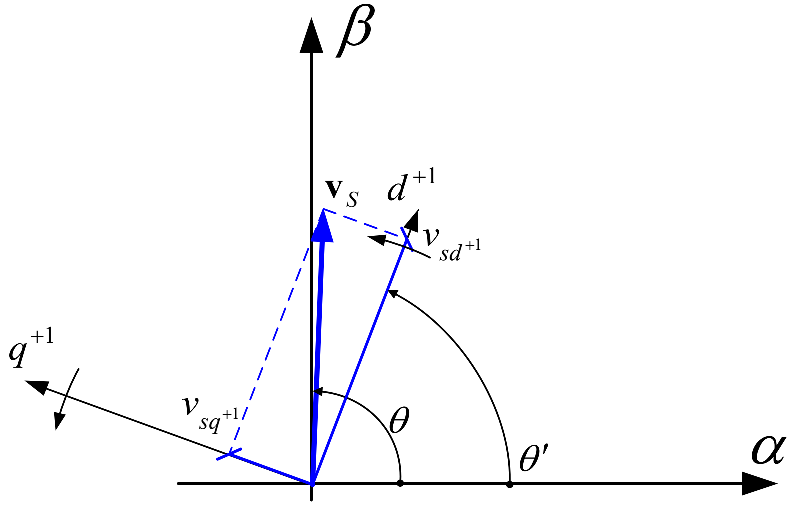

Small-Signal Propagation Path Through PLL

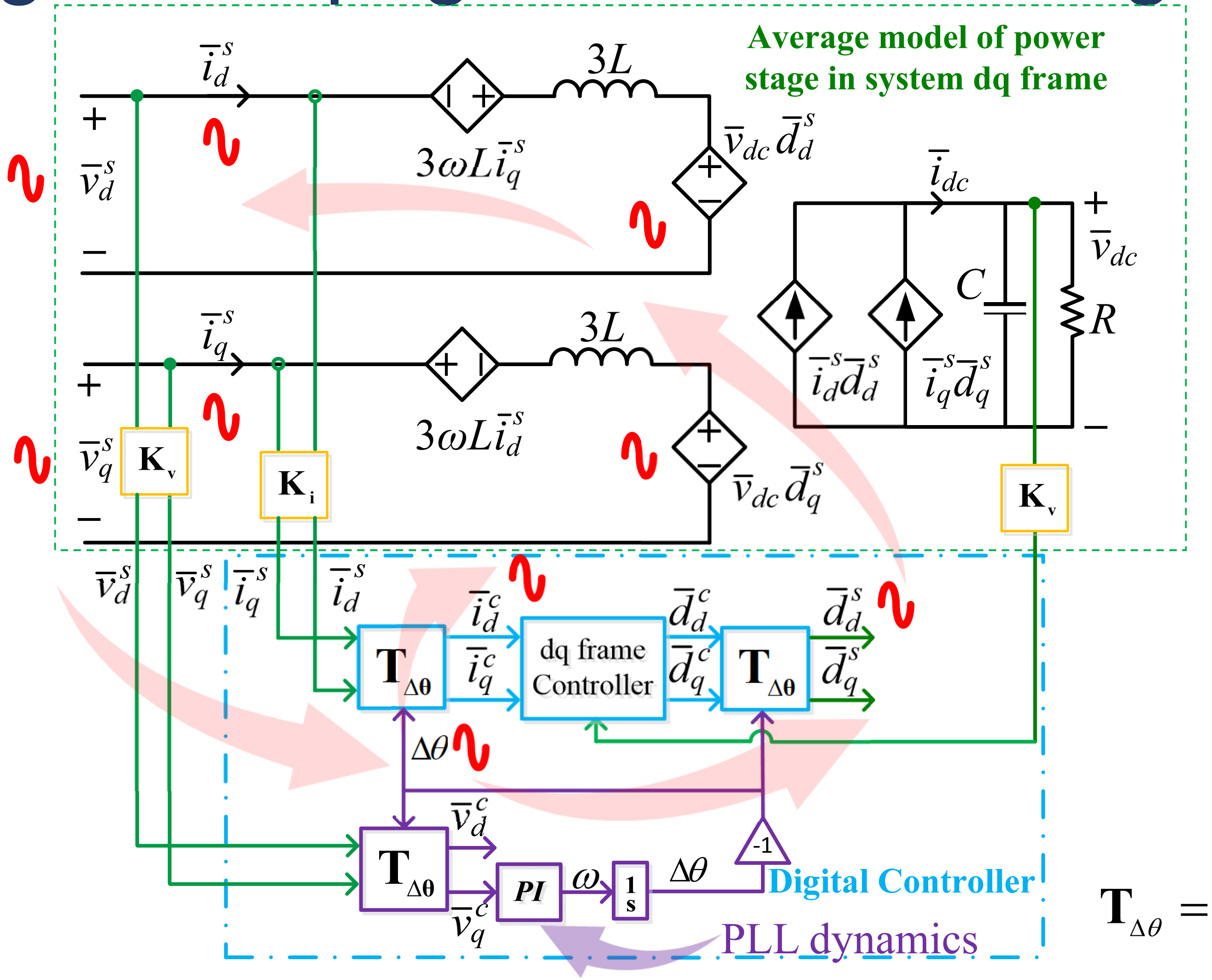

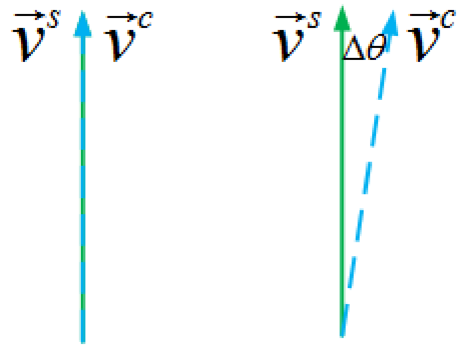

Under steady-state two vectors are aligned

Under perturbation two vectors are not aligned

$$\mathbf{T}_{\Delta\theta} = \begin{bmatrix} \cos(\Delta\theta) & \sin(\Delta\theta) \\ -\sin(\Delta\theta) & \cos(\Delta\theta) \end{bmatrix}$$

- Two dq frames: system dq frame and controller dq frame
- PLL dynamics influence input impedance of AFE

Small-Signal Model of AFE Impedance

$\mathbf{Y}_{\mathrm{in}}$: input admittance

$\mathbf{G}_{\mathrm{vd}}$: transfer function matrix from $\tilde{\vec{d}}^{s}$ to $\tilde{v}_{dc}$

$\mathbf{G}_{\mathrm{ve}}$: transfer function matrix from $\tilde{\vec{v}}^{s}$ to $\tilde{v}_{dc}$

$\mathbf{G}_{\mathrm{id}}$: transfer function matrix from $\tilde{\vec{d}}^{s}$ to $\tilde{\vec{i}}_{L}^{s}$

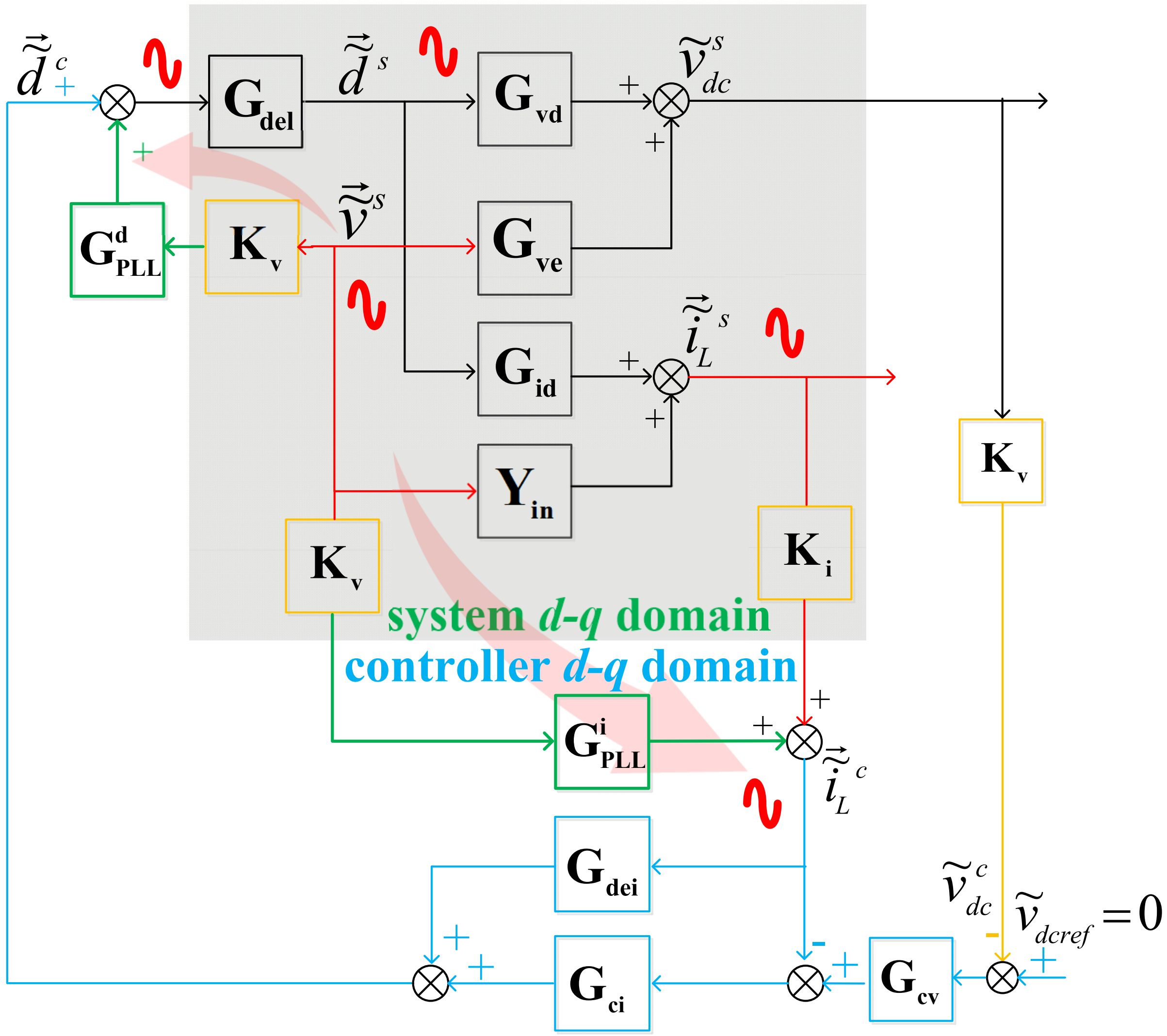

AFE Input Impedance Measurement Results

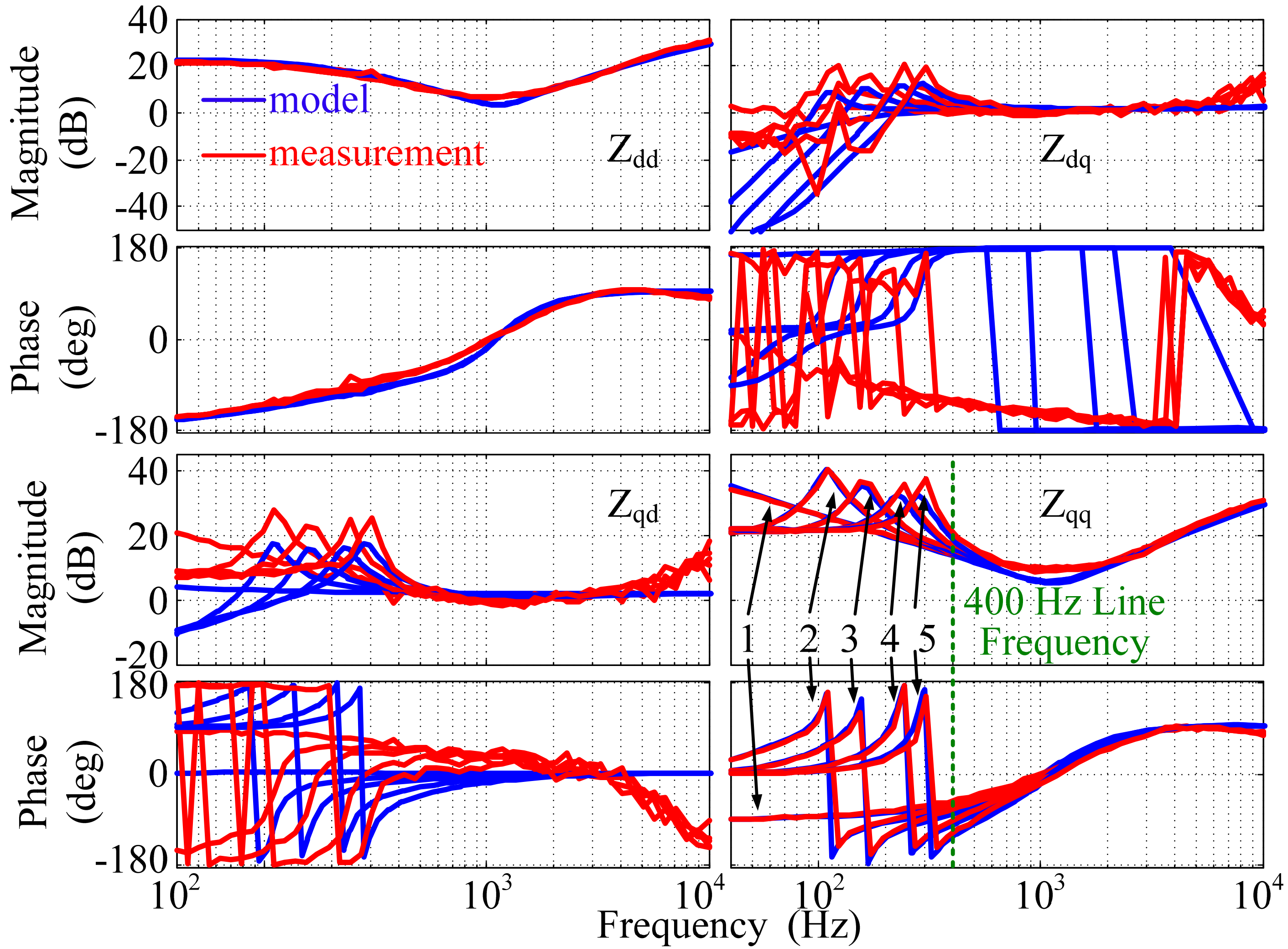

1: 1Hz PLL   2: 50 Hz PLL   3: 100 Hz PLL   4: 200 Hz PLL
5: 300 Hz PLL

Output Impedance of Grid-Tied Inverter

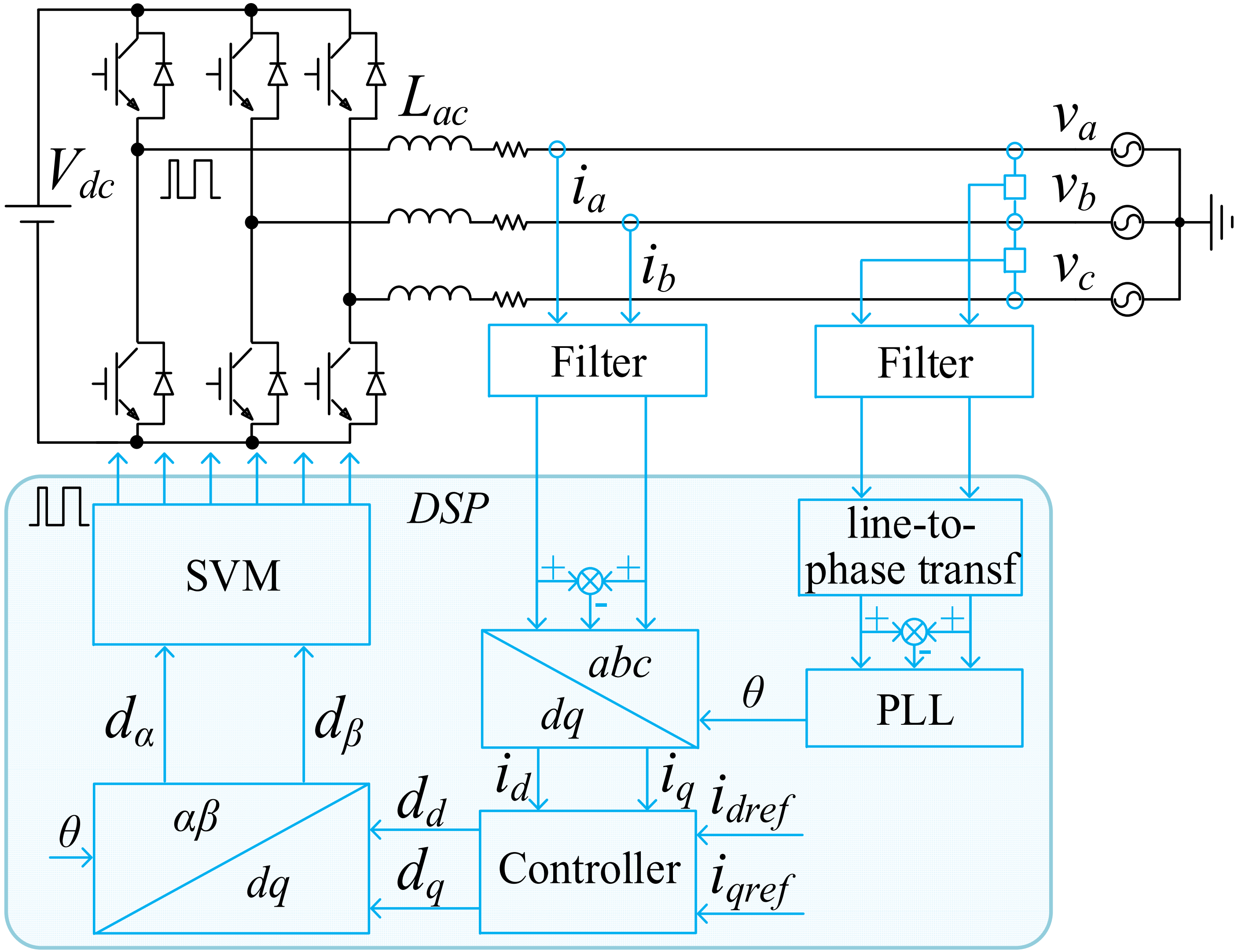

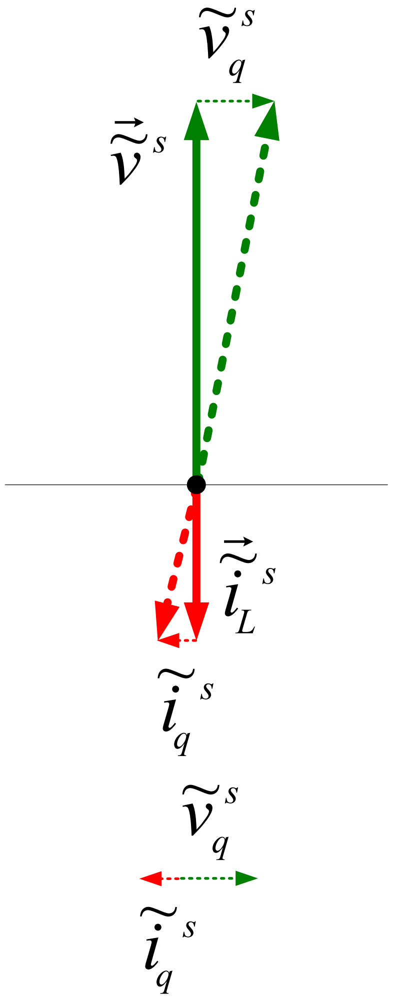

- **Negative incremental resistance in *q* channel!**

Inverter Impedance with PLL and Current Control

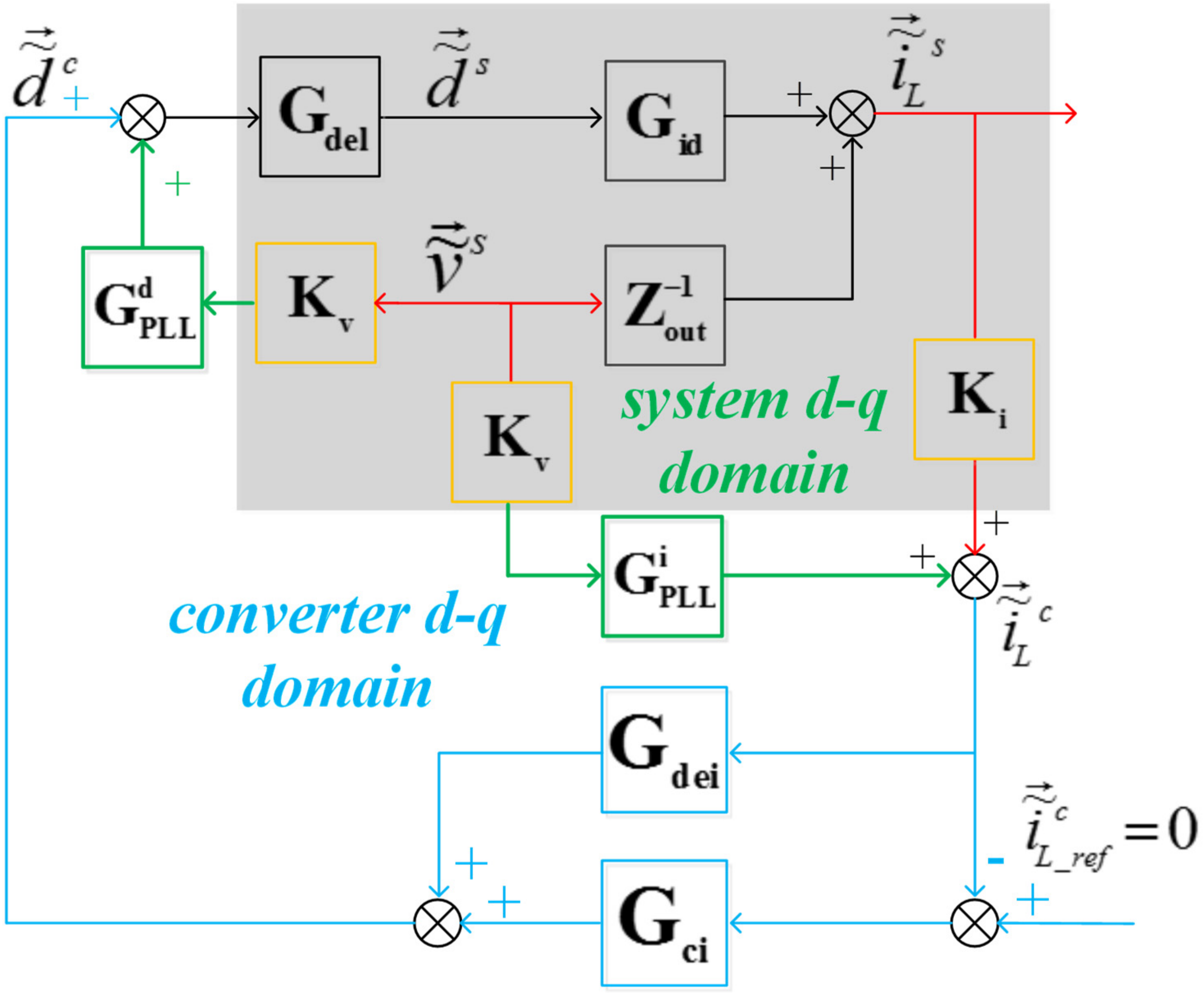

Inverter Impedance with PLL and Current Control

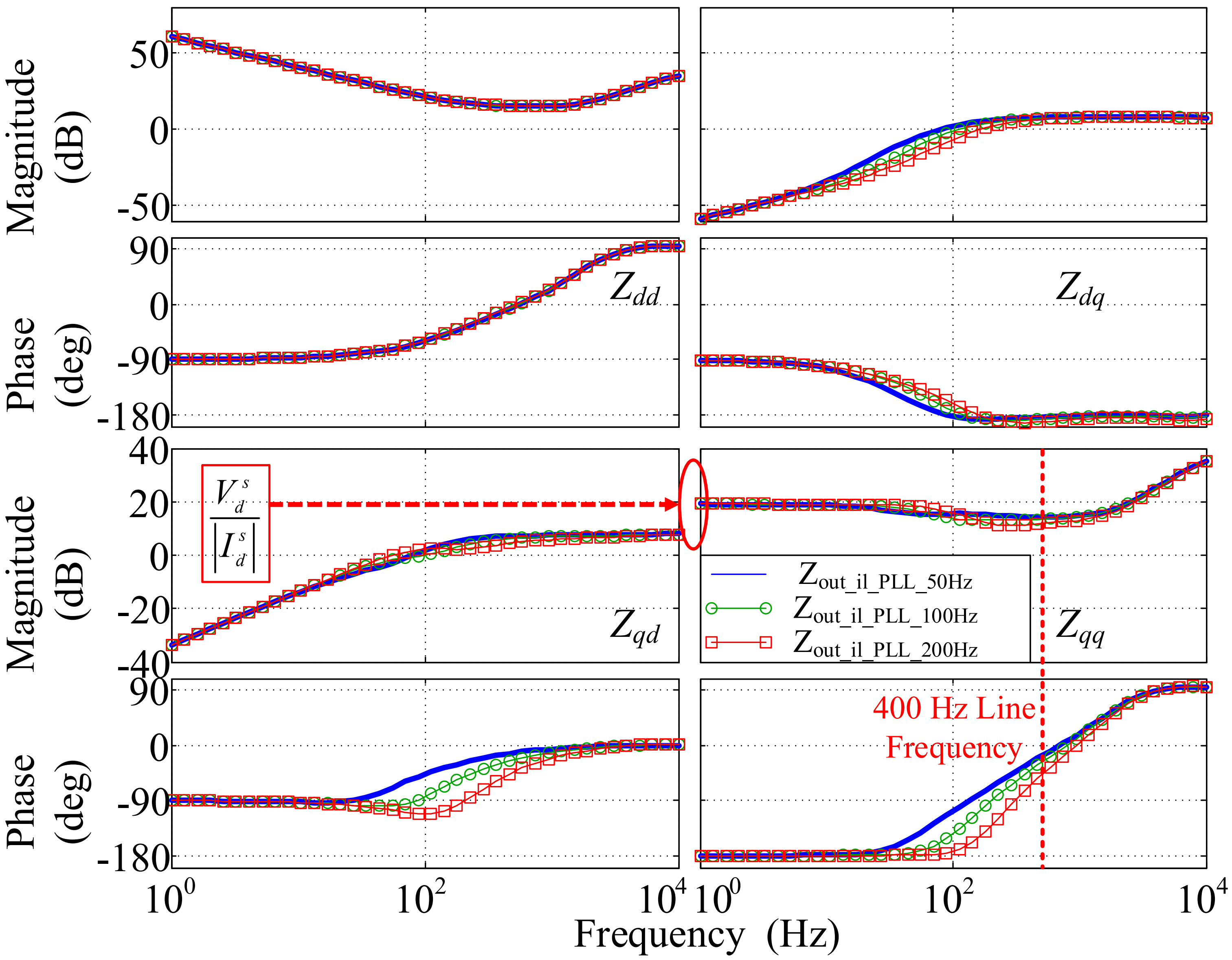

Outline

1. Introduction
2. Mathematical Framework
3. Switching Modeling and PWM
4. Average Modeling
5. Small-Signal Modeling
6. Closed-Loop Control
7. 3-Level Converters
8. Control System Synchronization
9. AC System Interactions
10. Electronic Synchronous Machine (Voltage Controlling Converter)

Balanced Three-Phase AC System Small-Signal Stability Analysis

Impedance based small-signal analysis for AC system

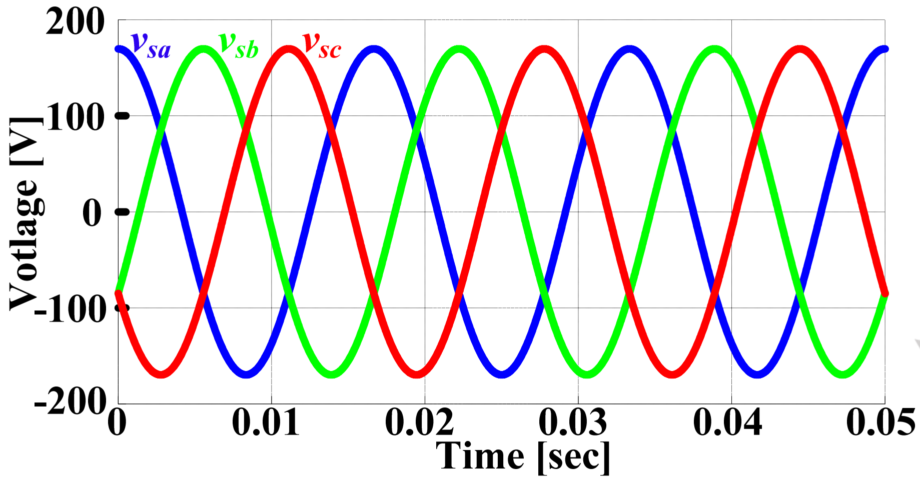

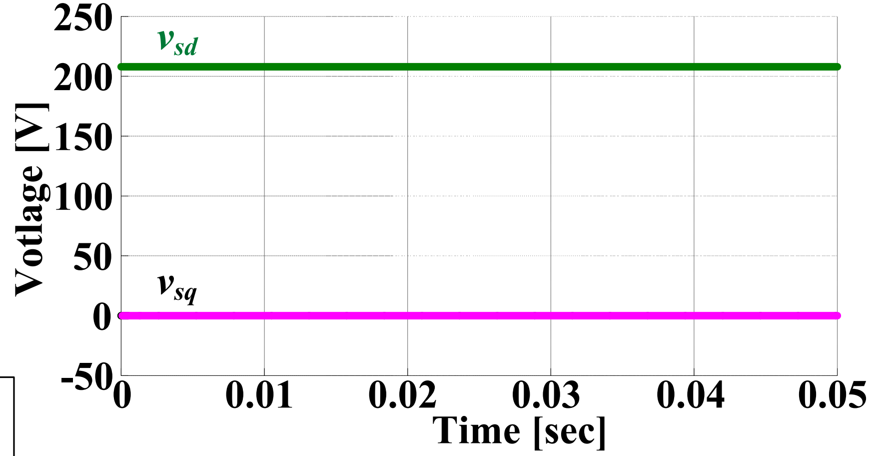

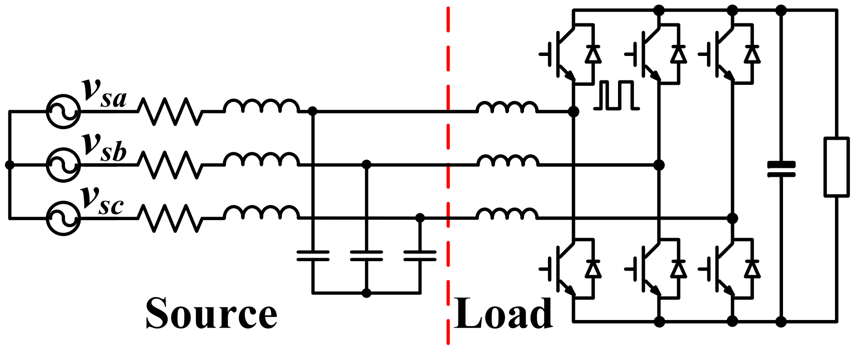

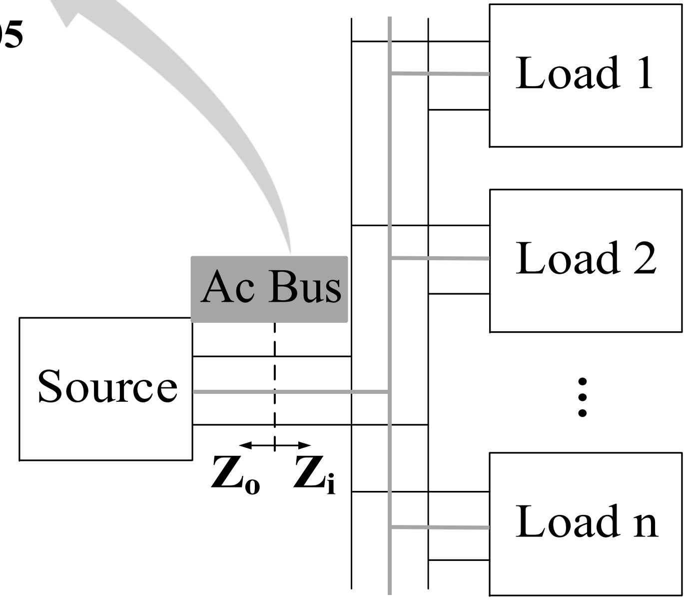

Synchronous rotating frame

- Standard small-signal analysis can be applied, like in DC systems

Stability at AC Interfaces

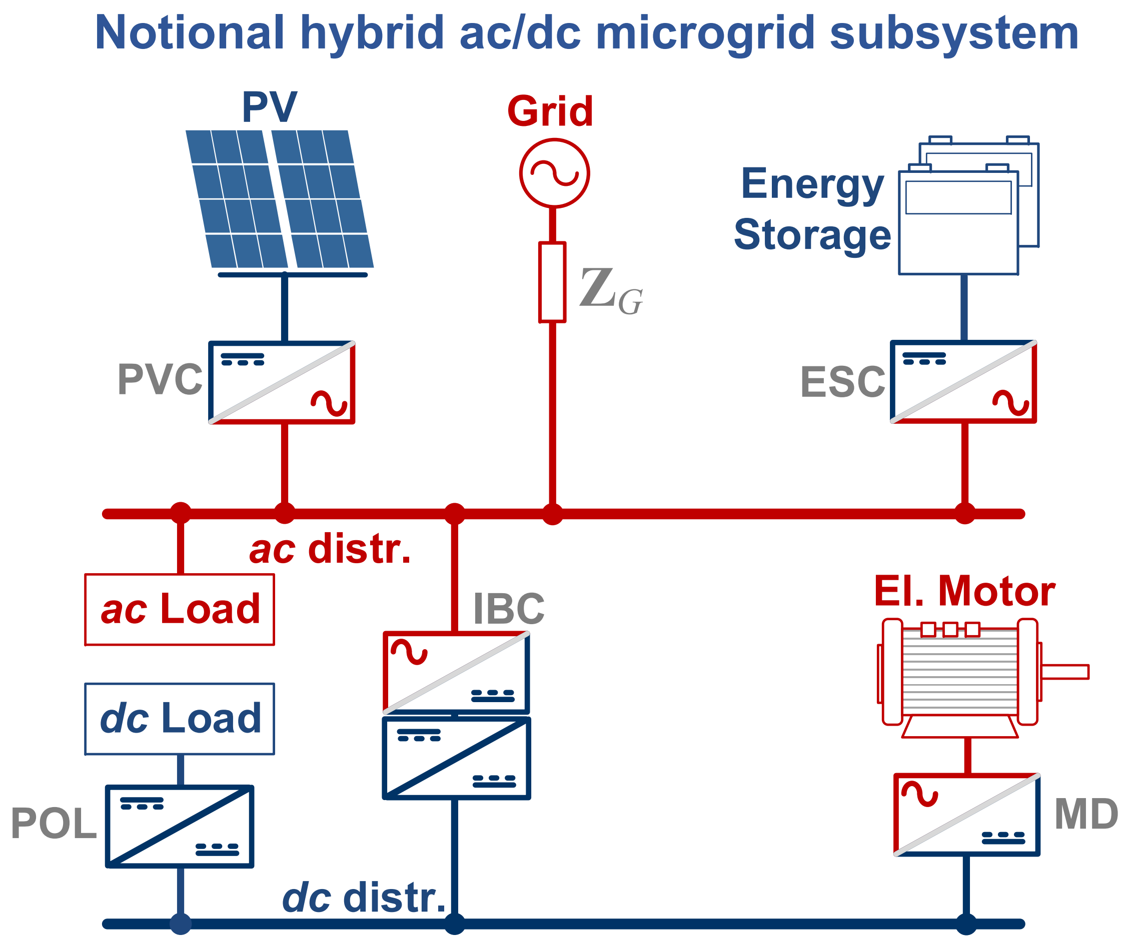

1- AC bus stability depends on output and input impedances

2- Stability must be ensured at every interface in the system

IBC – Intermediate Bus Converter
MD – Motor Drive
POL – Point of Load Converter

PVC – PV Converter
ESC – Energy Storage Converter

Balanced Three-Phase AC System Small-Signal Stability Analysis—Linearization

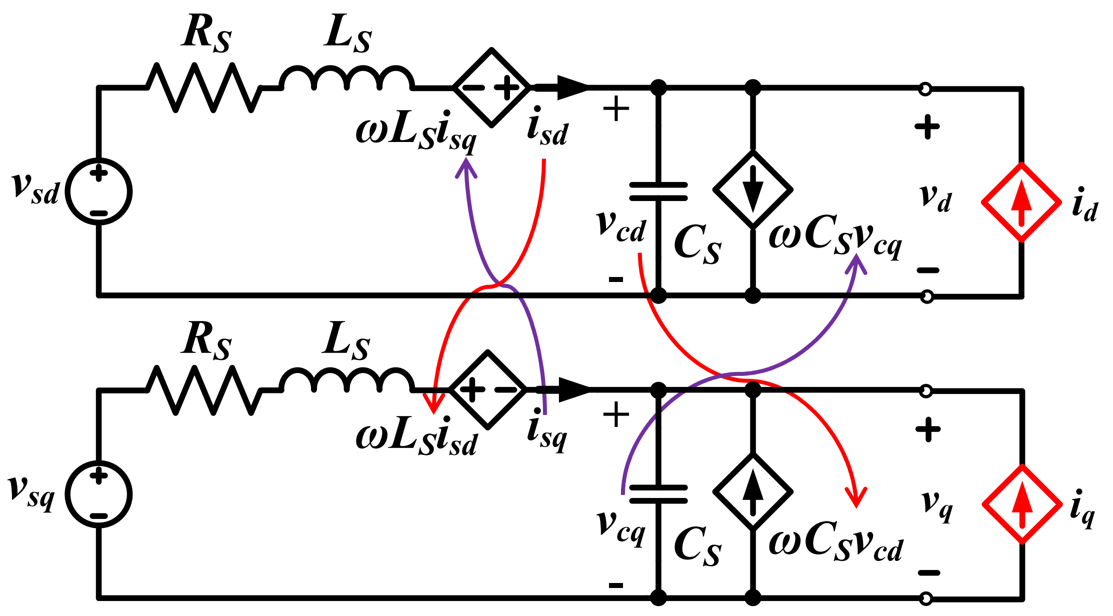

$$\begin{bmatrix} v_d(s) \\ v_q(s) \end{bmatrix} = \begin{bmatrix} Z_{dd}(s) & Z_{dq}(s) \\ Z_{qd}(s) & Z_{qq}(s) \end{bmatrix} \begin{bmatrix} i_d(s) \\ i_q(s) \end{bmatrix}$$

$$Z_{dd}(s) = \left.\frac{v_d(s)}{i_d(s)}\right|_{i_q=0}$$

$$Z_{qd}(s) = \left.\frac{v_q(s)}{i_d(s)}\right|_{i_q=0}$$

$$Z_{qq}(s) = \left.\frac{v_q(s)}{i_q(s)}\right|_{i_d=0}$$

$$Z_{dq}(s) = \left.\frac{v_d(s)}{i_q(s)}\right|_{i_d=0}$$

Balanced Three-Phase AC System Small-Signal Stability— Generalized Nyquist Criterion

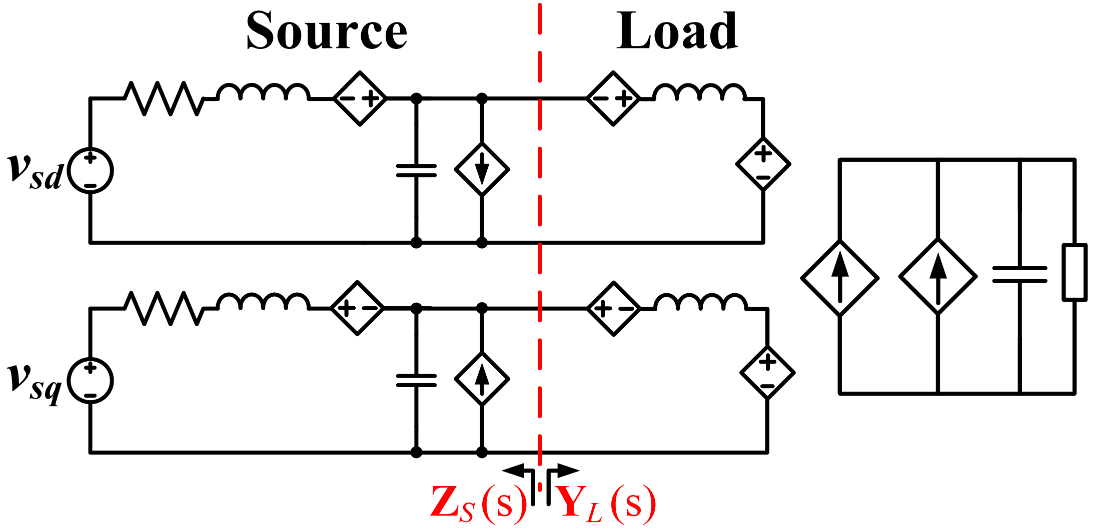

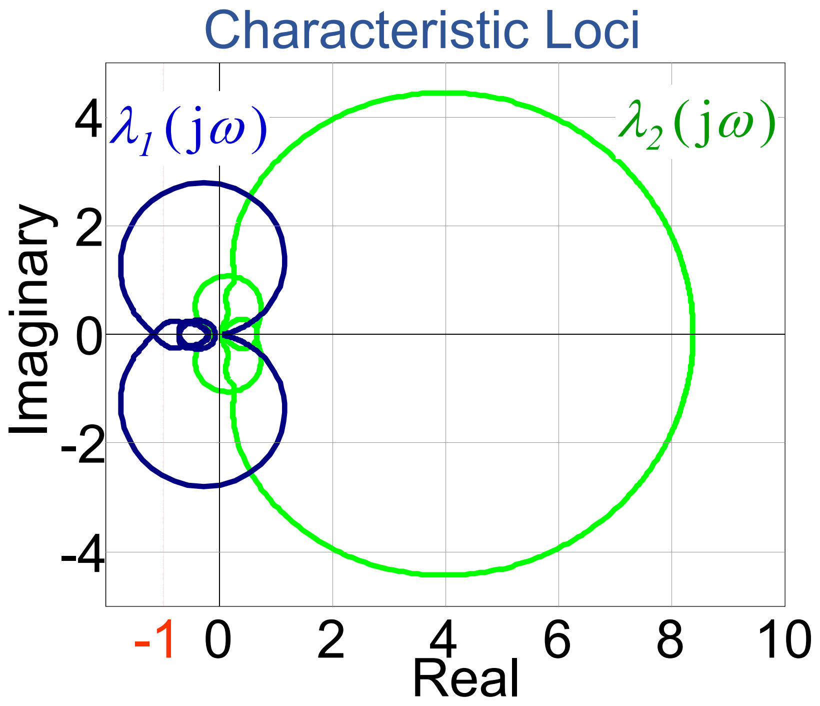

Return ratio is:

$$\mathbf{L}(s) = \mathbf{Z}_S(s)\cdot \mathbf{Y}_L(s) = \begin{bmatrix} Z_{dds} & Z_{dqs} \\ Z_{qds} & Z_{qqs} \end{bmatrix} \cdot \begin{bmatrix} Y_{dds} & Y_{dds} \\ Y_{dds} & Y_{dds} \end{bmatrix}$$

Generalized Nyquist Criterion (GNC)

$$\mathbf{L}(s) = \begin{bmatrix} L_{11}(s) & L_{12}(s) \\ L_{21}(s) & L_{22}(s) \end{bmatrix}$$

Eigenvalues of $\mathbf{L(s)}$ = $\lambda_1(s), \lambda_2(s)$

Balanced Three-Phase AC System Small-Signal Stability—Generalized Nyquist Criterion

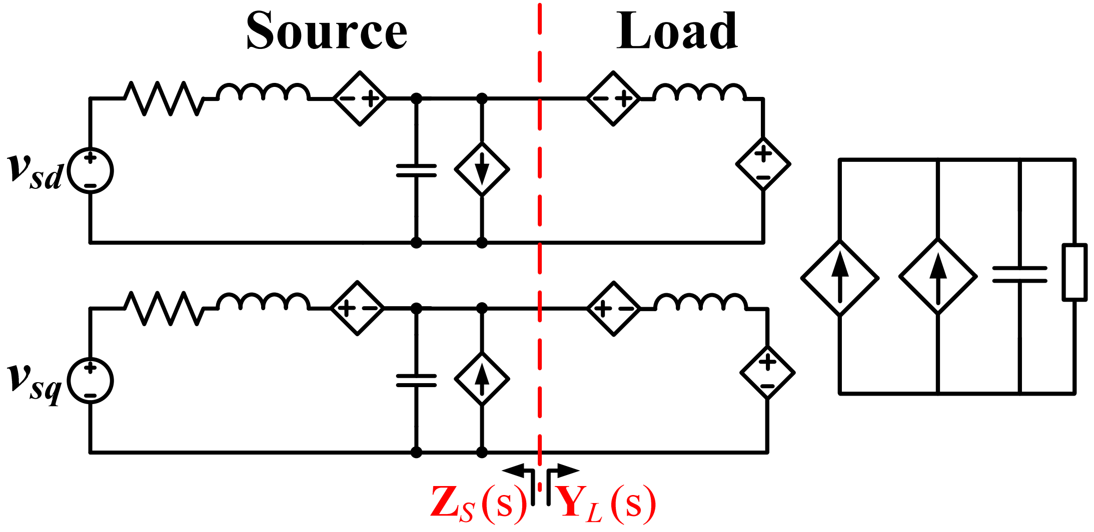

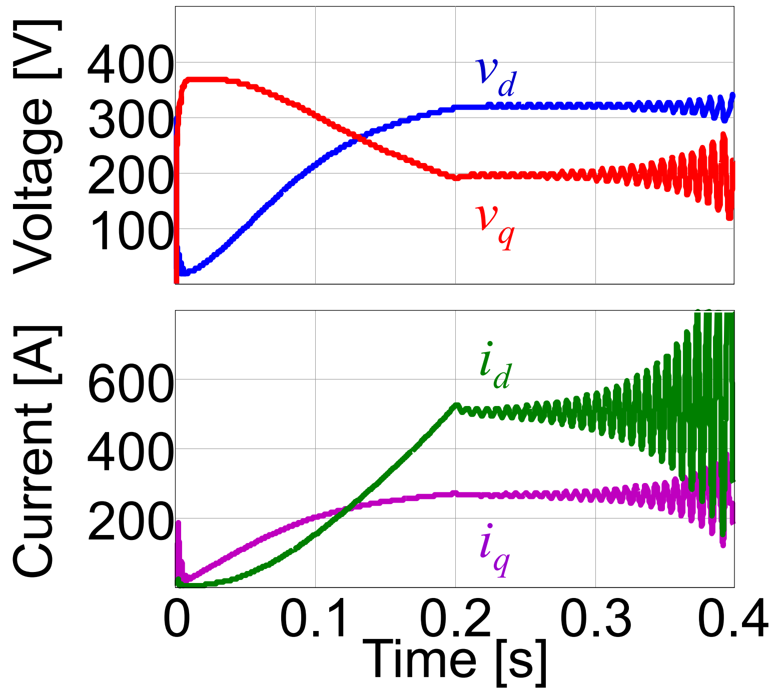

Return ratio is:

$$\mathbf{L}(s)=\mathbf{Z}_S(s)\cdot\mathbf{Y}_L(s)=\begin{bmatrix} Z_{dds} & Z_{dqs} \\ Z_{qds} & Z_{qqs} \end{bmatrix}\cdot\begin{bmatrix} Y_{dds} & Y_{dds} \\ Y_{dds} & Y_{dds} \end{bmatrix}$$

Generalized Nyquist Criterion (GNC)

$$\mathbf{L}(s)=\begin{bmatrix} L_{11}(s) & L_{12}(s) \\ L_{21}(s) & L_{22}(s) \end{bmatrix}$$

Eigenvalues of $\mathrm{L(s)} = \lambda_1(s), \lambda_2(s)$

Selected Types of System-Level Dynamic Interactions: *Constant Power Load*

Notional hybrid ac/dc microgrid subsystem

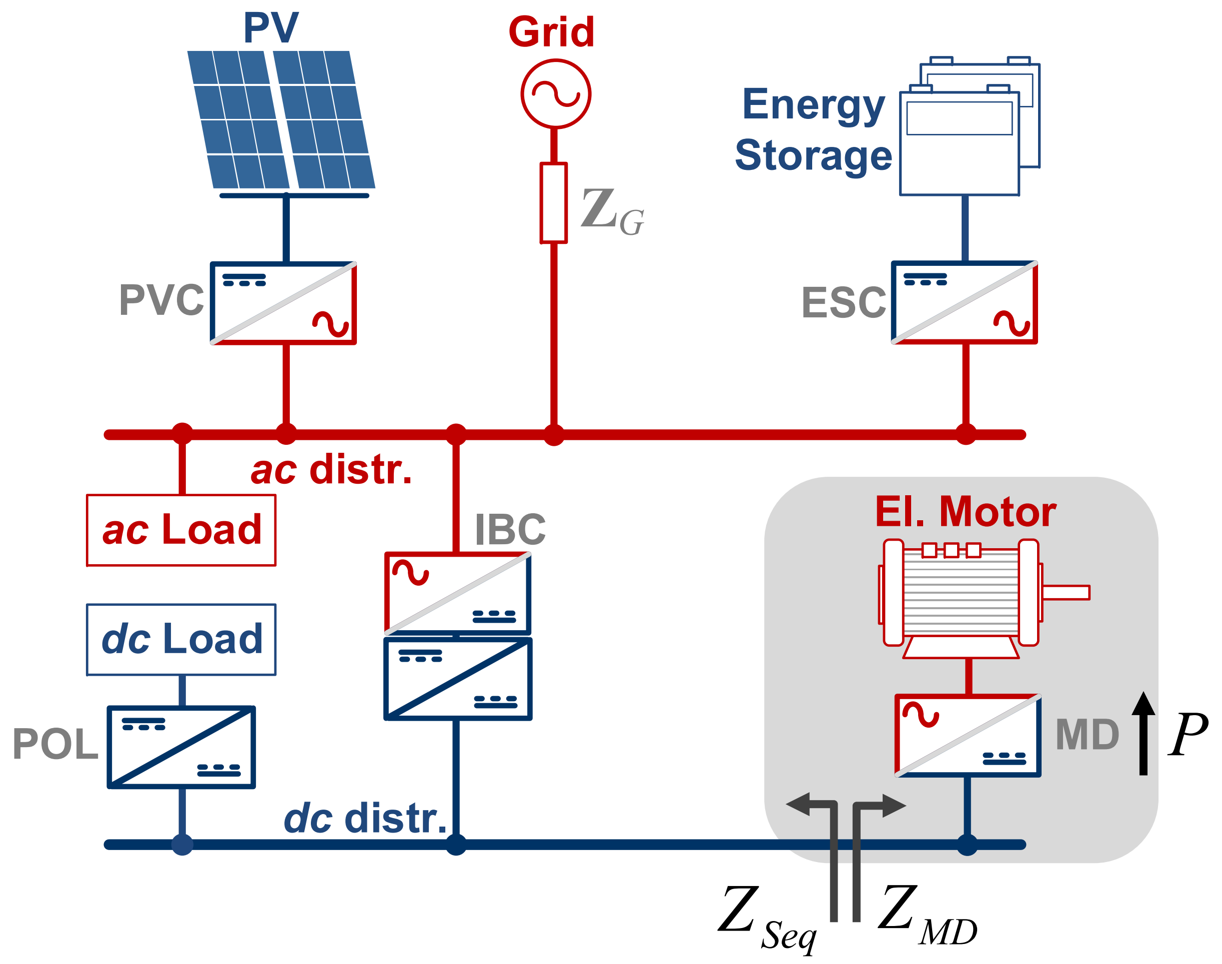

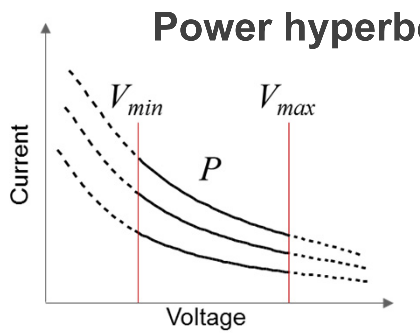

$$P = v_i i_i = const.$$

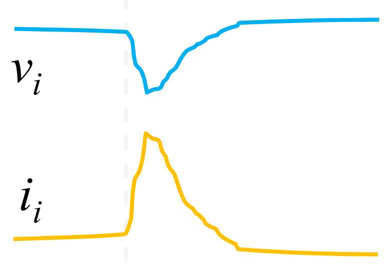

$$\Delta R = \frac{-\Delta v_i}{\Delta i_i}$$

Incremental Negative Resistor

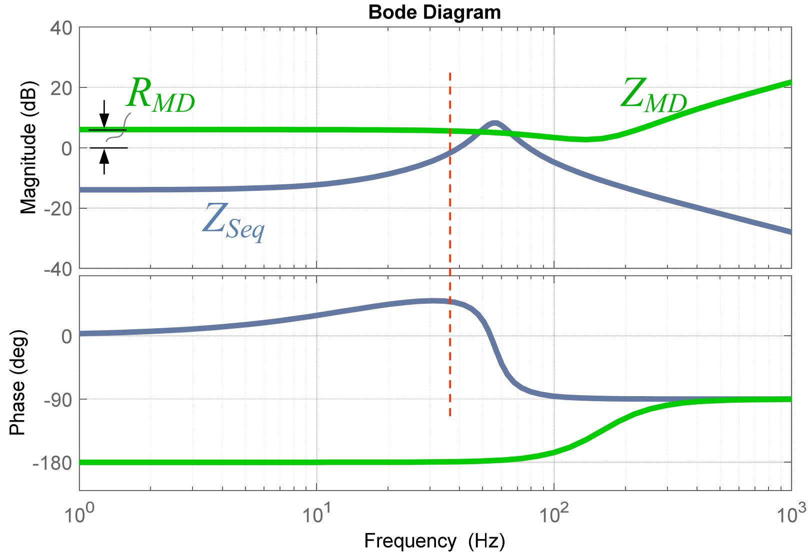

Selected Types of System-Level Dynamic Interactions: *Constant Power Load*

Notional hybrid ac/dc microgrid subsystem

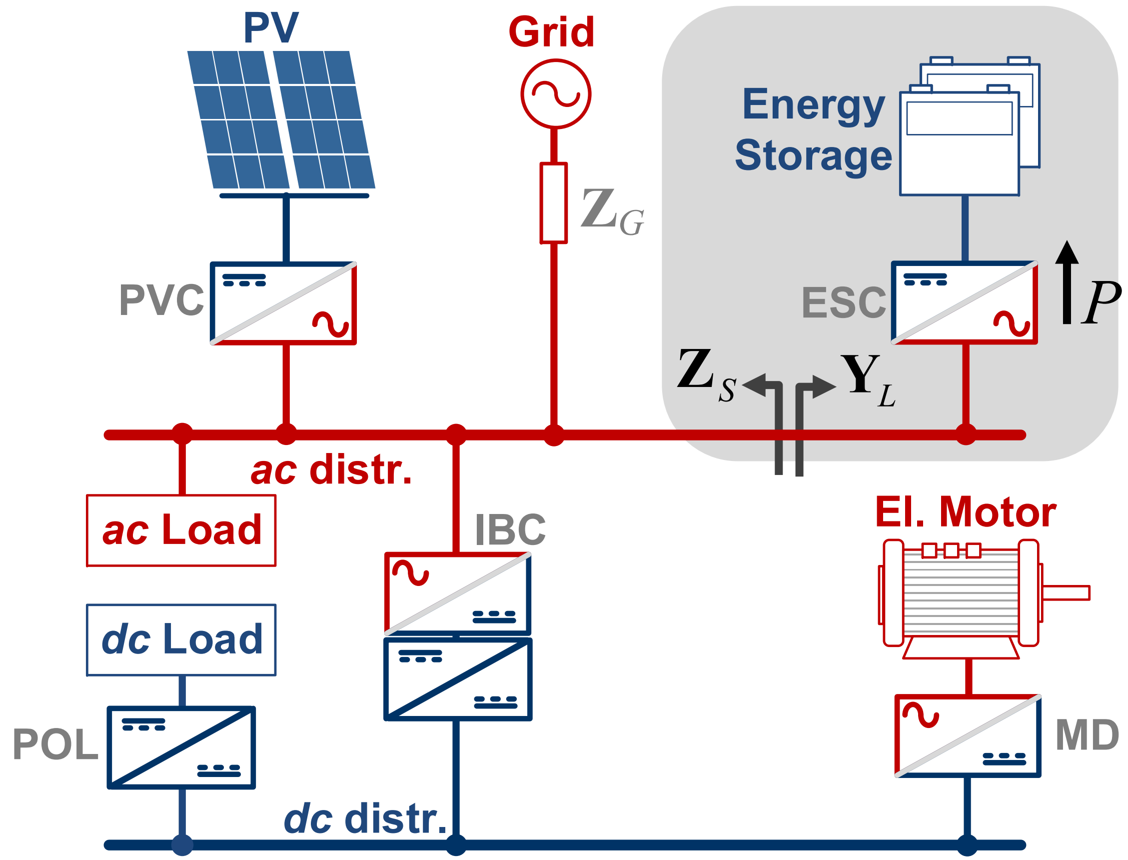

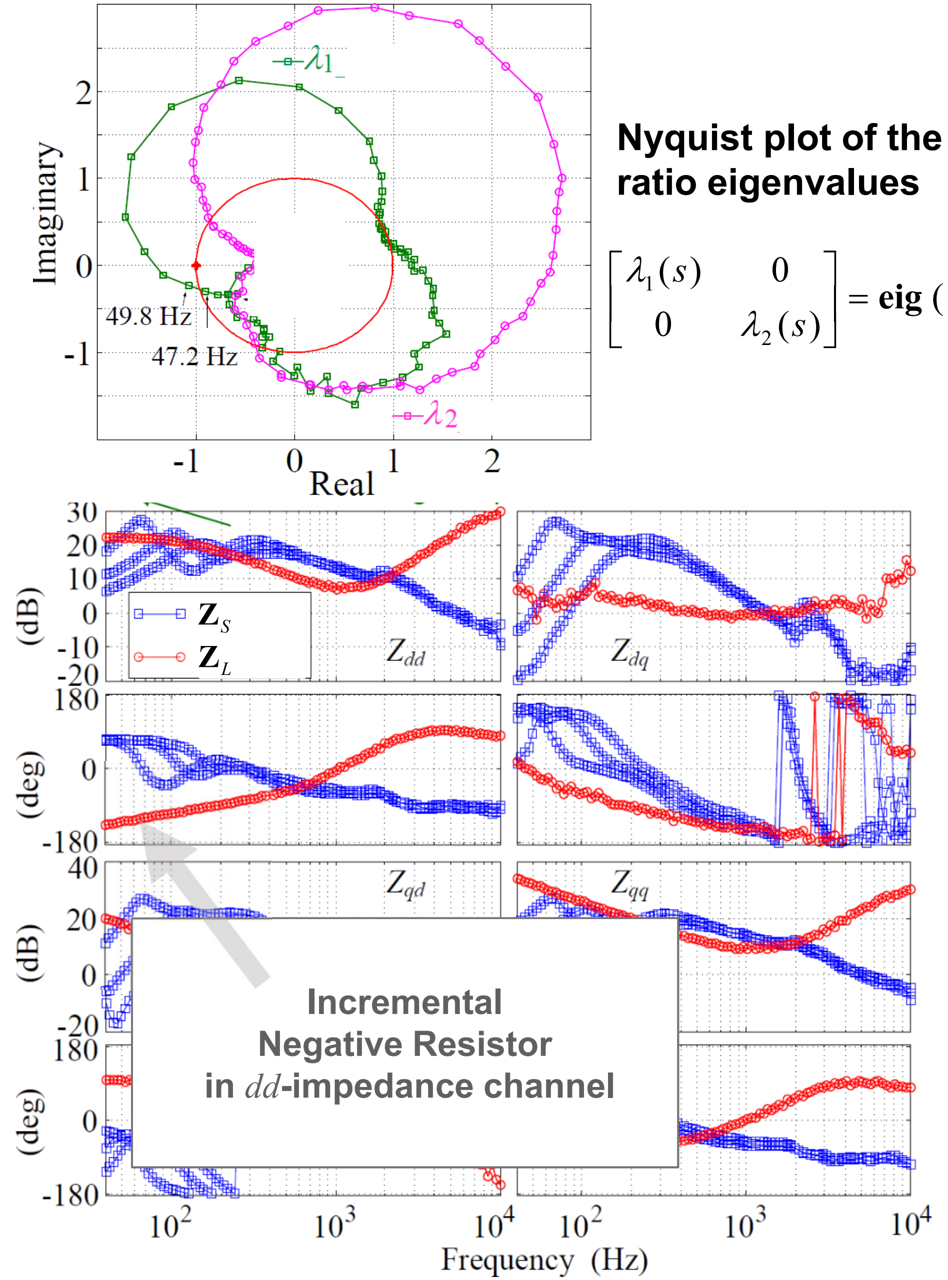

Nyquist plot of the return ratio eigenvalues

$$\begin{bmatrix} \lambda_1(s) & 0 \\ 0 & \lambda_2(s) \end{bmatrix} = \mathrm{eig}\,(\mathbf{Z_S Y_L})$$

Selected Types of System-Level Dynamic Interactions: *Synchronization*

(with power regeneration)

Notional hybrid ac/dc microgrid subsystem

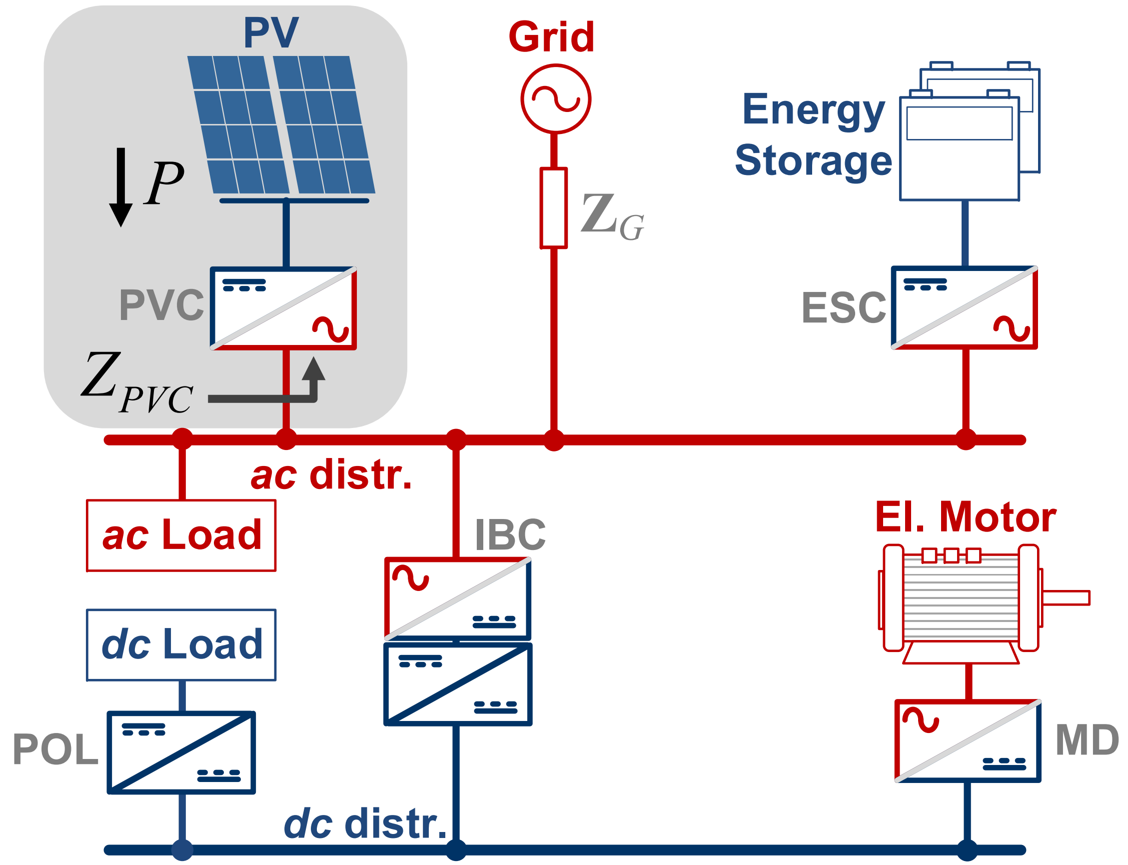

Interaction caused by the phase-locked loop (PLL)

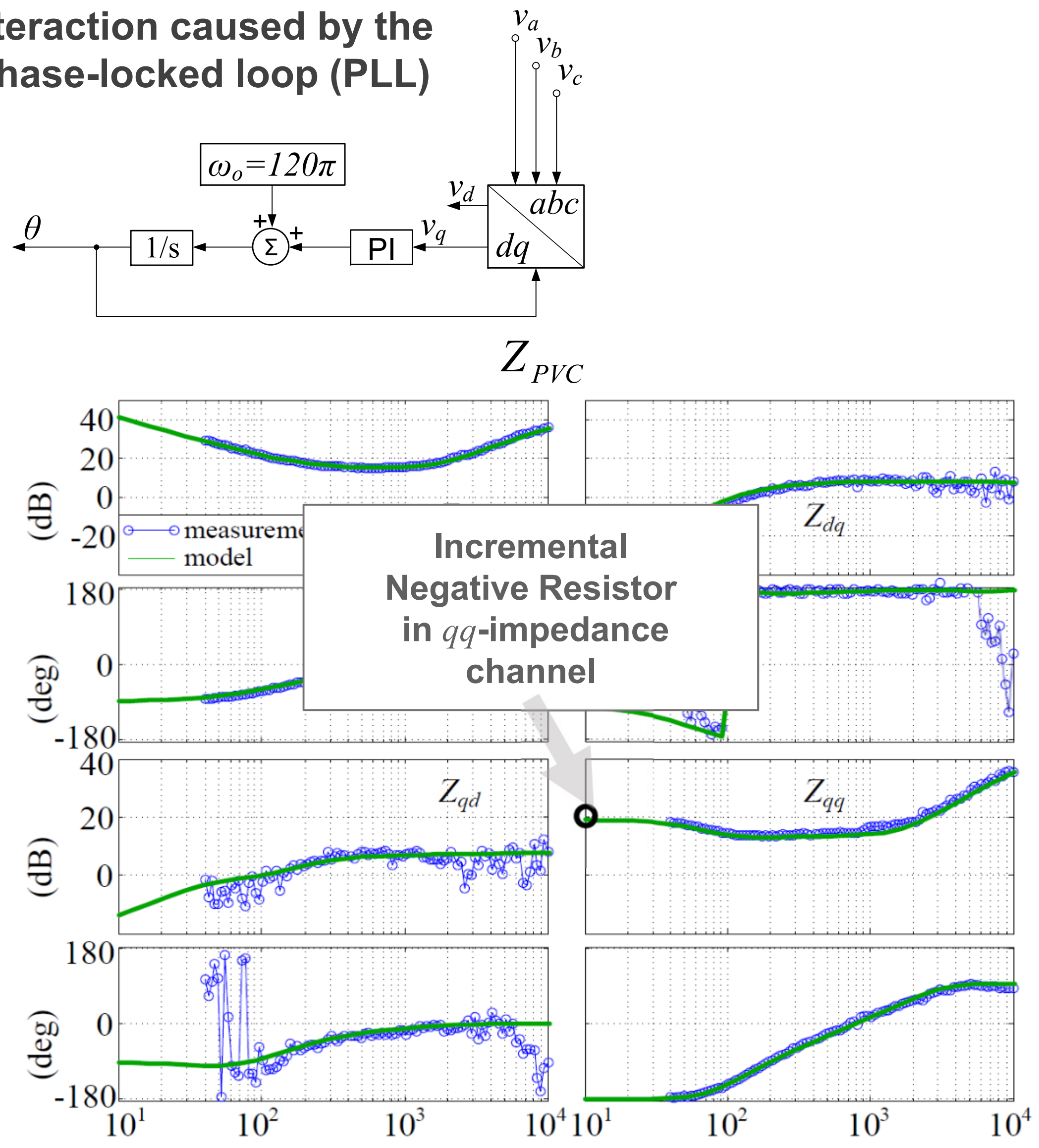

Selected Types of System-Level Dynamic Interactions: *Synchronization*

(with power regeneration)

Notional hybrid ac/dc microgrid subsystem

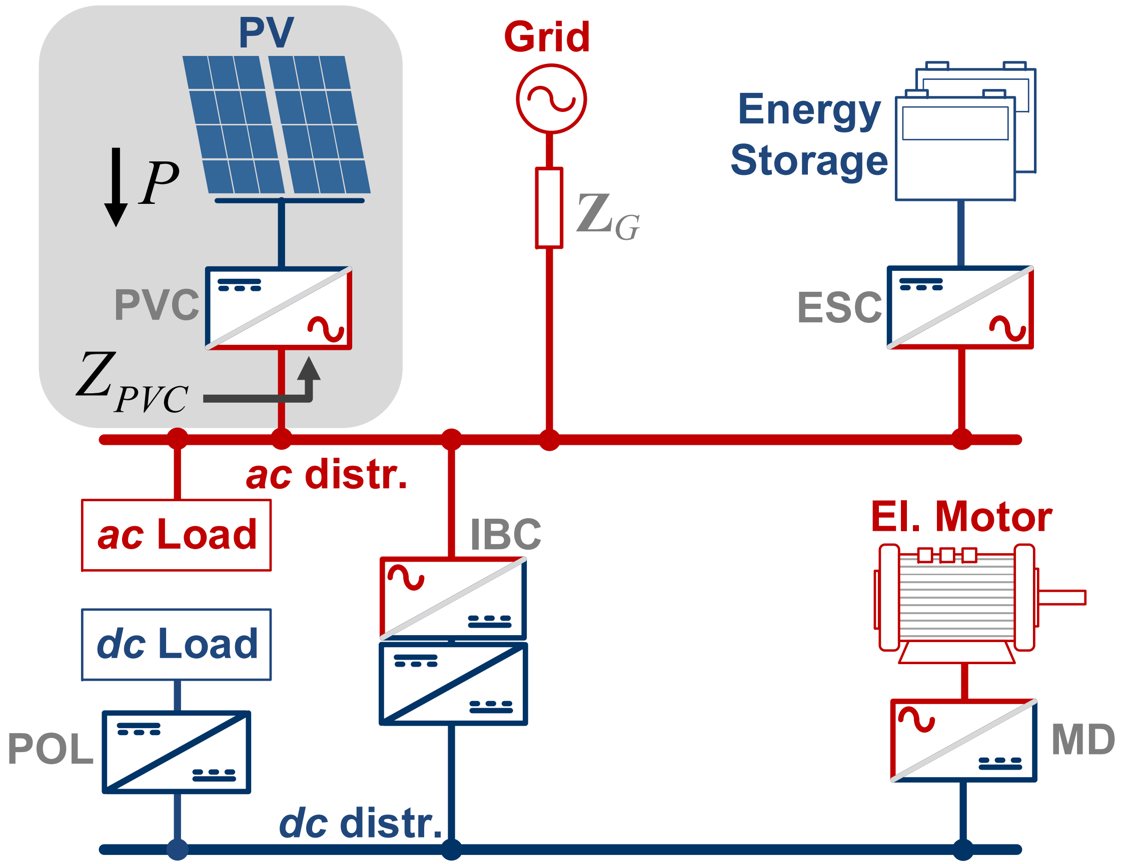

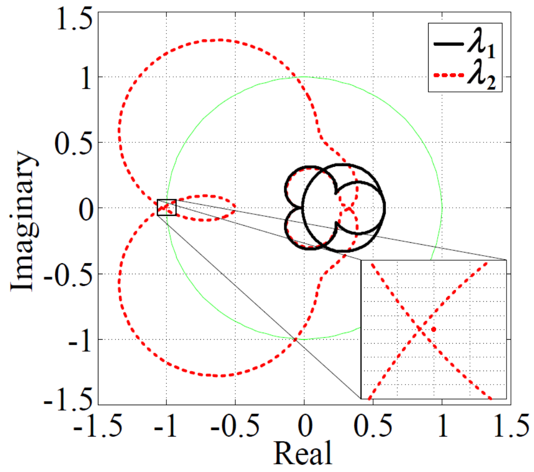

Nyquist plot of the return ration eigenvalues

$$\begin{bmatrix} \lambda_1(s) & 0 \\ 0 & \lambda_2(s) \end{bmatrix} = \mathbf{eig}(\mathbf{Z_S Y_L})$$

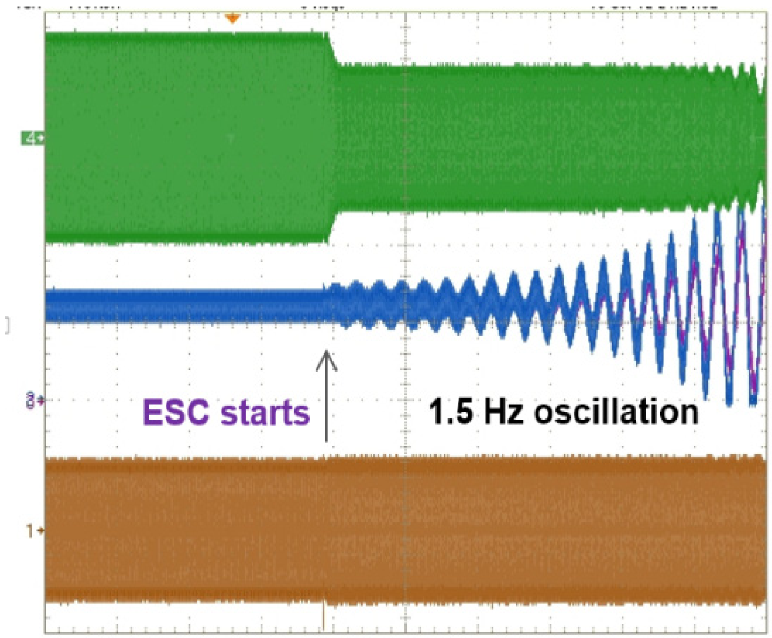

ac-bus voltage

PVC PLL frequency

ESC PLL frequency

VSI Phase A Current

Selected Types of System-Level Dynamic Interactions: *Aggregate Load Uncertainty*

Notional hybrid ac/dc microgrid subsystem

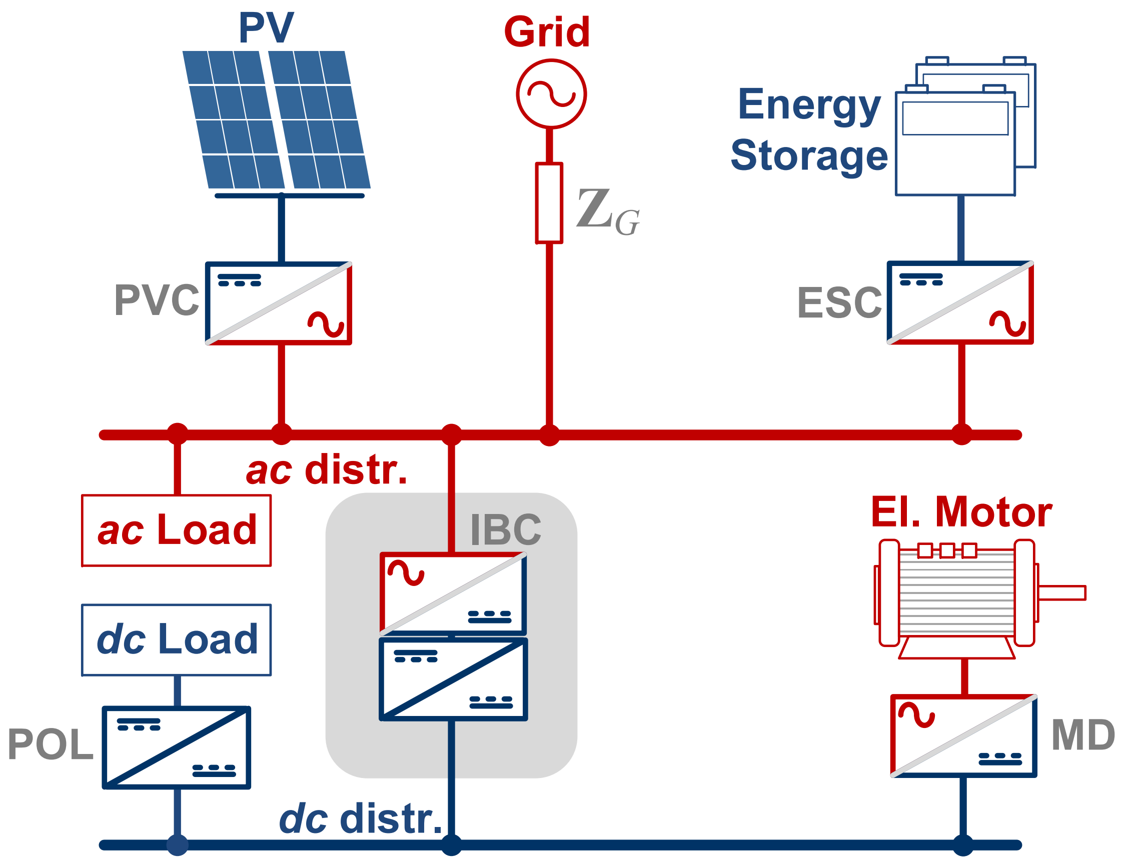

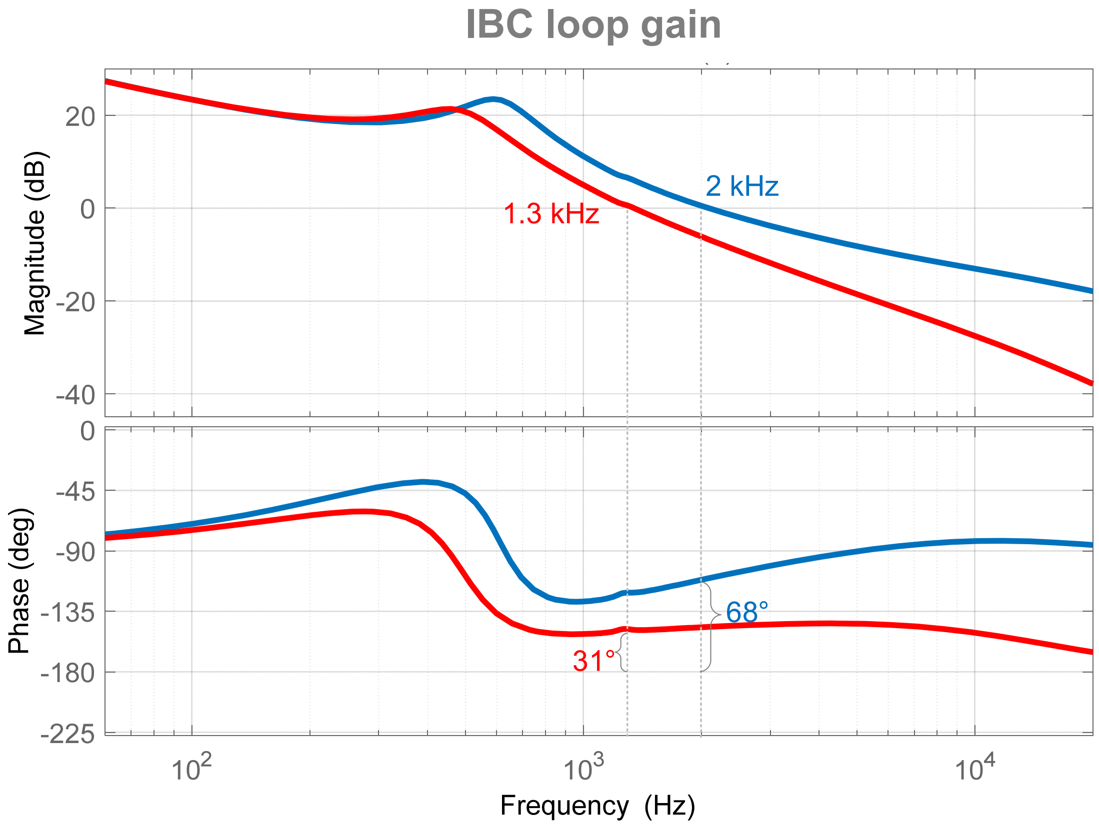

Instability in Traditional System Caused by Partial Loss of Generation

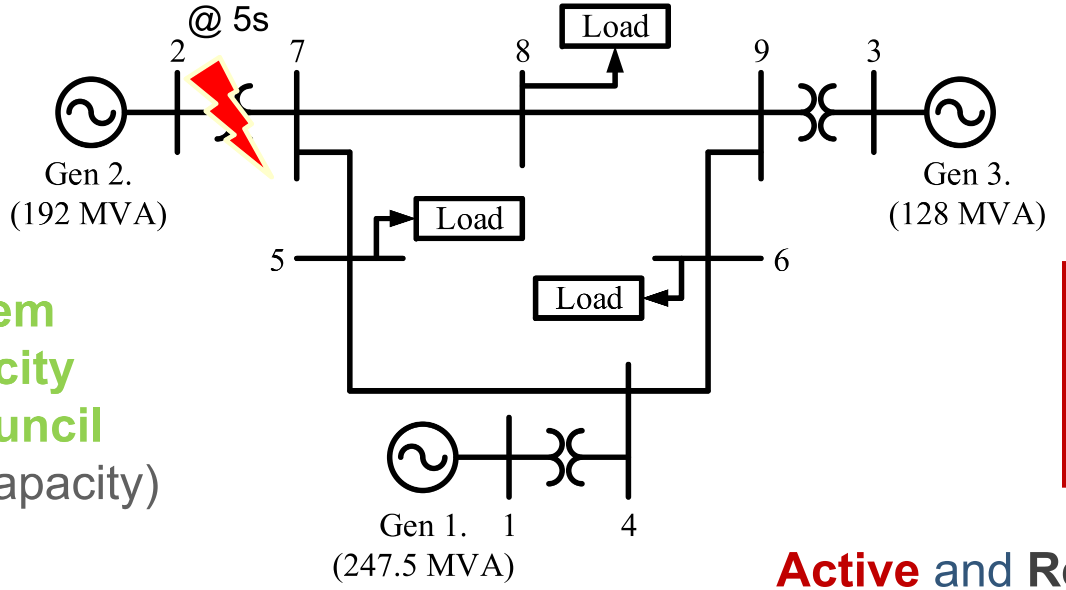

$$P_{Load}^{Total} < P_{Gen1} + P_{Gen2}$$

≈ 180 MW ≈ 370 MW

Large transient causes overall system instability due to undamped power oscillations between Generators 1 and 3.

9-bus subsystem
Western Electricity Coordinating Council
(240 GW Installed Capacity)

What if Generator at the bus 1 is replaced with the full-power grid interface converter operating as a virtual generator?

PV Farm

Active and **Reactive** Power at the bus No.4 during loss of generation transient

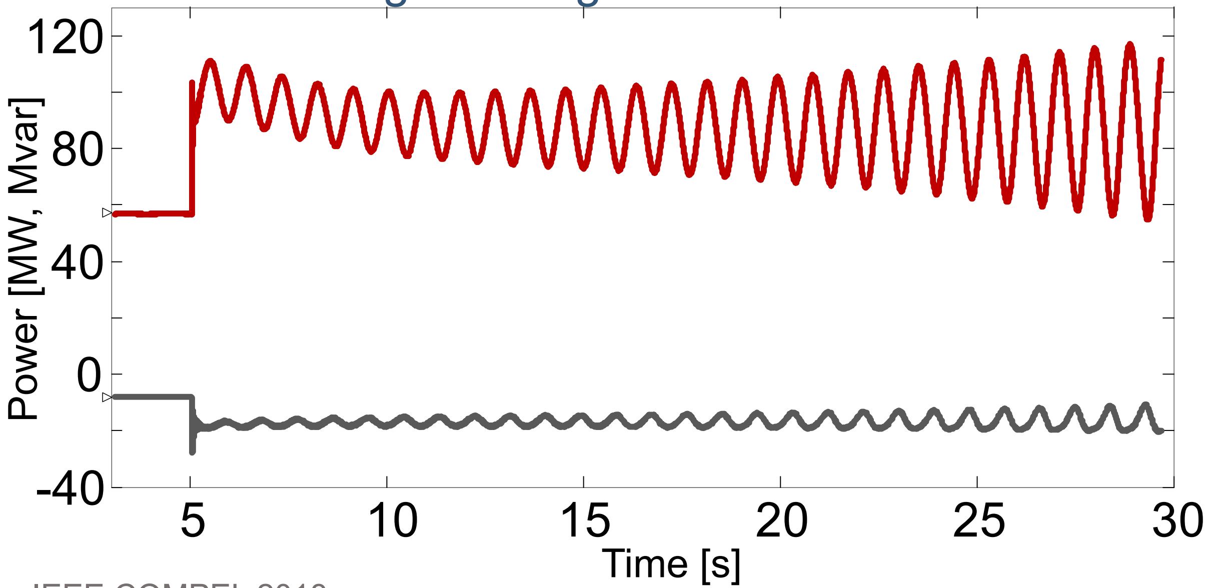

Outline

Average Model of a Power Electronics Converter
- Voltage Source Converter (VSC)-

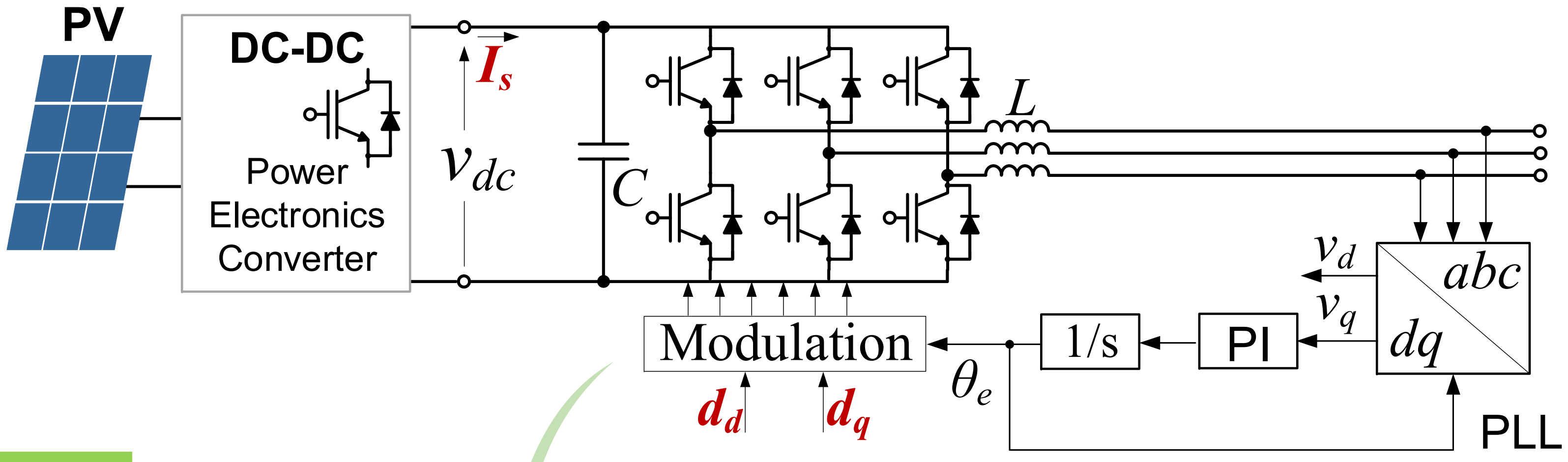

What is a relationship with a synchronous machine model?

dq **Transformation**

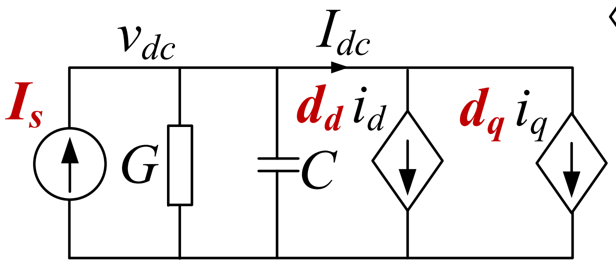

Dynamic (average) power converter model

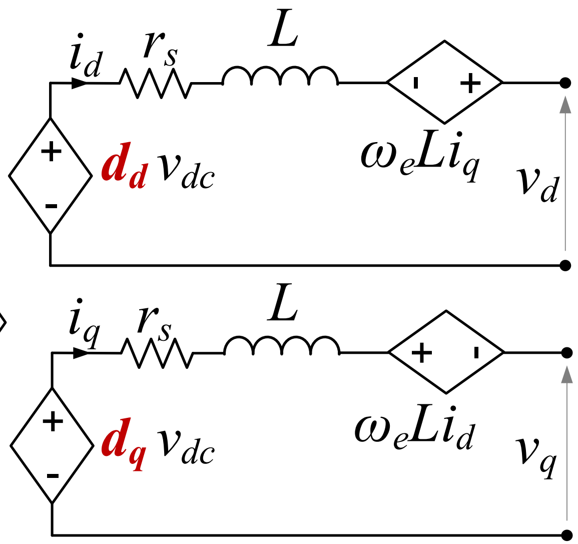

All-Electrical system

Model of a Synchronous Generator *- Salient-pole Rotor (Anisotropic) -*

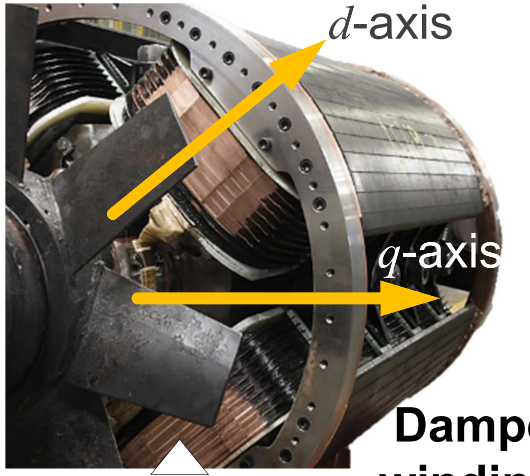

Field winding

Damper windings

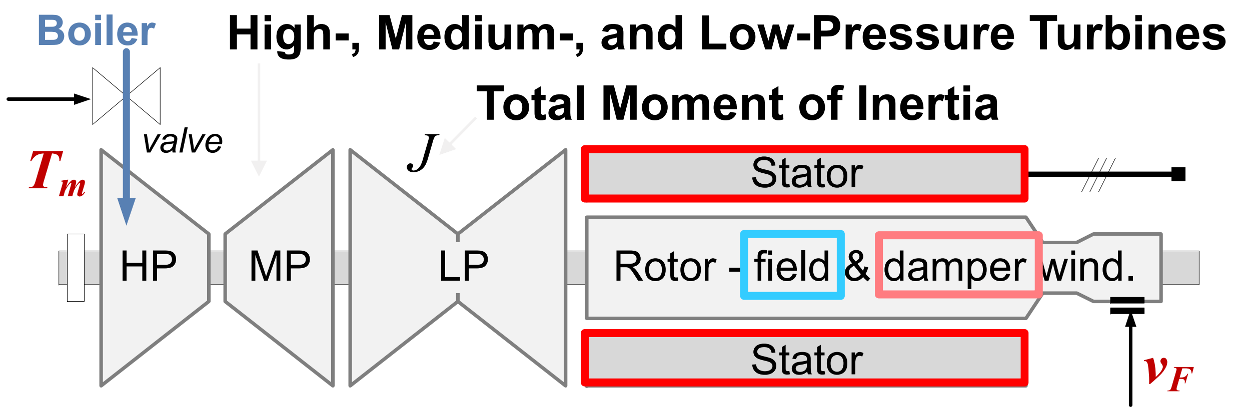

$$J\frac{\mathrm{d}\Omega}{\mathrm{d}t} = T_m - T_e - k_f\Omega$$

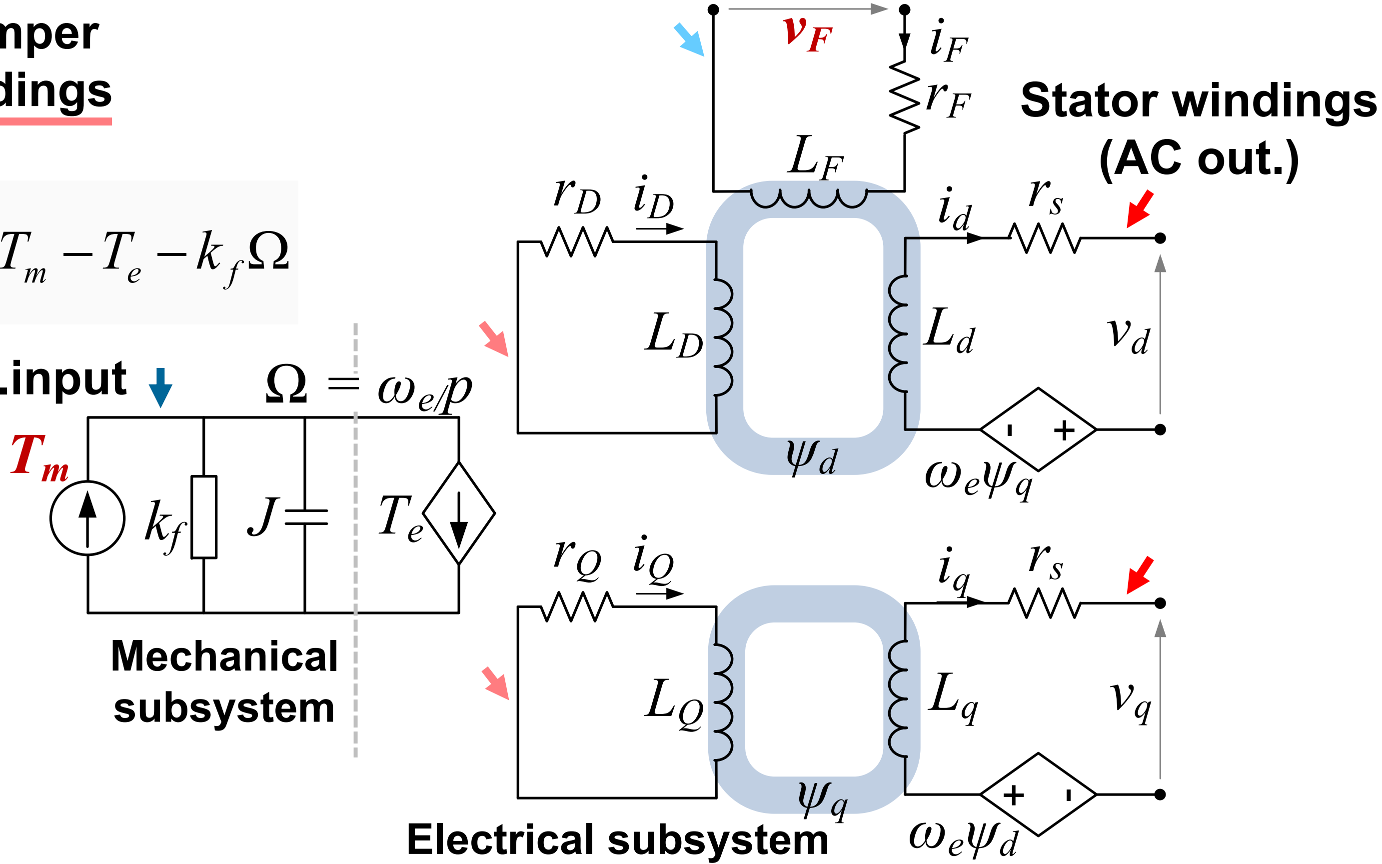

Electrical subsystem

Model of a Synchronous Generator - *Salient-pole Rotor (Anisotropic)* -

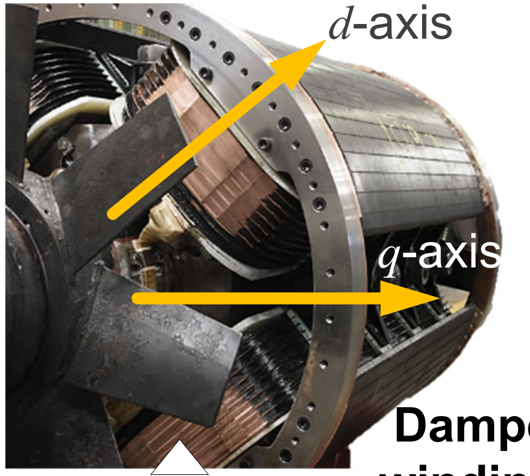

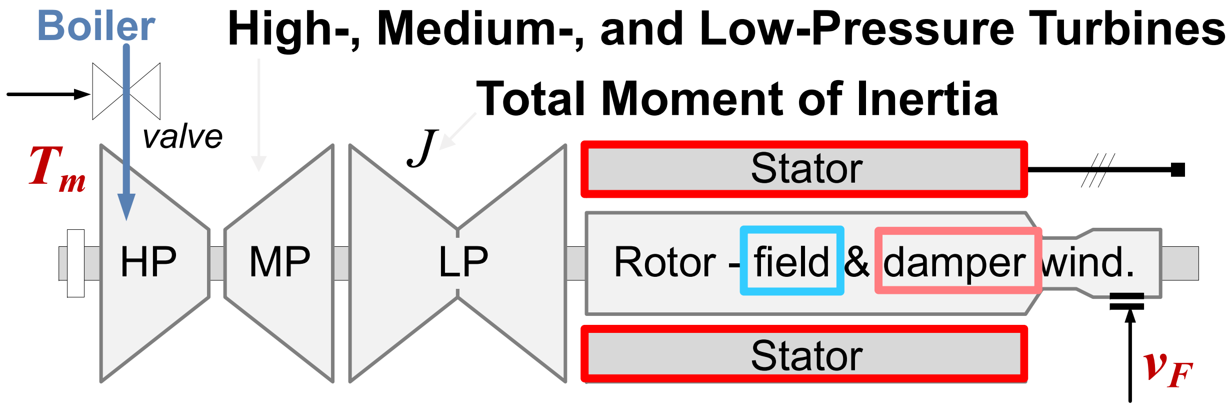

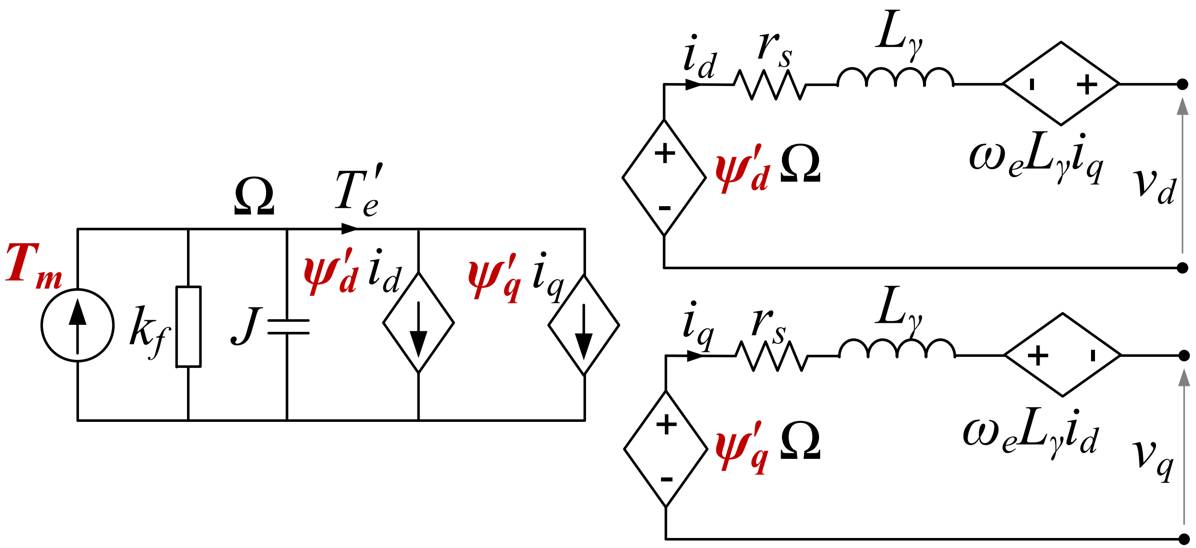

Electrical subsystem can be combined and "coupled" to an electrical equivalent of the mechanical subsystem…

Electrical subsystem

Supplementary slide

The machine equations can be rewritten into the following form, defining flux derivatives per rotor position rather than time (the main reason for this reformatting is to factor out the term dependent on the angular speed):

$$v_d = -r_s i_d - \omega_e \psi_q + \frac{\mathrm{d}\psi_d}{\mathrm{d}\theta_e}\frac{\mathrm{d}\theta_e}{\mathrm{d}t} = -r_s i_d - \omega_e \psi_q + \frac{\mathrm{d}\psi_d}{\mathrm{d}\theta_e}\omega_e = -r_s i_d + \Omega\, p(\frac{\mathrm{d}\psi_d}{\mathrm{d}\theta_e} - \psi_q)$$

$$v_q = -r_s i_q + \omega_e \psi_d + \frac{\mathrm{d}\psi_q}{\mathrm{d}\theta_e}\frac{\mathrm{d}\theta_e}{\mathrm{d}t} = -r_s i_q + \omega_e \psi_d + \frac{\mathrm{d}\psi_q}{\mathrm{d}\theta_e}\omega_e = -r_s i_q + \Omega\, p(\frac{\mathrm{d}\psi_q}{\mathrm{d}\theta_e} + \psi_d)$$

$$\Rightarrow \quad \begin{aligned} v_d &= -r_s i_d + \Omega \psi_d^{'} \\ v_q &= -r_s i_q + \Omega \psi_q^{'} \end{aligned}$$

Where:

$$\psi_d^{'} = p\left(\frac{\mathrm{d}\psi_d}{\mathrm{d}\theta_\mathrm{e}} - \psi_q\right)$$

$$\psi_q^{'} = p\left(\frac{\mathrm{d}\psi_q}{\mathrm{d}\theta_\mathrm{e}} + \psi_d\right)$$

Supplementary slide

Furthermore, active power at the machine terminals comprises following components: joules losses, rate of change of the energy accumulated in the magnetic field, and mechanical power converted to electrical:

$$P_{dq} = (i_d^2 + i_q^2) \cdot r_s + i_d \frac{\mathrm{d}\psi_d}{\mathrm{d}t} + i_q \frac{\mathrm{d}\psi_q}{\mathrm{d}t} + \omega_e (\psi_d i_q - \psi_q i_d) = (i_d^2 + i_q^2) \cdot r_s + P_{gap}$$

Assuming lossless electromechanical conversion from rotor to stator, all of the power (except joules losses) is delivered from the rotor (P_{gap}). Lumping this power into the form of an "equivalent" torque, it could be written:

$$T_e^{'} = \frac{P_{gap}}{\Omega} = \frac{1}{\Omega}\left(i_d \frac{\mathrm{d}\psi_d}{\mathrm{d}t} + i_q \frac{\mathrm{d}\psi_q}{\mathrm{d}t} \right) + \frac{\omega_e}{\Omega}(\psi_d i_q - \psi_q i_d) = i_d \psi_d^{'} + i_q \psi_q^{'}$$

Model of a Synchronous Generator - *Salient-pole Rotor (Anisotropic)* -

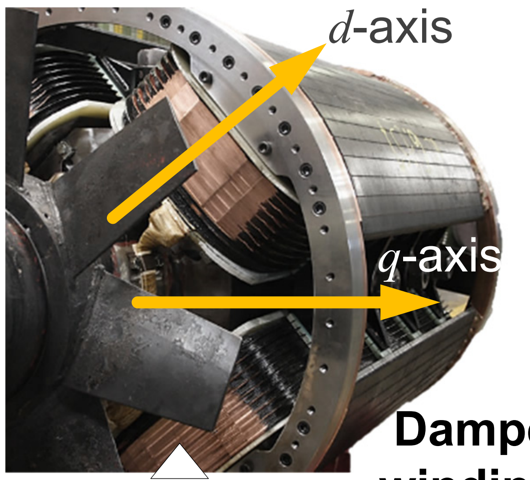

Field winding

Damper windings

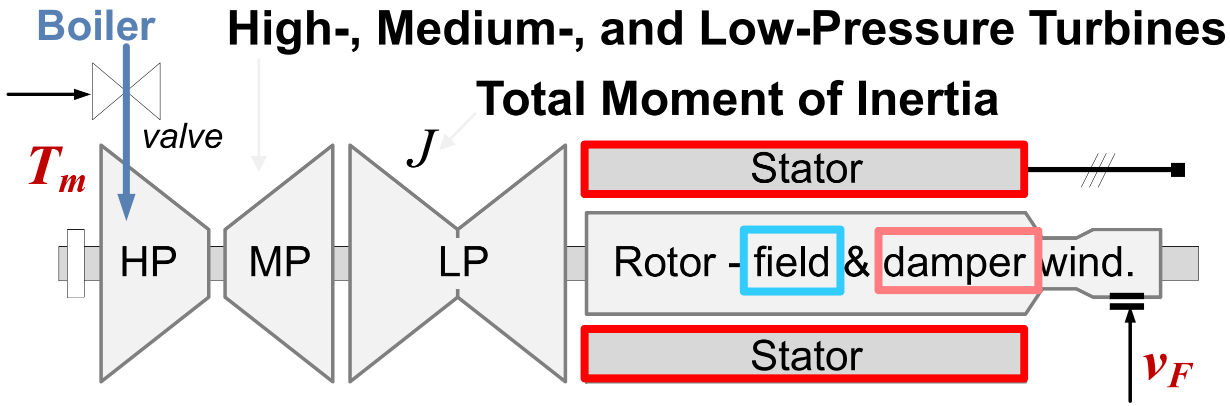

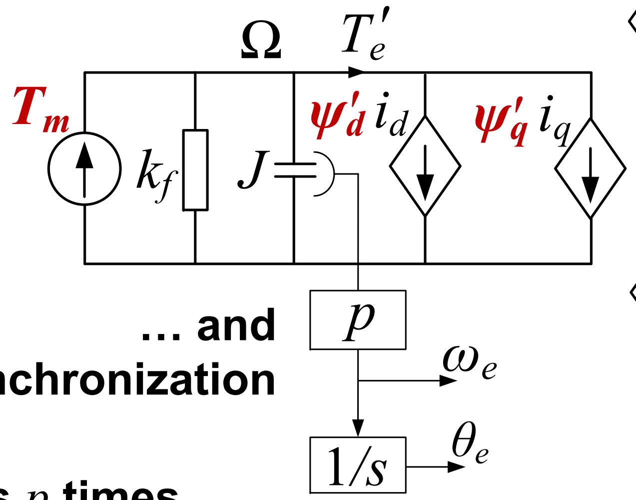

… and self- synchronization

ω_e **is** p **times higher than** Ω

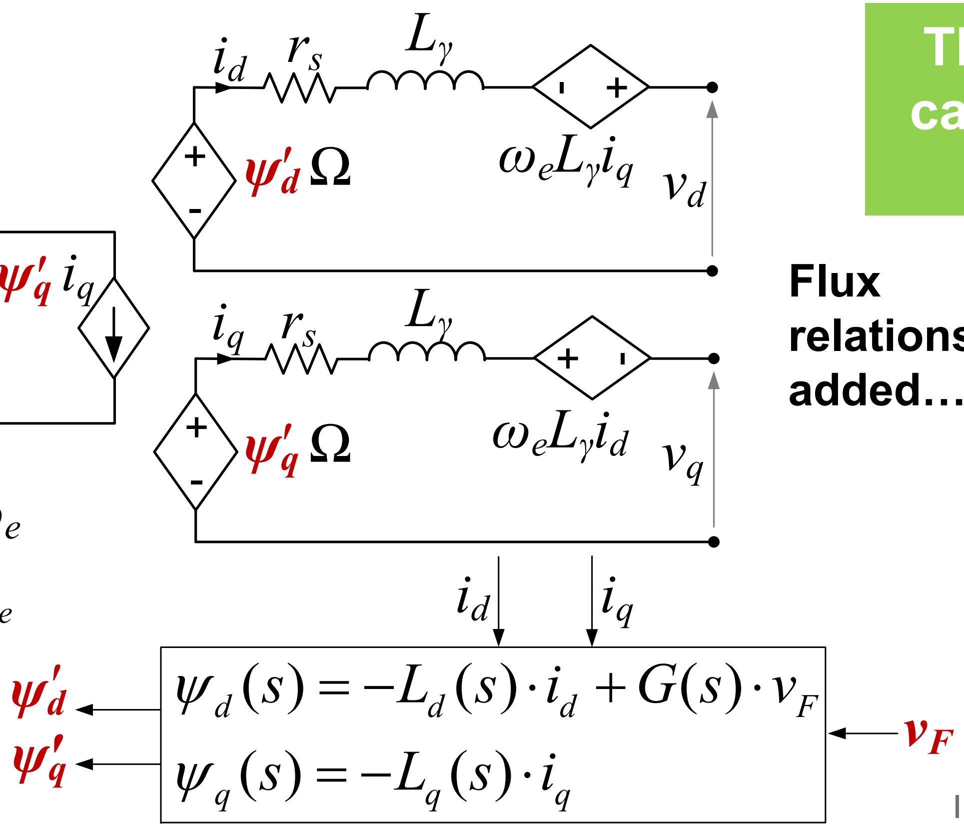

The same concept can now be applied to a converter!

Flux relationships added…

Electronic Synchronous Machine

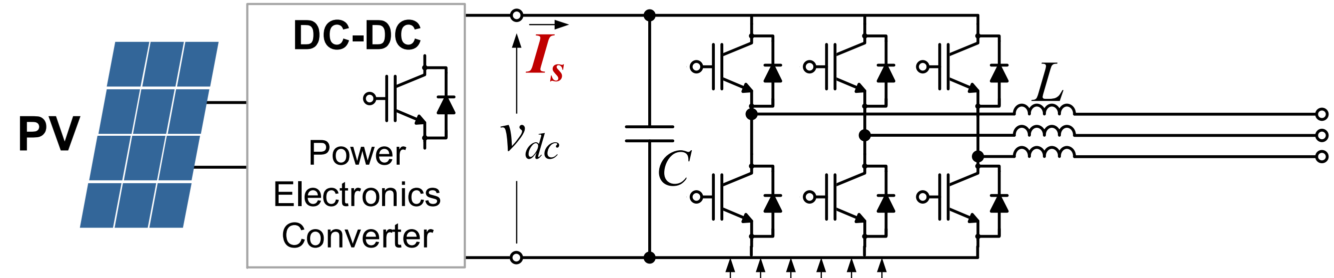

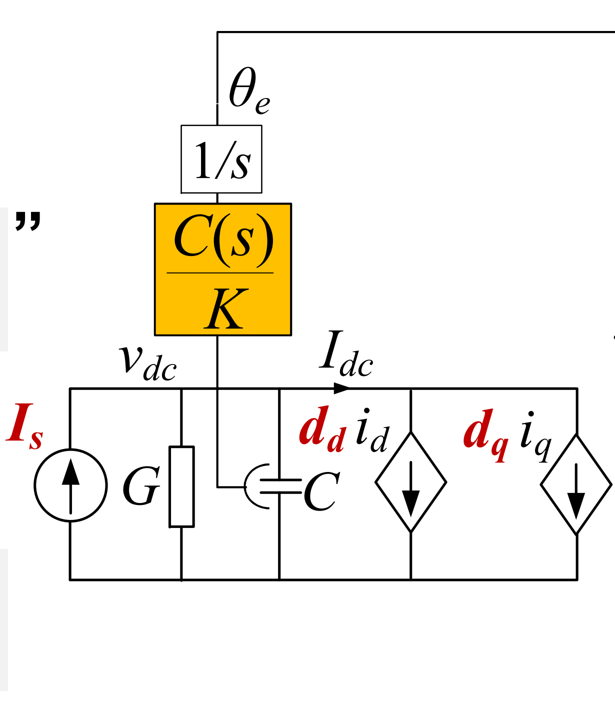

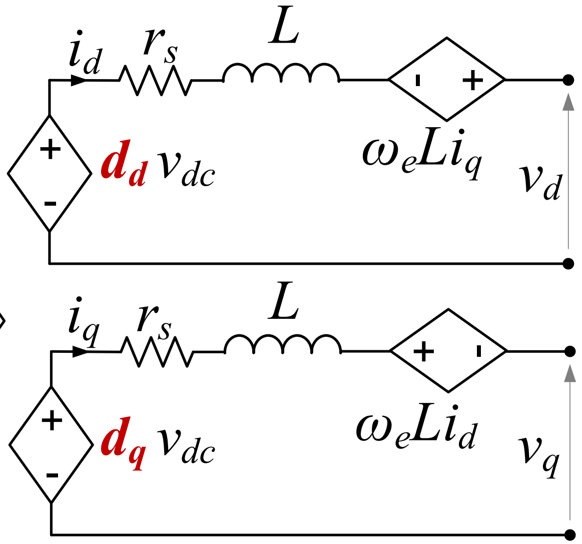

All that needs to be done to emulate a simple synchronous machine!

$$“\; J\frac{d\Omega}{dt} = T_m - T_e - k_f\Omega \;”$$

$$C\frac{dv_{dc}}{dt} = I_s - I_{dc} - Gv_{dc}$$

However, for emulation of the particular synchronous machine:

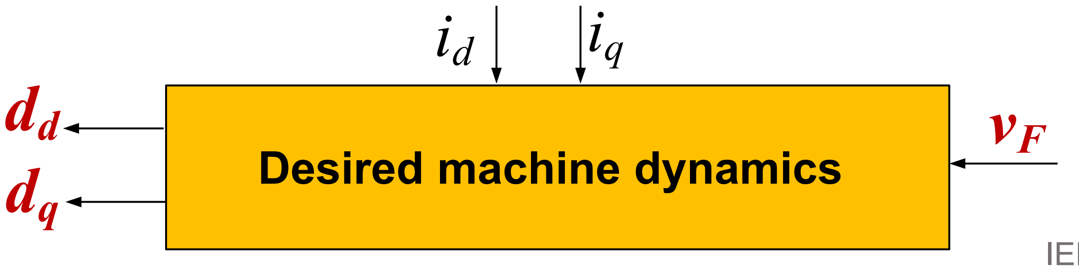

Supplementary slide

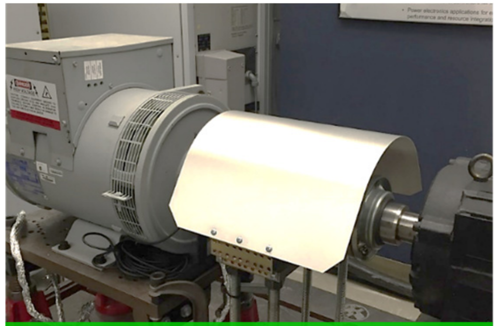

30 kW Synchronous Generator

$L_d(s)$, $L_q(s)$, **and** $G(s)$ **describe well an electrical dynamics of a synchronous machine including:**

- Field Winding
- Saliency
- Damper Windings

$$\psi_d(s) = -L_d(s)\cdot i_d + G(s)\cdot v_F$$
$$\psi_q(s) = -L_q(s)\cdot i_q$$

Measured point-by-point*

Curve-fitted transfer function

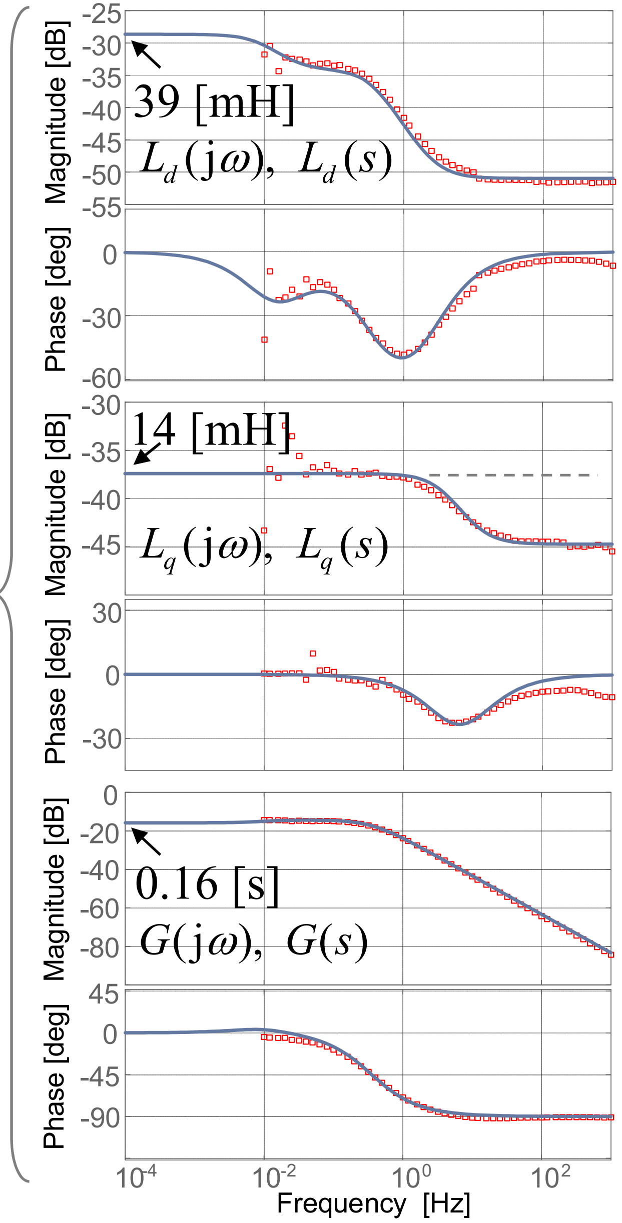

Additionally, mechanical dynamics estimated from two slow-down tests (in order to solve for k_f and J):

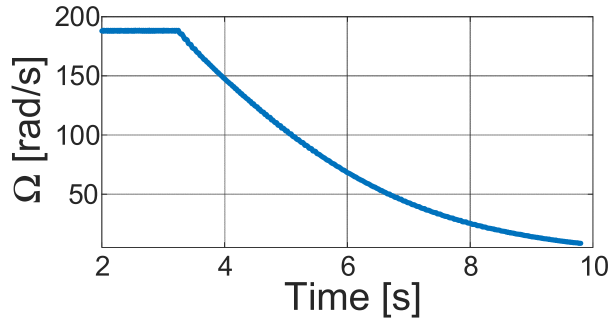

$$J = 0.32\ [\mathrm{kg\cdot m^2}]$$
$$k_f = 0.01\ [\mathrm{kg\cdot m^2/s}]$$

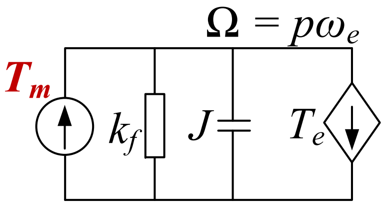

*IEEE guide for standstill frequency response (SSFR) testing - Std.115A-1987

Virtual Inertia

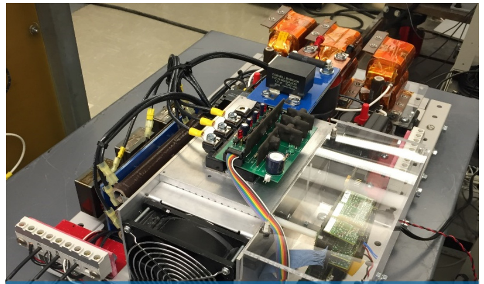

30 kW Voltage Source Converter (VSC)

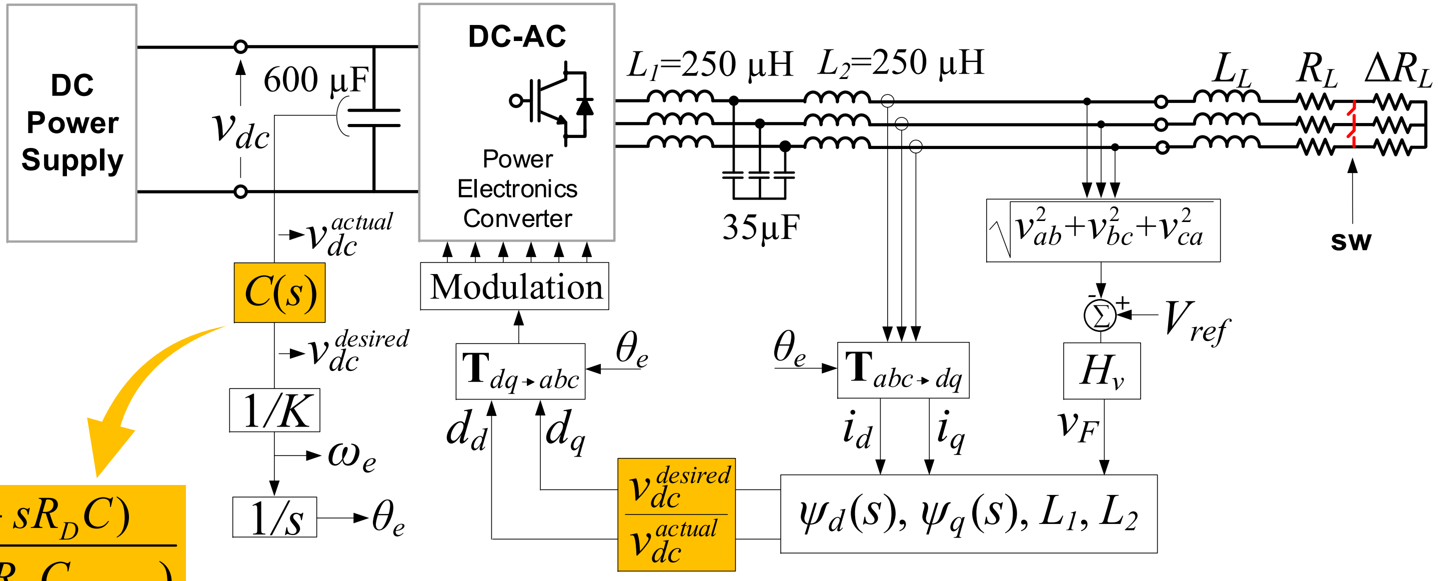

$$C(s)=\frac{R_D I_{dc}/V_{dc}-(1+sR_D C)}{R_D I_{dc}/V_{dc}-(1+sR_D C_{desired})}$$

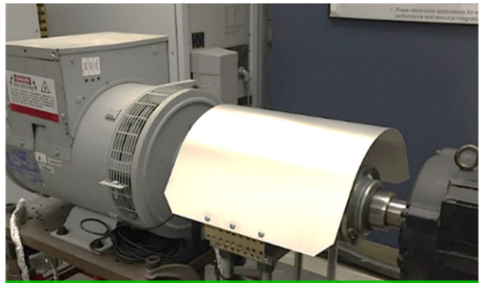

30 kW Synchronous Generator

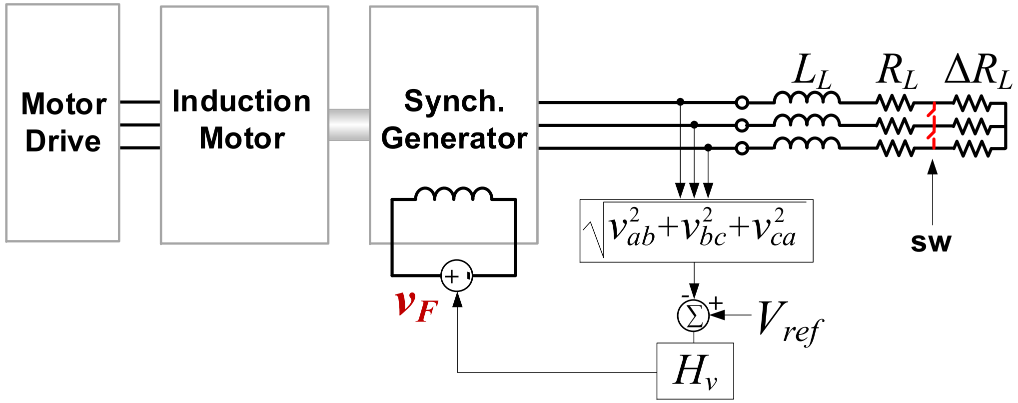

Virtual Inertia (cont'd)

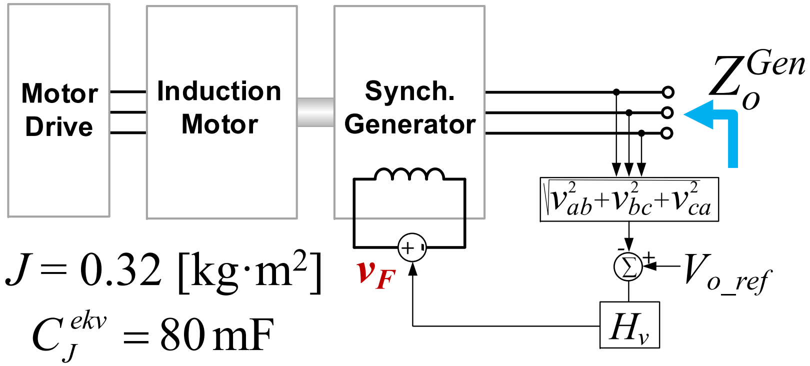

$J = 0.32$ [kg·m²]

$C_J^{ekv} = 80\,\text{mF}$

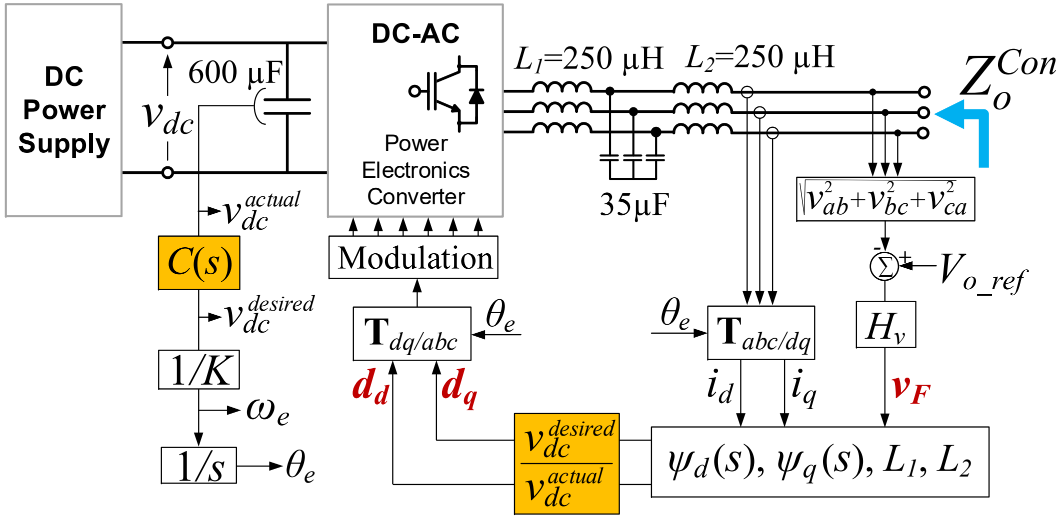

Output Impedance plots

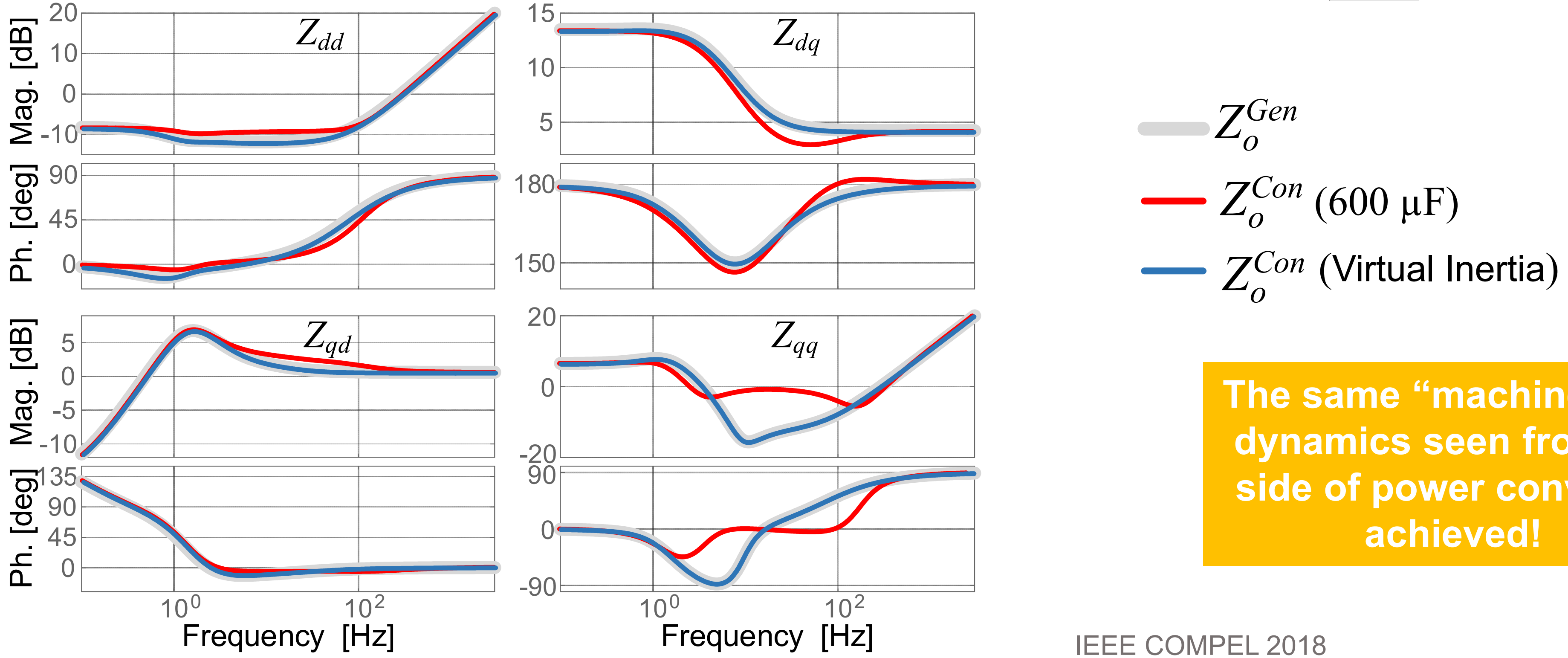

The same "machine-like" dynamics seen from AC side of power converter achieved!

Experimental Demonstration of the Equivalence

Machine and Converter Dynamics Fully Matched!

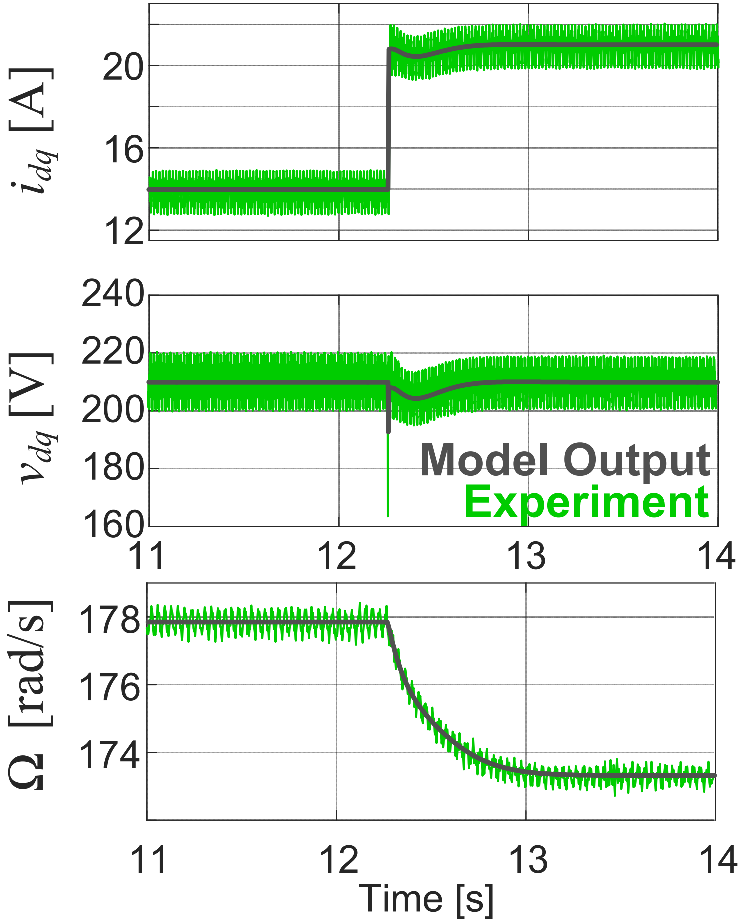

Capacitance equivalent to machine inertia:

$J = 0.32$ [kg·m²]

$C_J^{ekv} = 80\,\mathrm{mF}$

Compared to

$C = 600\,\mu\mathrm{F}$

130 times smaller capacitance!

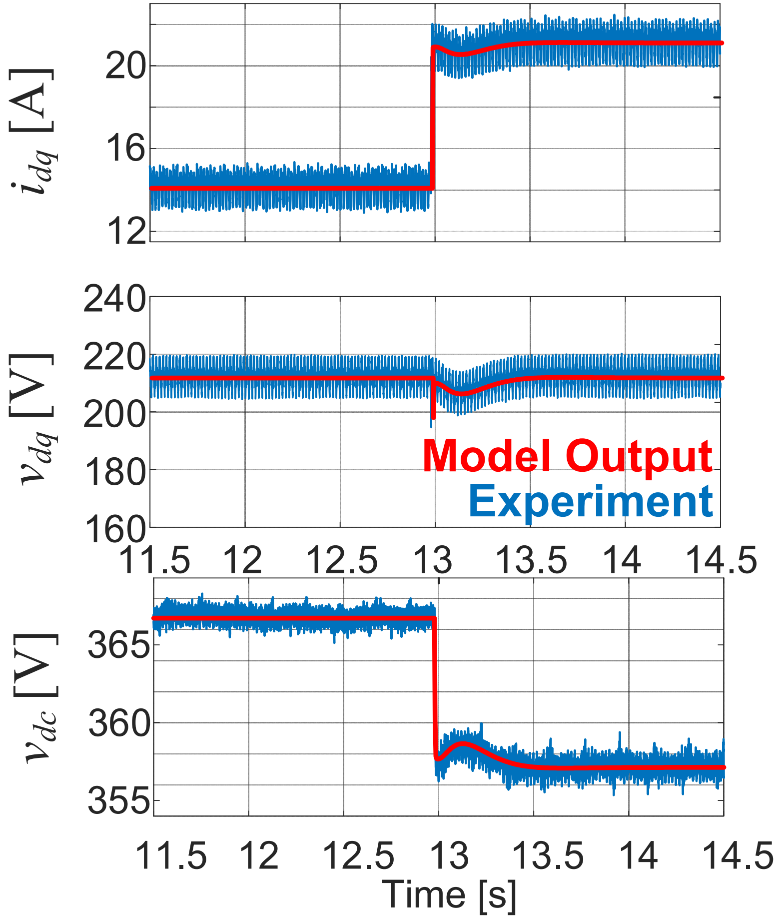

System-Level Operation with Real and Electronic Machine Coupled

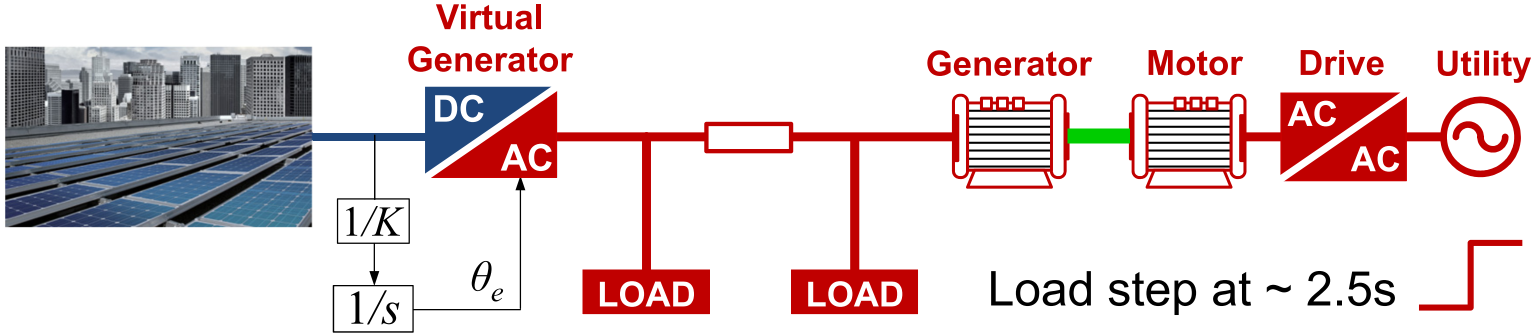

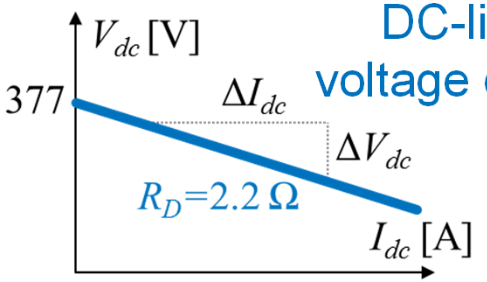

DC-link voltage droop

- Frequency of the *AC* –voltages and currents directly proportional to omega and DC-link voltage!
- Power converter synchronizes seamlessly with no PLL required

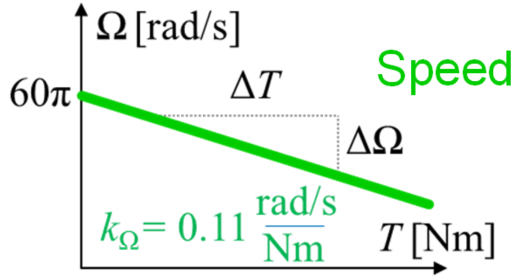

Speed droop

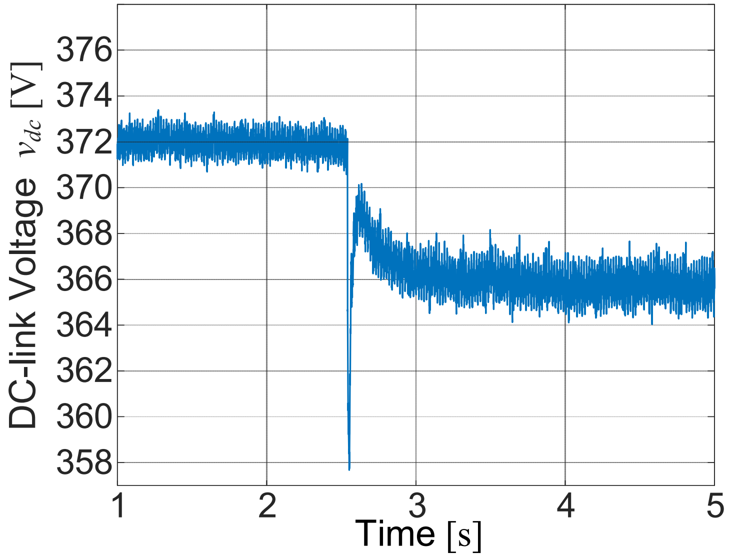

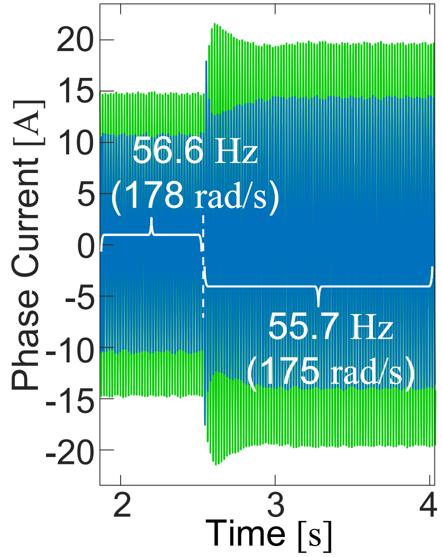

Generator current Converter current

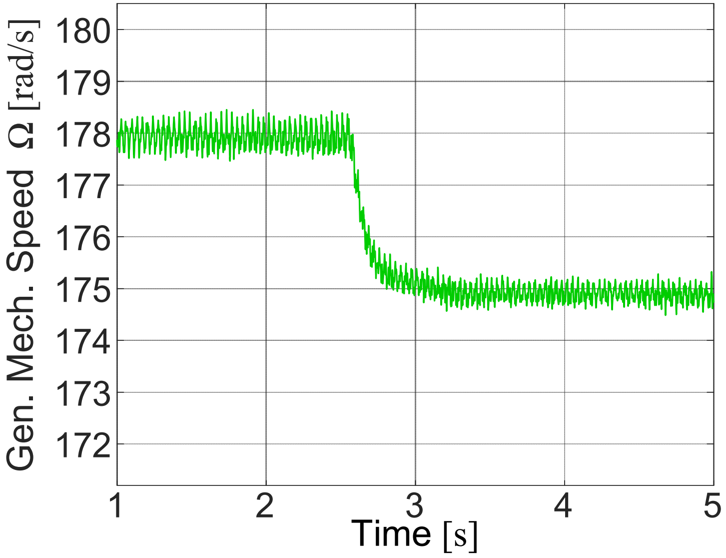

Mitigating Instability with Power Electronics-Interfaced Renewable Generation?

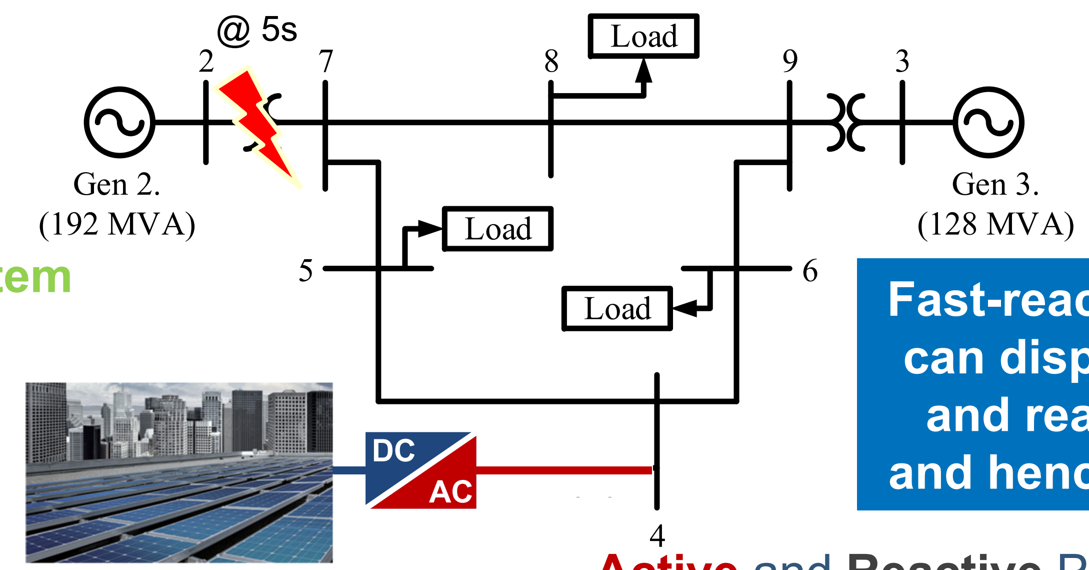

WECC
9-bus system

$$P_{Load}^{Total} < P_{Gen1} + P_{Gen2}$$

≈ 180 MW ≈ 370 MW

Fast-reacting power electronics can dispatch necessary active and reactive power very fast and hence stabilize the system!

Active and **Reactive** Power at the bus No.4 during loss of generation transient

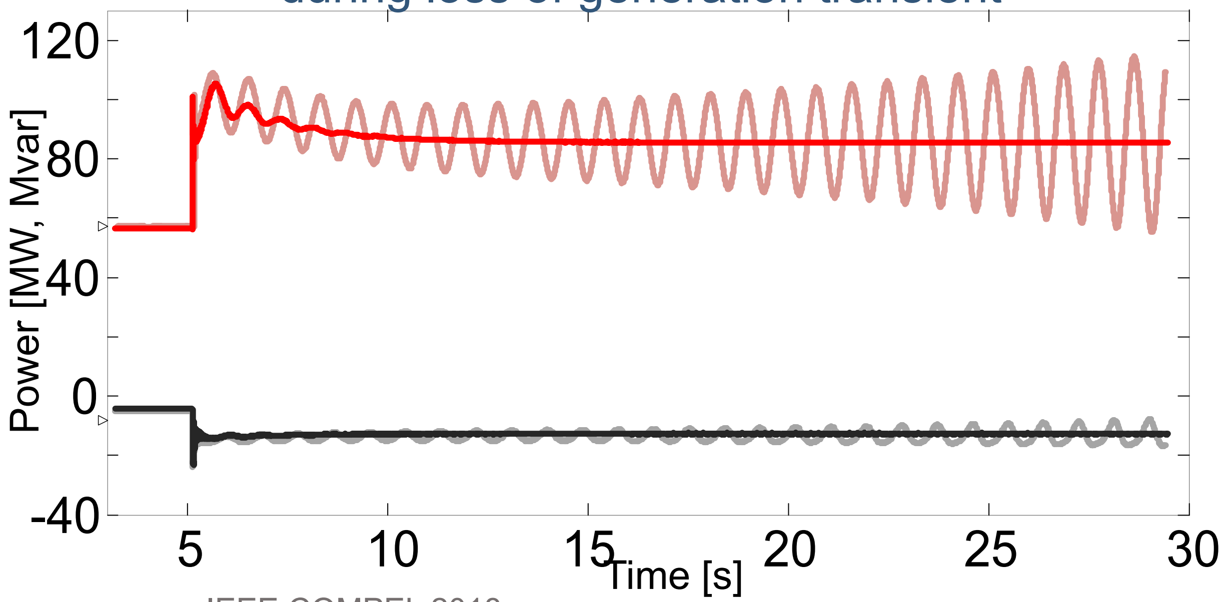

- **Replacing Generator 1 with a Virtual Generator behaving exactly the same as Generator 1**
- **However, if converter emulates lower inertia, instability can be avoided!**
- **Grid-tied converter <u>not</u> operating at peak power but regulating voltage and frequency!**

List of References - 1

[1] R. H. Park, “Two-reaction theory of synchronous machine I and II,” *AIEE Trans.*, vol. 48, and vol. 52, 1929 and 1993.

[2] P.C. Krause, *Analysis of Electric Machinery*, McGraw Hill, 1986.

[3] R. D. Middlebrook, and S. Cuk, “A general unified approach to modeling switching converter power stages,” *IEEE PESC’76*, Rec., 1976, pp. 18-34.

[4] K. D. T. Ngo, “Low frequency characterization of PWM converters,” *IEEE Trans. Power Electron.*, vol PE-1, 1986, pp. 223-230.

[5] P. T. Krein, J. Bentsman, R. M. Bass, and B. Lesieture, “On the use of averaging for the analysis of power electronic systems,” *IEEE Trans. Power Electron.*, vol. 5, no. 5, 1990, pp. 182-190.

[6] C. T. Rim, D. Y. Hu, and G. H. Cho, “Transformers as equivalent circuits for switches: general proofs and d-q transformation-based analyses,” *IEEE Trans. Ind. Appl.*, Vol. 26, no. 4, 1990, pp. 777-785.

[7] S. R. Sanders, J. M. Noworolski, X. Z. Liu, and G. C. Verghese, “Generalized averaging method for power conversion circuits,” *IEEE Trans. Power Electron.*, vol. 6, no. 2, 1991, pp. 251-259.

[9] P. Bauer, and J. B. Klaassens, “Dynamic modelling of AC power converters,” *IEEE PCC 1993 Rec.*, pp. 502-507, 1993.

[10] S. Hiti, D. Boroyevich, and C. Cuadros, “Small-signal modeling and control of three-phase PWM converters,” in *Proc. IEEE Ind. Applict. Soc. Annu. Meeting*, Oct. 1994, pp. 94-107.

[11] S. Hiti, and D. Boroyevich, “Small-signal modeling of three-phase PWM modulators,” in *Proc. IEEE Power Electron. Spec. Conf.*, Jun. 1996, pp. 550-555.

[12] S. Hiti, D. Boroyevich, and F. C. Lee, “A new control algorithm for three-phase PWM buck rectifier with input displacement factor compensation,” *IEEE Trans. Power Electron.*, vol. 9, no. 2, pp. 173-180, 1994.

List of References - 2

[12] H. Mao, D. Boroyevich, and F. C. Lee, "Novel reduced-order small-signal model of a three-phase PWM rectifier and its application in control design and system analysis," *IEEE Trans. Power Electron.*, vol. 13, no. 3, pp. 511-521.

[13] H. Soo-Bin, C. Nam-Sup, R. Chun-Taik, and C. Gyu-Hyeong, “Modeling and analysis of static and dynamic characteristics for buck-type-three-phase PWM rectifier by circuit dq transformation,” *IEEE Trans. Power Electron.*, vol. 13, no. 2, pp. 323-336, 1998.

[14] R. Zhang, F. C. Lee, D. Boroyevich, and M. Hengchun, “New high power, high performance power converter systems,” *IEEE Trans. Power Electron.*, vol. 15, no. 3, pp. 456-463, 2000.

[15] D. Ke, L. Ping, K. Yong, and C. Jian, “Decoupling current control for voltage source converter in synchronous rotating frame,” in *Proc. Power Electron. And Drive Sys.*, 2001, vol. 1, pp. 39-43.

[16] D. N. Zmood, D. G. Holmes, and G. H. Bode, “Frequency-domain analysis of three-phase linear current regulators,” *IEEE Trans. Ind. Appl.*, vol. 37, no. 2, pp. 601-610, 2001.

[17] Y. Yang, M. Kazerani, and V. H. Quintana, “Modeling, control and implementation of three-phase PWM converters,” *IEEE Trans. Power Electron.*, vol. 18, no. 3, pp. 857-864, 2003.

[18] R. Burgos, E. P. Wiechmann, and J. Holtz, “Complex state-space modeling and nonlinear control of active front-end converters,” *IEEE Trans. Ind. Electron.*, vol. 52, no. 2, pp. 363-377, 2005.

[19] M. Liserre, F. Blaabjerg, and S. Hansen, “Design and control of an LCL-filter-based three-phase active rectifier,” *IEEE Trans. Ind. Appl.*, vol. 41, no. 5, pp. 1281-1291, 2005.

[20] L. Yacoubi, K. Al-Haddad, L. A. Dessaint, and F. Fnaiech, “Linear and nonlinear control techniques for a three-phase three-level NPC boost rectifier,” *IEEE Trans. Ind. Electron.*, vol. 53, no. 6, pp. 1908-1918, 2006.

[21] S. Yongsug and T. A. Lipo, “Modeling and analysis of instantaneous active and reactive power for PWM AC/DC converter under generalized unbalanced network,” *IEEE Trans. On Power Electron.*, vol 21, no. 3, pp. 1530-1540, 2006.

[22] N. B. Hadj-Youssef, K. Ai-Haddad, H. Y. Kanaan, and F. Fnaiech, “Small-signal perturbation technique used for DSP-based identification of a three-phase three-level boost-type Vienna rectifier,” IET, Electric Power Appli., vol. 1, no. 2, pp. 199-208, 2007.

List of References - 3

[23] A. Tabesh and R. Iravani, "Multivariable dynamic model and robust control of a voltage-source converter for power system applications," *IEEE Trans. Power Del.*, vol. 24, no. 1, pp. 462-471, 2009.

[24] I. Cvetkovic et al. "Un-terminated, low-frequency terminal-behavioral d-q model of three-phase converters," in *Proc. ECCE, 2001 IEEE*, pp. 791-798.

[25] L. Harnefors, A. Antonopoulos, S. Norrga, L. Angquist, and H. P. Nee, "Dynamic analysis of modular multilevel converters," *IEEE Trans. Ind. Electron.*, vol. 60, no. 7, pp. 2526-2537, 2013.

[26] F. chierchie, L. Stefanazzi, E. E. Paolini, and A. R. Oliva, "Frequency analysis of PWM inverter with dead-time for arbitrary modulating signals," *IEEE Trans. Power Electron.*, vol. 29, pp. 2850-2860, Jun. 2014.

[27] F. Gonzalez-Espin, E. Figueres, G. Garcera, R. Gonzalez-Medina, and M. Pascual, "Measurement of the loop gain frequency response of digitally controlled power converters," *IEEE Trans. Ind. Electron.*, vol. 53, no. 5, vol. 57, pp. 2785-2796, Aug. 2010.

[28] B. Bahrani, A. Karimi, B. Rey, and A. Rufer, "Decoupled dq-current control of grid-tied voltage source converter using nonparametric models," *IEEE Trans. Ind. Electron.*, vol. 60, pp. 1356-1366, Apr. 2013.

[29] Texas Instrument, "PowerSUITE digital power supply software frequency response analyzer tool for C2000TM MCUs", available at http://www.ti.com/tool/SFRA#3.

[30] B. Wen, R. Burgos, P. Mattavelli, D. Boroyevich, "Experimental evaluation of voltage source inverter switching model with embedded C code controller," in *Proc. GCMS'13*, no. 8, 2013.

[31] C. Se-Kyo, "A phase tracking system for three-phase utility interface inverters," *IEEE Trans. Power Electron.*, vol. 15, no. 3, pp. 431-438, May 2000.

[32] F. Blaabjerg, R. Teodorescu, M. Liserre, and A. V. Timbus, "Overview of control and grid synchronization for distributed power generation systems," *IEEE Trans. Ind. Electron.*, vol. 53, no. 5, pp. 1398-1409, Oct. 2006.

List of References - 4

[33]L. Harnefors, "Modeling of Three-Phase Dynamic Systems Using Complex Transfer Functions and Transfer Matrices," *IEEE Trans. Ind. Electron.*, vol. 54, no. 4, pp. 2239-2248, Apr 2007.

[34] L. Harnefors, M. Bongiorno, and S. Lundberg, "Input-Admittance Calculation and Shaping for Controlled Voltage-Source Converters," *IEEE Trans. Ind. Electron.*, vol. 54, no. 6, pp. 3323-3334, Dec 2007.

[35] D. Dong, B. Wen, P. Mattavelli, D. Boroyevich, and Y. Xue, “Grid-synchronization modeling and its stability analysis for multi-paralleled three-phase inverter systems,” in *Proc. 28th Annu. Appl. Power Electron. Conf. Expo.*, Mar. 2013, pp. 439-446.

[36] Z. Yao, P. G. Therond, and B. Davat, "Stability analysis of power systems by the generalised Nyquist criterion," *International Conference on Control*, pp. 739-744, 1994.

[37] M. Belkhayat, "Stability Criterion for AC Power Systems with Regulated Loads," *Doctor of Philosophy*, Purdue University, 1997.

[38] E. A. A. Coelho, P. C. Cortizo, and P. F. D. Garcia, "Small-signal stability for parallel-connected inverters in stand-alone AC supply systems," *IEEE Transactions on Industry Applications*, vol. 38, no. 2, pp. 533-542, Mar 2002.

[39] Y. L. Familiant, K. A. Corzine, J. Huang, and M. Belkhayat, "AC Impedance Measurement Techniques," *IEEE International Conference on Electric Machines and Drive*s, pp. 1850-1857, 2005.

[40] J. Huang, K. Corzine, and M. Belkhayat, "Single-Phase ac Impedance Modeling for Stability of Integrated Power Systems," *2007 IEEE Electric Ship Technologies Symposium*, pp. 483-489, 2007.

[41] J. Huang, K. Corzine, and M. Belkhayat, "Single-Phase ac Impedance Modeling for Stability of Integrated Power Systems," *2007 IEEE Electric Ship Technologies Symposium*, pp. 483-489, 2007.

[42] R. Burgos, D. Boroyevich, F. Wang, K. Karimi, and G. Francis, "On the Ac stability of high power factor three-phase rectifiers," *IEEE Energy Conversion Congress and Exposition*, pp. 2047-2054, 2010.

[43] H. Jing, K. A. Corzine, and M. Belkhayat, "Small-Signal Impedance Measurement of Power-Electronics-Based AC Power Systems Using Line-to-Line Current Injection," *IEEE Transactions on Power Electronics*, vol. 24, no. 2, pp. 445-455, Feb 2009.

List of References - 5

[44] I. Cvetkovic, D. Boroyevich, D. Dong, P. Mattavelli, R. Burgos, M. Jaksic, et al., "Dynamic interactions in hybrid ac/dc electronic power distribution systems," *8th International Conference on Power Electronics - ECCE As*ia, pp. 2121-2128, 2011.

[45] I. Cvetkovic, M. Jaksic, D. Boroyevich, P. Mattavelli, F. Lee, Z. Shen, et al., "Un-terminated, low-frequency terminal-behavioral d-q model of three-phase converters," *IEEE Energy Conversion Congress and Exposition*, pp. 791-798, 2011.

[46] G. Francis, R. Burgos, D. Boroyevich, F. Wang, and K. Karimi, "An algorithm and implementation system for measuring impedance in the D-Q domain," *IEEE Energy Conversion Congress and Exposition*, pp. 3221-3228, 2011.

[47] J. Sun, "Impedance-Based Stability Criterion for Grid-Connected Inverters," *IEEE Transactions on Power Electronics*, vol. 26, no. 11, pp. 3075-3078, Nov 2011.

[48] V. Valdivia, A. Lazaro, A. Barrado, P. Zumel, Ferna, C. ndez, et al., "Impedance Identification Procedure of Three-Phase Balanced Voltage Source Inverters Based on Transient Response Measurements," *IEEE Transactions on Power Electronics*, vol. 26, no. 12, pp. 3810-3816.

[49] J. He, Y. W. Li, D. Bosnjak, and B. Harris, "Investigation and Active Damping of Multiple Resonances in a Parallel-Inverter-Based Microgrid," *IEEE Transactions on Power Electronics*, vol. 28, no. 1, pp. 234-246, Jan 2013.

[50] Z. Shen, M. Jaksic, P. Mattavelli, D. Boroyevich, J. Verhulst, and M. Belkhayat, "Design and implementation of three-phase AC impedance measurement unit (IMU) with series and shunt injection," *IEEE Applied Power Electronics Conference and Exposition*, pp. 2674-2681, 2013.

[51] Z. Shen, M. Jaksic, B. Zhou, P. Mattavelli, D. Boroyevich, J. Verhulst, et al., "Analysis of Phase Locked Loop (PLL) influence on DQ impedance measurement in three-phase AC systems," *IEEE Applied Power Electronics Conference and Exposition*, pp. 939-945, 2013.

[52] M. Jaksic, D. Boroyevich, R. Burgos, Z. Shen, I. Cvetkovic, and P. Mattavelli, "Modular interleaved single-phase series voltage injection converter used in small-signal dq impedance identification," *IEEE Energy Conversion Congress and Exposition*, pp. 3036-3045, 2014.

[53] F. Liu, J. Liu, H. Zhang, and D. Xue, "Stability Issues of Z+Z Type Cascade System in Hybrid Energy Storage System (HESS)," *IEEE Transactions on Power Elec*tronics, vol. 29, no. 11, pp. 5846-5859, Nov 2014.

List of References - 6

[54] T. Messo, J. Jokipii, J. Puukko, and T. Suntio, "Determining the Value of DC-Link Capacitance to Ensure Stable Operation of a Three-Phase Photovoltaic Inverter," *IEEE Transactions on Power Electronics*, vol. 29, no. 2, pp. 665-673, Feb 2014.

[55] T. Roinila, M. Vilkko, and J. Sun, "Online Grid Impedance Measurement Using Discrete-Interval Binary Sequence Injection," *IEEE Journal of Emerging and Selected Topics in Power Electronics*, vol. 2, no. 4, pp. 985-993, Feb 2014.

[56] D. Dong, B. Wen, D. Boroyevich, P. Mattavelli, and Y. Xue, "Analysis of Phase-Locked Loop Low-Frequency Stability in Three-Phase Grid-Connected Power Converters Considering Impedance Interactions," *IEEE Transactions on Industrial Electronics*, vol. 62, no. 1, pp. 310-321, Jan 2015.

[57] B. Wen, D. Boroyevich, R. Burgos, P. Mattavelli, and Z. Shen, "Small-Signal Stability Analysis of Three-Phase AC Systems in the Presence of Constant Power Loads Based on Measured d-q Frame Impedances," *IEEE Transactions on Power Electronics*, vol. 30, no. 10, pp. 5952-5963, Oct 2015.

[58] M. K. Bakhshizadeh, X. Wang, F. Blaabjerg, J. Hjerrild, Ł. Kocewiak, C. Bak, et al., "Couplings in Phase Domain Impedance Modeling of Grid-Connected Converters," *IEEE Transactions on Power Electronics*, vol. 31, no. 10, pp. 6792-6796, Oct 2016.

[59] S. Lissandron, L. Santa, P. Mattavelli, and B. Wen, "Experimental Validation for Impedance-Based Small-Signal Stability Analysis of Single-Phase Interconnected Power Systems With Grid-Feeding Inverters," *IEEE Journal of Emerging and Selected Topics in Power Electronics*, vol. 4, no. 1, pp. 103-115, March 2016.

[60] B. Wen, D. Boroyevich, R. Burgos, P. Mattavelli, and Z. Shen, "Analysis of D-Q Small-Signal Impedance of Grid-Tied Inverters," *IEEE Transactions on Power Electronics*, vol. 31, no. 1, pp. 675-687, Jan 2016.

[61] B. Wen, D. Dong, D. Boroyevich, R. Burgos, P. Mattavelli, and Z. Shen, "Impedance-Based Analysis of Grid-Synchronization Stability for Three-Phase Paralleled Converters," *IEEE Transactions on Power Electronics*, vol. 31, no. 1, pp. 26-38, Jan 2016.

[62] V. Salis, A. Costabeber, P. Zanchetta, and S. Cox, "Stability analysis of single-phase grid-feeding inverters with PLL using Harmonic Linearisation and Linear Time Periodic (LTP) theory," *IEEE 17th Workshop on Control and Modeling for Power Electronics (COMPEL)*, pp. 1-7, 2016.

List of References - 7

[63] W. Cao, Y. Ma, L. Yang, F. Wang, and L. Tolbert, "D-Q Impedance Based Stability Analysis and Parameter Design of Three-Phase Inverter-Based Ac Power Systems," *IEEE Transactions on Industrial Electronics*, vol. 64, no. 7, pp. 6017-6028, July 2017.

[64] M. Jakšić, Z. Shen, I. Cvetković, D. Boroyevich, R. Burgos, C. DiMarino, et al., "Medium-Voltage Impedance Measurement Unit for Assessing the System Stability of Electric Ships," *IEEE Transactions on Energy Conversion*, vol. 32, no. 2, pp. 829-841, Jun 2017.

[65] B. Wen, D. Boroyevich, R. Burgos, P. Mattavelli, and Z. Shen, "Inverse Nyquist Stability Criterion for Grid-Tied Inverters," *IEEE Transactions on Power Electronics*, vol. 32, no. 2, pp. 1548-1556, Feb 2017.

[66] I. Cvetkovic, D. Boroyevich, R. Burgos, C. Li, M. Jaksic, and P. Mattavelli, “Modeling of a virtual synchronous machine-based grid-interface converter for renewable energy systems integration,” in *Proc. COMPEL 2014*, pp. 1-7.

[67] I. Cvetkovi, D. Boroyevich, R. Burgos, C. Li, and P. Mattavelli, “Modeling and control of grid-connected voltage-source converters emulating isotropic and anisotropic synchronous machine,” in *Proc. COMPEL 2015*, pp. 1-5.

[68] I. Cvetkovi, et al. “Experimental verification of a virtual synchronous generator control concept,” in *Proc. COMPEL 2016*, pp. 1-8.

[69] R. Burgos, R. Lai, Y. Pei, F. Wang, D. Boroyevich, and J. Pou, “Space vector modulator for Vienna-type rectifier based on the equivalence between two-and three-level converters: a carrier-based implementation,” IEEE Trans. Power Electron., vol. 23, no. 4, pp. 1888-1898, 2008.

[70] R. Burgos, R. Lai, S. Rosado, F. Wang, D. Boroyevich, and J. Pou, “A full frequency range average model for Vienna-type rectifiers,” in *Proc. PESC 2008*, pp. 4495-4502.

[71] R. Lai, F. Wang, R. Burgos, D. Boroyevich, D. Jiang, and D. Zhang, “Average modeling and control design for Vienna-type rectifier considering the DC-link voltage balance,” *IEEE Trans. Power Electron.*, vol. 24, no. 11, pp. 2509-2522, 2009.

[72] J. Rocabert, A. Luna, F. Blaabjerg, and P. Rodriguesz, “Control of power converter in AC microgrids,” *IEEE Trans. Power Electron.*, vol. 27, no. 11, pp. 4734-4749, 2012.